TU/e EINDHOVEN UNIVERSITY OF TECHNOLOGY

The generation of molecules through plasma-surface interactions

Citation for published version (APA):
Helden, van, J. H. (2006). *The generation of molecules through plasma-surface interactions*. [Phd Thesis 1 (Research TU/e / Graduation TU/e), Applied Physics and Science Education]. Technische Universiteit Eindhoven. https://doi.org/10.6100/IR609971

DOI:
10.6100/IR609971

Document status and date:
Published: 01/01/2006

Document Version:
Publisher's PDF, also known as Version of Record (includes final page, issue and volume numbers)

Please check the document version of this publication:

• A submitted manuscript is the version of the article upon submission and before peer-review. There can be important differences between the submitted version and the official published version of record. People interested in the research are advised to contact the author for the final version of the publication, or visit the DOI to the publisher's website.
• The final author version and the galley proof are versions of the publication after peer review.
• The final published version features the final layout of the paper including the volume, issue and page numbers.

Link to publication

General rights
Copyright and moral rights for the publications made accessible in the public portal are retained by the authors and/or other copyright owners and it is a condition of accessing publications that users recognise and abide by the legal requirements associated with these rights.

• Users may download and print one copy of any publication from the public portal for the purpose of private study or research.
• You may not further distribute the material or use it for any profit-making activity or commercial gain
• You may freely distribute the URL identifying the publication in the public portal.

If the publication is distributed under the terms of Article 25fa of the Dutch Copyright Act, indicated by the "Taverne" license above, please follow below link for the End User Agreement:

www.tue.nl/taverne

Take down policy
If you believe that this document breaches copyright please contact us at:

openaccess@tue.nl

providing details and we will investigate your claim.

Download date: 04. Oct. 2023

The Generation of Molecules through Plasma–Surface Interactions

PROEFSCHRIFT

ter verkrijging van de graad van doctor aan de
Technische Universiteit Eindhoven, op gezag van de
Rector Magnificus, prof.dr.ir. C.J. van Duijn, voor een
commissie aangewezen door het College voor
Promoties in het openbaar te verdedigen
op maandag 19 juni 2006 om 16.00 uur

door

Jean-Pierre Hubertus van Helden

geboren te Susteren

Dit proefschrift is goedgekeurd door de promotoren:

prof.dr.ir. D.C. Schram
en
prof.dr.ir. M.C.M. van de Sanden

Copromotor:
dr. R.A.H. Engeln

The work described in this thesis is part of the research program of the Dutch Foundation for Fundamental Research on Matter (FOM) via project 95TF37: *"Thin layer deposition and surface modification. Plasmas in interaction with solid matter."*

CIP-DATA LIBRARY TECHNISCHE UNIVERSITEIT EINDHOVEN

Helden, Jean-Pierre Hubertus van

The generation of molecules through plasma-surface interactions / by Jean-Pierre Hubertus van Helden. – Eindhoven : Technische Universiteit Eindhoven, 2006. – Proefschrift.
ISBN-10: 90-386-2511-1
ISBN-13: 978-90-386-2511-9
NUR 926
Trefwoorden: plasmadiagnostiek / laserspetroscopie / plasma-wand interactie / plasmachemie / plasma katalyse
Subject headings: plasma diagnostics / laser spectroscopy / plasma-wall interactions / plasma chemistry / plasma catalysis

Printed by: Universiteitsdrukkerij Technische Universiteit Eindhoven
Cover: Picture of a substrate exposed to a nitrogen-oxygen plasma. The orange light is tentatively ascribed to the emission of excited NO_2 molecules generated through plasma-surface interactions.
Cover design: Jan-Willem Luyten

Contents

1 Introduction 1

1.1 General introduction 2

1.2 The aim of this work 4

1.3 The outline of the thesis 6

2 Phase-shift cavity ring-down spectroscopy to determine absolute line intensities 11

2.1 Introduction 12

2.2 Our experimental method 16

2.3 Results and discussion 18

2.4 Conclusion 24

2.5 Acknowledgement 24

3 The density of NH and NH_2 radicals in ammonia forming expanding plasmas 27

3.1 Introduction 28

3.2 Experimental details 30

3.3 Results 35

3.4 Conclusions 55

Appendix A 57

Appendix B 59

4 Plasma-activated catalytic generation of ammonia in N_2–H_2 plasmas 69

4.1 Introduction 70

4.2 Experimental details 72

4.3 Results and discussion 80

4.4 Conclusions 96

5 Evidence of surface production of excited molecules **101**
5.1 Introduction 102
5.2 Results and discussion 104
5.3 Conclusions 108

6 Resemblance in gas composition of Ar–N_2–O_2 plasmas and Ar–NO plasmas **113**
6.1 Introduction 114
6.2 Experimental details 116
6.3 Results and discussion 124
6.4 Conclusions 134

7 Mechanisms of molecule formation in Ar/N_2/O_2 plasmas **139**
7.1 Introduction 140
7.2 Experiment details 141
7.3 Results 147
7.4 Conclusion 164

8 General conclusions **171**

Summary **175**

Samenvatting **179**

Dankwoord **183**

Curriculum Vitae **185**

Chapter 1

Introduction

Abstract

The subject of this thesis is the generation of molecules in plasma and at the surfaces surrounding the plasma. Here, the plasma acts as catalyst, it dissociates the precursor molecules before they come in contact with a surface. Then the surface is mainly exposed to high fluxes of atomic and molecular *radicals* rather than molecules. The role of plasma-surface interactions in the generation of molecules by the association of radicals at a surface in low-pressure plasmas is investigated at the hand of two model systems. In the first one, surfaces are exposed to fluxes of nitrogen and hydrogen radicals and in the second one surfaces are exposed to fluxes of nitrogen and oxygen radicals. The molecules and radicals in these plasmas have been monitored with various diagnostic techniques. The thesis work is presented in the form of 6 stand-alone articles. In this introductory chapter, a general introduction to molecule formation in plasmas, the aim of the work and the outline of the thesis are given.

1.1 General introduction

Most industrial important chemicals are often synthesized in catalytic processes. In catalysis, a specific material, called the catalyst, accelerates the reaction rate of a chemical reaction by lowering the activation energy barrier of the reaction. A well-known example is the synthesis of ammonia from nitrogen and hydrogen gas on iron catalysts at typically 100 atm and $400°C$, known as the Haber-Bosch process. This process is considered as one of the most important discoveries in the history of industrial catalysis [1]. Furthermore it has often been called the most important invention of the 20th century [2] as ammonia is the key ingredient for artificial fertilizer. Today, about 500 million tons of fertilizer are produced using 1% of the world's energy supply [3], sustaining roughly 40% of the Earth's population [4]. Due to its importance for mankind, even today the process of ammonia synthesis is still investigated to fully understand the processes on the surface leading to ammonia and to increase its efficiency by using other catalysts, e.g. ruthenium [5]. According to general belief, the ammonia generation proceeds via the dissociative chemisorption of N_2 followed by the stepwise recombination of chemisorbed atomic nitrogen and hydrogen to NH_3 at the surface of the catalyst with NH and NH_2 as reaction intermediates [6].

A crucial step in the synthesis of molecules is the dissociation of the precursor molecules involved in the reaction. In ammonia synthesis, the dissociative chemisorption of N_2 molecules on the surface of the catalyst is the rate-limiting step, due to the binding energy of 9.6 eV of N_2 molecules. To lower the energy needed to dissociate nitrogen molecules and to perform the synthesis of ammonia at lower pressures, the use of excited nitrogen molecules was suggested by Nomura et al. [7]. The lowest excited state of N_2, $A^3\Sigma_u^+$ state lies at 6.2 eV; then only 3.4 eV is necessary to dissociate the nitrogen molecules. The production of excited N_2 can be achieved by a plasma and then other catalysts than iron or ruthenium may be used to enhance the ammonia production. However, the surface is still used as catalyst to form adsorbed nitrogen atoms by the dissociative adsorption of excited N_2 molecules or nitrogen molecular ions [8, 9]. The typical flux of atomic N radicals to the surface is therefore still low, approximately 10^{18} radicals/s, which limits the efficiency of the ammonia production.

Recently, a different way of generating ammonia with plasmas was proposed by Vankan et al. [10] by plasma-activated catalysis. They showed that ammonia can be formed efficiently in plasmas generated from mixtures of hydrogen and nitrogen.

In this process, high fluxes of hydrogen and nitrogen atomic radicals were produced with the expanding thermal plasma technique, i.e $\approx 10^{20}$ radicals/s [11], which is thus two orders of magnitude higher than in previous experiments in which a plasma was used (see e.g. [12]). Since the plasma is used to produce the radicals for the ammonia production and thus acts as catalyst, the process is called plasma-activated catalysis.

Despite the continuous research on ammonia synthesis, the formation of ammonia in plasmas is still not completely understood but it is believed that plasma-surface interactions play an important role. In 1989, Uyama and Matsumoto reported that zeolite added to the downstream plasma in high-frequency discharges facilitated the ammonia production by a factor two. This was ascribed to the surface reaction of NH_x radicals adsorbed on the zeolite with hydrogen atoms [13].

The generation of molecules seems evident for plasma synthesis of molecules, like ammonia, and for plasma etching, for which the conversion or removal of molecules is the essential process. However, also in deposition processes of materials, besides the depletion of molecules due to deposition the generation of new molecules is observed. These newly formed molecules, observed besides the injected molecules, can have an influence on the plasma chemistry, since the composition of the plasmas may be changed. For example, in the deposition of a–C:H, the precursor methane is converted into hydrogen and acetylene [14]. Another example is that in the deposition of a–Si:H and a–C:H films, the formation of hydrogen molecules by the association of hydrogen atoms at the walls of the plasma reactor is observed [15]. In the case of the deposition of a–Si:H, this leads to the loss of potential chemistry, as the H atoms are crucial for the production of the growth precursors from the injected silane gas (i.e. SiH_x radicals from SiH_4) and the formation of growth sites by the association of H atoms with H atoms present on the deposited layer [16].

In the case of expanding hydrogen plasmas, the generation of ro-vibrationally excited H_2 molecules is observed. The high rotational excitation of the hydrogen molecules suggests that they are produced by the surface association of H atoms: $H_{gas} + H_{ad} \longrightarrow H_{2\,gas}^{r,v}$ [17, 18]. The recombinative desorption of H atoms, leading to excited H_2 molecules is also an important mechanism in H^- formation [19]. In plasma chemistry, there is a debate on the importance of surface processes besides volume processes in the generation of molecules by association of radicals.

But not only in plasma chemistry, but also in the universe, more and more exotic molecules are observed in interstellar space and dark clouds. And also there, a similar debate on the relative importance of surface and volume processes in molecule formation is a central theme. One of the main molecules formed in space is H_2.

Nowadays, it is established that in interstellar medium H_2 is formed by association of H atoms on dust grains [20, 21]. Surface association is also assumed to be a possible mechanism for the formation of molecules like, H_2O, NH_3 and CH_4 [22] and recently also methanol [23].

To answer the question on the importance of plasma-surface interactions in the generation of molecules in plasma chemistry, several issues regarding this process have to be addressed. Firstly, which particles are arriving at the surface? The surface processes most probably depend on the amount of atomic and molecular radicals and molecules impinging on the surface. Secondly, the rate of surface processes can be enhanced if particles are excited as is the case of the dissociative adsorption of excited nitrogen molecules on a catalyst. Thirdly, the molecules formed are built from radicals which cover the surface, so the surface coverage has to be known. Fourthly, and probably the most important question is: Which molecules are formed if a surface is exposed to a variety of radicals and molecules? In connection herewith is the question, whether the formed molecules are electronically and/or ro-vibrationally excited and if the formation of molecules depends on the substrate material and temperature. Both issues are related again to the surface coverage and the abundance of the various adsorbing species. And finally, could the generation process of molecules be dependent on the fluxes of particles toward the surface.

1.2 The aim of this work

The subject of this thesis is the generation of molecules in plasma, in which plasma acts as catalyst to dissociate the precursor molecules already before they come in contact with a surface. As a result, the surface is mainly exposed to high fluxes of atomic and molecular *radicals*, i.e. $\approx 10^{20}$ radicals/s. The question investigated is: which molecules are formed and how? Especially, the role of plasma-surface interactions in the generation of molecules is studied.

The fluxes of reactive particles were created with the expanding thermal plasma (ETP) technique. The ETP technique is a remote technique in which reactive species are created in a high-pressure cascaded arc plasma source and the plasma processes take place downstream at lower pressure [24]. Due to this remote source approach, the dissociation and ionization in the plasma source are geometrically separated from the plasma chemistry in the vessel. In this way, the plasma production, plasma transport and plasma-surface interactions are separated, so the plasma conditions can be controlled independently from the downstream plasma chemistry. This allows inde-

pendent studies of the different aspects of the process in a relatively simple manner.

The generation of molecules by association of radicals at a surface was studied in plasmas containing mixtures of nitrogen and hydrogen, in which ammonia formation is observed. That plasma-surface interactions play a role in ammonia generation is generally accepted. To investigate whether also other molecules are mainly produced through plasma-surface interactions, a second system was studied. It concerns plasmas containing mixtures of nitrogen and oxygen in which NO is formed.

The experiments are performed in low-pressure recombining plasmas in conditions that several volume processes can be excluded. The importance of plasma-surface interactions is quantified by studying the generated molecules present in the gas phase. By varying the fluxes of atomic radicals to the surface, the role of the radicals in the production process of molecules is investigated. Furthermore, if the surface is exposed to high fluxes of radicals, the surface may become passivated under which conditions the dependence on the surface material may be minimized. The occurrence of surface processes are deduced from measurements in the gas phase, which also gives an indication of possible reaction mechanisms.

For the observation of generated molecules, advanced laser-based diagnostics are advantageous. Part of the thesis work was concerned with the introduction of new diagnostics to measure the densities of molecules and radicals in the plasmas. The laser based diagnostics range from single pass infrared spectroscopy to cavity ring-down spectroscopy. But also more standard techniques as mass spectrometry have been performed to obtain quantitative information on the molecules formed.

Although the study presented in this thesis is of fundamental nature, the generation of molecules in N_2–H_2 and N_2–O_2 plasmas is a subject of importance in various fields of research. For example, molecule generation in plasmas containing nitrogen and oxygen is of interest for understanding of the atmospheric and ionospheric physics [25], the re-entry studies of orbital space vehicles [26] and the air pollution cleaning by plasmas [27]. Furthermore, these two types of plasmas are also common in industrial environments, where they are used as sources of reactive particles, for the chemical synthesis of molecules, the deposition of materials like a–SiN_x:H for solar cell applications [28] or TiN diffusion barriers in the microelectronics industry by atomic layer deposition [29]. Plasmas containing nitrogen and oxygen are of relevance for example for sterilization processes in medicine [30] and the etching of materials [31]. More knowledge on the reaction mechanisms leading to generation of molecules in these plasmas can contribute to improvements of their usage in industry and could result in the development of new applications.

1.3 The outline of the thesis

To analyze the composition of plasmas, very sensitive diagnostics to monitor molecules and radicals are needed. In Chapter 2, a newly developed phase-shift cavity ring-down technique will be discussed. With this technique, not only densities can be determined, but also absolute absorption cross sections of transitions used to study molecules can be obtained. Furthermore, the effect of the amplified spontaneous emission on cavity ring-down measurements will be quantified.

For a complete understanding of plasmas of mixtures of nitrogen and hydrogen, the radicals involved in the plasma chemistry have to be characterized. However, information on absolute densities of the NH and NH_2 radicals in these plasmas is scarce. In Chapter 3, measurements on the NH_x radicals will be presented performed with a relative new technique, i.e. cavity ring-down spectroscopy. This technique made it possible to measure absolute NH_2 radical densities in N_2–H_2 plasmas. It will be shown that NH_2 radicals are formed by reactions between ammonia and H atoms. Subsequently, NH radicals can be formed by a reaction between NH_2 and H atoms. The NH radicals are also formed by reactions between N atoms and nitrogen ions and H_2 molecules in the supersonic expansion.

In Chapter 4, the efficiency and formation mechanism of ammonia generation in recombining plasmas generated from mixtures of N_2 and H_2 will be presented. It will be shown that efficient ammonia generation can be achieved, if the admitted nitrogen and hydrogen gas flows are appreciable dissociated.

In Chapter 5, the visual appearance of expanding nitrogen plasmas with or without oxygen is shown. The interaction of the plasma with a substrate leads to the appearance of additional light, which is ascribed to the formation of excited NO_2 molecules by association of N and/or O atoms at the substrate.

To further investigate this phenomenon, information on the molecules generated in these plasmas is essential. In Chapter 6, the steady state gas composition of plasmas produced from $Ar/N_2/O_2$ mixtures and Ar/NO mixtures measured with quantitative mass spectrometry will be discussed. It will be shown that these two types of plasmas have a strong resemblance in the gas composition, i.e. $\approx$ 5% NO and $\approx$ 95% N_2 and O_2 present in the plasma, although the starting conditions are completely different.

To quantify the relation between the gas composition and the surface processes, information on both has to be combined. In Chapter 7, measurements on the densities of molecules and the surface coverage of the reactor wall in expanding plasmas

containing mixtures of nitrogen and oxygen using time-resolved tunable diode laser absorption spectroscopy will be presented. It will be shown that under some conditions mainly NO and N are present at the surface and are stored in the metal wall. The molecule formation mechanisms leading to NO, N_2O and NO_2 molecules observed in these plasmas will be discussed.

Finally, in Chapter 8, the general conclusions of this thesis work are presented.

Bibliography

[1] K. Tamaru, in *in Catalytic Ammonia Synthesis*, edited by J.R. Jennings, page 1, Plenum, New York (1991).

[2] V. Smil, *Detonator of the population explosion*, Nature **400**, 415 (1999).

[3] B.E. Smith, *Nitrogenase reveals its inner secrets*, Science **297**, 1654 (2002).

[4] M.D. Fryzuk, *Ammonia transformed*, Nature **427**, 498 (2004).

[5] S.R. Tennison, in *in Catalytic Ammonia Synthesis*, edited by J.R. Jennings, page 303, Plenum, New York (1991).

[6] G. Ertl, in *in Catalytic Ammonia Synthesis*, edited by J.R. Jennings, page 109, Plenum, New York (1991).

[7] O. Nomura, H. Oyama, and Y. Sakamoto, *Ammonia synthesis at low pressures*, Sci. Paper IPCR **75**, 124 (1981).

[8] E.N. Eremin, A.N. Mal'tsev, and V.M. Belova, *Catalytic formation of ammonia in a barrier discharge*, Russ. J. Phys. Chem. **45**, 635 (1971).

[9] K.S. Yin and M. Venugopalan, *Plasma Chemical Synthesis. I. Effect of electrode material on the synthesis of ammonia*, Plasma Chem. Plasma Process. **3**, 343 (1983).

[10] P. Vankan, T. Rutten, S. Mazouffre, D.C. Schram, and R. Engeln, *Absolute density measurements of ammonia produced via plasma-activated catalysis*, Appl. Phys. Lett. **81**, 418 (2002).

[11] R. Engeln, S. Mazouffre, P. Vankan, D.C. Schram, and N. Sadeghi, *Flow dynamics and invasion by background gas of a supersonically expanding thermal plasma*, Plasma Sources Sci. Technol. **10**, 595 (2001).

[12] H. Kiyooka and O. Matsumoto, *Reaction scheme of ammonia synthesis in the ECR plasmas*, Plasma Chem. Plasma Process. **16**, 547 (1996).

[13] H. Uyama and O. Matsumoto, *Synthesis of ammonia in high-frequency discharges*, Plasma Chem. Plasma Process. **9**, 13 (1989).

[14] M.F.A.M. van Hest, A. de Graaf, M.C.M. van de Sanden, and D.C. Schram, *Use of in*

situ FTIR spectroscopy and mass spectrometry in an expanding hydrocarbon plasma, Plasma Sources Sci. Technol. **9**, 615 (2000).

[15] M.C.M. van de Sanden, R.J. Severens, R.F.G. Meulenbroeks, M.J. de Graaf, Z. Qing, D.K. Otorbaev, R. Engeln, J.W.A.M. Gielen, J.A.M. van der Mullen, and D.C. Schram, *The role of hydrogen during plasma beam deposition of amorphous thin films*, Surf. Coat. Technol. **74-75**, 1 (1995).

[16] W.M.M. Kessels, A. Leroux, M.G.H. Boogaarts, J.P.M. Hoefnagels, M.C.M. van de Sanden, and D.C. Schram, *Cavity ring down detection of SiH_3 in a remote SiH_4 plasma and comparison with model calculations and mass spectrometry*, J. Vac. Sci. Technol. A **19**, 467 (2001).

[17] P. Vankan, D.C. Schram, and R. Engeln, *High rotational excitation of molecular hydrogen in plasmas*, Chem. Phys. Lett. **400**, 196 (2004).

[18] P. Vankan, D.C. Schram, and R. Engeln, *Atomic and molecular hydrogen densities in a plasma expansion*, Plasma Sources Sci. Technol. **14**, 744 (2005).

[19] J. Amorim, J. Loureiro, and D. Schram, *Formation of H^- ions via vibrational excited molecules produced from recombinative wall desorption of H atoms in a low pressure H_2 positive column*, Chem. Phys. Lett. **346**, 443 (2001).

[20] L. Hornekær, A. Baurichter, V.V. Petrunin, D. Field, and A.C. Luntz, *Importance of surface morphology in interstellar H formation*, Science **302**, 1943 (2003).

[21] H.M. Cuppen and E. Herbst, *Monte Carlo simulations of H_2 formation on grains of varying surface roughness*, Mon. Not. R. Astron. Soc. 361 **361**, 565 (2005).

[22] D.A. Williams and E. Herbst, *It's a dusty Universe: surface science in space*, Surf. Sci. **500**, 823 (2002).

[23] S.M. Martin, J. Martin-Pintado, and R. Mauersberger, *Methanol detection in M82*, Astron. & Astrophys. **450**, L13 (2006).

[24] M.C.M. van de Sanden, R.J. Severens, W.M.M. Kessels, R.F.G. Meulenbroeks, and D. C. Schram, *Plasma chemistry aspects of a–Si:H deposition using an expanding thermal plasma*, J. Appl. Phys. **84**, 2426 (1998), **85**, 1243 (1999).

[25] E.C. Zipf and S.S. Prasad, *Production of nitrous oxide in the auroral D and E regions*, Nature **287**, 523 (1980).

[26] M. Capitelli (Ed), *Molecular Physics and Hypersonic Flows*, (NATO ASI Series C-482), Kluwer, Dordrecht (1996).

[27] B.M. Penetrante and S.E. Schultheis (Ed), *Non-Thermal Plasma Techniques for Pollution Control: Part A—Overview, Fundamentals and Supporting Technologies and Part B—Electron Beam and Electrical Discharge Processing*, Springer-Verlag, Berlin (1993).

[28] W.M.M. Kessels, F.J.H. van Assche, J. Hong, D.C. Schram, and M.C.M. van de Sanden, *Plasma diagnostic study of silicon nitride film growth in a remote Ar–H_2 – N_2–SiH_4 plasma: Role of N and SiH_n*, J. Vac. Sci. Technol. A **22**, 96 (2004).

[29] H. Kim, *Atomic layer deposition of metal and nitride thin films: Current research efforts and applications for semiconductor device processing*, J. Vac. Sci. Technol. B **21**, 2231 (2003).

[30] S. Moreau, M. Moisan, M. Tabbrizian, J. Barbeau, J. Pelletier, A. Ricard, and L'H. Yahia, *Using the flowing afterglow of a plasma to inactivate Bacilus subtilis spores: Influence of the operating conditions*, J. Appl. Phys. **88**, 1166 (2000).

[31] G.J.H. Brussaard, K.G.Y. Letourneur, M. Schaepkens, M.C.M. van de Sanden, and D.C. Schram, *Stripping of photoresist using a remote thermal Ar/O_2 and $Ar/N_2/O_2$ plasma*, J. Vac. Sci. Technol. B **21**, 61 (2003).

Chapter 2

Phase-shift cavity ring-down spectroscopy to determine absolute line intensities*

Abstract

Cavity ring-down detection techniques can sensitively determine frequency-dependent absorption cross sections of gasses. However, line-width problems and amplified spontaneous emission of the laser light source lower the technique's quantitative accuracy. Using phase-shift cavity ring-down spectroscopy (PSCRD), we measured absolute line intensities of the spin-forbidden transitions in the $b^1\Sigma_g^+(\nu' = 0) \leftarrow X^3\Sigma_g^-(\nu'' = 0)$ band of molecular oxygen. Our results were within 4% of values obtained from the HITRAN database, demonstrating the accuracy of PSCRD, when corrected for amplified spontaneous emission. Its high sensitivity (2×10^{-8} cm^{-1}), simplicity and high duty cycle make PSCRD a powerful diagnostic technique.

*J.H. van Helden, D.C. Schram and R. Engeln, Chem. Phys. Lett. **400**, 320 (2004)

2.1 Introduction

Absolute determinations of frequency-dependent absorption cross sections allow the physical and chemical community to accurately determine the density of absorbing species in absorption experiments. Cavity ring-down detection techniques offer several advantages over existing methods, and Berden et al. have summarized the schemes used up to the year 2000 [1]. One advantage is that the several-kilometer-long effective absorption path that can be realized in CRD considerably reduces sample volumes needed. This is especially useful when working with hazardous gases. Furthermore, CRD offers a powerful method to measure strong absorptions of species present in trace amounts and weak absorptions of abundant species.

CRD obtained absorption cross sections are, however, still not used in molecular spectroscopic databases such as HITRAN [2] because of doubts as to their accuracy. In pulsed CRD, the problems of producing quantitative accuracy were attributed to the so-called line-width problem [3, 4], and fitting non-exponential or multi-exponential transients [5]. Furthermore, Romanini et al. [6] have pointed out that amplified spontaneous emission (ASE) prevents CRD detection schemes from being quantitatively accurate. In this chapter, we show that accurate absolute line intensities can be obtained by phase-shift cavity ring-down (PSCRD) detection schemes and that they could be used in molecular spectroscopic databases without any hesitation. Specifically, we demonstrate that PSCRD spectroscopy in combination with an ASE correction model results in absolute line intensities of the spin-forbidden transitions in the $b^1\Sigma_g^+(\nu' = 0) \leftarrow X^3\Sigma_g^-(\nu'' = 0)$ band of molecular oxygen, the so-called "A-band," within 4% of the line intensities given by the HITRAN molecular spectroscopic database [2]. We also show that if the laser has a relatively large ASE component, a simple model can be used to correct the measurements for the phase shift introduced by this off-resonance emission.

In this chapter, we will first give a short overview of the history of CRD spectroscopy in Sec. 2.1.1. Next, in Sec. 2.2, the experimental details of the phase-shift cavity ring-down setup will be discussed followed by our experimental method to determine absolute line intensities. In the results and discussion section (Sec. 2.3), the measured absolute line intensities and the model to correct the measurements for the effects of ASE will be presented. In the last section the conclusions are presented.

2.1.1 A short history of CRD spectroscopy

Cavity ring-down spectroscopy (CRDS) and related techniques [1] are nowadays widely used for measuring electronic and vibrational transitions in gases, plasmas and solids. The different applications vary from the determination of absorption strengths of very weak transitions [6, 7], detection of molecules in molecular beams [8], the study of kinetic processes in plasma [9], trace gas detection in ambient air [3], exhaled human breath analysis [10], radical detection in flames [11], the study of surface processes [12] to the detection of defects in thin films [13]. Here, a short history of CRD detections schemes is given.

Anderson et al. [14] developed a technique to measure the reflectivity of laser mirrors. Subsequently, in 1988, O'Keefe and Deacon built on this idea and introduced a highly sensitive direct laser absorption technique to measure the absorption of a sample that is placed between two highly reflecting mirrors [15]. In their setup, a laser pulse is reflected many times within the optical cavity effectively increasing the path length through the sample. They showed that the decay rate of the light pulse confined between the two mirrors, rather than the magnitude of the absorption, is a sensitive measure of the absorption of the sample. Furthermore, the measurements are not sensitive to fluctuations of the light source. They called their technique cavity ring-down spectroscopy (CRDS). CRDS is non-intrusive, remote, and can easily be adapted to real time *in-situ* measurements of electronic and vibrational transitions in gases, plasmas and solids.

In pulsed CRDS, a pulsed laser light source leads to a relatively simple and straightforward set-up. Pulsed laser systems have the advantage of broad wavelength range but the system is rather bulky and very expensive and mostly the emitted power is too high for CRD experiments. Besides that, the duty cycle in a typical CRD experiment is low as the laser systems have a 10 – 100 Hz repetition rate which limits the data acquisition rate. In contrast to pulsed lasers, continuous wave (cw) lasers, especially diode lasers, are relatively cheap small plug-and-play lasers with powers in the preferable range (< 10 mW). Their only drawback is that only a limited wavelength range can be covered with one laser. Furthermore, the use of high-resolution cw lasers in CRDS makes it possible to reveal more detailed spectral features and accurate line profile measurements.

However, CRDS with cw lasers is experimentally more elaborate since the single mode behavior of cw lasers requires a resonance condition or so-called mode matching condition. To couple light into the high Q-factor optical cavity, the single mode

cw laser has to be mode-matched to one of the narrow modes of the optical cavity. To satisfy the resonance condition several cw-CRD schemes, i.e. CRD performed with a continuous laser, have been developed. Romanini et al. [16] introduced a scheme in which the cavity length is continuously modulated so that one of the cavity modes frequencies oscillates around the laser frequency. When the intensity build-up in the cavity exceeded a predefined threshold an acousto-optical modulator (AOM) with electric monitoring circuit is used to interrupt the laser beam and the intensity decay after the cavity is recorded as in a normal pulsed CRD experiment. In 1997, Romanini et al. [17] showed that diode lasers can be used in cw-CRD schemes using the same approach. Paldus et al. [18] introduced another scheme in which the cavity mode frequency is actively locked to the laser frequency and an optical switch is used to interrupt the laser light periodically to measure the intensity decay after the cavity as in a normal pulsed CRD experiment. A third approach was introduced by Hahn et al. [19] in which no optical switch was used. When the intensity build-up in the cavity exceeded a predefined threshold, the laser was fast detuned from an on-resonance to an off resonance condition after which the ring down transient was recorded. Although no AOM has to be used, a switching circuit is still required. With these techniques a high sensitivity was reached. Spence et al. [20] reported a sensitivity of 8.8×10^{-12} cm^{-1} Hz$^{-1/2}$ using a mode-locking approach.

Despite their high sensitivities, the complexity of the cw-CRD detection schemes [1] has prevented their widespread implementation. Furthermore, cw-CRD spectroscopy is in fact not a continuous technique at all as in almost all the cw-CRD detection schemes, the light coupling into the cavity is repetitively interrupted, requiring optical switching or fast digitizers to record ring-down transients.

In the last seven years, several less elaborate cw-CRD detection schemes have been introduced, by using the continuous character of cw lasers in combination with a so-called optically stable cavity to satisfy the resonance condition. These detection techniques are using a so-called optically stable cavity to satisfy the resonance condition [21]. Techniques based on this principle do not require any optical switching or control electronics to analyse ring down transients and thus allow continuous sampling of the cavity. An optically stable cavity has a quasi-continuum mode distribution due to the fact that the mirror separation d is set within the stability regime given by $0 < d < r$, $r < d < 2r$, with r the radius of curvature of the mirrors. As a result the narrow band cw laser beam will be coupled into the cavity via accidental coincidences of the frequency of one of the cavity modes with the laser frequency. The efficiency and the intensity of the light coupled into the cavity is determined by the overlap be-

tween the laser mode and the matching cavity mode, the jittering and finesse of the cavity.

In 1996, Engeln et al. [22] introduced the phase-shift cavity ring-down (PSCRD) technique, in which for the first time a continuous laser was used together with a high-finesse optically stable cavity. PSCRD, based on the ideas of Herbelin et al. [23], uses an intensity modulated cw laser beam. The modulated laser light undergoes a phase shift as it passes through a high-finesse optically stable cavity, and the absorption spectrum is extracted from the magnitude of the phase shift. An even simpler detection scheme with a high-finesse optically stable cavity was introduced in 1998, in the form of cavity enhanced absorption (CEA) [24]. In CEA, the light output of a continuous wave laser is sent directly onto the optical cavity and the absorption spectrum is extracted from a measurement of the time-integrated light intensity leaking out of the cavity as a function of laser wavelength. A similar approach was later adopted in integrated-cavity-output spectroscopy (ICOS) [25] and off-axis integrated-cavity-output spectroscopy (off-axis ICOS) [26]. Although the CEA-type techniques have a simple experimental setup, their sensitivity is in the same order as CRDS. The recorded spectrum however is a relative absorption spectrum expressed in loss of the empty cavity per round trip, i.e. $(1 - R)/d$. The spectrum can be put on an absolute scale by recording the CEA spectrum of a known amount of a certain gas or by obtaining the value of $(1 - R)/d$ using CRD of PSCRD spectroscopy.

Lewis et al. used PSCRD to measure integrated absorption cross sections of C-H ($\Delta\nu = 5$) and ($\Delta\nu = 6$) vibrational overtones of several hydrocarbons [27, 28]. They found good agreement between the integrated cross section of the C-H ($\Delta\nu = 5$) transition obtained from their PSCRD measurements and those obtained from FT-VIS measurements [27]. However, DeMille et al. [29] measured the C-H ($\Delta\nu = 6$) overtone absorptions with conventional pulsed CRD spectroscopy and found that the cross sections obtained by PSCRD were about 30% lower. In contrast, their values, obtained using pulsed CRD spectroscopy, compared favorably with values obtained using intra-cavity laser photo-acoustic spectroscopy. Although the reason for the discrepancy was not evident, they concluded that absolute absorption cross sections determined by PSCRD spectroscopy may not be accurate. This issue will be addressed in more detail in this chapter.

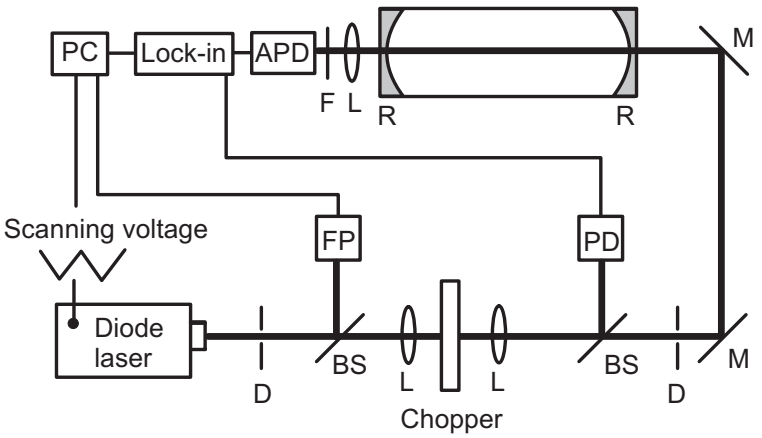

Figure 2.1: Schematic view of the phase-shift cavity ring-down spectrometer. D stands for diaphragm, BS for beam splitter, L for lens, F for filter, M for mirror, R for the high reflecting cavity ring-down mirrors, FP for Fabry-Perot, and (A)PD for (avalanche) photodiode detector.

2.2 Our experimental method

2.2.1 Experimental setup

Our light source was a narrow band cw diode laser (EOSI 2010 External Cavity Diode Laser) (Fig. 2.1). The laser had an effective line width of 1 MHz, was tunable in the 765 – 795 nm region, and had an output power of about 12 mW. Coarse scans were made by manually tuning the grating of the external cavity of the diode laser. While recording the absorption lines, the laser was scanned mode-hop free over about 2.8 cm^{-1} by step-wise adjusting the voltage applied to the piezo on which the grating was mounted. The laser light was focused and made parallel again by means of two lenses. A chopper was placed between the two lenses in such a way that it sinusoidally modulated the light intensity of the continuous laser beam (5 – 20 kHz). A sinusoidally modulated light beam is required in order to obtain the ring-down time from the phase shifts that are determined by the quality of the optical cavity as discussed in Section 2.2.2. The intensity modulated light beam was coupled into a high-finesse, 78.5 cm long, optically stable cavity formed by two highly reflective plano-concave mirrors. The mirrors were mounted on flexible bellows for accurate alignment, which were directly flanged onto a stainless steel vessel.

The mirrors (Newport SuperMirrors^{TM}) had a diameter of 1 inch, a radius of

curvature of $r = -1$ m and a maximum reflectivity of 0.99987 over the wavelength range: 761 – 876 nm. The mirror separation d was set within the stability regime given by the condition $0 < d < r$ and $r < d < 2r$ leading to an optically stable cavity [21]. As a result the narrow band cw laser beam coupled into the cavity on average 10% of the time. This coupling-time is dependent on the jittering and finesse of the cavity. To obtain a continuous sinusoidal signal exiting the cavity we introduced a modulation of several times the free spectral range (FSR) on the grating of the external cavity of the diode laser. This modulation ensured a predictable repetitive excitation of the cavity and also improved the signal to noise ratio significantly. In a typical experiment, the sinusoidally modulation on the piezo of the diode laser had a frequency of 1 kHz and an amplitude that corresponded to an optical frequency range of about 0.02 cm^{-1}, i.e. about 3 times the free spectral range of the cavity. Although this modulation introduced a broadening on the absorption spectra, it introduced no error in the determination of the line intensity. For determining the precise width of the absorption spectra, the amplitude of the modulation was lowered to about one FSR. Obviously, the way to record absorption spectra without this artificial broadening is to modulate the length of the CRD cavity over one or more FSRs. However, this was not possible with the present setup.

The light leaking out of the cavity was focused by a lens on an avalanche photodiode (Electron Tubes Inc. APD 50–2500) placed closely behind the cavity in order to ensure that all cavity modes were detected with equal probability. A broadband filter (750 – 850 nm) in front of the avalanche photodiode shielded the detection system from background light. The signal from the photodiode was analyzed by a lock-in amplifier (EG & G Model 7260 DSP). While recording an absorption line the transmission of a Fabry-Perot was recorded simultaneously for relative frequency calibration. We used a PCI card (National Instruments 6040E) with a PC together with a Labview program to control the scanning of the diode laser and to acquire the data generated by the lock-in amplifier and the Fabry-Perot signal.

For an absorption measurement the absolute value of the phase shift imposed by the empty cavity has to be known (see Section 2.2.2). This requires a so-called zero-phase-shift measurement to compensate for any phase shift introduced by the electronics. The zero-phase-shift was determined by directing the intensity modulated light beam around the cavity. With the lock-in amplifier the phase difference between the signal of the photo avalanche detector, which detects the light bypassing the cavity, and the photodiode in front of the cavity is set to zero (Fig. 1). The signal of the photodiode serves as the reference signal for the lock-in amplifier.

2.2.2 Determining absolute line intensities from phase shifts

When an optical cavity contains no absorbing medium, the photon lifetime $\tau_0(\nu)$, also called the ring-down time, of the empty cavity is solely caused by transmission and scattering losses at the mirrors, and is given by: $\tau_0(\nu) = d/(c|\ln R(\nu)|)$, where d is the length of the cavity, c the speed of light and $R(\nu)$ the reflectivity of the mirrors. When an absorbing medium with absorption coefficient $\kappa(\nu)$ is present in the cavity, the photon lifetime $\tau(\nu)$ of the optical cavity is given by (if $1 - R(\nu) << 1$):

$$\tau(\nu) = \frac{d/c}{1 - R(\nu) + \kappa(\nu)d} , \tag{2.1}$$

The absorption coefficient can be rewritten as $\kappa(\nu) = n_{v,J}\sigma(\nu)$, where $\sigma(\nu)$ is the frequency-dependent cross section and $n_{v,J}$ the number density in the lower level of the transition. The frequency-dependent absorption coefficient $\kappa(\nu)$ can easily be obtained from:

$$\kappa(\nu) = \frac{1}{c}\left(\frac{1}{\tau(\nu)} - \frac{1}{\tau_0(\nu)}\right). \tag{2.2}$$

Engeln et al. [22] have shown that the phase shift, $\phi(\nu)$, that is recorded during a PSCRD experiment, is related to the ring down time of the cavity, $\tau(\nu)$, as follows: $\tau(\nu) = \tan\phi(\nu)/\omega$, in which ω is the angular modulation frequency of the intensity. Eq. (2.2) can now be rewritten as:

$$\kappa(\nu) = \frac{\omega}{c}\left(\frac{1}{\tan\phi(\nu)} - \frac{1}{\tan\phi_0(\nu)}\right). \tag{2.3}$$

The line intensity $S(T)$ [cm^{-1}/(molecule cm^{-2})] as used in for instance the HITRAN database [2] was calculated using: $S(T) = \int \kappa(\nu)\mathrm{d}\nu/n$, with n the total density. It should be noted that the line intensity defined in this way is temperature dependent, via the Boltzmann relation between n and the density, $n_{v,J}$, of the level for which the absorption is measured.

2.3 Results and discussion

Fig. 2.2a illustrates a PSCRD measurement with a modulation amplitude of one FSR and its analysis. Here, the diode laser was scanned over the $^{\mathrm{P}}$P(29,29) transition of the $\mathrm{b}^1\Sigma_g^+(\nu' = 0) \leftarrow \mathrm{X}^3\Sigma_g^-(\nu'' = 0)$ band of molecular oxygen at 12999.96 cm^{-1} (open circle (◯)). The vessel was filled with 9.72 mbar of O_2 and the chopper frequency was set at 10 kHz, leading to an angular modulation frequency of the light intensity of $\omega = 2\pi \times 10$ kHz. The lock-in amplifier was set to an integration time of

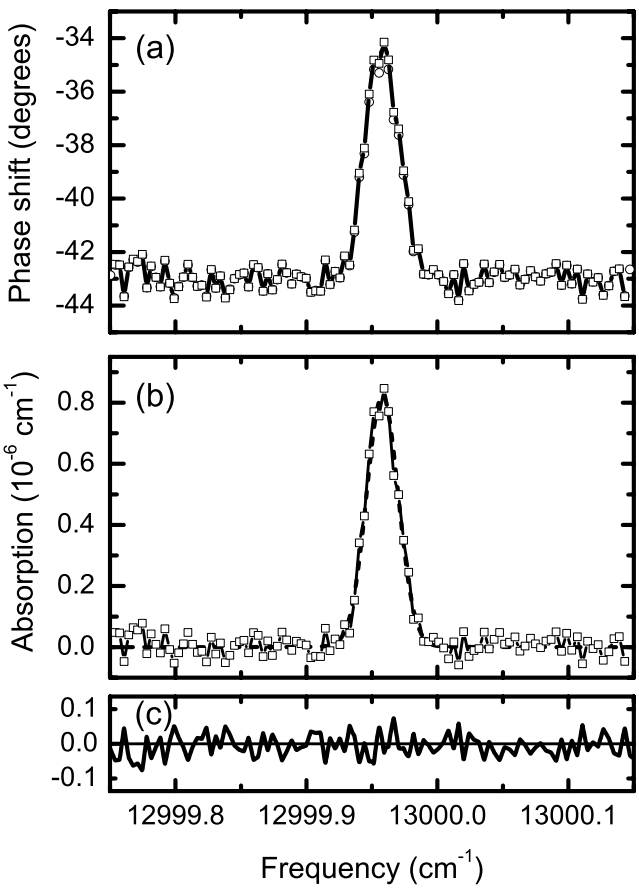

Figure 2.2: A PSCRD measurement of 9.72 mbar of O_2 for the $^{P}P(29,29)$ transition of the $b^1\Sigma_g^+(\nu' = 0) \leftarrow X^3\Sigma_g^-(\nu'' = 0)$ band of molecular oxygen. In (a) the measured phase (open circle (◯)) and the phase after the data analysis (open square (□)) is shown. In (b) the resulting absorption coefficient $\kappa(\nu)$ (solid line with open square (□)) together with a simulation based on the molecular parameters in the HITRAN database, assuming a temperature of 293 K and a pressure of 9.72 mbar, is shown (dashed line). The difference between the measured and calculated absorption profiles is give in (c).

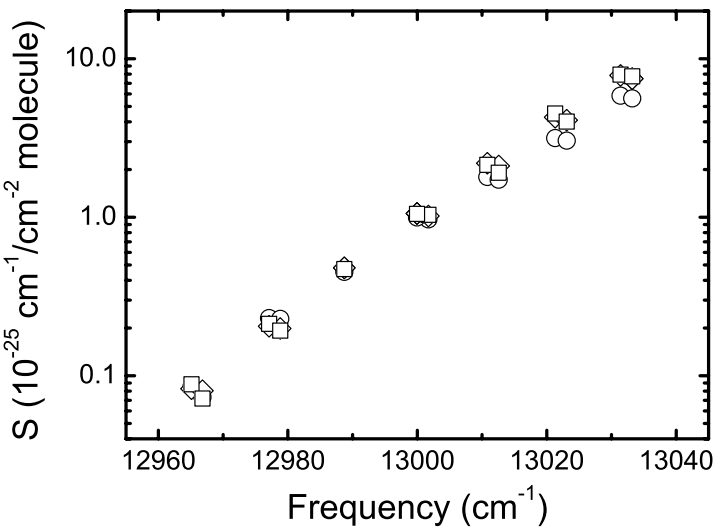

Figure 2.3: The measured absolute line intensities for all the recorded transitions in the region 12965.1 to 13033.2 cm^{-1} (open circle (◯)), the line intensities of the 2001 HITRAN database (open diamond(◇)) and the measured line intensities using the model to correct for the ASE (open square (□)).

500 milliseconds. From the baseline of the spectrum, i.e. ϕ_0, a ring-down time of 15 μs was determined.

Scans as shown in Fig. 2.2a were recorded for 13 absorption transitions in the oxygen A-band between 12965 and 13034 cm^{-1} with a modulation amplitude of three FSR. During these measurements we also recorded transitions in the $b(v' = 0) \leftarrow X(v'' = 0)$ band of $^{16}O^{18}O$ (natural abundance: 0.4%) and in the $b^1\Sigma_g^+(v' = 1) \leftarrow X^3\Sigma_g^-(v'' = 1)$ band of $^{16}O_2$. From these transitions the sensitivity of the setup was determined to be 2×10^{-8} cm^{-1} at an integration time of 500 milliseconds. From the measured values on the A-band and using Eq. (2.3) the line intensities were determined and plotted in Fig. 2.3 (open circle (◯)). Interference with the $^RQ(7,8)$ transition in the first hot-band of the A band prevented accurate determination of the absorption, and thus the line intensity, of the $^PQ(31,30)$ transition at 12990.46 cm^{-1}.

For comparison, we also plotted the line intensities given by the 2001 HITRAN database (open diamond(◇) in Fig. 2.3). The difference between our measured line intensities and the HITRAN values increases with increasing frequency. Amplified spontaneous emission (ASE) causes this. Although a diode laser is in principle a

single mode laser, it also emits ASE, and due to our broadband filter passing 750-850 nm and our mirrors with a reflectivity $R > 0.995$ over that wavelength range, the corresponding ASE also rang in the cavity and introduced a phase shift. When the single mode laser light is resonant with a molecular oxygen transition, the measured phase shift is thus the sum of the phase shift due to the oxygen resonance and the phase shift of the off-resonance ASE light.

We corrected for the ASE in the PSCRD absorption spectrum as follows. Let us assume that the intensity of the modulated beam with angular modulation frequency ω entering the cavity can be written as the sum of the intensity of the lasing beam with amplitude A_0 and the intensity of the ASE beam with amplitude B_0:

$$I(t) = A_0(1 + \sin(\omega t)) + B_0(1 + \sin(\omega t)). \tag{2.4}$$

The intensity $T(t)$ transmitted through the cavity is given by:

$$T(t) = (A - \Delta A)(1 + \sin(\omega t - \phi_0 + \Delta\phi_A)) + B(1 + \sin(\omega t - \phi_B)), \tag{2.5}$$

where A is the amplitude of the lasing beam, B the amplitude of the ASE beam, ΔA the amplitude change due to an absorption, ϕ_0 the phase shift due to the empty cavity, $\Delta\phi_A$ the phase change due to absorbing species in the cavity and ϕ_B the phase shift on the ASE due to all cavity losses. This can be rewritten as:

$$T(t) = \frac{(A + B) \times C}{\cos\Psi} \sin(\omega t - \phi_0 + \Psi) + A - \Delta A + B. \tag{2.6}$$

Herein is Ψ the measured phase shift on the modulation of the intensity of the light beam due to all cavity losses, which is given by:

$$\Psi = \arctan\left(\frac{A' \sin\Delta\phi_A + B' \sin(\phi_0 - \phi_B)}{A' \cos\Delta\phi_A + B' \cos(\phi_0 - \phi_B)}\right), \tag{2.7}$$

in which $A' = (A - \Delta A)/(A + B)$ and $B' = B/(A + B)$. C in Eq. (2.6) is the denominator of the term between brackets in Eq. (2.7).

The phase shift $\Delta\phi_A$ introduced by the molecular oxygen transition can be derived by solving Eq. (2.7) for each data point. The first step in this derivation is to determine the amplitude B and the phase ϕ_B of the ASE by measuring in conditions in which all narrow band laser light is absorbed. In that case, the measured amplitude and phase are only due to the ASE light; B and ϕ_B can then easily be determined. From this measurement also B' is determined. As an example, the PSCRD measurement of the amplitude and phase shift as measured at a pressure of 300 mbar O_2 for the $^{P}Q(23,22)$ transition at 13033.2 cm^{-1}, is presented in Fig. 2.4a.

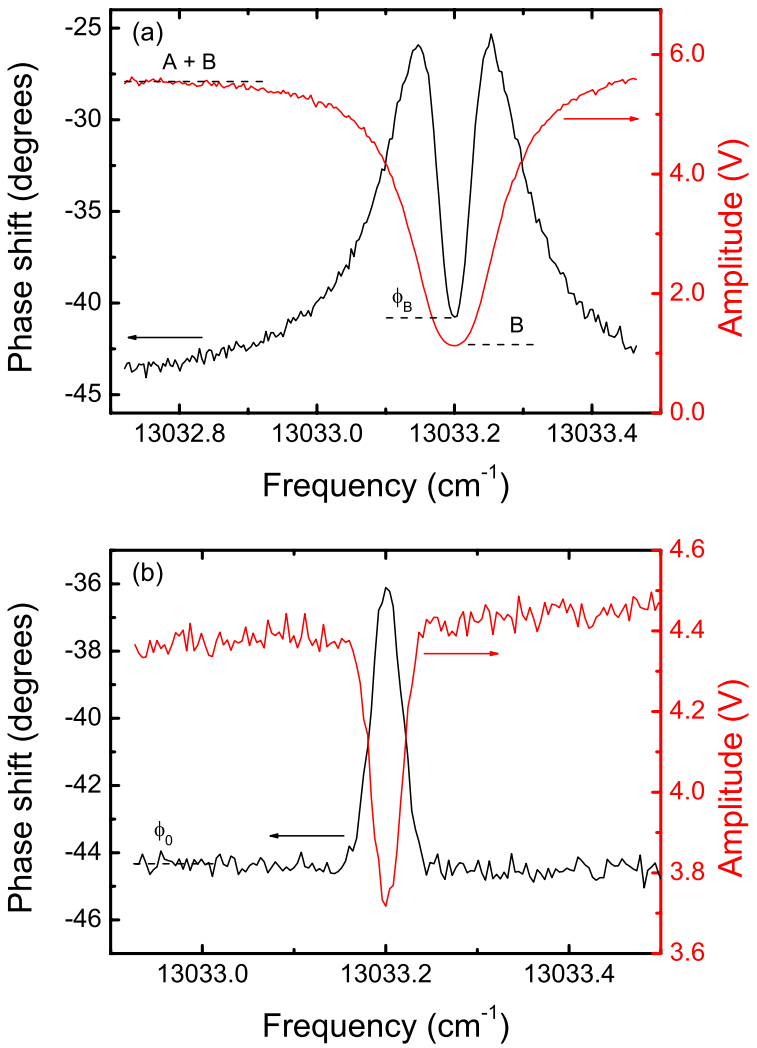

Figure 2.4: A PSCRD measurement of the amplitude and phase shift, i.e. Ψ of Eq. (2.7), recorded at a pressure of (a) 300 mbar and (b) 2 mbar of O_2 for the $^{P}Q(23,22)$ transition at 13033.2 cm^{-1}.

The phase shift decreases fast at the frequency where all narrow band laser light is absorbed and the recorded phase shift, ϕ_B, and amplitude, B, at that frequency are solely due to the ASE. In Fig. 2.4b, the phase shift and amplitude are presented for the same transition, but, recorded at a pressure of 2 mbar, i.e. it shows a measurement of the molecular oxygen transition in a condition without saturation. From this measurement the variables ΔA, i.e. the change in the amplitude spectrum due to an absorption, and ϕ_0 can be determined. With the value of B' from Fig. 2.4a and the value of the baseline of the amplitude from Fig. 2.4b, A' can be derived. With this information $\Delta\phi_A$ can now be determined (see Eq. (2.7)).

We note here that the amplitude can also be used to determine the line intensities and, again, the absorption has to be corrected for ASE (as in any absorption measurement) and also calibrated with the above described PSCRD technique.

Using the method described above, we determined the ASE amplitude and phase for all transitions between 13010.8 and 13033.2 cm^{-1}. The ASE contribution to the total amplitude, $B/(A+B)$, was about 20%. For transitions at frequencies lower than 13010.8 cm^{-1} the ASE amplitude and phase could not be determined, because the O_2 absorptions were not strong enough to absorb all narrow band laser light. Instead, the ASE around 12943 cm^{-1} has been determined using two strong argon transitions, i.e $1s_5 \rightarrow 2p_7$ and $1s_3 \rightarrow 2p_2$. For this measurement an argon plasma is created in the stainless steel vessel [30]. The ASE contribution to the total amplitude around 12943 cm^{-1} was about 4%. This means that the ASE contribution to the total amplitude, $B/(A+B)$, between 12965.1 and 13001.7 cm^{-1} was at least 4% and we used this value in the model for measurements below 13010.8 cm^{-1}.

An example of the result of the data analysis outlined above is shown in Fig. 2.2a for the measured phase (open circle (◯)) and, in Fig. 2.2b, the resulting absorption coefficient $\kappa(\nu)$ (solid line with open square (□)). In the same figure, a simulation based on the molecular parameters in the HITRAN database, assuming a temperature of 293 K and a pressure of 9.72 mbar, is shown (dashed line). The correspondence is remarkably good, as can be seen from the plot of the difference between the measured and calculated absorption profiles (Fig. 2.2c).

Using the model to correct for the ASE, the absolute line intensities for all the recorded transitions in the region 12965.1 to 13033.2 cm^{-1} were, on average, within 4% of values obtained from the HITRAN database (Fig. 2.3 (open square (□)). This 4% is within the estimated experimental measurement accuracy. Note that the line intensities measured during these PSCRD experiments differ over two orders in magnitude. Furthermore, several transitions were recorded at modulation frequen-

cies between 5 and 20 kHz and in the pressure range between 0.05 and 100 mbar. The line intensities deduced from these measurements, using the aforementioned data reduction procedure, were all within the reported accuracy. Only for a modulation frequency of 5 kHz, the line intensity could be determined less accurately. This is probably caused by the interference of the 5 kHz modulation frequency of the chopper and the 1 kHz modulation frequency on the grating of the external cavity of the diode laser.

2.4 Conclusion

The phase-shift cavity ring-down spectroscopy method described leads to accurately determined absolute line intensities. Specifically, the line intensities of transitions in the spin-forbidden $b^1\Sigma_g^+(\nu' = 0) \leftarrow X^3\Sigma_g^-(\nu'' = 0)$ band of molecular oxygen are within 4% of values obtained from the HITRAN molecular spectroscopic database, even over two orders of magnitude. Furthermore, we have shown that when the emission of the laser contains a relatively large ASE component, a simple model can be used to correct the measured signals for phase shifts introduced by the off-resonance ASE emission.

From our results, we conclude that with PSCRD spectroscopy, absorptions down to $2 \times 10^{-8}\mathrm{cm}^{-1}$ can be recorded in an integration time of 500 milliseconds. The high sensitivity together with its simplicity and high duty cycle makes PSCRD a very promising technique to accurately measure absolute line intensities.

2.5 Acknowledgement

The authors thank P. Hlavenka for his contribution during the early stage of the experiment and M.J.F. van de Sande, J.F.C. Jansen, A.B.M. Hüskens, and H.M.M. de Jong for their technical assistance. This work is part of the research program of the Foundation for Fundamental Research on Matter (FOM), which is financially supported by the Netherlands Organization for Scientific Research (NWO).

Bibliography

[1] G. Berden, R. Peeters, and G. Meijer, *Cavity ring-down spectroscopy: Experimental schemes and applications,* Int. Rev. Phys. Chem. **18**, 565 (2000).

[2] L.S. Rothman, A. Barbe, D. Chris Benner, L.R. Brown, C. Camy-Peyret, M.R. Carleer, K. Chance, C. Clerbaux, V. Dana, V.M. Devi, A. Fayt, J.-M. Flaud, R.R. Gamache, A. Goldman, D. Jacquemart, K.W. Jucks, W.J. Lafferty, J.-Y. Mandin, S.T. Massie, V. Nemtchinov, D.A. Newnham, A. Perrin, C.P. Rinsland, J. Schroeder, K.M. Smith, M.A.H. Smith, K. Tang, R.A. Toth, J. Vander Auwera, P. Varanasi, and K. Yoshino, *The HITRAN molecular spectroscopic database: edition of 2000 including updates through 2001*, J. Quant. Spectrosc. Radiat. Transfer **82**, 5 (2003).

[3] R.T. Jongma, M.H.G. Boogaarts, I. Holleman, and G. Meijer, *Trace gas detection with cavity ring down spectroscopy*, Rev. Sci. Instrum. **66**, 2821 (1995).

[4] P. Zalicki and R.N. Zare, *Cavity ring-down spectroscopy for quantitative absorption measurements*, J. Chem. Phys. **102**, 2708 (1995).

[5] W. Hogervorst W. Ubachs H. Naus, I.H.M. van Stokkum, *Quantitative analysis of decay transients applied to a multimode pulsed cavity ringdown experiment*, Appl. Opt. **40**, 4416 (2001).

[6] D. Romanini and K.K. Lehmann, *Ring-down cavity absorption spectroscopy of the very weak HCN overtone bands with six, seven and eight stretching quanta*, J. Chem. Phys. **99**, 6287 (1993).

[7] R.D. van Zee, J.T. Hodges, and J.P. Looney, *Pulsed, single-mode cavity ringdown spectroscopy*, Appl. Opt. **38**, 3951 (1999).

[8] M.G.H. Boogaarts and G. Meijer, *Measurement of the beam intensity in a laser desorption jet-cooling mass spectrometer*, J. Chem. Phys. **103**, 5269 (1995).

[9] J.P.M. Hoefnagels, A.A.E. Stevens, M.G.H. Boogaarts, W.M.M. Kessels, and M.C.M. van de Sanden, *Time-resolved cavity ring-down spectroscopic study of the gas phase and surface loss rates of Si and SiH_3 plasma radicals*, Chem. Phys. Lett. **360**, 189 (2002).

[10] H. Dahnke, D. Kleine, P. Hering, and M. Mürtz, *Real-time monitoring of ethane in human breath using mid-infrared cavity leak-out spectroscopy*, Appl. Phys. B **72**, 971 (2001).

[11] R.L. Stolk and J.J. ter Meulen, *Laser diagnostics of CH in a diamond depositing flame*, Diamond Relat. Mater. **8**, 1251 (1999).

[12] A.C.R. Pipino, *Ultrasensitive surface spectroscopy with a miniature optical resonator*, Phys. Rev. Lett. **83**, 3093 (1999).

[13] I.M.P. Aarts, B. Hoex, A.H.M. Smets, R. Engeln, W.M.M. Kessels, and M.C.M. van de Sanden, *Direct and highly sensitive measurement of defect-related absorption in amorphous silicon thin films by cavity ringdown spectroscopy*, Appl. Phys. Lett. **84**, 3079 (2004).

[14] D.Z. Anderson, J.C. Frisch, and Carl S. Masser, *Mirror reflectometer based on optical cavity decay time*, Appl. Opt. **23**, 1238 (1984).

[15] A. O'Keefe and D. Deacon, *Cavity ring-down optical spectrometer for absorption measurements using a pulsed laser source*, Rev. Sci. Instrum. **59**, 2544 (1988).

[16] D. Romanini, A.A. Kachanov, N. Sadeghi, and F. Stoeckel, *CW cavity ring down spectroscopy*, Chem. Phys. Lett. **264**, 316 (1997).

[17] D. Romanini, A.A. Kachanov, and F. Stoeckel, *Diode laser cavity ring down spectroscopy*, Chem. Phys. Lett. **270**, 538 (1997).

[18] B.A. Paldus, C.C. Harb, T.G. Spence, B. Wilke, J. Xie, and J.S. Harris, *Cavity-locked ring-down spectroscopy*, J. Appl. Phys. **83**, 3991 (1998).

[19] J.W. Hahn, Y.S. Yoo, J.Y. Lee, J.W. Kim, and H.-W. Lee, *Cavity ringdown spectroscopy with a continuous-wave laser: calculation of coupling efficiency and a new spectrometer design*, Appl. Opt. **38**, 1859 (1999).

[20] T.G. Spence, C.C. Harb, B.A. Paldus, R.N. Zare, B. Willeke, and R.L. Byer, *A laser-locked cavity ring-down spectrometer employing an analog detection scheme*, Rev. Sci. Instrum. **71**, 347 (2000).

[21] G. Meijer, M.G.H. Boogaarts, R.T. Jongma, D.H. Parker, and A.M. Wodtke, *Coherent cavity ring down spectroscopy*, Chem. Phys. Lett. **217**, 112 (1994).

[22] R. Engeln, G. von Helden, G. Berden, and G. Meijer, *Phase shift cavity ring down absorption spectroscopy*, Chem. Phys. Lett. **262**, 105 (1996).

[23] J.M. Herbelin, J.A. McKay, M.A. Kwok, R.H. Ueunten, D.S. Urevig, D.J. Spencer, and D.J. Benard, *Sensitive measurement of photon lifetime and true reflectances in an optical cavity by a phase-shift method*, Appl. Opt. **19**, 144 (1980).

[24] R. Engeln, G. Berden, R. Peeters, and G. Meijer, *Cavity enhanced absorption and cavity enhanced magnetic rotation spectroscopy*, Rev. Sci. Instrum. **69**, 3763 (1998).

[25] A. O'Keefe, *Integrated cavity output analysis of ultra-weak absorption*, Chem. Phys. Lett. **293**, 331 (1998).

[26] J.B. Paul, L. Lapson, and J.G. Anderson, *Ultrasensitive absorption spectroscopy with a high-finesse optical cavity and off-axis alignment*, Appl. Opt. **40**, 4904 (2001).

[27] E.K. Lewis, C.J. Moehnke, and C.E. Manzanares, *Phase shift cavity ring down and FT-VIS measurements of C–H ($\Delta\nu = 5$) vibrational overtone absorptions*, Chem. Phys. Lett. **394**, 25 (2004).

[28] E.K. Lewis, D. Reynolds, X. Li, G. de Villele, C. Leduc, D.L. Cede no, and C. Manzanares I, *Phase shift cavity ring-down measurement of C–H ($\Delta\nu = 6$) vibrational overtone absorptions*, Chem. Phys. Lett. **334**, 357 (2001).

[29] S. DeMille, R.H. deLaat, R.M. Tanner, R.L. Brooks, and N.P.C. Westwood, *Comparison of CRDS to ICL-PAS and phase-shift CRDS spectroscopies for the absolute intensities of $C-H$ ($\Delta\nu_{CH} = 6$) overtone absorptions*, Chem. Phys. Lett. **366**, 383 (2002).

[30] A.J.M. Buuron, D.K. Otorbaev, M.C.M. van de Sanden, and D.C. Schram, *Absorption spectroscopy on the argon first excited state in an expanding thermal arc plasma*, Phys. Rev. E **50**, 1383 (1994).

Chapter 3

The density of NH and NH_2 radicals in ammonia forming expanding plasmas

Abstract

We measured the densities of NH and NH_2 radicals by cavity ring-down spectroscopy in N_2–H_2 plasmas expanding from a remote thermal plasma source and in N_2 plasmas to which H_2 was added in the background. The NH_2 radical was observed via transitions in the $(0,9,0) \leftarrow (0,0,0)$ band of the $\tilde{A}^2A_1 \leftarrow \tilde{X}^2B_1$ electronic transition and the NH radical via transitions in the (0,0), (1,1) and (2,2) vibrational bands of the $A^3\Pi \leftarrow X^3\Sigma^-$ electronic transition. From the results, we conclude that the NH_2 radicals are formed by reactions of NH_3 molecules, produced at the walls of the plasma reactor, with H atoms emitted by the plasma source. The NH radicals are mainly produced via the reaction of N with H_2 with also a possible contribution of N^+ with H_2. The NH radicals can also be produced by H abstraction of NH_2 radicals. The flux densities of the NH_x radicals is appreciable in the first part of the expansion. Further downstream in the expansion they are further dissociated and the densities become smaller than those of the atomic radicals. It is concluded that NH_x radicals play an important, though indirect, role in the ammonia production at the surface.

3.1 Introduction

Plasmas containing nitrogen and hydrogen are extensively studied because of their widespread applications in research and industry for the (surface) treatment of materials. These plasma are e.g. used for the nitriding of materials [1], deposition of amorphous silicon nitride (a–SiN_x:H) films [2], plasma assisted atomic layer deposition of TiN thin films [3], etching of organic low *k* films [4], and the chemical synthesis of ammonia [5–8]. Despite their widespread application, only limited information is available on the role of the NH_x radical species in the plasma chemistry of N_2–H_2 plasmas.

It has been shown that ammonia can be formed efficiently in plasmas generated from mixtures of hydrogen and nitrogen, i.e. more than 10% of the total background pressure became ammonia [9]. The ammonia production in N_2–H_2 plasmas is well studied and the ammonia density has been predicted fairly well from a self-consistent model assuming that NH_3 is mainly produced at the surface of the vessel [1, 10, 11]. The formation of ammonia is generally ascribed to stepwise addition reactions between absorbed nitrogen and hydrogen containing radicals at the surface and incoming radicals and molecules [11, 12]. NH_3 is thus formed by subsequent hydrogenation of absorbed nitrogen atoms and the intermediates NH and NH_2 at the surface.

The NH and NH_2 radicals are included in models describing the plasma chemistry in N_2–H_2 plasmas. However information on absolute densities of NH_x radicals in these plasmas is scarce. The density of NH has been determined with laser-induced fluorescence (LIF) in flowing discharges and post discharges [13, 14]. The interaction of NH and NH_2 radicals with the surface of different materials has been addressed by Fisher and co-workers, using a molecular plasma beam in combination with laser-induced fluorescence for spatial imaging of the radicals [15–17]. Furthermore, mass spectrometry and emission measurements have been performed on NH_x species in the gas phase and with XPS on the surface [18, 19]. LIF measurements on NH_2 are hampered by the effective collisional quenching of the upper electronic state (fluorescence quenching rate of 9.3×10^6 s^{-1}) [20]. Moreover, absolute density measurements are difficult to perform, since the production of a known amount of NH_2 for calibration of LIF is not a simple task. Although NH_2 has been detected with intracavity laser absorption spectroscopy (ICLAS) [21, 22] and cavity ring-down spectroscopy [23, 24], the technique was to the best of our knowledge not yet used to measure NH_2 densities in N_2–H_2 plasmas. Furthermore, to determine the absolute densities of NH_x radicals spectroscopic information is needed to determine the den-

sity distribution over all possible states. We present here a detailed overview of the determination of absolute densities of NH and NH_2, as the information for NH and NH_2 is currently scattered over a number of papers and books.

To obtain more insight in the role of the NH_x species in N_2–H_2 plasmas, we measured the densities of NH_x ($x = 1,2$) radicals at three positions in the plasma using cavity ring-down spectroscopy. Two plasmas were studied in which ammonia generation has been observed [8, 9], both created with the expanding thermal plasma (ETP) technique. The first was an expanding N_2 plasma to which H_2 was added in the background and the second concerned expanding N_2–H_2 plasmas with both gases applied through the plasma source. In experiments with an expanding H_2 plasma to which N_2 was added in the background, no ammonia was observed and therefore that plasma will not be discussed here.

The ETP technique is a remote technique in which ions and radicals are created in a high-pressure cascaded arc plasma source and the plasma chemistry takes place downstream at lower pressure [25]. The plasma expands supersonically through a conically shaped nozzle into a low-pressure vessel (typically 20 Pa), and after a stationary shock, expands subsonically towards the other end of the process chamber. Due to the remote source approach, the dissociation and ionization in the plasma source are geometrically separated from the plasma chemistry in the vessel. In this way, the plasma production, plasma transport and plasma-surface interactions are separated, so the plasma conditions can be controlled independently from the downstream plasma chemistry, which allows independent studies of the different aspects of the process in a relatively simple manner.

In this work the plasma source is fed with nitrogen (with hydrogen added in the background) or with a mixture of nitrogen and hydrogen. From previous experiments, we know that for operation in nitrogen a substantial dissociation is obtained. The N/N_2 ratio at the plasma source exit is estimated to be 0.5, corresponding to a dissociation degree of 35% and a N-flow of 6 ssc/s [26]. Pure hydrogen source operation yields dissociation degrees in the order of 10%, thus 3 scc/s H flow at maximum [27]. We will assume that the H and N flows from a N_2–H_2 arc source to be similar to the pure N_2 or H_2 operation. We are now interested in the NH and NH_2 densities and their formation kinetics in these plasmas.

In this chapter, we will first describe the basics of the ETP technique (Sec. 3.2.1). Next, in Sec. 3.2.2, the experimental details of the cavity ring-down setup used to measure the NH and NH_2 radicals will be discussed. In the results section (Sec. 3.3), the measured spectra and obtained densities of the NH_x radicals will be presented

and discussed and finally the main reactions in the plasma leading to the observed NH_x radical density will be evaluated. In the last section the conclusions are presented.

3.2 Experimental details

3.2.1 Expanding thermal plasma setup

In order to obtain high fluxes of nitrogen and/or hydrogen radicals in the experiments, plasmas from mixtures of nitrogen and hydrogen were created with the expanding thermal plasma (ETP) technique. The technique has been described extensively in the literature (see e.g. [25, 28]). Here, only a short description of the main constituents of the setup is given. In the DC cascaded arc plasma source a sub-atmospheric (typically 0.4 bar) plasma is created with a power of around 5 kW. The cascaded arc source consists of a 4 diameter narrow channel of 5 water-cooled insulated copper plates with a total length of 30 mm. The cascaded plates are at the potential from the plasma. The last plate acts as the common anode for the discharge. A gas flow is admitted to the channel and a dc current is drawn from the three cathodes to the grounded anode plate producing the plasma. The high heavy particle temperature of approximately 1 eV leads to almost full dissociation of molecular gases when these are injected in the arc. The plasma is close to local thermal equilibrium ($T_{heavyparticles} \simeq T_e$) and characterized by a high electron density $n_e \approx 10^{22}$ m^{-3}, and a modest electron temperature $T_e \approx 1$ eV. The pressure gradient between source (>100 kPa) and process chamber (typically 20 Pa) causes a supersonic expansion and a stationary shock at approximately 3 cm (see Sec. 3.2.2), followed by a subsonic expansion towards the other end of the process chamber. As there is no power dissipation anymore in the process chamber, the plasma is recombining and the enthalpy is carried out in expansion by the ions or atomic radicals. In the expansion, the electron temperature T_e decreases to 0.1 – 0.3 eV and the electron density downstream is in the order of 10^{18} m^{-3}. The electron temperature is too low for electron induced dissociation or excitation processes to play a role [25].

Molecular gases can be injected into the background of the plasma vessel, i.e. into the re-circulation flow in the chamber. The injected molecules, together with molecules generated by the plasma itself, possibly in interaction with surface, form the basis of influx in the expanding plasma beam. It has been established that diffusion inwards occurs mainly in the subsonic region; it can also already occur in

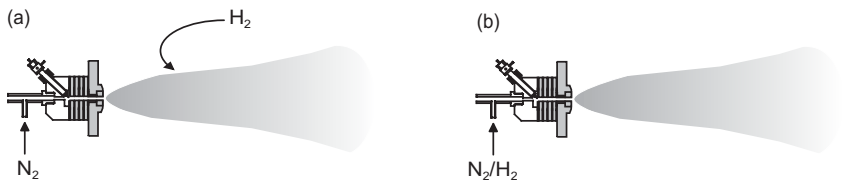

Figure 3.1: Schematic representation of the expanding plasma jet for both types of plasmas: (a) Expanding N_2 plasma to which H_2 was injected in the background; (b) Expanding N_2–H_2 plasma.

the supersonic region if the flow is rarefied at low pressure [27, 29]. As a result, the gas mixture in the re-circulating flow in the periphery of the chamber is mixed into the forward plasma emanating from the source. The molecules diffusing into the expanding plasma can undergo charge-transfer, and subsequently dissociative recombination reactions with the N^+ ions emanating from the source, leading to atomic and/or molecular radicals. Furthermore, the molecules diffusing into the beam may undergo abstraction reactions with atomic radicals leading to additional radicals. Direct generation of molecules in the volume by two or three particle reactions from atomic or molecular radicals can be excluded, since these reactions are too slow to lead to any significant production under our low-pressure conditions (mostly < 100 Pa). Note that the transit time from the plasma source to the other end of the plasma reactor, relevant for "forward" kinetics, is short (< 1 ms). However, the residence time, relevant for background kinetics, is relatively long (0.1 – 1 s), so there two particle reactions can take place.

We studied two different experimental situations: expanding N_2 plasmas with H_2 injected in the background and expanding N_2–H_2 plasmas as schematically depicted in Fig. 3.1. In both plasmas, the generation of ammonia in the downstream section is observed [8, 9]. The formation of ammonia molecules in the background by two particle nitrogen-hydrogen reactions involving atomic and molecular radicals can be excluded, since processes leading to ammonia at typical temperatures for the radicals in the background of 1000 K are too slow to lead to production. The formation of molecules at the surface is much more likely; the surface acts as the third body in this case. This means that most of the (atomic) radicals will arrive at the surface at which they will adsorb or reflect. If reflected, the density will increase until the consumption by adsorption is equal to the production of that radical. At the surface, new molecules can be generated which subsequently desorb. This process is called

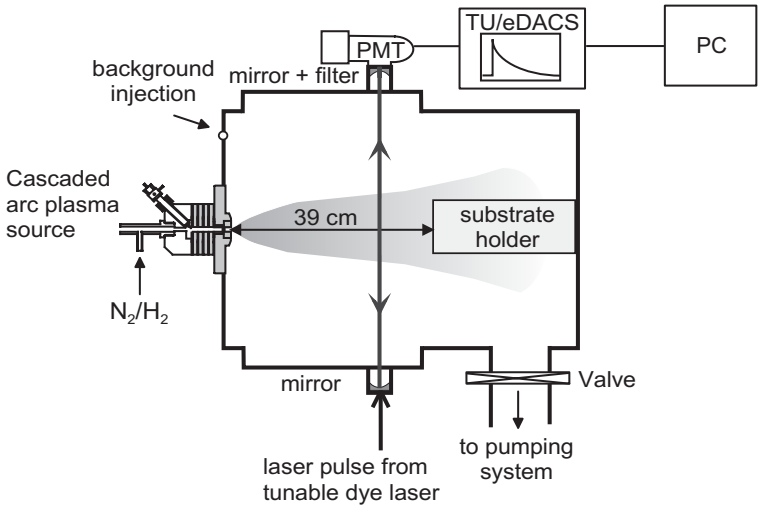

Figure 3.2: Schematic representation of the expanding thermal plasma (ETP) setup together with the cavity ring-down setup including a TU/eDACS data acquisition system.

plasma-activated catalysis, since a plasma is used as a catalyst to produce the radicals for the molecule production at the surface [8]. Note that the produced molecules may still undergo reactions in the re-circulating flow in the background of the plasma vessel, during the lifetime of (active) particles in the background.

The setup was equipped with a residual gas analyzer for mass spectrometry measurements, which was situated on top of the vessel at 56 cm from the source in the plasma beam. Absolute concentrations of the stable gas species N_2, H_2 and NH_3 were obtained by calibrating the mass spectrometer signals by injecting the relevant gases into the plasma chamber at various known pressures in the absence of a plasma.

3.2.2 Cavity ring-down spectroscopy

We measured the density of NH and NH_2 radicals in the downstream plasma using cavity ring-down spectroscopy (CRDS) at three positions on the axis ($z = 10, 21$ and 36 cm) from the plasma source (Fig. 3.2). CRDS is an absolute absorption technique based on the measurement of the decay rate of a light pulse confined in an optical cavity rather than the magnitude of the absorption [30]. The optical cavity is formed by two highly reflective plano-concave mirrors. The effective multi-passing of the laser pulse within the optical cavity makes CRDS a highly sensitive technique.

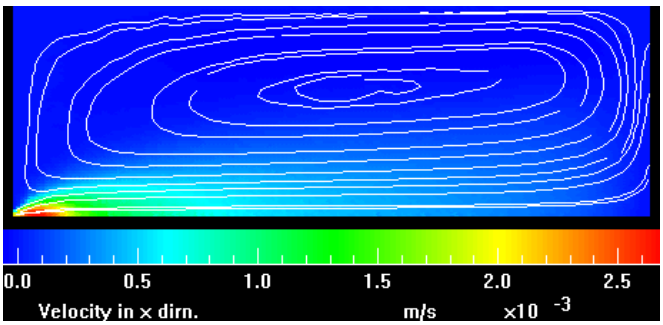

Figure 3.3: Illustration of the flow pattern of the plasma for an argon plasma (55 sccs Ar, $p = 22$ Pa). The picture shows the top part of a cross section through the vessel, which has a radius of 20 cm and a length of 50 cm.

Furthermore, the technique is insensitive to light intensity fluctuations of the light source and is therefore not affected by pulse-to-pulse fluctuations of the laser system. The exponential decay of the light leaking out of the cavity can be expressed by a ring-down time τ. When an optical cavity contains no absorbing medium, the decay is solely caused by transmission and scattering losses and is given by: $\tau_0(\nu) = d/(c|\ln R(\nu)|)$. Herein is d the length of the cavity, c the speed of light and $R(\nu)$ the reflectivity of the mirrors. When an absorbing medium is present in the cavity, the decay becomes faster and is expressed by means of a ring-down time $\tau(\nu)$ (if $1 - R(\nu) \ll 1$):

$$\tau(\nu) = \frac{d/c}{1 - R(\nu) + A(\nu)}. \tag{3.1}$$

The frequency dependent absorption per pass $A(\nu)$ can be rewritten as $A(\nu) = n_{v,J}\sigma(\nu)l$, where $\sigma(\nu)$ is the frequency-dependent cross-section, l the absorption path length and $n_{v,J}$ the number density in the lower level of the transition of the absorbing species. When the value of the absorption cross-section is known, the absorption per pass $A(\nu)$ can easily be obtained by measuring the ring-down time with and without absorbing plasma.

In order to determine absolute densities of the NH and NH_2 radicals, an assumption has to be made on the path length over which the radicals absorb and the spatial distribution. This value is based on data on the plasma expansion. The flow pattern consists of a supersonic expansion, a shock front and a subsonic beam of roughly constant diameter and flow lines ending in the pumps. At the periphery recirculation vortices are present, illustrated in Fig. 3.3 for an argon plasma. Particles from the source or forward radicals produced like NH and NH_2 diffuse out of the forward

plasma beam in the recirculation vortices and arrive finally at the vessel walls.

The cavity ring-down measurements were performed in the subsonic region of the expansion. Previously reported results on plasma expansions show that the plasma beam diameter at $z = 10$ cm is roughly twice the distance between the nozzle and the position of the stationary shock Z_M in the plasma [27]. The position of the stationary shock Z_M is given by [31]:

$$Z_M = 1.8 \cdot 10^{-2} \sqrt{\frac{\hat{\Phi}}{p_b}} \sqrt[4]{A\hat{T}_s}, \tag{3.2}$$

in which $\hat{\Phi}$ is the flow in sccs (1 sccs is equivalent to 2.5×10^{19} s^{-1}), p_b the background pressure in Pa, A the atomic mass number and $\hat{T}_s$ the source temperature at the axis in eV. In the case of an expanding N_2–H_2 plasma, Z_M is $\lesssim 3$ cm depending on the ratio of N_2 and H_2. In the case of a pure expanding N_2 plasma $Z_M \approx 4$ cm. This means that at the shock position the plasma beam diameter is around 7 cm. In our calculation of the density of the radicals, we used an absorption path length in the plasma of 10 cm at $z = 10$ cm. With increasing distance from the plasma source the absorption path length increases due to the diffusion of NH and NH_2 radicals out of the plasma beam. Diffusion out of the plasma beam has also previously been observed for N and H atoms in N_2 and H_2 plasmas. The diffusion is induced by the density gradient for these radicals between the plasma beam and the periphery caused by surface association [26, 32]. The absorption path length at $z = 21$ cm and $z = 36$ cm is estimated to be respectively 20 cm and 30 cm [33, 34]. In the calculations a homogeneous density distribution of the radicals over the absorption path length is assumed.

Reactions between radicals and ions in the plasma beam and nitrogen and hydrogen molecules diffusing into the plasma beam first occur at the outside of the plasma beam [35–37]. These profile effects would result in a smaller effective absorption path length and thus a higher radical density by as large as a factor of 2.

A tunable Sirah PrecisionScan-D dye laser pumped by the second harmonic output of a Nd:YAG laser (Spectra-Physics GCR-4) produced ≈ 8 ns laser pulses at a repetition rate of 10 Hz. To measure NH absorptions, the dye laser was operated on Pyridine 1 dye, to create laser light around 680 nm. The laser beam was subsequently frequency doubled using a KDP crystal resulting in laser pulses around 340 nm. To measure NH_2 absorptions, the dye laser was operated on Rhodamine B, resulting in laser light around 600 nm. To avoid optical saturation of the transitions of interest, an UV attenuator was placed in the laser beam in the first experimental

configuration and in the latter experiment the amplifier stage of the dye laser was not implemented. The intensity of the laser pulses was further reduced by a set of filters, leading to a typical pulse energy of $\sim$ 100 μJ in front of the cavity.

The laser pulses were coupled into a 112 cm long optical cavity formed by two highly reflective plano-concave mirrors. The mirrors were mounted on flexible bellows for accurate alignment, which were directly flanged onto the stainless steel vessel in which the plasma expanded. The mirrors (Laser-Optik) had a diameter of 1 inch, a radius of curvature of $r = -1$ m and a reflectivity of $R \sim 0.997$ at 340 nm for the NH detection and a reflectivity of $R \sim 0.999$ at 560 nm for the NH_2 detection. Immediately in front of the mirrors an argon flow was injected to protect the mirrors from reactive plasma species. The light leaking out of the cavity through the second mirror was detected by a photomultiplier tube (Hamamatsu R928) placed closely behind the cavity in order to ensure that all cavity modes were detected with equal probability. An interference bandpass filter in front of the photomultiplier shielded the detection system from the plasma light.

The CRD transient of every laser shot was individually processed by means of a state-of-the-art 100 MHz, 12 bits data acquisition system (TU/eDACS [38, 39]). All recorded CRDS transients were single exponential and were analyzed by a weighted least squares fit of the logarithmic of the transient, yielding the ring-down time of the light intensity in the cavity. To improve the signal-to-noise ratio, the averaged ring-down time of 20 laser shots was taken for all measurements. The baseline of the NH_2 spectra was affected by an oscillating behavior of the CRD signals, which is a known artefact for mirrors in the wavelength range around 600 nm [40]. This behavior hampered the baseline correction procedure and resulted in a slightly lower experimental accuracy compared to the NH measurements. We note that no optical saturation took place, since the integrated absorption as a function of the laser energy coupled into the cavity was measured to be constant for both NH and NH_2 radicals.

3.3 Results

3.3.1 Determining absolute densities of the NH_2 radical

The NH_2 radical was observed via transitions in the $(0,9,0) \leftarrow (0,0,0)$ band of $\tilde{A}^2A_1 \leftarrow \tilde{X}^2B_1$ electronic transition around 597.5 nm. The radical is a highly asymmetric top molecule with an H-N-H angle around 110° in the ground state, while it has a nearly linear configuration in the excited state. The electronic band spectrum

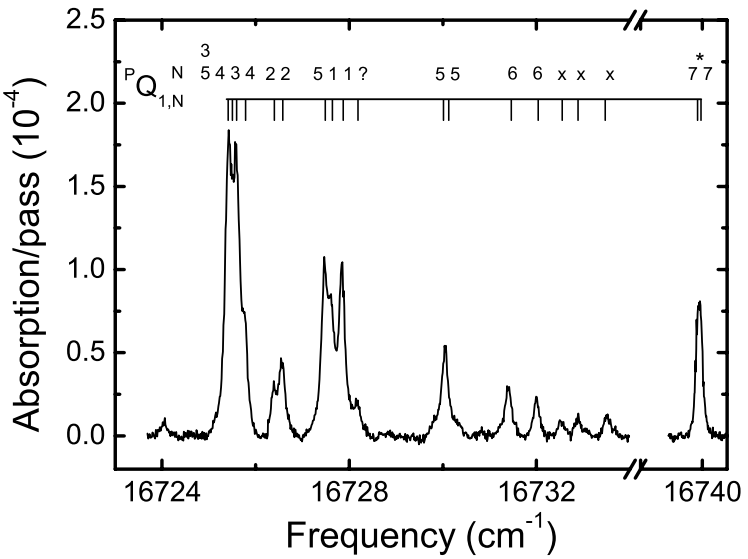

Figure 3.4: The NH_2 spectrum as measured with cavity ring-down spectroscopy at $z = 21$ cm. The plasma source was operated on a mixture of 5 sccs N_2 and 11.67 sccs H_2 at an arc current of 55 A. The background pressure was 20 Pa. The line positions reported in literature are indicated by ticks in the upper part of the graph and the rotational assignments for the ${}^PQ_{1,N}$ branch of the Σ vibronic sub-band are given [41]. The "isolated" spin doublet line ${}^PQ_{1,N}(7)$ line at 16739.90 cm^{-1} was used for the density measurements (marked by an asterisk). The lines marked by a cross are lines which are not part of the ${}^PQ_{1,N}$ branch, but are assigned in literature (see text) and the line marked with a question mark is not assigned.

($\tilde{A}^2A_1 \leftarrow \tilde{X}^2B_1$) of NH_2 in the visible (380 – 830 nm) consists mainly of transitions of a long progression of bands $(0, v_2, 0) \leftarrow (0, 0, 0)$ of the bending vibration of NH_2 [42]†. Fig 3.4 shows a typical spectrum containing lines of the ${}^PQ_{1,N}$ branch of the Σ vibronic sub-band as measured in a N_2–H_2 plasma at a position of $z = 21$ cm from the plasma source. The rotational branch is denoted as: ${}^{\Delta K_a}\Delta N_{K_a,K_c}$ [42], where K_a and K_c are the quantum numbers of rotation about the *a* and *c* axes. The line positions and rotational assignments are obtained from Ross et al. [41]. The transitions in this branch obey the *c*-type selection rules: $\Delta J = \Delta N = 0$, $\Delta K_a = -1$ and $\Delta K_c = 0$. Furthermore, each line with quantum number N, the total angular

† Notation for ν_2 used in this chapter is according to the linear molecule convention. The correlation between the linear and bent notation for vibrational numbering is:
$\nu_2(\text{linear}) = 2\nu_2(\text{bent}) + K_a + 1$

momentum apart from electronic spin, consist of two levels F_1 and F_2 due to spin-rotation splitting. The F_1 levels have $J = N+1/2$ and the F_2 levels have $J = N-1/2$. The lines marked by a cross are not part of the ${}^PQ_{1,N}$ branch of the Σ vibronic sub-band, but are assigned in literature as a line of the ${}^RR_{1,N}$ branch of the Δ vibronic sub-band (left cross) and lines of the ${}^PP_{1,N-1}$ branch of the Σ vibronic sub-band. The line marked with a question mark is not assigned in literature. The spin doublet line ${}^PQ_{1,N}(5)$ at a center frequency of 16730.07 cm^{-1} is associated with a multiple perturbation.

The density of NH_2 was determined by scanning the laser over the "isolated" spin doublet line ${}^PQ_{1,N}(7)$ at a center frequency of 16739.90 cm^{-1} (597.375 nm) (marked by an asterisk in Fig. 3.4). This line is the most studied NH_2 transition since it is an isolated line. It is therefore one of the few lines of the NH_2 absorption spectrum for which the oscillator strength has been reported [43, 44]. To determine the integrated absorption of the spin doublet line, and its line profile, the doublet splitting was set to a value of 3.44 GHz and the ratio of the area of the two components of the doublet line was set at 0.81, as determined by Kohse-Höinghaus et al. [43]. The density of NH_2 in the ${}^PQ_{1,N}(7)$ line was obtained using a value of the integrated absorption cross section of $\sigma_{int} = 7.4 \times 10^{-21}$ m^2 cm^{-1}, which was calculated from the oscillator strength reported in the literature by Votsmeier et al. [44] (See Appendix A). The density calculated in this way is insensitive to the laser line-width and the Doppler broadening effect.

The total NH_2 density was calculated by taking into account the density distribution over all possible states, which is determined by the kinetic, rotational and vibrational temperatures of the NH_2 radicals. The kinetic gas temperature of the radicals was obtained from the Doppler broadening by deconvoluting the experimental absorption lines into a Lorentzian laser profile and a Gaussian Doppler contribution. This procedure yielded a laser line-width of 0.064 ± 0.01 cm^{-1} at 16739.90 cm^{-1}, which is consistent with the manufacturer's specifications [45] and previous values determined for this laser system [38]. From the measured ${}^PQ_{1,N}(7)$ line and the spectra, an average kinetic NH_2 gas temperature of 1775 ± 200 K was determined for $z = 10$ and 21 cm from the plasma source, and 1350 ± 250 K for $z = 36$ cm. The measured temperatures point to the fact that these NH_2 radicals are only present in the plasma beam and not in the periphery, where the temperatures are much lower. The NH_2 kinetic gas temperature is in agreement with previous measured temperatures of NH_x radicals in expanding Ar–NH_3 plasmas [33], with measured temperatures of radicals in expanding plasmas of different gas mixtures [38] and with the temperature

of H atoms in e.g. Ar–H_2 plasmas as measured with TALIF [46]. These measurements all concerned radical species which are primarily present in the plasma beam and not (or much less) in the periphery. The rotational and vibrational temperatures of the NH_2 radicals could not be determined. It can be argued that since the NH_2 kinetic gas temperatures reflects the gas temperature in the plasma expansion, the NH_2 radicals in the plasma are already thermalized by elastic collisions with other particles. We therefore assume that the rotational and vibrational temperatures are equal to the kinetic gas temperature.

We thus calculated the total NH_2 density assuming a Boltzmann density distribution over the rotational and vibrational energy states with a rotational and vibrational temperature of 1775 K for $z = 10$ and 21 cm and 1350 K for $z = 36$ cm. The Boltzmann fraction f_b for NH_2 is reported in the literature by Green and Miller [47] and Kohse-Höinghaus et al. [43]:

$$f_b = \frac{3}{4}\frac{(2J''+1)}{g''Q_rQ_v}\exp[-\frac{E_{rot}}{kT_{rot}}]\exp[-\frac{E_{vib}}{kT_{vib}}]. \tag{3.3}$$

The factor 3/4 occurs due to the nuclear spin of the H atoms, J'' and g'' are the total rotational quantum number including spin and the electron-spin degeneracy of the lower state, Q_r and Q_v are the rotational and vibrational partition functions, and E_{rot} and E_{vib} are the rotational and vibrational energy of the lower state and T_{rot} and T_{vib} are the rotational and vibrational temperature, respectively. We note that g'' is equal to 1, since the integrated absorption of the measured line contained both components of the spin-doublet. The partition functions Q_r and Q_v are given by Green and Miller [47]. E_{vib} is given by Herzberg [48] and $E_{rot} = hcF(J)$, in which $F(J)$ is the experimentally determined rotational term value as reported by Ross et al. [41]. The total NH_2 density [m^{-3}] at $z = 10$ cm can then be calculated from the integrated absorption A_{int} [cm^{-1}] using an absorption path length $l = 0.1$ m and $T = 1775$ K:

$$n_{NH_2} = \frac{A_{int}}{\sigma_{int}l}\frac{1}{f_b} = 2.33 \times 10^{23}A_{int}. \tag{3.4}$$

The complete derivation of the total density of NH_2 is given in appendix A.

The oscillator strengths of the other transitions in the ${}^PQ_{1,N}$ branch are not known. In Table 3.1, the oscillator strengths of the measured transitions in the ${}^PQ_{1,N}$ branch are presented as determined from the spectrum depicted in Fig. 3.4 assuming a Boltzmann density distribution at 1775 K. We also determined the oscillator strengths for the same transitions from the data published in Fig. 4 of the paper of Rahinov et al. as published in Appl. Phys. B [24], in which NH_2 was measured

Table 3.1: Oscillator strengths for part of the transitions in the ${}^{P}Q_{1,N}$ branch of the Σ vibronic sub-band in the $(0,9,0) \leftarrow (0,0,0)$ band of the $\tilde{A}^2A_1 \leftarrow \tilde{X}^2B_1$ electronic transition of NH_2. The oscillator strengths were determined from the spectrum plotted in Fig. 3.4 and from data published in Fig. 4 of the paper of Rahinov et al. as published in Appl. Phys. B [24]. The rotational assignments are given as: ${}^{F'}N'_{K'_aK'_c} - {}^{F''}N''_{K''_aK''_c}$, where F indicates which of the two levels F_1 and F_2 due to spin-rotation splitting are involved in the transitions.

Rotational assignment	frequency (cm^{-1})	oscillator strength (this work)	oscillator strength [24]
${}^{1}1_{01} - {}^{1}1_{11}$	16727.872	3.52×10^{-4}	1.05×10^{-4}
${}^{2}1_{01} - {}^{2}1_{11}$	16727.638	4.76×10^{-4}	1.63×10^{-4}
${}^{1}2_{02} - {}^{1}2_{12}$	16726.579	1.02×10^{-4}	4.47×10^{-5}
${}^{2}2_{02} - {}^{2}2_{12}$	16726.398	8.20×10^{-5}	4.15×10^{-5}
${}^{1}3_{03} - {}^{1}3_{13}$	16725.594	2.93×10^{-4}	1.04×10^{-4}
${}^{1}4_{04} - {}^{1}4_{14}$	16725.784	9.27×10^{-5}	3.75×10^{-5}
${}^{2}5_{05} - {}^{2}5_{15}$	16727.488	1.52×10^{-4}	7.63×10^{-5}
${}^{1}6_{06} - {}^{1}6_{16}$	16731.463	4.18×10^{-5}	3.02×10^{-5}
${}^{2}6_{06} - {}^{2}6_{16}$	16732.038	3.34×10^{-5}	2.83×10^{-5}

under conditions in which a Boltzmann density distribution can be assumed. They measured a NH_2 spectrum produced by ammonia pyrolysis in a quartz cell at 890 K and at a pressure of 1.6 kPa. The obtained oscillator strengths using a Boltzmann distribution at 890 K are also presented in Table 3.1. Our oscillator strengths are higher, at lower N up to a factor 3.5. This could be caused by the fact that the lower J transitions are overlapping, which hampered the determination of the integrated absorption.

3.3.2 Determining absolute densities of the NH radical

The NH radical was observed via transitions in the (0,0), (1,1) and (2,2) vibrational bands of the $A^3\Pi \leftarrow X^3\Sigma^-$ electronic transition around 340 nm [49, 50]. The electronic band spectrum of NH at 336 nm consists mainly of transitions of the nine branches for which the selection rules $\Delta K = \Delta J = 0, \pm 1$ apply, since $A^3\Pi \leftarrow X^3\Sigma^-$ is a Hund's coupling case (b) to case (b) electronic transition. The other branches with $\Delta K \neq \Delta J$ are very weak, except at lower J where a transition from Hund's coupling case (b) to case (a) in the $A^3\Pi$ state occurs. Furthermore, for each value of K, the total angular momentum apart from electronic spin, there are three

levels denoted as F_1, F_2 and F_3 due to spin-orbit coupling. The quantum number for the total angular momentum J of the three levels are $J = K + 1$ for the F_1 levels, $J = K$ for the F_2 levels and $J = K - 1$ for the F_3 levels. The rotational branch is denoted as: $\Delta J_{F_i', F_i''}$, where F_i' and F_i'' indicate the upper and lower state F level [51].

In Fig. 3.5, the spectra are depicted as measured at the positions $z = 10, 20$ and 36 cm from the plasma source in N_2 plasmas with H_2 injected in the background of the vessel (Figures on the left) and in N_2–H_2 plasmas (Figures on the right). The measured spectra at $z = 10$ cm for both plasmas contain strong rotational lines in the (0,0), (1,1) and (2,2) vibrational bands of the $A^3\Pi \leftarrow X^3\Sigma^-$ electronic transition. The line positions are plotted as ticks in the upper part of the figures. The line positions and rotational assignment have been reported in literature by Brazier et al. [49] and were simulated using the ROTSPEC software package using the molecular parameters given by Brazier et al. At $z = 10$ cm, all strong lines reported in the literature, up to the rotational level $J = 18$ in the $v = 2$ state were observed in N_2 plasmas with H_2 injected in the background of the vessel. At the same position in a N_2–H_2 plasma, only rotational lines up to $J = 11$ were observed. At $z = 21$ cm and $z = 36$ cm, all the lines of the (2,2) band, except for two lines with low J, have completely disappeared in expanding N_2 plasmas with H_2 injected in the background of the vessel. In N_2–H_2 plasmas no lines of the (2,2) band were observed at these positions. The clear presence of transitions in the (1,1) and (2,2) bands indicates that the density distribution over the rotational and vibrational states are non-Boltzmann as will be discussed in more detail further on.

The density of NH was determined by scanning the laser over the "isolated" $P_{33}(9)$ line at a center frequency of 29444.28 cm^{-1} (339.62 nm) (marked by an asterisk in Figures 3.5(a) and 3.5(b)). The density of NH in the $P_{33}(9)$ line was obtained using a value of the integrated absorption cross section of $\sigma_{int} = 8.3 \times 10^{-21}$ m^2 cm^{-1}, which was calculated from the Einstein coefficient for spontaneous emission based on information reported in the literature by Lents [50] and Schadee [52] (See Appendix B). The density calculated in this way is insensitive to the laser linewidth and the Doppler broadening effect. The total NH density was calculated by taking into account the density distribution over all possible states, which is determined by the kinetic, rotational and vibrational temperatures of the NH radicals. The pronounced presence of the (1,1) and (2,2) bands indicates that the density distributions over the rotational and vibrational states are non-Boltzmann. The kinetic temperature of the NH radicals was again obtained from the Doppler broadening

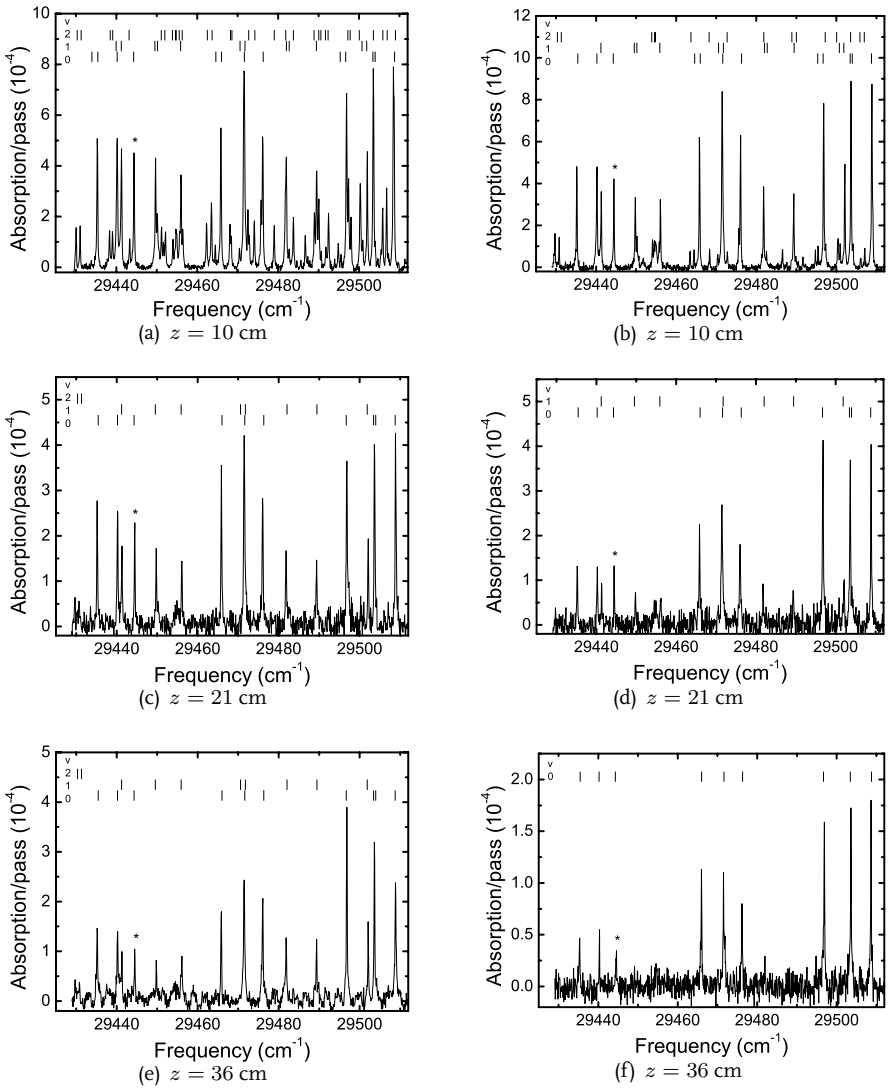

Figure 3.5: The NH spectra as measured with cavity ring-down spectroscopy at $z = 10, 21$ and 36 cm. The plasma source was operated on 16.67 sccs N_2 while 5.56 sccs H_2 was injected in the background (Figures on the left) and on a mixture of 5 sccs N_2 and 11.67 sccs H_2 applied through the arc (Figures on the right). The arc current was 55 A and the background pressure was 20 Pa. The line positions reported in literature by Brazier et al. [49] and from the ROTSPEC software package are indicated by ticks in the upper part of the graph for the vibrational bands (0,0) (1,1) and (2,2). The "isolated" $P_{33}(9)$ line at a center frequency of 29444.28 cm^{-1} was used for the density measurements (marked by an asterisk).

by deconvoluting the experimental absorption lines into a Lorentzian laser profile and a Gaussian Doppler contribution. This procedure yielded a laser line-width of 0.11 ± 0.01 cm^{-1} at 29444.28 cm^{-1}. The average kinetic NH gas temperature at the three positions from the plasma source proved to be the same as for the NH_2 radicals, so 1775 ± 200 K at $z = 10$ and 21 cm from the plasma source, and 1350 ± 250 K for $z = 36$ cm. As in the downstream plasma all particles are collisionally coupled, the temperatures of the various particles are expected to be the same.

To determine in how far the rotational density distribution could be characterized by a Boltzmann distribution, we extracted the rotational temperature of the NH radicals from a Boltzmann plot using the recorded spectra. The rotational density distribution at a temperature T_{rot} is given by:

$$n(J) \propto (2J+1)\exp(-E_{rot}(J)/kT_{rot}), \tag{3.5}$$

where $2J+1$ is the statistical weight of the rotational level in the lower state, k the Boltzmann constant and $E_{rot}(J)$ is the energy of the rotational level in the lower state. The density $n(J)$ is given by:

$$n(J) = A_{int}(J)/(\sigma_{int}(J)l), \tag{3.6}$$

where $A_{int}(J)$ is the integrated absorption of the measured transition, $\sigma_{int}(J)$ is the integrated absorption cross section of the measured transition and l the absorption path length of the radicals in the plasma.

The density in the various rotational levels $n(J)$ for the (0,0), (1,1) and (2,2) vibrational bands were determined using the integrated cross sections derived from the Einstein coefficients for spontaneous emission. These were derived from the information reported in the literature by Lents [50] for the (0,0) and (1,1) bands [50] and from an average of reported values in literature as summarized by Seong et al. for the (2,2) band [53]. The complete derivation is given in Appendix B.

A Boltzmann plot of the spectrum at $z = 10$ cm depicted in Fig. 3.5(a) is shown in Fig. 3.6, in which the statistically weighted densities $n(J)/(2J+1)$ observed in an expanding N_2 plasma with H_2 injected in the background of the vessel are plotted as function of the internal energy (rotational and vibrational). The low rotational levels in the three vibrational states were populated according to a Boltzmann distribution with $T_{rot} = 1775 \pm 80$ K. This value is equal to the kinetic temperature of the NH radicals. The density distribution in the low rotational levels indicates a thermalization of the radicals with the kinetic gas temperature by inelastic collisions with other particles. However, the high rotational levels, $J \geq 12$, in the $v = 2$ vibrational

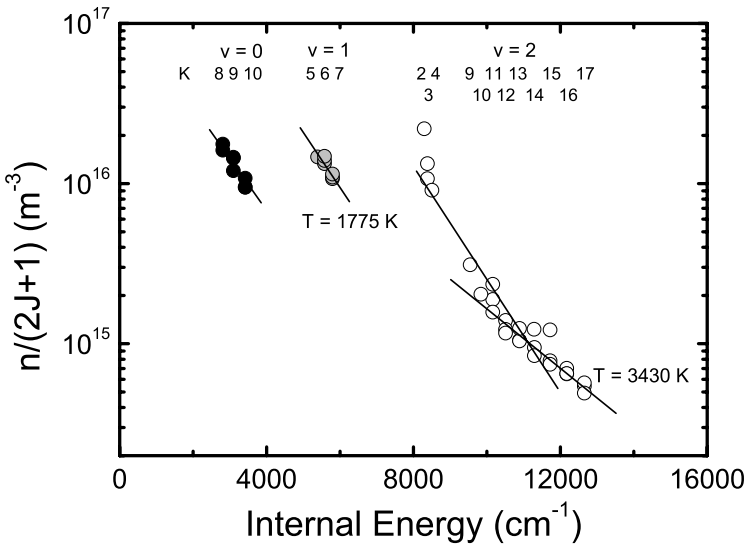

Figure 3.6: The statistically weighted densities $n(J)/(2J+1)$ of the observed rotational levels at $z = 10$ cm in a N_2 plasma with H_2 injected in the background of the vessel as a function of the total internal energy (rotation and vibration). The spectrum is shown in Fig. 3.5(a). The plasma source was operated on 16.67 sccs N_2 while 5.56 sccs H_2 was injected in the background at an arc current of 55 A and a background pressure of 20 Pa. For $v = 2$, the rotational levels with $K > 12$ have a rotational temperature above the kinetic gas temperature.

state were populated according to a temperature of 3430 ± 1300 K. This could also be true for the high rotational levels in other vibrational states, but transitions from these states were outside the measured spectral range. A similar density distribution over the rotational and vibrational states has been observed previously in $H_2^{(r,v)}$ molecules produced in expanding H_2 plasmas [54, 55]. In that case the production of $H_2^{(r,v)}$ molecules occurs at the surface by the exothermic association of an incoming H atom with an H atom at the surface. In the present case the excitation must be the result of the formation process, as [56]:

$$N^+ + H_2 \longrightarrow NH + H^+ \text{and } N + H_2 \longrightarrow NH + H. \tag{3.7}$$

The rotational levels of $v = 2$ are no longer occupied at $z = 20$ and 36 cm. The NH radicals in these states have experienced enough collisions in the drift time to relax to rotational levels in the lower vibrational states. From the Boltzmann plots at $z = 20$ and $z = 36$ cm (Fig. 3.7a), we concluded that the rotational temperature

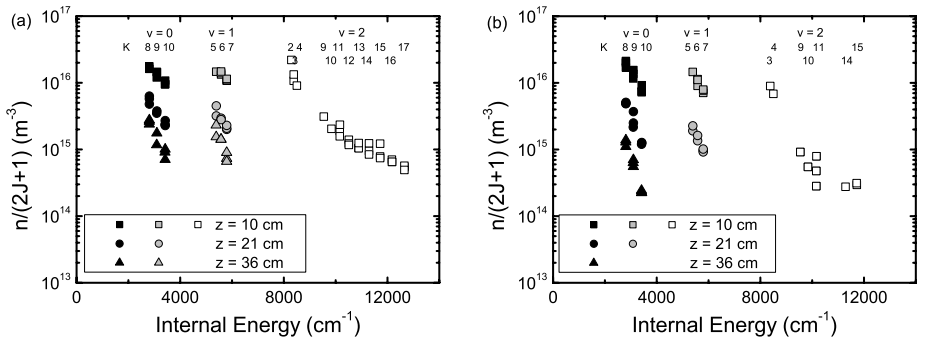

Figure 3.7: The statistically weighted densities $n(J)/(2J+1)$ of the observed rotational levels at $z = 10, 21$ and 36 cm in N_2 plasmas with H_2 injected in the background of the vessel (Figure on the left) and in expanding N_2–H_2 plasmas as a function of the total internal energy (rotation and vibration). The plasma source was operated on 16.67 sccs N_2 while 5.56 sccs H_2 was injected in the background and on a mixture of 5 sccs N_2 and 11.67 sccs H_2 applied through the arc at an arc current of 55 A. The background pressure was 20 Pa.

equals the kinetic gas temperature, i.e. respectively 1775 K and 1350 K. From Boltzmann plots of the recorded spectra in N_2–H_2 plasmas (Fig. 3.7b), we extracted that the rotational levels in all vibrational states at all three positions from the plasma source were populated according to a rotational temperature equal to the kinetic gas temperature at all three positions, even for the $v = 2$ band.

That the rotational density distribution could be characterized by a Boltzmann distribution, does not automatically imply that also the vibrational density distribution is a Boltzmann distribution. Since the energy spacing between the various vibrational levels is larger than the energy spacing between the rotational levels, the relaxation of the vibrational distribution to a Boltzmann distribution at the gas kinetic temperature takes more inelastic collisions and thus time. Therefore, first the total NH density in the vibrational states was calculated assuming a rotational Boltzmann distribution. The rotational Boltzmann fraction $f_{b,rot}$ for NH is taken from Herzberg [48]:

$$f_{b,rot} = \frac{(2J+1)}{Q_r} \exp[-\frac{E_{rot}(K)}{kT_{rot}}]. \tag{3.8}$$

J is the quantum number of the total angular momentum of the lower level and Q_r the rotational partition function. The partition functions Q_r can be approximated by the classical expression given by Herzberg [48]. The total NH density [m^{-3}] in the (0,0) band at $z = 10$ cm can then be calculated using the integrated absorption A_{int}

[cm^{-1}] and an absorption path length of the radicals in the plasma $l = 0.1$ m, and $T = 1775$ K:

$$n_{NH} = \frac{A_{int}}{\sigma_{int} l} \frac{1}{f_b} = 2.06 \times 10^{22} A_{int}. \quad (3.9)$$

The complete derivation of the total NH in a vibrational state is given in appendix B.

From the distribution of the NH density over the vibrational states, we concluded that at all three positions in N_2 plasmas with H_2 injected in the background of the vessel, the vibrational distribution is non-Boltzmann. Also in N_2–H_2 plasmas, the vibrational distribution is non-Boltzmann, except at $z = 36$ cm, were the total NH density distribution is in accordance with a Boltzmann distribution at 1350 K. We estimated in first order the total density by adding the densities in the various vibrational states we measured. The NH density distribution over the vibrational states was only measured in some plasma conditions. In order to calculate also the total NH density under all conditions investigated, we assume that at a certain position from the plasma source, the percentage of the total density present in the (0,0) band remains constant if the plasma conditions are changed. This percentage was determined from the measured spectra presented in Fig. 3.5.

3.3.3 Formation kinetics of NH and NH_2 radicals

We studied two different experimental situations: expanding N_2 plasmas with H_2 injected in the background and expanding N_2–H_2 plasmas in which both gases are fed through the plasma source. It has already been established that in both plasmas, ammonia can be formed [8, 9]. In experiments with an expanding H_2 plasma to which N_2 was added in the background, no ammonia was observed and therefore that plasma will not be discussed here. The highest efficiency of ammonia production is reached if both nitrogen and hydrogen are flowing through the cascaded arc. The ammonia density in the background in a N_2 plasma with H_2 injected in the background of the vessel is plotted as function of the hydrogen flow rate relative to the total flow rate in Fig. 3.8. Also the ammonia density as measured in the background of a N_2–H_2 plasma is plotted in Fig. 3.8. The formation mechanism of the NH_x radicals under these two experimental conditions has been studied and the results will be reported in the next two subsections.

N_2 plasma with H_2 injected in the background

In the first experimental situation (Fig. 3.1a), a nitrogen plasma was created with a flow of 16.67 sccs (standard cm^3 s^{-1}) N_2 flowing through the arc. The current

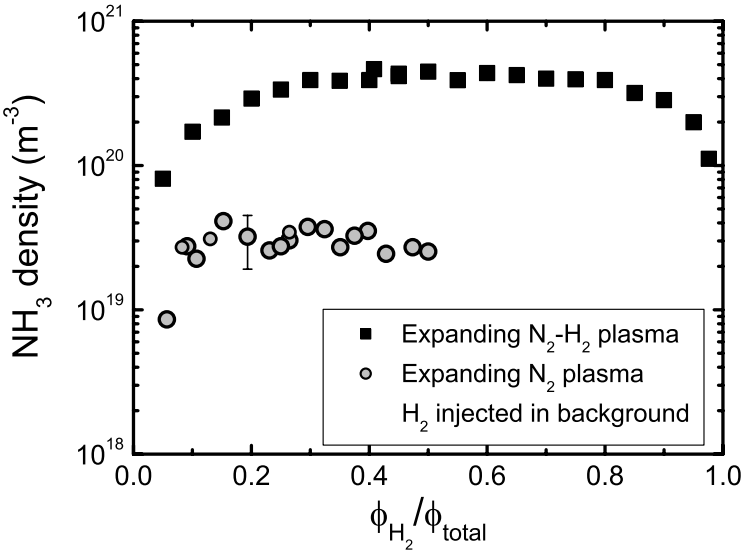

Figure 3.8: Ammonia density as measured in the background of the plasma reactor with mass spectrometry as function of the relative hydrogen flow rate for two different experimental situations. 1. Nitrogen is applied through the arc at a flow rate of 16.67 sccs, while hydrogen is injected into the background of the vessel. 2. Both nitrogen and hydrogen are applied through the arc at a total flow rate of 16.67 sccs. In both cases, the arc current was 55 A and the background pressure was kept constant at 20 Pa.

through the arc was set at 55 A and the downstream pressure was kept constant at 20 Pa by adjusting the gate valve to the pump. In a pure nitrogen plasma, the dissociation degree of N_2 in the arc is expected to be around 35%, and an ionization degree of around 1 – 5 % is attained [26, 57]. The densities of the meta-stable N atoms N(^{2}P) and N(^{2}D) emanating from the plasma source are expected to be at maximum 20% of the N(^{4}S) atoms (assuming a thermal population at a temperature of 1 eV). In the expansion, the N(^{2}P) and N(^{2}D) densities will decrease fast due to de-excitation by collisions with electrons, which is the most dominant in the first few cm of the plasma expansion ($k_e \approx 10^{-13}$ m^3 s^{-1}) [58]). Next, the meta-stable atoms are de-excited by collisions with N(^{4}S) atoms, and N_2 molecules (rate constant of 4.1×10^{-17} m^3 s^{-1} [26]). The same applies to the N(^{2}D) and N(^{2}P) atoms generated in dissociative recombination of N_2^+ ions. This source represents a maximum of a few percentage of the flow (equal to the initial N^+ flow). It is thus to be expected that the N(^{2}D) and N(^{2}P) densities are much smaller (< 1%) than the N(^{4}S) density.

Next, also the density of meta-stable molecules, N_2(A) needs to be considered. The density of N_2(A) at the source exit will already be small at the arc exit, i.e. $N_2(A)/N_2(X) \leq 10^{-2}$, and the density will also decrease fast by electron and N induced de-activation. Previously, meta-stable $N_2(A^3\Sigma_u^+)$ molecules have been observed in expanding pure nitrogen plasmas; they were assumed to be produced by surface association of N atoms. This observation was made in a low flow, low current nitrogen plasma with only a relative low N^+ ion density. These N^+ ions are a major loss channel for N_2(A) molecules by resonant charge-transfer. In the present plasma conditions a higher ion density than in those experiments was produced and the $N_2(A^3\Sigma_u^+)$ molecules are efficiently lost by charge-transfer reactions with N^+[59] or by collisions with N atoms [60]. Therefore, we concluded that the role of meta-stable atoms and molecules is small compared to that of N atoms. Thus the main chemistry is initiated by N(^{4}S) atoms and N^+ ions.

Hydrogen molecules were injected in the background of the vessel with a flow rate of 0 – 16.67 sccs. The hydrogen molecules can first be dissociated by N^+ ions emanating from the plasma source via the charge-transfer reaction followed by dissociative recombination, producing two H atoms and one N atom [56]:

$$N^+ + H_2 \longrightarrow NH^+ + H \tag{3.10}$$

$$NH^+ + e \longrightarrow N + H \tag{3.11}$$

with rate constants of 5.4×10^{-16} and 2×10^{-13} m^3 s^{-1}, respectively. Vankan et al. showed that the observed ammonia in plasma of mixtures of nitrogen and hydrogen can be explained using these reactions [8]. However, also the reaction between nitrogen ions and hydrogen molecules resulting in NH radicals should be considered:

$$N^+ + H_2 \longrightarrow NH + H^+. \tag{3.12}$$

To the best of our knowledge, no information is reported on this reaction in literature. As the reaction is resonant, we will assume that it has a rate constant of 5×10^{-16} m^3 s^{-1} similar as that of reaction 3.10.

The measured density of NH is plotted in Fig. 3.9 as a function of the hydrogen flow rate relative to the total flow rate of nitrogen and hydrogen at $z = 10, 21$ and 36 cm. We note that no NH_2 was detected in N_2 plasmas with H_2 injected in the background of the vessel. This means that the NH_2 density is below our detection limit of about 3×10^{16} m^{-3}. From the recorded spectra, shown in Sec. 3.3.2, the rotational and kinetic gas temperatures have been deduced. These temperatures are in agreement with previous measurements on radicals produced in the plasma beam

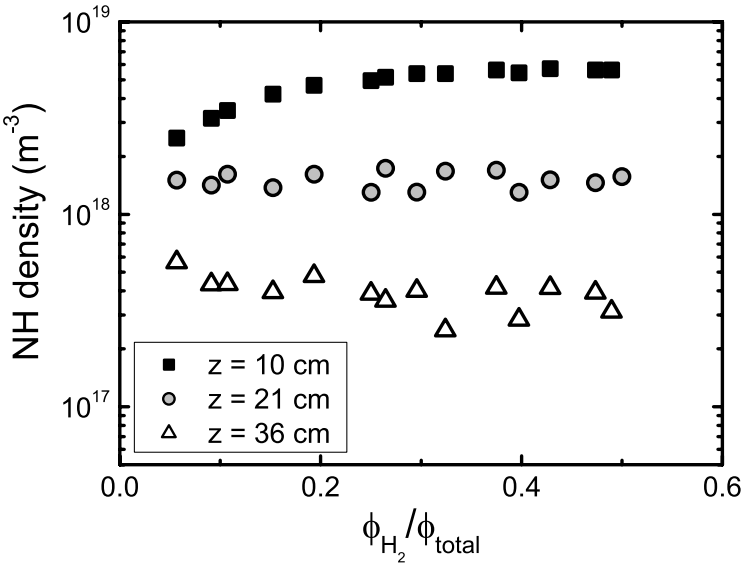

Figure 3.9: The NH density as a function of the hydrogen flow rate relative to the total flow rate of nitrogen and hydrogen measured by cavity ring-down spectroscopy. The plasma source was operated on 16.67 sccs N_2 at an arc current of 55 A, while a varying H_2 flow (0 – 16.67 sccs) was injected in the background. The background pressure was kept at 20 Pa.

[33, 38]. This indicates that also in these experiments the NH_x radicals are produced in the plasma expansion.

Now, the reaction mechanisms leading to the production of NH, while no NH_2 is produced will be evaluated. As a starting point, we first summarize the results of a previous study on the production of NH and NH_2 radicals in an Ar–NH_3 plasma expansion [33]. From that study, we concluded that in the presence of Ar^+ ions, the charge-transfer reaction:

$$Ar^+ + NH_3 \longrightarrow Ar + NH_3^+, \tag{3.13}$$

which has a reaction constant of 1.6×10^{-15} m^3 s^{-1} [61] with subsequently dissociative recombination of the molecular ion with electrons is the most important source of NH radicals:

$$\begin{aligned} NH_3^+ + e &\longrightarrow NH_2 + H, \\ &\longrightarrow NH + pH_2 + (2-2p)H \quad (p = 0, 1), \\ &\longrightarrow N + qH_2 + (2-2q)H \quad (q = 0, 1). \end{aligned} \tag{3.14}$$

Furthermore, we had then to assume that the branching ratio of the dissociative recombination reaction of NH_3^+ (reaction (3.14)), not known in literature, is mainly to NH (80%) and NH_2 (20%), and negligible to N. We also concluded that the values of p and q in reaction (3.14) can be set to zero. The dissociative recombination reaction typically has a rate constant of $1 \times 10^{-13}/\sqrt{\hat{T}_e}$ m^3 s^{-1} [62], which gives a rate of 2×10^{-13} m^3 s^{-1} for an electron temperature around $\hat{T}_e = 0.3$ eV. It was also shown that the following reactions play a significant role in the production of NH_2 radicals:

$$NH_3^+ + NH_3 \longrightarrow NH_4^+ + NH_2, \tag{3.15}$$

which has a reaction rate of 1.7×10^{-15} m^3 s^{-1} [63] and

$$NH_3 + H \longrightarrow NH_2 + H_2. \tag{3.16}$$

The latter has a rather low rate constant of 4×10^{-18} m^3 s^{-1} at a temperature of 1750 K due to an activation energy of 4991 K [64]. However, it was shown that the reaction rate is increased by a factor 7.5 due to the presence of energetic H atoms in the plasma, i.e the rate constant is 2.5×10^{-17} m^3 s^{-1}.

Above, we discussed the generation of NH_x from NH_3 in NH_3 fed plasmas. However, it should be noted that also in these plasmas new molecules are generated. In fact, if dissociated, the radicals primarily lead to the formation of N_2 and H_2 and in less extend to NH_3 ($\sim$ 10%). In the present experiments, N_2 and H_2 (downstream or in arc source) are injected. NH_3 is expected to be formed to an amount of $\leq$ 10%. Hence, also kinetics with H_2 and N and H radicals need to be considered.

Following this line of thought for the production of NH and NH_2 radicals in an Ar–NH_3 plasma expansion, the most likely reactions are then charge-transfer reactions between N^+ and NH_3 or H_2 as charge-transfer reactions involving ammonia, was also the dominant reaction mechanism in Ar–NH_3 plasmas. We note that under optimal conditions a significant amount of background gas in our vessel is ammonia (Fig. 3.8), which can diffuse into the plasma beam. The NH_x radicals are produced by first a charge-transfer reaction between ammonia and N^+ from the plasma source leading to mainly NH_3^+ (see Table 3.2):

$$N^+ + NH_3 \longrightarrow N + NH_3^+, \tag{3.17}$$

with a reaction rate of 2×10^{-15} m^3 s^{-1}. Subsequently, the molecular ions recombine dissociatively with electrons, reaction (3.14), leading to mainly NH radicals. There are however, several issues which indicate that this reaction is most probably not the dominant mechanism for NH production. The measured NH density is higher than

expected from these reactions and we should also have observed NH_2. Furthermore, the maximum in NH density is observed at $z = 10$ cm, which indicates that NH_3 the has to diffuse already into the plasma beam in the supersonic expansion, which is much more difficult for ammonia than for H_2 due to its higher mass.

We therefore suggest a second reaction which could explain the observed NH density and also the fact that no NH_2 was detected. This is the reaction between nitrogen ions and hydrogen molecules resulting in NH radicals:

$$N^+ + H_2 \longrightarrow NH + H^+, \tag{3.18}$$

for which we assume a similar reaction rate as in (3.10) of 5.4×10^{-16} m^3 s^{-1}. That more H_2 than NH_3 is observed in this plasma, and that H_2 can diffuse into the plasma beam already in the supersonic expansion supports this reaction mechanism.

However, the N^+ density is at maximum about 10^{18} m^{-3} (with no H_2 present), whereas the density of atomic nitrogen in the plasma expansion is about 1×10^{20} m^{-3} [26]. It is observed that NH is only produce before $z = 10$ cm. There are not enough ions in the plasma to produce a NH density of 6×10^{18} m^{-3} by charge-transfer reactions. The only explanation is that the reaction between atomic N and H_2 resulting in NH is more important than expected in the first 10 cm:

$$N + H_2 \longrightarrow NH + H \qquad k = 3.9 \times 10^{-16} \exp(\frac{-15775}{T})\ \mathrm{m^{-3}\,s^{-1}}. \tag{3.19}$$

which has a rate constant of 5.3×10^{-20} m^3 s^{-1} at 1775 K, due to its high activation energy of 15775 K [56]. The rate of this reaction will be higher in the supersonic expansion region and first part of subsonic expansion, where H_2 molecules can diffuse into the plasma expansion. There N atoms with kinetic energies in excess of 0.5 – 1 eV are expected [26]. Namely, thermal energies of a few thousand K are possible in the first few cm after the shock. Also substantial rotational-vibrational excitation of $H_2^{(r,v)}$ molecules has been observed [54, 55]. We therefore assume that in total approximately 1 eV of energy is available to the particles involved in the reaction, which would give a rate constant of 1×10^{-16} m^3 s^{-1}.

It is observed that the NH density has a maximum at $z = 10$ cm and decreases further downstream. This is due to the loss of NH radicals due to diffusion out of the plasma beam. The NH radicals can also be destroyed by abstraction reactions with N and H atoms or by reactions between two NH radicals resulting in N_2 and H_2 molecules and N and H atoms (R8)–(R11) (see Table 3.2).

From a comparison of the rate coefficients of neutral-neutral reactions and charge-transfer reactions and of the expected abundance of species in the plasma expansion,

Table 3.2: Reactions and rate constants.

No.			Reaction	rate constant ($m^3\ s^{-1}$)	Ref.
R1	$N^+ + NH_3$	$\longrightarrow$	$N + NH_3{}^+$	2×10^{-15}	[56]
		$\longrightarrow$	$HN_2^+ + H_2$	2.2×10^{-16}	
		$\longrightarrow$	$H_2N^+ + NH$	2.2×10^{-16}	
R2	$N^+ + H_2$	$\longrightarrow$	$NH^+ + H$	5.4×10^{-16}	[56]
		$\longrightarrow$	$NH + H^+$	$\approx 5 \times 10^{-16}$ [a]	
R3	$NH_3^+ + e$	$\longrightarrow$	$NH_2 + H$	3.6×10^{-14} [b]	
		$\longrightarrow$	$NH + 2H$	1.4×10^{-13}	
R4	$NH^+ + e$	$\longrightarrow$	$N + H$	2×10^{-13} [b]	
R5	$HN_2^+ + e$	$\longrightarrow$	$NH + N$	2.6×10^{-14}	[65]
		$\longrightarrow$	$H + N_2$	1.4×10^{-14}	
R6	$H_2N^+ + e$	$\longrightarrow$	$H_2 + N$	2×10^{-13} [b]	
R7	$N + H_2$	$\longrightarrow$	$NH + H$	$3.8 \times 10^{-16} \exp(-15775/T)$	[56]
R8	$NH + H$	$\longrightarrow$	$N + H_2$	$8.3 \times 10^{-17} \exp(-1000/T)$	[56]
R9	$NH + N$	$\longrightarrow$	$N_2 + H$	$1.8 \times 10^{-17} T^{0.5}$	[56]
R10	$NH + NH$	$\longrightarrow$	$N_2 + 2H$	8.5×10^{-17}	[10]
R11	$NH + NH$	$\longrightarrow$	$N + NH_2$	$1.7 \times 10^{-18} (T/300)^{1.5}$	[10]
R12	$NH_2 + H$	$\longrightarrow$	$NH + H_2$	3.2×10^{-17}	[56]
R13	$N + NH_2$	$\longrightarrow$	$N_2 + 2H$	1.2×10^{-16}	[10]
R14	$NH + NH_2$	$\longrightarrow$	$NH_3 + N$	1.7×10^{-17}	[10]
R15	$NH_3 + H$	$\longrightarrow$	$NH_2 + H_2$	$9.0 \times 10^{-25} T^{2.4} \exp(-4991/T)$	[64]

[a] Estimated rate constant for charge-transfer reactions as no information is available in literature.
[b] Estimated rate constant for dissociative recombination reactions.

we conclude that hydrogen transfer reactions are dominant in the production of NH radicals. The results can be explained if we assume that a reaction between N and H_2 takes place in which NH is formed. The charge-transfer reactions between N^+ and H_2 (or NH_3) can not be excluded, but the expected abundance of N^+ compared to the N atom abundance suggests that the latter are mainly responsible for the NH formation. That no NH_2 is observed supports the suggested reaction mechanism for NH production. The flux density of the NH radicals in the plasma beam at $z = 10$ cm, assuming a velocity of 1000 m/s, is about $6 \times 10^{21}\ m^{-2}\ s^{-1}$. This gives a flow of NH radicals of about 5×10^{19} radicals/s, which is thus a flow of 2 sccs. It was previously determined that the N flux in pure nitrogen plasma is about 6 ssc/s. This means that a significant part of the radical flux are NH radicals, which can contribute to the

generation of N_2, H_2 and ammonia molecules. The further downstream densities of the NH radicals are smaller because of diffusion loss and abstraction reactions. It can therefore be argued that at the end, at the vessel surfaces mainly the resulting N and H atoms play a key role in the generation of molecules.

N_2–H_2 plasma

In the second experimental situation (Fig. 3.1b), the plasma was produced with both nitrogen and hydrogen applied through the cascaded arc with a total flow of 16.67 sccs. In these experiments, the hydrogen flow rate relative to the total flow rate was varied. Also in these experiments, the current through the arc was 55 A and the downstream pressure was kept constant at 20 Pa. In the plasma source, the gas mixture of nitrogen and hydrogen is almost fully dissociated. However, the hydrogen atoms will partially recombine at the surface of the nozzle to form (excited) hydrogen molecules [54]. This loss mechanism is less important for the nitrogen atoms, since the association rate for nitrogen atoms is lower than for hydrogen atoms. The loss probability of H atoms on a stainless steel surfaces is reported in literature to be around 0.2 [32, 66], whereas values for N atoms vary from 7×10^{-2} to 8×10^{-3} [67, 68]. The ions emanating from the plasma source are lost very fast - most probably even faster than in the previous case as now H_2 is emanating from the source - via the same mechanisms as mentioned before.

The NH and NH_2 densities determined at the three positions from the plasma source ($z = 10, 21, 36$ cm) are plotted as a function of the hydrogen flow relative to the total flow rate of nitrogen and hydrogen in Fig. 3.10. Again the NH_x radicals are primarily found in the forward plasma beam. Also in this plasma, the rotational temperature and kinetic gas temperature of the NH_x radicals reflects the gas temperature in a plasma expansion. No NH_2 was detected outside the plasma beam, at $r = 10$ cm from the z-axis (and $z = 41.5$ cm) from the nozzle. Both observations indicate that the NH_x radicals are produced in the plasma expansion. The difference in the measured NH spectra in this plasma compared with the NH spectra in N_2 plasmas with H_2 injected in the background of the vessel, indicates that the generation of the NH_x radicals in both situations is governed by a different mechanism.

At low hydrogen flows, the main reaction mechanism leading to NH radicals is the same as for a N_2 plasmas with H_2 injected in the background of the vessel, i.e. formation of NH by a reaction between N atoms and H_2 molecules. When the hydrogen flow increases and the nitrogen flow decreases, the N atom flow will decrease

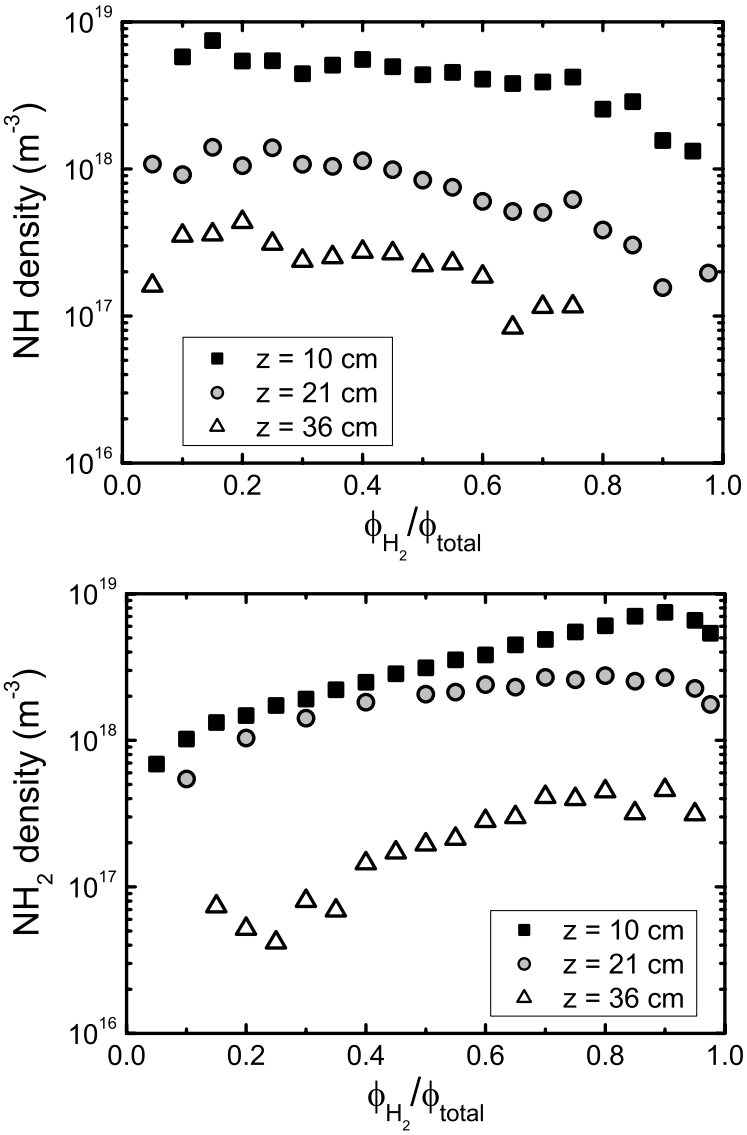

Figure 3.10: The densities of NH_2 and NH as a function of the hydrogen flow rate relative to the to the total flow rate of nitrogen and hydrogen as measured by cavity ring-down spectroscopy at $z = 10, 21$ and 36 cm. Both nitrogen and hydrogen are applied through the arc at a total flow rate of 16.67 sccs at an arc current of 55 A. The background pressure was kept at 20 Pa.

and the remaining N atoms will react with H_2 resulting in NH radicals. This would lead to a decreasing NH density with increasing hydrogen flow rate and decreasing N_2 flow. The observed decrease of the NH density is somewhat weaker than expected on basis of the flow ratio. Furthermore, the presence of NH_2 radicals at low hydrogen flow indicates that a second mechanism has to be taken into account, which is dominant in the production of the NH_x radicals at high hydrogen flows through the arc. When the plasma contains more and more hydrogen atoms, the NH_x radicals are also produced by reactions between H atoms and NH_3 molecules leading to NH_2 and subsequently the reaction between H and NH_2 leading to NH, reactions (R15) and (R12) in Table 3.2. This is underlined by the stronger increase of NH_2 compared to the trend of ammonia in Fig. 3.8 and that maximum NH_2 density is observed at high hydrogen flows. As more hydrogen is injected in the plasma source, more H atoms are emanating from the plasma source, leading to more ammonia, which can be dissociated again in the plasma beam by the H atoms. Furthermore, the rate constant of reaction (R15) is estimated to be higher than reported in literature, as also became clear from earlier reported Ar–NH_3 experiments [33]. Similar as previously estimated for the N atoms, it is also expected that the H atoms emanating from the plasma source have an kinetic energy in excess of 0.5 – 1 eV in the supersonic expansion region and first part of subsonic expansion to overcome the activation energy in this reaction, resulting in a rate constant of $0.6 - 1.0 \times 10^{-16}$ m^3 s^{-1}.

It is observed that the NH density has again its maximum at $z = 10$ cm and decreases further downstream. The NH densities as function of the relative H_2 flow show the same H_2 dependence at the three positions in the plasma beam. Furthermore, the gradient of the NH density as function of the measured position in the plasma beam has a constant factor of about 5 between positions. Both observations suggest that the loss mechanism of NH is the same for all three positions measured. Also now the loss of NH radicals is due to diffusion out of the plasma beam of the radicals and abstraction reactions with N and H atoms or by reactions between two NH radicals, reactions (R8)–(R11) (see Table 3.2).

The gradient of the NH_2 density as function of the measured position in the plasma beam gives a factor two between $z = 10$ cm and $z = 20$ cm, whereas it is a factor 10 between $z = 21$ cm and $z = 36$ cm. That this factor is not constant as it is in the case of NH, can be explained as follows. The NH_2 radicals are produced in a reaction between H atoms and NH_3 molecules, which also still can take place after $z = 10$ cm. Thus in contrast to the NH radicals, the NH_2 radicals are still produced after $z = 10$ cm. This counteracts the loss of NH_2 radicals due to diffusion out of the

plasma beam of the radicals and by abstraction reactions with H atoms. After $z = 21$ cm, the density of the NH_2 radicals is determined by these processes as almost no production occurs.

In conclusion, two mechanisms are responsible for the production of NH_x radicals in N_2–H_2 plasmas. At low hydrogen flows, the production of NH via the reaction of N atoms and and H_2 molecules is dominant. At higher H_2 flows, the N density diminishes and the formation of NH and NH_2 is governed by reactions between H and NH_3. The resulting NH_2 reacts then again with H, resulting in NH radicals. The flux density of the NH_x radicals in the plasma beam at $z = 10$ cm is about 1×10^{22} m^{-2} s^{-1}, assuming that the velocity of the NH radicals is the same as of the N radicals, i.e. 1000 m/s. This gives a flow of NH_x radicals of about 1×10^{20} radicals/s, which is thus a flow of 4 sccs. This means that the NH_x radicals form a significant part of the radical flux in the plasma used to generate N_2, H_2 and ammonia molecules.

3.4 Conclusions

We measured the densities of NH and NH_2 radicals at three positions from plasma source by cavity ring-down spectroscopy in expanding N_2 plasmas to which H_2 was added in the background and in expanding N_2–H_2 plasmas. The NH_2 radical was observed via transitions in the $(0, 9, 0) \leftarrow (0, 0, 0)$ band of the $\tilde{A}^2A_1 \leftarrow \tilde{X}^2B_1$ electronic transition. From a measured NH_2 spectrum, we determined the oscillator strengths of part of the transitions in the ${}^PQ_{1,N}$ branch of the Σ vibronic sub-band. The NH radical was observed via transitions in the (0,0), (1,1) and (2,2) vibrational bands of the $A^3\Pi \leftarrow X^3\Sigma^-$ electronic transition. For both radicals an overview of the calculation of the integrated absorption cross section and the determination of the total density is given.

From the density distribution of the rotational states of the NH radical in an expanding N_2 plasma with H_2 injected in the background, we concluded that the low rotational levels in the three vibrational states were populated according to a Boltzmann distribution. However, at $z = 10$ cm the high rotational levels, $J \geq 12$, in the $v = 2$ vibrational state were overpopulated. At the other two positions the rotational levels of $v = 2$ were not anymore observable. In N_2–H_2 plasmas the rotational levels in all vibrational states were populated according to a Boltzmann distribution at the three positions in the plasma expansion. Furthermore, from the distribution of the NH densities over the vibrational states, we concluded that at all three positions in both types of plasmas the vibrational distribution is non-Boltzmann, except at $z = 36$

cm in N_2–H_2 plasmas.

In both plasmas that have been studied, the NH_x radicals are produced in the plasma expansion. The difference in the measured NH spectra for both types of plasmas as function of the position from the plasma source indicates that the generation of the NH_x radicals is governed by two different mechanisms. The results of expanding N_2 plasmas to which H_2 was added in the background point to a formation of NH by a reaction between N atoms and H_2 molecules. In expanding N_2–H_2 plasmas, two mechanisms are responsible for the production of NH radicals.

The NH production at low hydrogen flows occurs in the same way as mentioned above, thus via N and H_2. But at high hydrogen flows, and thus a lower N flow, NH is formed by abstraction from NH_2, which is on its turn formed in a reaction between H and NH_3. That NH_2 was not detected in the case hydrogen is added to a N_2 plasma indicates that in this plasma reactions involving ammonia play no significant role in the production of NH_x radicals. The flux densities of the NH_x radicals at $z = 10$ cm represent a flux of $0.5 - 1 \times 10^{20}$ radicals/s. This represents a significant contribution to the total radical flux used for the generation of N_2, hydrogen and NH_3 molecules. At further downstream positions these fluxes are smaller because of diffusion loss and by abstraction reactions. It is therefore feasible that at the end the NH_x radicals play an indirect role and that at the surfaces mainly the resulting N and H atoms play a key role in the generation of molecules.

Appendix A

Total density of NH_2 using the absorption cross section of the $\tilde{A}^2A_1 \leftarrow \tilde{X}^2B_1(0,9,0) \leftarrow (0,0,0)\Sigma^P Q_{1,N}(7)$ transition in NH_2 at 16739.90 cm^{-1}

The total density of NH_2 can be calculated from the measured integrated absorption using the oscillator strength reported by Votsmeier et al. [44] and the molecular parameters reported by Green and Miller [47] assuming a Boltzmann density distribution over the rotational and vibrational energy states. The relation between the integrated absorption cross section σ_{int} and the oscillator strength f_{ik} for a transition from the lower level i to the upper level k is given by [69]:

$$\sigma_{int} = \int_0^\infty \sigma_{ik}(\nu)\,\mathrm{d}\nu = \frac{e^2}{4\varepsilon_0 m_e c} f_{ik}. \tag{3.20}$$

Using the fundamental physical constants for the electron mass m_e, elementary charge e, the dielectric constant ε_0, the speed of light c and the oscillator strength $f_{ik} = 8.36 \times 10^{-5}$ reported by Votsmeier et al. [44], we found the following value for the integrated absorption cross section:

$$\sigma_{int} = 2.21 \times 10^{-10}\,\mathrm{m^2\,Hz} = 7.37 \times 10^{-21}\,\mathrm{m^2\,cm^{-1}}. \tag{3.21}$$

The corresponding peak absorption cross section σ_{peak} at a gas temperature T can now be calculated by incorporating the line shape function $\Phi(0,a)$ that depends on the pressure-dependent broadening parameter a [21, 44]:

$$\sigma_{peak} = \sigma_{int}\Phi(0,a). \tag{3.22}$$

For the low working pressures in our experimental conditions, pressure broadening is negligible [23] and $\Phi(0,a)$ is a pure Gaussian line shape function ($a = 0$), so that $\Phi(0,a)$ can be written as a function of the Doppler width $\Delta\nu_D$:

$$\Phi(0,a) = \sqrt{\frac{4ln2}{\pi}}\frac{1}{\Delta\nu_D}. \tag{3.23}$$

$\Delta\nu_D$ is the full width half maximum of the Doppler broadened line profile and is given by:

$$\Delta\nu_D = \frac{\nu}{c}\sqrt{\frac{8kTln2}{m}} = 7.16 \times 10^{-7}\nu\sqrt{\frac{T}{M}}, \tag{3.24}$$

where ν is the absorption frequency, k is the Boltzmann's constant, T the gas temperature, m the mass of the NH_2 molecule, and M its molecular weight in amu. This

results in a peak absorption cross section at $T = 1775$ K of:

$$\sigma_{peak} = 5.51 \times 10^{-20}\,\mathrm{m}^2. \tag{3.25}$$

The density of NH_2 in the ${}^{P}Q_{1,N}(7)$ line can be calculated from the measured integrated absorption A_{int} [cm^{-1}]:

$$n_{NH_2,N=7} = \frac{A_{int}}{\sigma_{int} \cdot l}, \tag{3.26}$$

where l is the absorption path length of the radicals in the optical cavity. Assuming a Boltzmann distribution for the densities in the rotational and vibrational states, the total NH_2 density is given by:

$$n_{NH_2} = \frac{n_{NH_{2,N=7}}}{f_b}, \tag{3.27}$$

The Boltzmann fraction f_b for NH_2 is reported in the literature by Green and Miller [47] and Kohse-Höinghaus et al. [43]:

$$f_b = \frac{3}{4}\frac{(2J''+1)}{g''Q_rQ_v}\exp[-\frac{E_{rot}}{kT_{rot}}]\exp[-\frac{E_{vib}}{kT_{vib}}]. \tag{3.28}$$

The factor 3/4 occurs due to the nuclear spin of the H atoms, J'' and g'' are the total rotational quantum number including spin and the electron-spin degeneracy of the lower state, Q_r and Q_v are the rotational and vibrational partition functions, and E_{rot} and E_{vib} are the rotational and vibrational energy of the lower state and T_{rot} and E_{rot} are the rotational and vibrational temperature, respectively. We note that g'' is equal to 1, since the integrated absorption of the spin doublet line contained both components of the spin-doublet. The vibrational energy E_{vib} for the NH_2 molecules is given by Herzberg [48]:

$$E_{vib} = hc\,\omega_1(n_1 + 1/2) + hc\,\omega_2(n_2 + 1/2) + hc\,\omega_3(n_3 + 1/2), \tag{3.29}$$

in which h is Planck's constant, ω_1, ω_2 and ω_3 are the vibrational constants and n_1, n_2 and n_3 the vibrational quantum numbers of the lower state. The rotational energy E_{rot} is given by the following formula:

$$E_{rot} = hcF(J), \tag{3.30}$$

where $F(J)$ is the experimentally determined rotational term value as reported by Ross et al. [41]. The vibrational partition function Q_v including the zero-point energy of vibration is given by Green and Miller :

$$Q_v = \frac{\exp\left[-\frac{hc\omega_1}{2kT}\right]}{1-\exp\left[-\frac{hc\omega_1}{kT}\right]} \cdot \frac{\exp\left[-\frac{hc\omega_2}{2kT}\right]}{1-\exp\left[-\frac{hc\omega_2}{kT}\right]} \cdot \frac{\exp\left[-\frac{hc\omega_3}{2kT}\right]}{1-\exp\left[-\frac{hc\omega_3}{kT}\right]}. \tag{3.31}$$

The rotational partition function Q_r for NH_2, which is an asymmetric top molecule, can be estimated by [47, 48]:

$$Q_r = \frac{\sqrt{\pi}}{\sigma}\sqrt{\frac{8\pi^2 I_A\, kT}{h^2}}\sqrt{\frac{8\pi^2 I_B\, kT}{h^2}}\sqrt{\frac{8\pi^2 I_C\, kT}{h^2}} \tag{3.32}$$

In this equation, σ is the symmetry number and I_A, I_B and I_C are the moments of inertia of the NH_2 molecule. The symmetry number σ is equal to two. Using the moments of inertia and the vibrational frequencies reported by Green and Miller [47] and assuming equal rotational and vibrational temperatures of 1775 K, we can write the total NH_2 density [m^{-3})] as a function of the measured integrated absorption A_{int} [cm^{-1}]. At $z = 10$ cm, where $l = 0.1$ m, this results in:

$$n_{NH_2} = \frac{A_{int}}{\sigma_{int} \cdot l}\frac{1}{f_b} = 2.33 \times 10^{23} A_{int}. \tag{3.33}$$

Appendix B

Total density of NH using the absorption cross section of the $A^3\Pi(\nu' = 0) \leftarrow X^3\Sigma^-(\nu'' = 0)P_{33}(9)$ transition in NH at 29444.128 cm^{-1}

The total density of NH can be calculated from the integrated absorption using the Einstein coefficient for spontaneous emission on the basis of the information reported by Lents [50] and Schadee [52] and the molecular parameters reported by Brazier et al. [49] assuming a Boltzmann distribution over the rotational states. The integrated absorption cross section σ_{int} is directly related to the Einstein coefficient of spontaneous emission A_{ki} [69]:

$$\sigma_{int} = \frac{g_k}{g_i}\frac{c^2}{8\pi\nu^2}A_{ki}, \tag{3.34}$$

where g_i and g_k are the degeneracy of the lower level i and upper level k and c the speed of light and ν the absorption frequency. Subsequently, the Einstein coefficient for emission A_{ki} can be related to the electronic-vibrational transition probability $A_{v'v''}$ by the following expression:

$$A_{ki} = A_{v'v''}\frac{S_{J'J''}}{g'_e(2J'+1)(2S'+1)}, \tag{3.35}$$

where $S_{J'J''}$ is the Hönl-London factor belonging to the transition, g'_e is the electron degeneracy of the upper level, S' is the total spin of the upper state and J' is the

quantum number of the total angular momentum of the upper state. The electronic-vibrational transition probability $A_{v'v''}$ for the (0,0) and (1,1) bands are reported in the literature by Lents [50]; the values are $A_{00} = 2.32 \times 10^6$ and $A_{11} = 2.76 \times 10^6$. For the (2,2) band we used the average of reported values in literature as summarized by Seong et al. [53], resulting in $A_{22} = 2.93 \times 10^6$.

Here, the complete derivation of the density in the $v = 0$ vibrational state using the $A^3\Pi(\nu' = 0) \leftarrow X^3\Sigma^-(\nu'' = 0)$ $P_{33}(9)$ transition in NH at 29444.128 cm^{-1} will be described. In the subsequent derivation, singly primed coefficients pertain to the upper Π state and doubly primed coefficients to the lower Σ state and J is the quantum number of the total angular momentum of the lower state, i.e. $J = 9$. For this transition, $S_{J'J''}$ in Eq. 3.35 is the Hönl-London factor $P_{33}(J)$ for the lines in the P_{33} branch as given by Schadee [52]:

$$\begin{aligned} P_{33} &= \frac{(J-1)(J+1)}{8JC_3'(J-1)}[(J-2)u_{3+}'(J-1)g''(J) + 4(J-1)\sqrt{J(J+1)}s''(J) \\ &\quad + Ju_{3-}'(J-1)g''(J)]^2, \end{aligned} \tag{3.36}$$

with the following coefficients:

$$g(J) = \left[\frac{F_2(J) - F_1(J)}{F_3(J) - F_1(J)}\right]^{\frac{1}{2}}, \tag{3.37}$$

$$S(J) = \left[\frac{F_3(J) - F_2(J)}{F_3(J) - F_1(J)}\right]^{\frac{1}{2}}, \tag{3.38}$$

where $F_i(J)$ are the term values and:

$$\begin{aligned} F_2(J) - F_1(J) &= [(B_v - \tfrac{1}{2}\gamma - \lambda)^2 + 4J(J+1)(B_v - \tfrac{1}{2}\gamma)^2]^{\frac{1}{2}} \\ &\quad -(B_v - \tfrac{1}{2}\gamma - \lambda), \end{aligned} \tag{3.39}$$

$$\begin{aligned} F_3(J) - F_2(J) &= [(B_v - \tfrac{1}{2}\gamma - \lambda)^2 + 4J(J+1)(B_v - \tfrac{1}{2}\gamma)^2]^{\frac{1}{2}} \\ &\quad +(B_v - \tfrac{1}{2}\gamma - \lambda), \end{aligned} \tag{3.40}$$

$$F_3(J) - F_1(J) = 2[(B_v - \tfrac{1}{2}\gamma - \lambda)^2 + 4J(J+1)(B_v - \tfrac{1}{2}\gamma)^2]^{\frac{1}{2}}, \tag{3.41}$$

and the coefficients:

$$u_{3\pm}(J) = [(Y-2)^2 + 4J(J+2)]^{\frac{1}{2}} \pm (Y-2), \tag{3.42}$$

$$\begin{aligned} C_3(J) &= Y(Y-4)(J-1)(J+2) + 2(2J+1)J(J+1)(J+2) \\ &\quad -(Y-2)[(Y-2)^2 + 4J(J+2)]^{\frac{1}{2}} + Y(Y-4) - 4(J+1). \end{aligned} \tag{3.43}$$

The molecular constant γ represents the spin-rotation interaction, λ is the splitting constant, B_v the rotational constant, and Y represents the coupling constant between the nuclear spin S and the orbital angular momentum Λ. The electron degeneracies of the Σ and Π states are $(2S+1)$ and $2(2S+1)$, respectively [51]. Using the molecular constants of the electronic states ($A^3\Pi$ and $X^3\Sigma^-$) of the NH radical reported by Brazier et al. [49] and the electronic-vibrational transition probability A_{00} reported by Lents [50], we can calculate the Einstein coefficient for emission of the $P_{33}(9)$ line:

$$A_{ki} = 6.07 \times 10^4\,\mathrm{s}^{-1} \tag{3.44}$$

Using Eq. 3.34 and $g_k = 2(J-1)+1)$ and $g_i = (2J+1)$ with $J = 9$ we find for the integrated absorption cross section:

$$\sigma_{int} = 2.49 \times 10^{-10}\,\mathrm{m}^2\,\mathrm{Hz} = 8.30 \times 10^{-21}\,\mathrm{m}^2\,\mathrm{cm}^{-1}. \tag{3.45}$$

The corresponding peak absorption cross section σ_{peak} at a gas temperature T can be calculated according to same procedure as for the NH_2 radical [Eqs. (3.22) – (3.24)]. This results in a peak absorption cross section at $T = 1775$ K of:

$$\sigma_{peak} = 3.4 \times 10^{-20}\,\mathrm{m}^2. \tag{3.46}$$

The density of NH in the $P_{33}(9)$ line can be calculated from the measured integrated absorption A_{int} [cm^{-1}]:

$$n_{NH_2,J=9} = \frac{A_{int}}{\sigma_{int} \cdot l}, \tag{3.47}$$

where l is the absorption path length of the radicals in the optical cavity. The total density in the $v = 0$ vibrational state assuming a Boltzmann distribution for the densities in the rotational states is given by:

$$n_{NH_{v=0}} = \frac{n_{NH_{J=9}}}{f_{b,rot}}. \tag{3.48}$$

The rotational Boltzmann fraction $f_{b,rot}$ at a rotational temperature T_{rot} for NH is taken from Herzberg [48]:

$$f_{b,rot} = \frac{(2J+1)}{Q_r} \exp[-\frac{E_{rot}(K)}{kT_{rot}}], \tag{3.49}$$

where J is the quantum number of the total angular momentum of the lower level and E_{rot} the rotational energy:

$$E_{rot}(K) = hcB_vK(K+1), \tag{3.50}$$

in which B_v is the rotational constant, and K the total angular momentum of the lower level apart from electronic spin. The rotational partition function Q_r for the diatomic NH molecule can be approximated by the classical expression [48]:

$$Q_r = \frac{kT}{hcB_v}. \tag{3.51}$$

Using the molecular constants reported by Brazier et al. [49] and assuming a rotational temperature of 1775 K, the total density in the $v = 0$ vibrational state [m^{-3}] can be calculated as a function of the measured integrated absorption A_{int} [cm^{-1}]:

$$n_{NH_{v=0}} = \frac{A_{int}}{\sigma_{int} \cdot l} \frac{1}{f_{b,rot}} = 2.06 \times 10^{22} A_{int}. \tag{3.52}$$

In the case one can assume a Boltzmann distribution for the densities in the rotational and vibrational states, the total NH density can be calculated with Eq. 3.48 with $f_{b,rot}$ replaced by f_b which is given by:

$$f_b = \frac{(2J+1)}{Q_r Q_v} \exp[-\frac{E_{rot}}{kT_{rot}}] \exp[-\frac{E_{vib}}{kT_{vib}}]. \tag{3.53}$$

The vibrational energy E_{vib} is given by Herzberg [48]:

$$E_{vib}(n) = hc\,\omega_1(n + 1/2), \tag{3.54}$$

ω_1 is the vibrational constant and n the vibrational quantum number of the lower state. The vibrational partition function Q_v including the zero-point energy of vibration is given by Herzberg [48]:

$$Q_v = \frac{\exp\left[-\frac{hc\omega_1}{2kT}\right]}{1 - \exp\left[-\frac{hc\omega_1}{kT}\right]} \tag{3.55}$$

Then the total NH density at $z = 10$ cm, where $l = 0.1$ m, is given by:

$$n_{NH} = \frac{A_{int}}{\sigma_{int} \cdot l} \frac{1}{f_b} = 2.22 \times 10^{22} A_{int}. \tag{3.56}$$

Bibliography

[1] A. Ricard, B.F. Gordiets, M.J. Pinheiro, C.M. Ferreira, G. Baravian, J. Amorim, S. Bockel, and H. Michel, *Diagnostic and modeling of N_2–H_2 discharges for iron nitriding*, Eur. Phys. J. Appl. **4**, 87 (1998).

[2] W.M.M. Kessels, F.J.H. van Assche, J. Hong, D.C. Schram, and M.C.M. van de Sanden, *Plasma diagnostic study of silicon nitride film growth in a remote Ar–H_2–N_2–SiH_4 plasma: Role of N and SiH_n*, J. Vac. Sci. Technol. A **22**, 96 (2004).

[3] H. Kim, *Atomic layer deposition of metal and nitride thin films: Current research efforts and applications for semiconductor device processing,* J. Vac. Sci. Technol. B **21**, 2231 (2003).

[4] H. Nagai, M. Hiramatsu, M. Hori, and T. Goto, *Etching organic low dielectric film in ultra-high frequency plasma using N_2/H_2 and N_2/NH_3 gases,* J. Appl. Phys. **94**, 1362 (2003).

[5] E.N. Eremin, *Kinetics and catalysis of reactions in electrical discharge plasmas (application of the specific energy method),* Russ. J. Phys. Chem. **49**, 1112 (1975).

[6] H. Uyama and O. Matsumoto, *Synthesis of ammonia in high-frequency discharges,* Plasma Chem. Plasma Process. **9**, 13 (1989).

[7] K.S. Yin and M. Venugopalan, *Plasma Chemical Synthesis. I. Effect of electrode material on the synthesis of ammonia,* Plasma Chem. Plasma Process. **3**, 343 (1983).

[8] P. Vankan, T. Rutten, S. Mazouffre, D.C. Schram, and R. Engeln, *Absolute density measurements of ammonia produced via plasma-activated catalysis,* Appl. Phys. Lett. **81**, 418 (2002).

[9] J.H. van Helden, W. Wagemans, P. Vankan, T. Rutten, D.C. Schram, and R. Engeln, 16th International Sysmposium on Plasma Chemistry, Taormina, Italy, June 22-27, 2003.

[10] B. Gordiets, C.M. Ferreira, M.J. Pinheiro, and A. Ricard, *Self-consistent kinetic model of low-pressure N_2–H_2 flowing discharges: I. Volume processes,* Plasma Sources Sci. Technol. **7**, 363 (1998).

[11] B. Gordiets, C.M. Ferreira, M.J. Pinheiro, and A. Ricard, *Self-consistent kinetic model of low-pressure N_2–H_2 flowing discharges: II. Surface processes and densities of N, H, NH_3,* Plasma Sources Sci. Technol. **7**, 379 (1998).

[12] J.L. Jauberteau, I. Jauberteau, and J. Aubreton, *NH_3 and $NH_{x<3}$ radicals synthesis downstream a microwave discharge sustained in an Ar–N_2–H_2 gas mixture. Study of surface reactive processes and determination of rate constants,* J. Phys. D: Appl. Phys. **35**, 665 (2002).

[13] J. Amorim, G. Baravian, and A. Ricard, *Production of N, H, and NH active species in N_2–H_2 flowing discharges,* Plasma Chem. Plasma Process **15**, 721 (1995).

[14] S. Bockel, J. Amorim, G. Baravian, A. Ricard, and P. Stratil, *A spectroscopic study of active species in DC and HF flowing discharges in N_2–H_2 and Ar–N_2–H_2 mixtures,* Plasma Sources Sci. Technol. **5**, 567 (1996).

[15] E.R. Fisher, P. Ho, W.G. Breiland, and R.J. Buss, *Laser studies of the reactivity of $NH(X^3\Sigma^-)$ with the surface of sllicon nitride,* J. Phys. Chem. **96**, 9855 (1992).

[16] P.R. McCurdy, C.I. Butoi, K.L. Williams, and E.R. Fisher, *Surface interactions of NH_2 radicals in NH_3 plasmas,* J. Phys. Chem. B **103**, 6919 (1999).

[17] M.L. Steen, K.R. Kull, and E.R. Fisher, *Comparison of surface interactions for NH and NH_2 on polymer and metal substrates during NH_3 plasma processing,* J. Appl. Phys. **92**, 55 (2002).

[18] H. Uyama nd O. Matsumoto, *Synthesis of ammonia in high-frequency discharges. II. Synthe-*

sis of ammonia in a microwave discharge under various conditions, Plasma Chem. Plasma Process. **9**, 421 (1989).

[19] H. Kiyooka and O. Matsumoto, *Reaction schemes of ammonia synthesis in the ECR plasmas*, Plasma Chem. Plasma Process. **16**, 547 (1996).

[20] J.B. Halpern, G. Hancock, M. Lenzi, and K.H. Welge, *Laser induced fluorescence from $NH_2(^2A_1)$. State selected radiative lifetimes and collisional de-excitation rates*, J. Chem. Phys. **63**, 4808 (1975).

[21] I. Rahinov, N. Ditzian, A. Goldman, and S. Cheskis, *NH_2 radical formation by ammonia pyrolysis in a temperature range of 800–1000 K*, Appl. Phys. B **77**, 541 (2003).

[22] I. Derzy, V.A. Lozovsky, N. Ditzian, I. Rahinov, and S. Cheskis, Absorption spectroscopy measurements of NH and NH_2. Absolute concentrations in methane/air flames doped with N_2O, in *Proc. Combust. Insti.*, volume 28, page 1741, 2000.

[23] G. Friedrichs, M. Colberg, M. Fikri, Z. Huang, J. Neumann, and F. Temps, *Validation of the extended simultaneous kinetics and ringdown model by measurements of the reaction NH_2 + NO*, J. Phys. Chem. A **109**, 4785 (2005).

[24] I. Rahinov, A. Goldman, and S. Cheskis, *Intracavity laser absorption spectroscopy and cavity ring-down spectroscopy in low-pressure flames*, Appl. Phys. B **81**, 143 (2005).

[25] M.C.M. van de Sanden, R.J. Severens, W.M.M. Kessels, R.F.G. Meulenbroeks, and D. C. Schram, *Plasma chemistry aspects of a–Si:H deposition using an expanding thermal plasma*, J. Appl. Phys. **84**, 2426 (1998), **85**, 1243 (1999).

[26] S. Mazouffre, I. Bakker, P. Vankan, R. Engeln, and D.C. Schram, *Two-photon laser induced fluorescence spectroscopy performed on free nitrogen plasma jets*, Plasma Sources Sci. Technol. **11**, 439 (2002).

[27] R. Engeln, S. Mazouffre, P. Vankan, D.C. Schram, and N. Sadeghi, *Flow dynamics and invasion by background gas of a supersonically expanding thermal plasma*, Plasma Sources Sci. Technol. **10**, 595 (2001).

[28] M.C.M. van de Sanden, J.M. de Regt, G.M. Jansen, J.A.M. van der Mullen, D.C. Schram, and B. van der Sijde, *A combined Thomson-Rayleigh scattering diagnostic using an intensified photodiode array*, Rev. Sci. Instrum. **63**, 3369 (1992).

[29] P. Vankan, S. Mazouffre, R. Engeln, and D. C. Schram, *Inflow and shock formation in supersonic, rarefied plasma expansions*, Phys. Plasmas **12**, 102303 (2005).

[30] K.W. Busch and M.A. Busch, *Cavity-Ringdown Spectroscopy – An Ultratrace-Absorption Measurement Technique*, American Chemical Society, Washington (1998).

[31] P.J.W. Vankan, *Molecules and atoms in a hydrogen plasma expansion*, PhD thesis, Eindhoven University of Technology, Eindhoven, 2005, available on-line at

http://alexandria.tue.nl/extra2/200510358.pdf.

[32] S. Mazouffre, P. Vankan, R. Engeln, and D. C. Schram, *Influence of surface chemistry on the transport of H atoms in a supersonic hydrogen plasma jet,* Phys. Plasmas **8**, 3824 (2001).

[33] P.J. van den Oever, J.H. van Helden, C.C.H. Lamers, R. Engeln, D.C. Schram, M.C.M. van de Sanden, and W.M.M. Kessels, *Density and production of NH and NH_2 in an Ar–NH_3 expanding plasma jet,* J. Appl. Phys. **98**, 093301 (2005).

[34] W.M.M. Kessels, A. Leroux, M.G.H. Boogaarts, J.P.M. Hoefnagels, M.C.M. van de Sanden, and D.C. Schram, *Cavity ring down detection of SiH_3 in a remote SiH_4 plasma and comparison with model calculations and mass spectrometry,* J. Vac. Sci. Technol. A **19**, 467 (2001).

[35] R.F.G. Meulenbroeks, A.J. van Beek, A.J.G. van Helvoort, M.C.M. van de Sanden, and D.C. Schram, *Argon-hydrogen plasma jet investigated by active and passive spectroscopic means,* Phys. Rev. E **49**, 4397 (1994).

[36] S. Mazouffre, M.G.H. Boogaarts, I.S.J. Bakker, P. Vankan, R. Engeln, and D. C. Schram, *Transport of ground-state hydrogen atoms in a plasma expansion,* Phys. Rev. E **64**, 016411 (2001).

[37] G.J.H. Brussaard, *Remote arc generated plasma in diatomic gases,* PhD thesis, Eindhoven University of Technology, Eindhoven, 1999, available on-line at http://alexandria.tue.nl/extra2/9900312.pdf.

[38] J.P.M. Hoefnagels, Y. Barrell, W.M.M. Kessels, and M.C.M. van de Sanden, *Time-resolved cavity ringdown study of the Si and SiH_3 surface reaction probability during plasma deposition of a–Si:H at different substrate temperatures,* J. Appl. Phys. **96**, 4094 (2004).

[39] Technical Laboratory Automation Group, Eindhoven University of Technology, Den Dolech 2, 5600 MB Eindhoven, The Netherlands.

[40] D. Romanini and K.K. Lehmann, *Ring-down cavity absorption spectroscopy of the very weak HCN overtone bands with six, seven and eight stretching quanta,* 99 , 6287 (1993).

[41] S.C. Ross and F.W. Birss, *The absorption spectrum of NH_2 in the region 5300 to 6800* , J. Mol. Spectrosc. **129**, 436 (1988).

[42] K. Dressler and D.A. Ramsay, *The electronic absorption spectra of NH_2 and ND_2,* Philos. Trans. R. Soc. London, Ser. A **251**, 553 (1959).

[43] K. Kohse-Höinghaus, D.F. Davidson, A.Y. Chang, and R.K. Hanson, *Quantitative NH_2 concentration determination in shock tube laser-absorption experiments,* J. Quant. Spectrosc. Radiat. Transfer **42**, 1 (1989).

[44] M. Votsmeier, S. Song, D.F. Davidson, and R.K. Hanson, *Shock tube study of monomethylamine thermal decomposition and NH_2 high temperature absorption coefficient,* Int. J. Chem.

Kinet. **31**, 323 (1999).

[45] Sirah Laser- und Plasmatechnik GmbH, Darmstadt, Germany, *Manual PrecisionScan-D dye laser*, 1999.

[46] S. Mazouffre, *Transport phenomena in plasma expansions containing hydrogen*, PhD thesis, Eindhoven University of Technology, Eindhoven, 2001, http://alexandria.tue.nl/extra2/200142219.pdf.

[47] R.M. Green and J.A. Miller, *The measurement of relative concentration profiles of NH_2 using laser absorption spectroscopy*, J.Quant. Spectrosc. Radiat. Transfer **4**, 313 (1981).

[48] G. Herzberg, *Molecular spectra and molecular structure*, volume II. Infrared and Raman Spectra of Polyatomic Molecules, Van Nostrand, Princeton (1966).

[49] C.R. Brazier, R.S. Ram, and P.F. Bernath, *Fourier transform spectroscopy of the $A^3\Pi - X^3\Sigma^-$ transition of NH*, J. Mol. Spectrosc. **120**, 381 (1986).

[50] J.M. Lents, *An evaluation of molecular constants and transition probabilities for the NH free radical*, J.Quant. Spectrosc. Radiat. Transfer **13**, 297 (1973).

[51] G. Herzberg, *Molecular spectra and molecular structure*, volume I. Spectra of Diatomic Molecules, Van Nostrand, Princeton (1965).

[52] A. Schadee, *Hönl-London factors for $^3\Pi - {}^3\Sigma^-$ and $^3\Sigma^- - {}^3\Pi$ transitions with intermediate coupling*, Astron. & Astrophys. **41**, 213 (1975).

[53] J. Seong, J.K. Park, and H. Sun, *Transition dipole moments, transition probabilities, and radiative lifetimes for NH by ab initio effective valence shell Hamiltonian*, Chem. Phys. Lett. **228**, 443 (1994).

[54] P. Vankan, D.C. Schram, and R. Engeln, *High rotational excitation of molecular hydrogen in plasmas*, Chem. Phys. Lett. **400**, 196 (2004).

[55] P. Vankan, D.C. Schram, and R. Engeln, *Atomic and molecular hydrogen densities in a plasma expansion*, Plasma Sources Sci. Technol. **14**, 744 (2005).

[56] M. Capitelli, C.M. Ferreira, B.F. Gordiets, and A.I. Osipov, *Plasma kinetics in atmospheric gases*, Springer-Verlag, Berlin (2000).

[57] R.P. Dahiya, M.J. de Graaf, R.J. Severens, H. Swelsen, M.C.M. van de Sanden, and D.C. Schram, *Dissociative recombination in cascaded arc generated Ar-N_2 and N_2 expanding plasma*, Phys. Plasmas **1**, 2086 (1994).

[58] J.A.M. van der Mullen, *Excitation equilibria in plasmas; a classification*, Phys. Rep. **191**, 110 (1990).

[59] G.J.H. Brussaard, E. Aldea, M.C.M. van de Sanden, G. Dinescu, and D.C. Schram, *Evidence of charge exchange between N^+ and $N_2(A^3\Sigma_u^+)$ in a low-temperature nitrogen plasma*, Chem. Phys. Lett. **290**, 379 (1998).

[60] G. Cernogora, C.M. Ferreira, L. Hochard, M. Touzeau, and J. Loureiro, *Vibrational populations of $N_2(A)$ in a pure N_2 glow discharge,* J. Phys. B **17**, 4429 (1984).

[61] R. Derai amd G. Mauclaire and R. Marx, *Energy disposal in thermal-energy charge-transfer reactions: Ar^+, Kr^+ and Xe^+ with NH_3,* Chem. Phys. Lett. **86**, 275 (1982).

[62] J. Perrin, O. Leroy, and M.C. Bordage, *Cross-sections, rate constants and transport coefficients in silane plasma chemistry,* Contrib. Plasma Phys. **36**, 3 (1996).

[63] M.P. Skrzypkowski and R. Johnsen, *Electron-temperature dependence of the recombination of $NH_4^+(NH_3)_n$ ions with electrons,* Chem. Phys. Lett. **274**, 473 (1997).

[64] T. Ko, P. Marshall, and A. Fontijn, *Rate coefficients for the $H + NH_3$ reaction over a wide temperature range,* J. Phys. Chem. **94**, 1401 (1990).

[65] W.D. Geppert, R. Thomas, J. Semaniak, A. Ehlerding, T.J. Millar, F. Österdahl, M.A. Ugglas, N. Djuric, A. Paál, and M. Larsson, *Dissociative recombination of N_2H^+: Evidence for fracture of the N-N bond,* Astrophys. J. **609**, 459 (2004).

[66] P. Kae-Nune, J. Perrin, J. Jolly, and J. Guillon, *Surface recombination probabilities of H on stainless steel, a–Si:H and oxidized silicon determined by threshold ionization mass spectrometry in H_2 RF discharges,* Surf. Sci. **360**, L495 (1996).

[67] H. Singh, J. W. Coburn, and D. B. Graves, *Recombination coefficients of O and N radicals on stainless steel,* J. Appl. Phys. **88**, 3748 (2000).

[68] S.F. Adams and T.A. Miller, *Surface and volume loss of atomic nitrogen in a parallel plate rf discharge reactor,* Plasma Sources Sci. Technol. **9**, 248 (2000).

[69] A.P. Thorne, *Spectrophysics,* Chapman and Hall & Science Paperbacks London (1974).

Chapter 4

Plasma-activated catalytic generation of ammonia in N_2–H_2 plasmas

Abstract

We investigated the efficiency and formation mechanism of ammonia generation in recombining plasmas generated from mixtures of N_2 and H_2 under various plasma conditions and plasma reactor geometries. We show that by using an atomic nitrogen and hydrogen source, ammonia can be formed efficiently, i.e. more than 10% of the total background pressure is measured to be ammonia. These results show a strong similarity with results reported in literature. It is concluded that ammonia is formed via plasma-surface interactions by the successive hydrogenation of adsorbed nitrogen atoms and the intermediates NH and NH_2 at the surface of the plasma reactor.

4.1 Introduction

The synthesis of ammonia from nitrogen and hydrogen gas on iron catalysts, known as the Haber-Bosch process, is considered as one of the most important discoveries in the history of industrial catalysis [1] and has often been called the most important invention of the 20th century [2]. Today, the artificial fertilizer produced with the Haber-Bosch process is responsible for sustaining roughly 40% of the Earth's population [3]. Because of its importance, even today the process of ammonia synthesis is investigated, to fully understand the processes on the surface leading to ammonia and to increase its efficiency, e.g. by using other catalysts as ruthenium [4, 5]. The general picture is that the ammonia generation proceeds via dissociative chemisorption of N_2 followed by stepwise recombination of chemisorbed atomic nitrogen and hydrogen to NH_3 at the surface of the catalyst with NH and NH_2 as reaction intermediates [6, 7]. The rate-limiting step in the ammonia synthesis is the dissociative chemisorption of N_2 molecules on the surface of the catalyst, due to the binding energy of 9.6 eV of N_2.

Nomura et al. [8] suggested that excited N_2 molecules would improve the dissociative adsorption of N_2. The lowest excited state of N_2, the $A^3\Sigma_u^+$ state, lies at 6.2 eV; then only 3.4 eV is necessary to dissociate the nitrogen molecule. The production of excited N_2 or even direct production of N atoms can be achieved by a plasma and then other catalysts than iron or ruthenium may be used to enhance the ammonia production.

In 1971 Eremin et al. [9] showed that the synthesis of ammonia in mixtures of nitrogen and hydrogen in a barrier discharge was increased by a factor of 1.5 to 4, when respectively copper, nickel, iron or platinum wires were wound on the inner electrode of the reactor. It was shown by various research groups in the world that ammonia production using plasmas is dependent on the type of wall material (up to a factor 3) [10–13]. The wall is namely still used as a catalyst to form adsorbed nitrogen atoms by the dissociative adsorption of excited N_2 molecules or nitrogen molecular ions. In 1989, Uyama and Matsumoto reported that zeolite added to the downstream plasma in high-frequency discharges facilitated the ammonia production. This enhancement can at least partly be ascribed to a change in effective surface area. The ammonia production was ascribed to the surface reaction of NH_x radicals adsorbed on the zeolite with hydrogen atoms [14]. The formation of ammonia in plasmas is still not completely understood but it is assumed that plasma-surface interactions play an important role. The formation of ammonia is generally ascribed to stepwise

addition reactions between adsorbed nitrogen and hydrogen containing radicals at the surface and incoming N and H containing radicals [15–18].

Plasma-surface interactions are not only observed in the ammonia generation. For example, recombinative desorption of H atoms, leading to excited H_2 molecules is an important mechanism in H^- formation [19]. In expanding hydrogen plasmas, the generation of ro-vibrationally excited H_2 molecules is observed. The high rotational excitation of the hydrogen molecules suggests that they are produced by the surface association of H atoms: $H_{gas} + H_{ad} \longrightarrow H_{2\ gas}^{r,v}$ [20, 21].

To gain a better understanding of plasma-surface interactions that take place during the generation of stable molecules, we have chosen to investigate the formation of ammonia in plasmas of mixtures of nitrogen and hydrogen in more detail. Plasmas containing nitrogen and hydrogen are also extensively studied because of their widespread applications in research and industrial environments. In this chapter, we present measurements of the density of ammonia in recombining plasmas generated from mixtures of N_2 and H_2 with the remote expanding thermal plasma (ETP) technique [22]. In the experiments, the plasma acts as catalyst to dissociate the precursor molecules already before they come in contact with a surface. Then the surface is exposed to fluxes of atomic and molecular *radicals* rather than molecules. The process is called plasma-activated catalysis. We note that in our experiments, the N and H radicals are already produced in the plasma source and as a result the flux of N and H radicals to the surface is up to 10^{21} m^{-2} s^{-1} [23–25], which is at least one order of magnitude higher than in previous experiments in which a plasma was used, (see e.g. [12]). In the present experiments the fluxes of radicals at the surface of the vessel are several tens of mono-layers per second.

Previously, we have shown that ammonia can be formed efficiently in plasmas generated from mixtures of hydrogen and nitrogen via plasma-activated catalysis [26]. In this study, fluxes of hydrogen and nitrogen radicals are produced in a high-density plasma source with high dissociation degree. The plasma then expands into a low-pressure vessel, where most of the atomic radicals will arrive at the reactor wall at which they may reflect, but will finally adsorb. There new molecules can be generated which subsequently may desorb. In this way the dissociation in the plasma source is geometrically separated from the production zone of the molecules. Because the plasma production, plasma transport and plasma-surface interactions are separated, the plasma conditions can be controlled independently from the downstream plasma chemistry, which allows independent studies of the different aspects of the process in a relatively simple manner.

We studied the formation of ammonia in expanding plasmas generated from: (a) expanding Ar plasma to which mixtures of N_2 and H_2 were added; (b) expanding N_2 plasma to which H_2 was added; (c) expanding N_2–H_2 plasma. The density of NH_3 was measured with three different detection techniques, i.e. mass spectrometry, cavity enhanced absorption spectroscopy (CEA) and tunable diode laser absorption spectroscopy (TDLAS). With massa spectrometry, also N_2 and H_2 can be detected, which is not possible with the two laser techniques. The laser techniques have the advantage that the measurements are not hampered by the presence of water as may be the case for ammonia using mass spectrometry. We investigated the efficiency and formation mechanism of ammonia generation in these plasmas under various plasma conditions and in three different plasma reactors, with different geometries.

We will first describe the basics of the ETP technique (Sec. 4.2.1). Next, in Sec. 4.2.2, the experimental details of the three techniques used to measure ammonia will be discussed, i.e. mass spectrometry, cavity enhanced absorption spectroscopy and tunable diode laser absorption spectroscopy. In Sec. 4.3, we present the measured ammonia densities in the various plasmas. The conclusions are presented in the last section.

4.2 Experimental details

4.2.1 Expanding thermal plasma setup

The experiments were performed on three similar plasma reactors, all of the ETP type. Two of them (HNO and Depo II) are very similar in dimensions and flow pattern. The third one, on which most measurements were performed is different in the sense that it is much longer; it has a smaller surface to volume ratio and produced particles are more easily lost. The recombining plasmas were generated with the expanding thermal plasma (ETP) technique, described extensively in the literature (see e.g. [22]), to obtain high fluxes of reactive species in the experiments. The ETP technique is a remote technique in which reactive species are created in a high-pressure cascaded arc plasma source and the plasma processes take place downstream at lower pressure (Fig. 4.1). Here, only a short description of the main constituents is given.

In the DC cascaded arc plasma source a sub-atmospheric (typically 400kPa) plasma is created with a power of 2 – 8 kW. The cascaded arc source consists of a 4 mm diameter bore channel of 5 water-cooled insulated copper plates with a total length

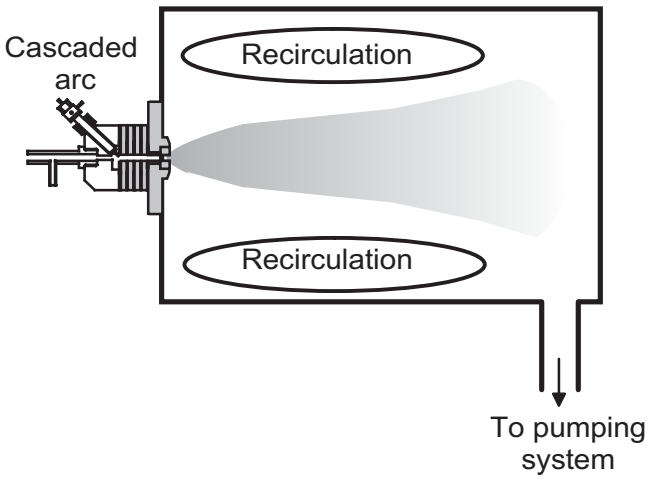

Figure 4.1: Schematic representation of the plasma source, vacuum vessel, and the plasma expansion with the recirculation flow in the chamber. The width of the process chamber in all set-ups was 0.4 m, and the length of the plasma reactors was respectively 0.4 m (HNO), 0.6 m (Depo II) and 2 m (PLEXIS).

of 30 mm. The cascaded plates are at floating potential. The last plate acts as the common anode for the discharge. A gas flow is admitted to the channel and a dc current is drawn from the three cathodes concentrically placed around the channel, to the grounded anode plate producing the plasma. The high heavy particle temperature of approaching 1 eV leads to almost full dissociation of molecular gases when these are injected in the arc. The plasma expands supersonically through a conically shaped nozzle into a low-pressure vessel (typically 20 Pa), and after a stationary shock, expands subsonically towards the other end of the process chamber. As there is no power input anymore in the process chamber, the plasma is recombining. Furthermore, in the expansion, the electron temperature decreases to 0.1 – 0.3 eV. Dissociation and excitation by electrons can be neglected at these temperatures.

The resulting high-density plasma has an ionization degree of around 12% in argon [27] and around 1 – 5% in pure nitrogen and mixtures of nitrogen and hydrogen [24, 28]. The current through the arc channel was set to 55 A in the experiments reported here and the voltage over the arc ranged from 40 V in argon plasmas to 150 V for N_2–H_2 plasmas. In the experiments, the pressure in the vessel was varied between 20 and 100 Pa by adjusting the gate valve to the pump.

N_2 and H_2 gas can also be injected into the background of the plasma vessel, i.e.

into the re-circulation flow in the chamber. If the source is operated on argon (or nitrogen), the injected molecules, together with molecules generated in the plasma vessel, form the basis of influx in the expanding plasma beam. It has been established that diffusion inwards occurs mainly in the subsonic region, but can also already occur in the supersonic region if the flow is rarefied at low pressure [23, 25]. As a result, the gas mixture in the re-circulating flow in the periphery of the chamber is mixed into the forward plasma beam emanating from the source. Molecules which diffuse into the expanding plasma beam can undergo charge-transfer with Ar^+ (or N^+) ions emanating from the source. Subsequent dissociative recombination reactions lead to atomic and/or molecular radicals. Furthermore, the monomers may undergo abstraction reactions with radicals, e.g. H atoms, leading to additional radicals.

Production of molecules out of atomic or molecular radicals in the volume by three particle reactions can be excluded, since these reactions are too slow to lead to any significant production under our low-pressure conditions (mostly < 100 Pa). This is certainly true for the time in the plasma beam, which is short (< 1 ms). It holds even for the relatively long (0.1 – 1 s) residence time of particles, relevant for the background kinetics. However, during the residence time molecules may undergo reactions in the re-circulating flow in the background of the plasma vessel, since even the lifetime of active particles as N and H atoms in the background is relatively long.

To study possible contribution of the generation of ammonia in the gas phase through bimolecular nitrogen-hydrogen reactions in our experiments, we modeled the chemistry in the expanding plasma beam and in the recirculation flow by a reaction model using the chemical kinetic software package CHEMKIN [29] and all possible reactions in N_2–H_2 plasmas and their rate constants as given in ref [30]. From the results, we conclude that less than 1% of the measured ammonia density can be formed in the expanding plasma beam and that ammonia generation is not possible via gas phase reactions during the residence time in the vessel. Though we can not exclude the possibility that ammonia is formed at the end of the plasma source, when both nitrogen and hydrogen are fed through the plasma source, it is clear that also dissociation is very effective there. The results that will be shown, indicate that ammonia formation at the end of the plasma source does probably not take place.

If the production of ammonia is due to plasma-surface interactions a larger “active” surface to “active” volume ratio should lead to more ammonia production. The word “active” underlines the fact that the plasma(-surface) chemistry is dependent on geometry of the plasma reactors, i.e. the total surface or volume of the plasma

reactor is not always used in the processes. The "active" surface to volume ratio is determined by the combination of the flow pattern of the plasma in the reactor and the total surface to volume ratio.

An indication that flow pattern and surface to volume ratio is important is offered by the use of three reactors of the same type (ETP-remote source), but different geometries. At one hand there is a long, very effectively pumped PLEXIS dedicated to these studies and in which most experiments were performed. At the other hand, two other similar machines HNO and Depo II, which are much shorter with a larger surface to volume ratio are used. All these experiments have clean stainless steel walls. It is to be expected that in the last two machines the surface generation is more effective than in the airy PLEXIS machine. This on itself provides already an indication of the significance of surface plasma interaction for molecule generation.

The flow patterns in the vessel leading to the recirculation flows, depicted in Fig. 4.1, influence the plasma-surface interactions as they determine the effective area exposed to the fluxes of radicals. Due to the recirculation flows, the complete wall of HNO and Depo II is exposed to a high flux of reactive radicals. On the other hand, PLEXIS has an effective length of around 2 meters, which is a factor of 4 longer in comparison with HNO. In that case, not one recirculation pattern, but more recirculation patterns may exist along the length of PLEXIS [31].

It is evident that in PLEXIS, the loss of chemistry may be faster than in the relatively short Depo II and HNO experiments. Also the S/V ratio of the Depo II (14 m^{-1}) and HNO (16 m^{-1}) machines is roughly a factor 3 larger than that of PLEXIS (4 m^{-1}). We will later see, that the effectivity of molecule production is correspondingly smaller in PLEXIS compared to the Depo II and HNO experiments.

In this respect also a difference in location of arrival of radicals may play a role. Hydrogen atoms diffuse more readily out of the plasma beam and arrive at surfaces closer to the source, whereas the heavier N atoms will arrive more at the downstream side. Also this "mass-defocusing" effect may be more serious in the long PLEXIS machine than in the shorter other experiments. But as mentioned before, we will first discuss the results obtained in PLEXIS and later return to this issue.

4.2.2 Diagnostics

Mass spectrometry

Depo II and HNO were equipped with a mass spectrometer for mass spectrometry measurements of the stable species present in the background of the plasma. In

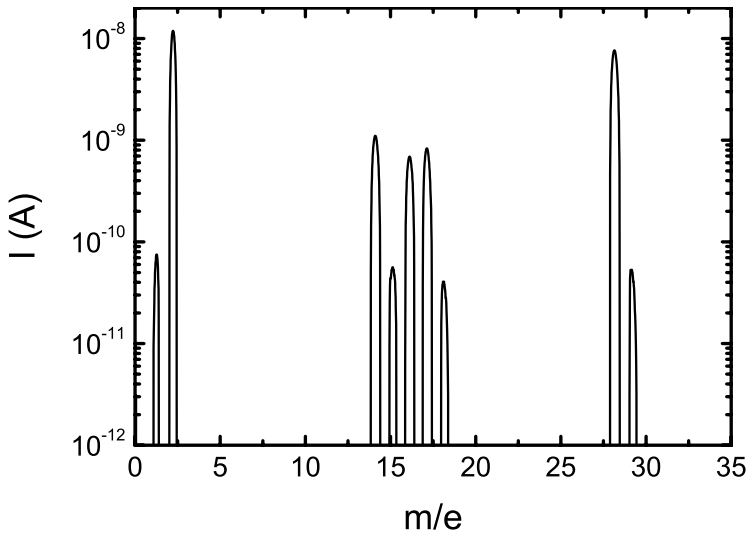

Figure 4.2: Mass scan as measured in expanding N_2–H_2 plasmas (HNO set-up). Both nitrogen and hydrogen were applied through the arc (0.8 slm N_2 and 1.2 slm H_2). The arc current was 55 A; the background pressure was kept constant at 20 Pa. NH_3 (m/e $= 15, 16, 17$), N_2 (m/e $= 14, 28, 29$) and H_2 (m/e $= 1, 2$) and H_2O (m/e $= 18, 17, 16$) are detected.

the case of Depo II, a residual gas analyzer (Balzers Prisma 200 Quadrupole RGA) was attached, with a pinhole to sample the gas in the reactor. HNO was equipped with a quadrupole mass spectrometer (Balzers QMS 421C) on top of the reactor and the mass spectra were measured by sampling the gas through a controlled all-metal regulating valve (UDV 035). The operating pressure in the mass spectrometer unit was in the 10^{-7} – 10^{-6} mbar range depending on the chamber pressure. The mass spectrometer unit was pumped to a pressure in the range of 10^{-5} to 10^{-9} mbar with two vacuum pumps in series, a turbo pump (Balzers TPU 180H, 180 litre/s) and a rotary vane pump (Edwards RV3, 3 m^3/h). Absolute concentrations of the stable gas species N_2, H_2 and NH_3 were obtained by calibrating the mass spectrometer signals by injecting the relevant gases into the chamber at various known pressures.

In Fig. 4.2, a typical mass scan, after background substraction, is shown as measured in a expanding N_2–H_2 plasma, with 0.8 slm (standard liter s^{-1}) N_2 and 1.2 slm H_2 flowing through the arc. The arc current was 55 A and the background pressure was 20 Pa. From the mass spectrometry measurements, we concluded that next to NH_3 (m/e $= 15, 16, 17$), N_2 (m/e $= 14, 28, 29$) and H_2 (m/e $= 1, 2$) and a small

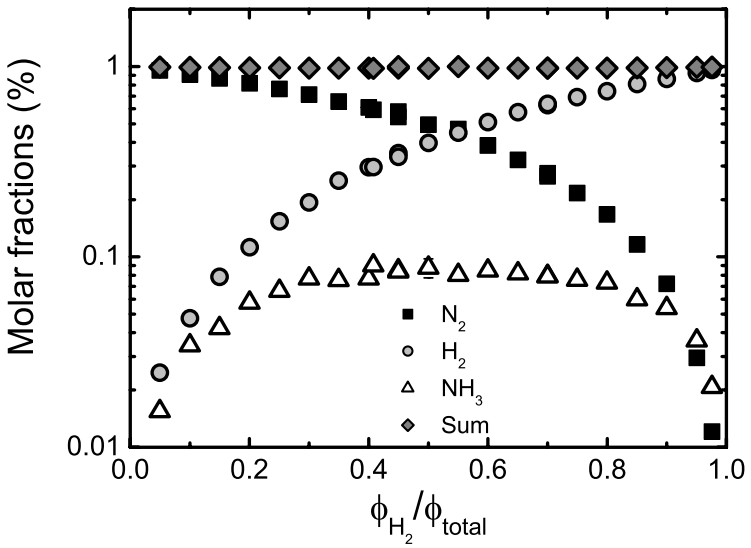

Figure 4.3: Relative amount of N_2, H_2, and NH_3 as measured by mass spectrometry as a function of the relative hydrogen flow rate in expanding N_2–H_2 plasmas (HNO set-up). Both nitrogen and hydrogen were applied through the arc at a total flow rate of 1 slm. The arc current was 55 A; the background pressure was kept constant at 20 Pa.

amount of H_2O (m/e $= 18, 17, 16$), no other species were present in the plasma. In particular, no significant amounts of N_2H_4 and of N_3H are found, confirming the generally observed dominance of NH_3 (and N_2 and H_2) generation.

To show that this is valid for all relative hydrogen flow rates, the resulting molar fractions of NH_3, and N_2 and H_2 are shown in Fig. 4.3, measured for a total flow of 1 slm (mass scan of Fig. 4.2 for 2 slm).

Cavity enhanced absorption spectroscopy

In PLEXIS, we measured the density of NH_3 with cavity enhanced absorption (CEA) spectroscopy [32]. CEA spectroscopy with this set-up has been performed previously to measure the ammonia generation in N_2-H_2 plasma [26], to study the ammonia spectrum in the 1.5 μm region [33], and to demonstrate the feasibility of open-path trace gas detection of ammonia with CEA [34].

The recorded ammonia spectra represented an average of 1000 scans, i.e. a measurement took about 30 s of acquisition time. After every measurement a spectrum

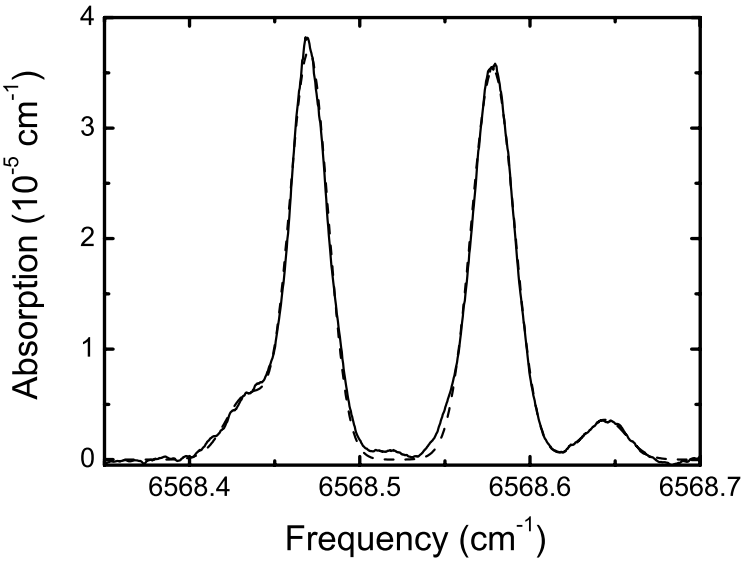

Figure 4.4: Typical NH_3 CEA spectrum measured in a vessel in which a N_2–H_2 plasma expands. The dashed line is a fit assuming four Gaussian line profiles. The plasma source was operated on a mixture of 0.8 slm N_2 and 1.2 slm H_2 and at an arc current of 55 A. The background pressure was 20 Pa.

was recorded without laser radiation coupled into the cavity to correct the ammonia spectra for the emission of the plasma. We note that the absorption spectrum over the full scanning range appears directly on the display of an oscilloscope in a fraction of a second. The recorded spectrum is a relative absorption spectrum expressed in loss of the empty cavity per round trip, i.e. $(1 - R)/d$. In contrast with cavity ring-down spectroscopy (CRDS) methods discussed in Chapters 2 and 3, the factor $(1 - R)/d$ can not directly be determined in this experimental configuration. The spectrum has to be put on an absolute scale by measuring this factor using pulsed CRDS or phase-shift cavity ring-down (PSCRD) spectroscopy or by recording the CEA spectrum of a known amount of a certain gas. We obtained the factor by recording the CEA spectrum of a known amount of water in the same frequency range as in which the ammonia transitions were measured. The H_2O transitions that were measured were the $6_{51} \leftarrow 5_{42}$ and the $6_{52} \leftarrow 5_{41}$ rotational transitions of the $(1,1,3) \leftarrow (0,0,0)$ vibrational band, and have integrated absorption cross-sections of 1.13×10^{-24} cm^{-1}/(molecule cm^{-2}) and 3.39×10^{-24} cm^{-1}/(molecule cm^{-2}), respectively [35]. Using these transition strength and the known density of

the ground-state water molecules of 2×10^{23} m^{-3}, the factor $(1 - R)/d$ was determined as $(5.5 \pm 0.5) \times 10^{-5}$ cm^{-1}. Since d was 1.1 m, a reflectivity of the mirrors of $R = 0.994 \pm 0.006$ was deduced from repeated measurements, which is in agreement with the manufacturer's specifications. The absolute absorption can be determined by using the formula:

$$\kappa(\nu) = \left(\frac{S_0(\nu)}{S(\nu)} - 1 \right) \left(\frac{1 - R}{d} \right), \tag{4.1}$$

where $S(\nu) = I_0 \tau$ is the time-integrated intensity with absorption in the cavity and $S_0(\nu) = I_0 \tau_0$ is the signal in an empty cavity, i.e. the baseline, with I_0 the laser intensity inside the cavity.

In Fig. 4.4, a typical ammonia spectrum as measured in an expanding N_2–H_2 plasma is shown. All CEA measurements have been performed at about 20 cm downstream from the exit of the arc. However, it was verified that the NH_3 density was not dependent on the measurement position in the plasma by shifting the arc source. We concluded that NH_3 is present in the background.

The observed transitions of ammonia in the wavelength region presented here are strong lines from the combination band $\nu_1 + 2\nu_4$ reported by Lundsberg-Nielsen et al. [36]. Of the four transitions shown in Fig. 4.4, three are reported in literature with the line positions 6568.299, 6568.401, and 6568.463 cm^{-1}, and absorption coefficients, 7.556×10^{-4}, 7.602×10^{-4}, and 0.948×10^{-4} cm^{-1} Torr^{-1}. The shoulder on the left side of the first transition has been reported by Peeters et al. [34], but was not used in our data analysis since its absorption coefficient is not known.

Tunable diode laser absorption spectroscopy

In PLEXIS, we also detected NH_3 in the downstream plasma by tunable diode laser absorption spectroscopy (TDLAS) at 70 cm from the plasma source. The infrared multi-component acquisition (IRMA) system of the INP institute in Greifswald consists of four independent tunable diode lasers, which can be multiplexed. With this system, the mole fractions of several molecules can be simultaneously measured with millisecond time resolution. The laser beam from the IRMA system was directed twice through the vessel by the use of a retroreflector, to increase the path length and thus the sensitivity by a factor of two. Also it allowed the detectors to be located the same table of the IRMA system as the diode lasers.

The density of the produced NH_3 was monitored as function of various experimental parameters as the nitrogen and hydrogen flows, the background pressure in

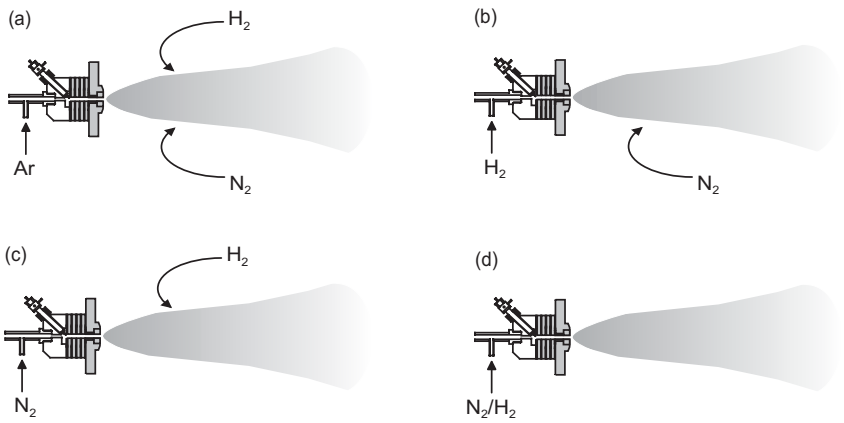

Figure 4.5: Schematic representation of the expanding plasma jet for the three types of plasmas: (a) Ar plasma to which mixtures of N_2 and H_2 were added in the background; (b) H_2 plasma with N_2 injected into the background; (c) N_2 plasma with H_2 injected in the background; (d) N_2–H_2 plasma.

the plasma vessel, and the arc current. The density of ammonia was observed via the transition at 770.914 cm^{-1} with the line strength 2.445×10^{-20} cm^{-1}/(molecule cm^{-2}). We should note, that also information on the temperature obtained by analysis of the Doppler width of the measured transitions, i.e T = 450 K, points to primarily presence of NH_3 in the background. The results of the TDLAS measurements were in agreement with the mass spectrometry measurements.

4.3 Results and discussion

We studied the ammonia generation in four different expanding plasmas generated from mixtures of nitrogen and hydrogen as schematic depicted in Fig. 4.5: (a) expanding Ar plasma to which mixtures of N_2 and H_2 were added; (b) expanding H_2 plasma to which N_2 was added; (c) expanding N_2 plasma to which H_2 was added; (d) expanding N_2-H_2 plasma. These plasma conditions were chosen to study the relation between the NH_3 production and the fluxes of atomic N and H radicals. In the conditions from (a) to (d), the amount of produced N and H atoms in the plasma increases and thus the flux of radicals towards the surface. In condition (a), the dissociation of N_2 and H_2 and thus the creation of N and H atoms can be controlled as the N and H radicals are produced in the plasma expansion by charge-transfer reactions.

In conditions (b) and (c), the fluxes of respectively H and N atoms is optimized by applying the gas through the plasma source, while respectively N_2 and H_2 molecules are admixed. In the final situation (d), both N_2 and H_2 are fed through the plasma source, creating a plasma beam of mainly N and H atoms. In this way, the dependence of the ammonia production on the plasma composition and the role of N and H atomic radicals can be studied.

4.3.1 Expanding Ar plasma with N_2 and H_2 injected in the background

In the first experimental situation, an expanding argon plasma was created with 3 slm argon applied through the arc, and nitrogen and hydrogen were injected downstream into the background of the vessel. These measurements were performed in PLEXIS, with a short nozzle installed in the plasma source. The characteristics of expanding Ar plasmas created with the cascaded arc source have been described extensively in literature [27] and here only the main issues will be discussed briefly. In the case of an expanding argon plasma, the plasma source emanates a partially ionized (12%) argon flow. The meta-stable argon density Ar_m^* formed in three particle recombination processes of the argon ions is typically a factor of 10 lower than the argon ion density [37] and we neglect the contribution of these states to the plasma chemistry. Molecules injected in the background mix with the recirculating flow of which a part invades in the expanding plasma beam. These molecules are dissociated by charge-transfer reactions with argon ions from the plasma source followed by dissociative recombination leading to atomic N and H radicals:

$$\mathrm{Ar^+ + N_2 \longrightarrow Ar + N_2^+} \qquad k \approx 2\times10^{-16}\ \mathrm{m^3\,s^{-1}}, \qquad [38] \qquad (4.2)$$

$$\mathrm{Ar^+ + H_2 \longrightarrow ArH^+ + H} \qquad k = 1.1\times10^{-15}\ \mathrm{m^3\,s^{-1}}, \qquad [39] \qquad (4.3)$$

$$\mathrm{N_2^+ + e \longrightarrow N^* + N} \qquad k \approx 10^{-13}\ \mathrm{m^3\,s^{-1}}, \qquad [38] \qquad (4.4)$$

$$\mathrm{ArH^+ + e \longrightarrow Ar + H} \qquad k \approx 10^{-13}\ \mathrm{m^3\,s^{-1}}. \qquad [39] \qquad (4.5)$$

In Fig. 4.6, the measured ammonia density as function of the hydrogen flow rate relative to the total flow rate of nitrogen and hydrogen is depicted for three different conditions as measured by TDLAS on the PLEXIS setup. In two conditions an Ar flow of 3 slm was applied through the arc at an arc current of 55 A, and a total flow of nitrogen and hydrogen of 0.3 slm was injected in the background. The two conditions only differ in the value of the background pressure, i.e. 20 versus 100 Pa. At 55 A, the Ar flow is partially ionized (12%), i.e. an Ar^+ ion flow of 0.36 slm, as determined from Langmuir probe measurements in the argon expansion [40], is

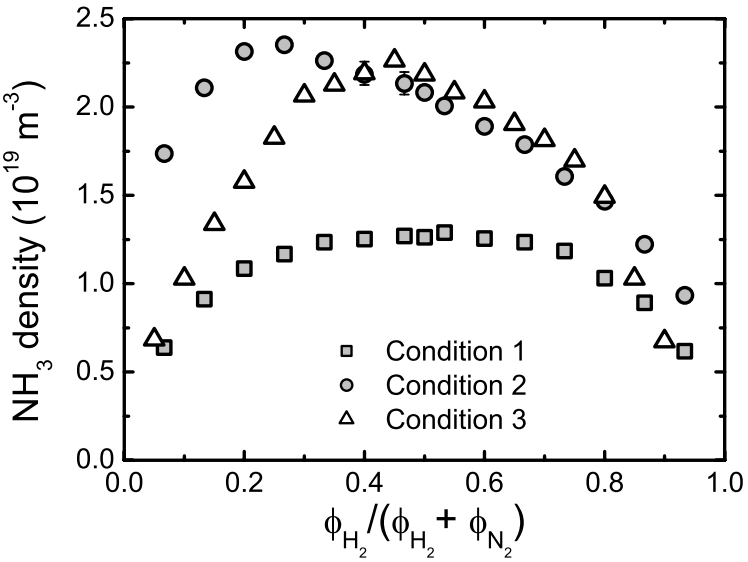

Figure 4.6: Ammonia density in expanding Ar plasmas with N_2 and H_2 injected in the background. In conditions 1 and 2, the argon plasma was created with a flow of 3 slm Ar flowing through the arc. Simultaneously, a mixture of N_2 and H_2 molecules was admixed into the background of the vessel with a total flow rate of 0.3 slm. The arc current was set at 55 A; the background pressure was 20 Pa in condition 1 and 100 Pa in condition 2. In condition 3, the argon plasma was created with a flow of 5 slm Ar flowing through the arc, while $\phi_{N_2} + \phi_{H_2} = 0.5$ slm. The arc current was set at 75 A; the background pressure was 20 Pa.

injected into the vessel. Thus the Ar^+ ion flow is approximately equal to the total injected flow of N_2 and H_2 molecules, thus a significant dissociation can be expected. In the third condition, an Ar flow of 5 slm was applied through the arc at an arc current of 75 A, and a total flow of nitrogen and hydrogen of 0.5 slm was injected in the background at a constant pressure of 20 Pa. In this case, the Ar^+ ion flow was 0.65 slm, i.e. $\phi_{Ar^+} \approx \phi_{N_2} + \phi_{H_2}$. The ammonia density in the third condition is a factor 1.8 higher compared to condition 1, which shows that the ammonia production is determined by the dissociation of the injected N_2 and H_2. The maximum in ammonia density is not observed at the stoichiometric ratio of H_2 and N_2 in NH_3, but at lower fractions of H_2. The reason for this is that the Ar^+ ions are needed for the dissociation of both nitrogen and hydrogen molecules. Meulenbroeks et al. [39] have shown that the presence of small amounts of hydrogen in expanding plasmas,

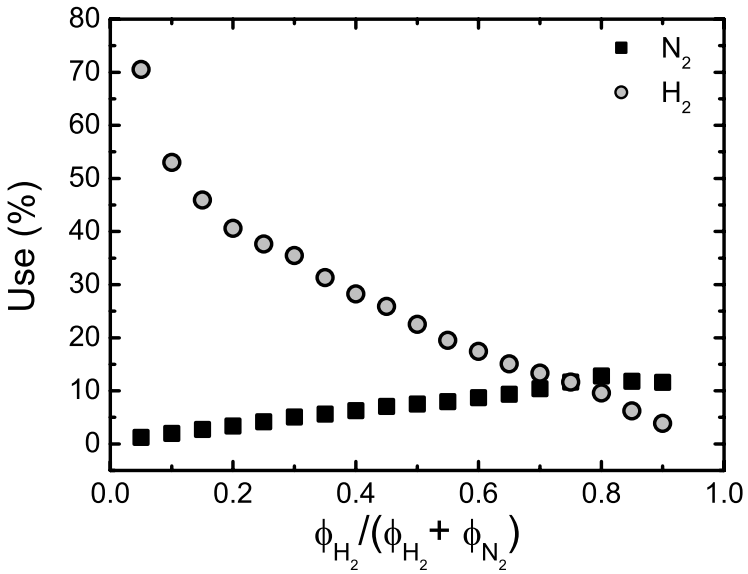

Figure 4.7: The use of N_2 and H_2 in condition 3 of Fig. 4.6 as a function of the relative hydrogen flow rate.

leads to a strong decrease in the ionization degree of the plasma expansion. Also in this plasma, the charge-transfer reaction of Ar^+ with molecular hydrogen is 5 times faster than the reaction with molecular nitrogen (reaction (4.2) versus (4.3)). This means that less nitrogen is dissociated in the presence of hydrogen. The optimal N to H ratio leading to maximum NH_3 production is therefore already reached at lower hydrogen flows.

At 100 Pa, the maximum in ammonia production shifts to even lower hydrogen flows. At this higher pressure, the charge-transfer reaction of Ar with H_2 is faster, so now even at lower relative hydrogen flows, the ions are already almost completely consumed by hydrogen molecules. Thus at higher relative hydrogen flows smaller amounts of atomic nitrogen are formed. The optimum ratio between N and H atoms at the surface to form ammonia is therefore already reached at lower hydrogen flows.

Since only NH_3, N_2 and H_2 (besides Ar), are present in the plasma (Sec. 4.2.2), the use of N_2 and H_2 to form NH_3 can be calculated from Fig. 4.6. The use of $N_2(H_2)$ is defined as the amount of N(H) atoms in the formed NH_3 divided by the amount of N(H) atoms admitted to the system in the form of $N_2(H_2)$. The use of H_2 and N_2 gas for the plasmas is plotted in Fig. 4.7 as a function of the relative hydrogen flow for the third condition. At small hydrogen flows, the fraction of the admitted

H_2, which is used for NH_3 formation increases to 70%. On the other hand, the use of nitrogen at small nitrogen flows, thus high hydrogen flows, is always below 15%. This discrepancy can be explained by the fact that the dissociation of nitrogen decreases in the presence of hydrogen.

4.3.2 Expanding H_2 plasma with N_2 injected in the background

The plasma source was operated on 2 slm H_2 at an arc current of 55 A. The background pressure in the experiments was 20 Pa. Simultaneously, 0 – 1.5 slm N_2 was injected downstream. Under this experimental condition no ammonia was detected with the CEA technique in PLEXIS. From the detection limit of our CEA setup we conclude that less than 10^{18} m^{-3} ammonia is produced. The reason for this is that under this plasma condition only very few ions leave the source and thus N atoms can only be produced by the reaction [30]:

$$H + N_2 \longrightarrow NH + N \qquad k = 2.7 \times 10^{-17} T^{0.5} \exp\left(\frac{-75900}{T}\right) \ m^3\,s^{-1}. \tag{4.6}$$

However, this reaction is too endothermic to be effective. The conclusion that can be drawn from these results is that for the production of ammonia both H_2 and N_2 needs to be dissociated and thus H atoms and N atoms are essential. Also, the surface of the plasma vessel, most probably saturated with H atoms, does not act as a catalyst to dissociate nitrogen molecules.

4.3.3 Expanding N_2 plasma with H_2 injected in the background

In PLEXIS, the ammonia generation in expanding argon plasmas to which nitrogen and hydrogen were admixed was hampered by the amount of N radicals produced in the plasma (Sec. 4.3.1). To increase the amount of N radicals, a better approach is to generate an expanding nitrogen plasma and adding hydrogen downstream into the plasma. In a pure nitrogen plasma, the dissociation degree of N_2 in the arc is expected to be up to 35%, while an ionization degree of around 1 – 5% is reached [24, 28]. The densities of the meta-stable N atoms, $N(^2P)$ and $N(^2D)$, emanating from the plasma source are expected to be at maximum in the order of 20% of the $N(^4S)$ atoms (assuming a thermal population at a temperature of 1 eV). In the expansion, the $N(^2D)$ and $N(^2D)$ densities decrease due to de-excitation by collisions with electrons, $N(^4S)$ atoms, N_2 molecules and the nozzle wall. De-excitation will also limit the densities of meta-stable N atoms produced in the expansion by disso-

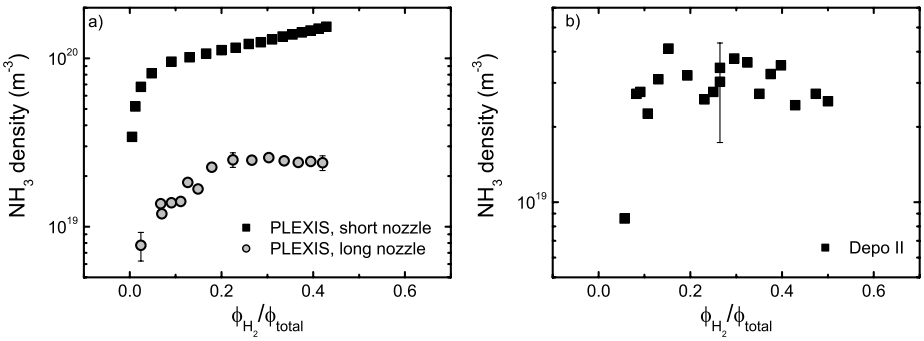

Figure 4.8: Ammonia density in expanding N_2 plasmas with H_2 injected in the background. a) The nitrogen plasma was created with a flow of 2 slm in PLEXIS flowing through the arc. Simultaneously, hydrogen molecules were admixed into the background of the vessel with a flow rate of 0 – 1.5 slm. The arc current was set at 55 A; the background pressure was 100 Pa. b) The nitrogen plasma in Depo II was created with 1 slm N_2 while the other conditions were the same. The background pressure was 20 Pa.

ciative recombination of N_2^+ with electrons. Note that the maximum production via N_2^+ would be limited by the ionization degree of the plasma.

The ammonia density as measured in PLEXIS is plotted in Fig. 4.8a) as a function of the hydrogen flow rate relative to the total flow rate. The ammonia densities in PLEXIS with a long (length of $L = 14$ mm) and a short nozzle ($L = 7$ mm) were measured by CEA spectroscopy and TDLAS, respectively. In both cases the calibrations were verified with mass spectrometry. In the experiments, the plasma source was operated on 2 slm N_2 at an arc current of 55 A. Simultaneously, hydrogen molecules were admixed into the background of the vessel with a flow rate of 0 – 1.45 slm. The downstream pressure was kept constant at 100 Pa.

With long nozzle installed the ammonia density increased with increasing hydrogen flow and saturated at a level of 2.5×10^{19} m^{-3} for relative hydrogen flows larger than 0.26 (Fig. 4.8a). This means that at $T = 600$ K, which is determined from the Doppler width of the measured ammonia transitions, 0.2% of the background gas is ammonia. For the short nozzle the NH_3 density becomes a factor of 5 higher. Also the relative use of hydrogen at low flows increases. This must be ascribed to a higher dissociation degree of the N_2 gases injected in the source.

The saturation of the ammonia density can be explained by noting that the hy-

drogen molecules, which are injected in the background, can only be dissociated by N atoms and N^+ ions emanating from the arc. Vankan et al. [26] explained the ammonia production in these plasmas by the fact that hydrogen molecules can efficiently be dissociated by charge-transfer reactions with N^+ followed by dissociative recombination [30]:

$$N^+ + H_2 \longrightarrow NH^+ + H \qquad k = 5.4 \cdot 10^{-16}\ m^3\,s^{-1} \tag{4.7}$$

$$NH^+ + e \longrightarrow N + H \qquad k \approx 10^{-13}\ m^3\,s^{-1}, \tag{4.8}$$

producing two H atoms and one N atom, all of which can be used for the production of ammonia. As was suggested in Chapter 3, the reaction between nitrogen ions and hydrogen molecules could also result in NH radicals and H ions:

$$N^+ + H_2 \longrightarrow NH + H^+. \tag{4.9}$$

However, in Chapter 3, it has been shown that mainly N atoms are responsible for the dissociation of H_2 resulting in NH radicals [30]:

$$N + H_2 \longrightarrow NH + H, \tag{4.10}$$

which has a rate constant of $1 \times 10^{-16}\ m^3\ s^{-1}$ in these experiments (see Chapter 3). This is underlined by the observation that a shorter nozzle results in more ammonia production. The production of H containing radicals (H, NH) will increase until all N atoms and N^+ ions are consumed limited by the time these reactions can take place. This also explains the saturation, as adding more H_2 molecules does not lead to the production of more H atoms, and thus no extra NH_3 is produced. It can be argued that due to abstraction reactions of NH with N and H atoms, finally at the surfaces mainly the resulting N and H atoms play a key role in the generation of ammonia.

It was proven in previous experiments by Vankan et al. [41] that in pure expanding H_2 plasmas the use of a short nozzle results in a 10 times higher atomic H flux. This is because the main loss channel for atomic hydrogen is surface recombination on the nozzle surface. By shortening the length of the nozzle, the surface area is reduced and thus the atomic flux is increased. Although we did not measure the atomic N flux in pure nitrogen plasmas produced using the short nozzle, we assume that this loss mechanism is similarly important for the nitrogen atoms since the ammonia increased by using a short nozzle. This conclusion must be drawn, despite the fact that the reported values of loss probability of H and N atoms on copper differ appreciably. The loss probability of H atoms and N atoms on copper surfaces is reported to be 0.3 to 0.5 [42, 43] and 3.9×10^{-2} to 8.5×10^{-4} [44, 45], respectively.

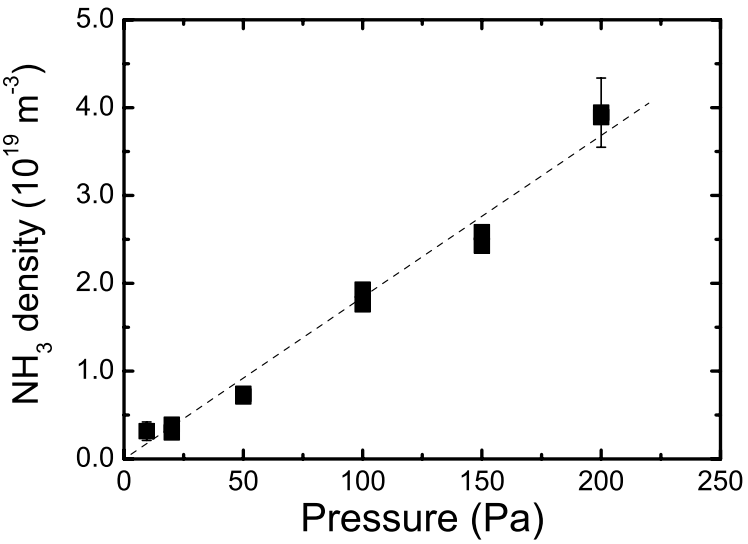

Figure 4.9: Ammonia density as a function of the background pressure in the vessel as measured with CEA spectroscopy. The plasma is created with 2 slm N_2 flowing through the arc at an arc current of 55 A and 0.45 slm H_2 injected in the background.

In Depo II, the ammonia density was measured with mass spectrometry in the conditions in which also the NH radicals have been measured (see Chapter 3). The ammonia density with long nozzle installed, operated at 1 slm N_2 and a constant pressure of 20 Pa, saturated at a level of 3×10^{19} m^{-3} for relative hydrogen flows larger than 0.13 (Fig. 4.8b). This means that 0.6% of the background gas was ammonia. The ammonia density in PLEXIS saturated at twice the relative hydrogen flow, because the initial nitrogen flow is also twice as large, leading to twice as much N atoms and N^+ ions. From the measurements presented in Chapter 3, we determined that the flux density of the NH radicals in the plasma beam at 10 cm from the nozzle exit is about 6×10^{21} m^{-2} s^{-1}, which corresponds to a flow of about 5×10^{19} NH radicals/s, i.e. a flow of 2 sccs. In reaction 4.10, next to NH also H atoms are produced. This means that in the residence time of 0.2 seconds, about 2×10^{19} H atoms can arrive at the surface. This would result in 7×10^{18} NH_3 molecules in the residence time. The amount of ammonia molecules in the residence time is 1.5×10^{18}. This indicates that an efficiency of 20% procent is achieved in the experiments.

At the condition of 0.45 slm H_2 injected in the background, the ammonia density was measured as function of the background pressure from 10 to 200 Pa as shown in Fig. 4.9. The measured ammonia density shows a linear dependence on pressure.

This can be explained in the following way. Assume that only N and H atomic radicals are involved in the production of ammonia. The H atoms are mainly produced by the reaction between N atoms and H_2 molecules. The atomic N flow is only dependent on the cascaded arc source parameters and remains thus constant, when the pressure in the vessel is changed. This means that the amount of H produced in the experiments is independent of pressure. The total amount of NH_3 formed is then also constant, but its residence time in the vessel increases with increasing pressure, i.e. $n_{NH_3} \propto \tau$. And since τ is linearly dependent on the pressure in the vessel, the ammonia density should also increase linearly with increasing pressure. Furthermore, this indicates that three particle reactions are not responsible for the ammonia production, because the ammonia density would then show a stronger than linear dependence on the pressure, which is not observed. Moreover, under all conditions, the density of ammonia proved to be independent of the axial and lateral position in the plasma jet at which the CEA spectrum was taken. This shows that ammonia is not produced in the expanding plasma jet. All this evidence points to the conclusion that ammonia is mainly produced at the vessel wall.

4.3.4 Expanding N_2–H_2 plasma

In the previous section (Sec. 4.3.3), the ammonia generation was limited by the amount of H radicals produced in the plasma by the dissociation of H_2 by N atoms form the source. To optimize the dissociation of both nitrogen and hydrogen, the plasma in the fourth experimental situation was produced with both nitrogen and hydrogen fed through the plasma source. The experiments were performed on all three plasma reactors, which all had clean stainless steel walls. In HNO and PLEXIS the total flow was 2 slm, and in Depo II the total flow was 1 slm. The current through the arc was set at 55 A and the downstream pressure was kept constant at 20 Pa. In the experiments, the hydrogen flow rate relative to the total flow rate was varied. The plasma contains mainly nitrogen and hydrogen atoms and molecules, since most of the ions (N^+, H^+) are lost very fast - most probably even faster than in the previous case as now H_2 is already present in the source - via charge-transfer reactions with hydrogen molecules in the beginning of the expansion.

In Fig. 4.10, the ammonia molar fractions as function of the hydrogen flow rate relative to the total flow rate as was measured in the N_2–H_2 plasmas in the three setups is plotted. In case of HNO and Depo II, the ammonia density was measured with mass spectrometry. The ammonia densities in PLEXIS in the experiments with

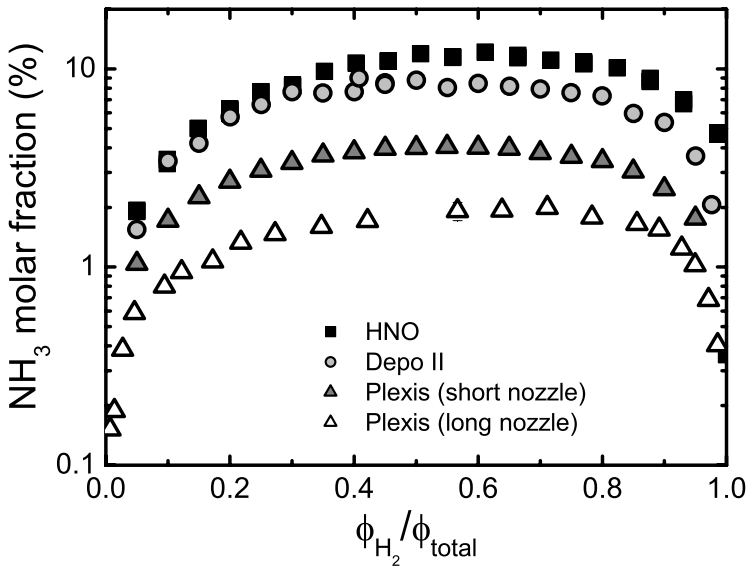

Figure 4.10: Relative amount of ammonia as a function of the relative hydrogen flow rate in expanding N_2–H_2 plasmas. Both nitrogen and hydrogen were applied through the arc. In PLEXIS and HNO at a total flow rate of 2 slm and in Depo II at a total flow rate of 1 slm. The arc current was 55 A; the background pressure was kept constant at 20 Pa.

the long and short nozzles were measured by CEA spectroscopy and TDLAS, respectively. The maximum ammonia molar fraction increased from 2% in PLEXIS to about 10% in Depo II and HNO. The normalized NH_3 molar fractions are plotted in Fig. 4.11, which shows that the trend of ammonia as a function of the hydrogen flow rate relative to the total flow rate is the same in all set-ups. Only the absolute amounts differ: the production is the largest in HNO and Depo II, the two smaller volume machines and the smallest in PLEXIS, with the large long volume. This is in agreement with the remarks made in 4.2.1 that we expected that the ammonia density is dependent on the "active" surface to volume ratio and should be the highest in HNO and Depo II, and to be the lowest in PLEXIS. This is again in line with the picture that the ammonia is generated via plasma-surface interactions.

The maximum ammonia production is not observed at the stoichiometric ratio of hydrogen and nitrogen in ammonia. This is a priori not to be expected, since the dissociation degree of the plasma source for different flow ratios of N_2 and H_2 could change a lot. For expanding N_2–H_2 plasma the ammonia density increased

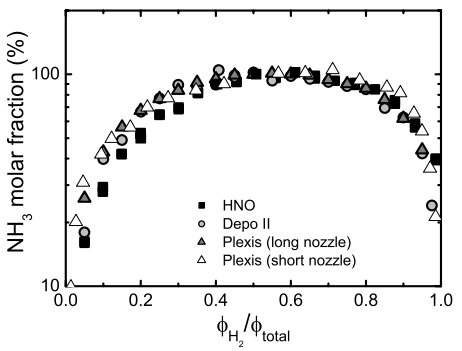

Figure 4.11: Normalized ammonia molar fraction as a function of the relative hydrogen flow rate in expanding N_2–H_2 plasmas

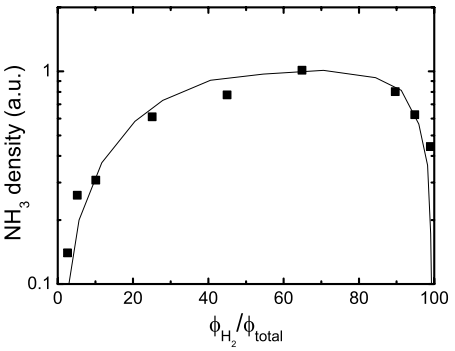

Figure 4.12: NH_3 density (in relative units) as function of the relative hydrogen flow rate in a low-pressure (2 Torr) flowing discharge. Reproduced from Fig. 6 of [15]. The curve presents a self-consistent model in which it is assumed that NH_3 is mainly produced at the surface of the vessel.

by a factor 2 in PLEXIS, when the long nozzle was replaced by a short nozzle. The same reasoning as mentioned in Section 4.3.3 is also applicable to expanding N_2–H_2 plasmas for the N and H fluxes in these plasmas. We can again only state that the increase in ammonia generation with the short nozzle is in agreement with an increase of N and H fluxes. Furthermore, this shows that the ammonia in the plasma chamber does not originate from plasma-surface interactions at the nozzle wall, but from the surface in the vessel. Because then a decrease in the NH_3 generation would have been observed.

The trend of the ammonia molar fraction as function of the hydrogen flow rate relative to the total flow rate as shown in Fig. 4.10, is generally observed in N_2–H_2 plasmas (r.f, microwave, barrier discharge, low-pressure D.C. flowing discharge) [9, 46, 47]. The measured relative NH_3 density as a function of the H_2 percentage in a low-pressure N_2–H_2 flowing discharge as measured by Gordiets et al. [15] is depicted in Fig. 4.12. Also depicted in this figure is the result of a self-consistent model in which it is assumed that NH_3 is mainly produced at the surface of the vessel by the stepwise addition reactions between adsorbed nitrogen and hydrogen containing radicals at the surface and incoming atomic N and H radicals [15]. Their proposed reaction mechanism at the surface was validated by others [17, 18] and can

be simplified as follows:

$$\mathrm{N(s) + H \longrightarrow NH(s)} \tag{4.11}$$

$$\mathrm{H(s) + N \longrightarrow NH(s)} \tag{4.12}$$

$$\mathrm{NH(s) + H \longrightarrow NH_2(s)} \tag{4.13}$$

$$\mathrm{NH(s) + H_2 \longrightarrow NH_3(s) \longrightarrow NH_3(g)} \tag{4.14}$$

$$\mathrm{NH_2(s) + H \longrightarrow NH_3(s) \longrightarrow NH_3(g)} \tag{4.15}$$

From the similarity of Fig. 4.12 with our measurements, we conclude again that also in the present experiments ammonia is formed at the surface through plasma-surface interactions, with the same reaction mechanism.

Influence of surface material on ammonia production

To investigate the influence of the wall material of the plasma reactor on the ammonia production in expanding N_2–H_2 plasma, we measured the ammonia density in a clean stainless steel vessel and with a 1 μm a–SiN_x layer deposited on the reactor wall in Depo II. For the a–SiN_x deposition, the arc was operated on pure Ar with a flow of 55 sccs at an arc current of 45 A with a typical voltage of 40 V. A flow of 17 sccs NH_3 was injected through the nozzle and 2.5 sccs SiH_4 was injected through a ring situated 10 cm downstream from the nozzle. The deposition time was 2'30". The ammonia molar fraction as deduced from mass spectrometry measurements, as a function of the relative hydrogen flow rate proves to be the same for both wall materials (Fig. 4.13). This indicates that the ammonia production is independent of the wall material. This seems to be in contrast to experiments of various research groups in the world in which it was shown that the ammonia production is dependent on the type of wall material [9–13]. However, a major difference with our experiments is that in those experiments the wall is used to form adsorbed nitrogen atoms by the dissociative adsorption of excited N_2 molecules or nitrogen molecular ions. The adsorbed nitrogen atoms react with impinging hydrogen atoms or molecules formed in the plasma. In our experiments, the N and H radicals are already produced in the plasma source and as a result the fluxes of N and H radicals to the surface are around 10^{21} m^{-2} s^{-1} [23], which is one order of magnitude higher than in the other experiments. One has observed an increase of the N density in the plasma beam when a–SiN_x is deposited on the walls of Depo II. This seems to suggest that less nitrogen is adsorbed at the wall [48], but it could also be caused by a slightly less generation of

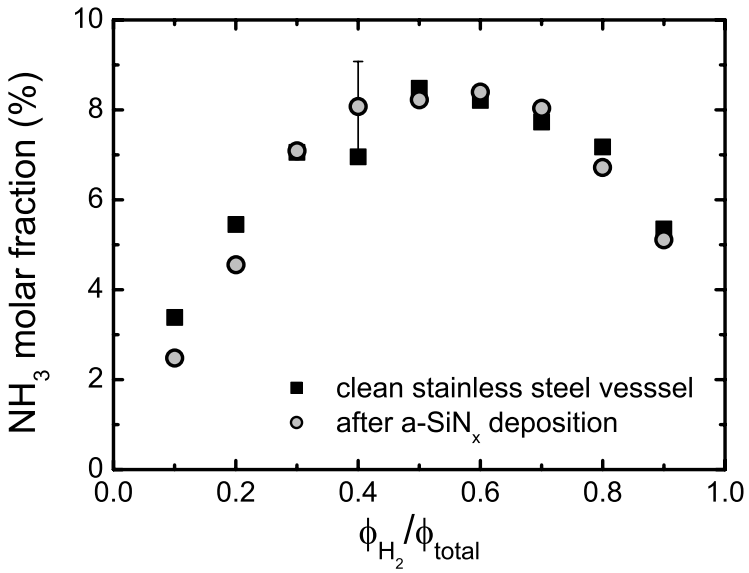

Figure 4.13: Ammonia molar fraction as a function of the relative hydrogen flow rate as measured by mass spectrometry in expanding N_2–H_2 plasmas with and without SiN deposited on the reactor wall. Both nitrogen and hydrogen were applied through the arc at a total flow rate of 1 slm. The arc current was 55 A; the background pressure was kept constant at 20 Pa.

H_2 leaving more ions to dissociate N_2. The effect of a–SiN_x on the atomic H radicals has not been studied.

We measured that the ammonia molar fraction is independent of the wall material, which indicates that the amount of N at the surface is not a limiting factor in the ammonia production and that the H flux to the surface is most likely not changed by a a–SiN_x deposited wall. The high N and H flux to the surface leads to a surface covered with N and H radicals and other molecular radicals. This coverage passivates the surface, i.e. it is more or less independent of the actual wall material. Then, the actual chemistry may take place in an additional layer at the passivated surface. The presence of weakly bonded radicals at a surface was previously suggested by Gordiets et al. [49] to explain the NO production in N_2–O_2 plasmas, by Gelb et al. [50] to explain atomic recombination on surfaces and was observed in ammonia decomposition experiments on ruthenium [51].

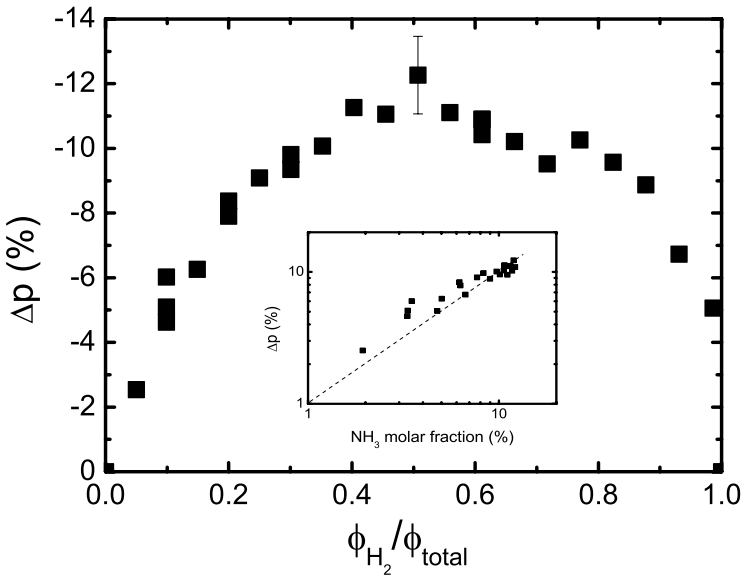

Figure 4.14: Relative decrease of the pressure in the vessel as a function of the relative hydrogen flow rate as measured in expanding N_2–H_2 Both gases were applied through the arc with a total flow of 2 slm at an arc current of 55 A. The starting background pressure was 22 Pa for a pure nitrogen plasma. The inset shows the relative decrease in pressure as a function of the ammonia molar fraction as measured by mass spectrometry.

Pressure decrease

In most experiments discussed until now in this chapter, the pressure was kept constant while the hydrogen flow rate relative to the total flow rate was changed. In experiments with a constant flow through the plasma source, constant pumping speed, assuming a constant temperature, and no change in the amount of particles in the vessel, one expects a constant pressure in the vessel. In our experiments, in which N_2 and H_2 mixtures are used as gas mixture in the plasma source, ammonia is formed. Consider the production of ammonia from nitrogen and hydrogen by the reaction: $N_2 + 3H_2 \rightarrow 2NH_3$. This means that if two molecules of NH_3 are formed from one N_2 molecule and three H_2 molecules, the total number of molecules decreases with two. Since the pressure in the vessel is linearly dependent on the number of molecules, we should observe a pressure decrease in the vessel with the same trend as in Fig. 4.10. With a starting background pressure of 22 Pa for a pure nitrogen plasma, a

relative pressure decrease was found with a maximum of 11% in HNO for expanding N_2–H_2 as shown in Fig. 4.14. The observed pressure change occurred only when the plasma source was operated on a mixture of N_2 and H_2; the pressure was observed to remain constant at 22 Pa for the pure hydrogen and nitrogen plasmas. This decrease is not due to the pumping system as the pumping capacity is constant and independent of the gas type. Secondly, it is not caused by a temperature change, because the pressure is observed to change almost instantaneously after adjustment of the flows. The relative decrease in pressure is proportional to the ammonia molar fraction as measured by mass spectrometry with a slope 1 (see inset Fig. 4.14), which validates the calibration and that indeed more than 10% of the total background pressure is ammonia.

Efficiency of the ammonia generation

As only NH_3, N_2 and H_2, are present in the plasma (Sec. 4.2.2), the use of N_2 and H_2 must be equivalent to the amount of gas needed to produce NH_3. The use and thus use of N_2 and H_2 gases as determined from the mass spectrometry measurements in HNO are plotted in Fig. 4.15. The results at low flows of N_2 and H_2 indicate that the minority gas is almost fully dissociated, i.e a dissociation degree of at least 60% for H_2 gas and 48% for N_2 gas. This means that about 10^{20} atomic N and H radicals per second arrive at the reactor wall at which they will react with particles at the surface. That in HNO 11% of the background gas is ammonia, is a remarkable result if one compares this with the total ammonia that could have been produced in our experimental conditions.

Let us assume that a dissociation degree of 60% for H_2 and 48% for N_2 gas are applicable over the whole range of the hydrogen flow rate relative to the total flow rate of nitrogen and hydrogen. Furthermore, we assume that all H and N atoms are used to produce ammonia, i.e. 3 H atoms per 1 N atom, only limited by the availability of one of the atomic radicals. The maximum ammonia molar fraction that could have been generated in the experiments would have been 30% at a relative hydrogen ratio of 0.7. This means that an efficiency in the ammonia generation of 33% is achieved in our experiments.

The use of H_2 and N_2 can be made plausible in a picture that at the passivated (stainless steel) surface only H atoms, N atoms and NH_x ($x = 1, 2$) radicals can be present. At small hydrogen fractions the surface will then only be covered with N and NH_x radicals. Incoming N radicals form N_2 molecules by association with N

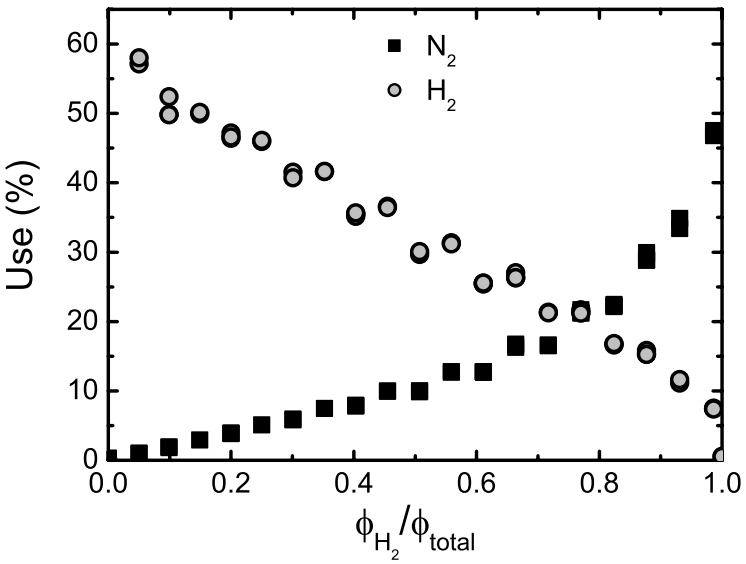

Figure 4.15: The use of N_2 and H_2 as a function of the relative hydrogen flow rate as measured in expanding N_2–H_2 plasmas by mass spectrometry. Both gases were applied through the arc with a total flow of 2 slm at an arc current of 55 A.

atoms on the surface or adsorb at surface sites. The few H atoms impinging at the surface will readily form NH_x radicals and finally NH_3 which desorbs. With increasing hydrogen flows, the H-coverage on the surface increases. Then, the H atoms impinging at the surface are more and more converted back into H_2 molecules or adsorb at surface sites or are used to form NH_x radicals. The N-atom flux towards the surface decreases with increasing hydrogen flow. As a result, the N atoms impinging on the surface react mainly with H atoms on the surface leading to NH radicals on the surface. These are quickly hydrogenated by the incoming H atom flux. This results in an increasing use of N_2. The above picture is in agreement with the general proposed reaction mechanism for the ammonia production at the surface in N_2–H_2 plasmas [15, 17, 18], but also in surface studies related to catalysis [6, 7, 52–54]. In conclusion, ammonia is mainly produced by association of atomic and molecular radicals at the surface, i.e. by the successive hydrogenation of adsorbed nitrogen atoms and the intermediates NH and NH_2 at the surface of the plasma reactor.

4.4 Conclusions

We studied the ammonia generation in four different types of expanding plasmas containing mixtures of nitrogen and hydrogen. In these experiments the plasma acts as catalyst to dissociate the precursor molecules and the surface is then exposed to large fluxes of atomic and molecular radicals. The efficiency and formation mechanisms of ammonia generation were determined under various plasma conditions and in three similar plasma reactors, with different geometries. Three diagnostic techniques, i.e. mass spectrometry, cavity enhanced absorption spectroscopy and tunable diode laser absorption spectroscopy, were employed to measure the ammonia density.

We have shown that the ammonia production is strongly dependent on the fluxes of N and H and probably NH_x radicals to the surface. The ammonia density was the highest in the plasma reactor with the highest "active" surface to volume ratio a relatively small volume. By using an atomic nitrogen and hydrogen source, ammonia can be formed efficiently, i.e. more than 10% of the total background pressure is measured to be ammonia. The ammonia production proved to be independent of wall material. The explanation is that the high fluxes of N and H radicals in our experiments are two orders of magnitude higher. This results in a passivated surface, covered with N, H and NH and NH_2 radicals. The presence of an additional layer at a passivated surface could then play a role in the formation of ammonia at the surface. Our results for N_2–H_2 plasma are in agreement with reported trends in literature, which were explained by the production of ammonia at the surface through plasma-surface interactions. We therefore conclude that ammonia is formed via plasma-surface interactions by stepwise addition reactions between adsorbed nitrogen and hydrogen containing radicals at the surface and incoming atomic H radicals, i.e. by the successive hydrogenation of adsorbed nitrogen atoms and the intermediates NH and NH_2 at the surface of the plasma reactor.

We note that by using two different cascaded arc plasma sources, one operated on H_2 and optimized to produce most efficiently H atoms and one operated on N_2 delivering N atoms would probably result in an even higher ammonia production.

Bibliography

[1] K. Tamaru, in *Catalytic Ammonia Synthesis*, edited by J.R. Jennings, page 1, Plenum, New York (1991).

[2] V. Smil, *Detonator of the population explosion*, Nature **400**, 415 (1999).

[3] M.D. Fryzuk, *Ammonia transformed*, Nature **427**, 498 (2004).

[4] S.R. Tennison, in *Catalytic Ammonia Synthesis*, edited by J.R. Jennings, page 303, Plenum, New York (1991).

[5] K. Aika, *Heterogeneous catalysis of ammonia synthesis at room temperature and atmospheric pressure*, Angew. Chem. Int. Ed. Engl. **25**, 558 (1986).

[6] G. Ertl, in *Catalytic Ammonia Synthesis*, edited by J.R. Jennings, page 109, Plenum, New York (1991).

[7] C. Zhang, Z.-P. Liu, and P. Hu, *Stepwise addition reactions in ammonia synthesis: A first principles study*, J. Chem. Phys. **115**, 609 (2001).

[8] O. Nomura, H. Oyama, and Y. Sakamoto, *Ammonia synthesis at low pressures*, Sci. Paper IPCR **75**, 124 (1981).

[9] E.N. Eremin, A.N. Mal'tsev, and V.M. Belova, *Catalytic formation of ammonia in a barrier discharge*, Russ. J. Phys. Chem. **45**, 635 (1971).

[10] K.S. Yin and M. Venugopalan, *Plasma Chemical Synthesis. I. Effect of electrode material on the synthesis of ammonia*, Plasma Chem. Plasma Process. **3**, 343 (1983).

[11] M. Tanaka, H. Uyama, and O. Matsumoto, *Synergistic effects of catalysts and plasmas on the synthesis of ammonia and hydrazine*, Plasma Chem. Plasma Process. **14**, 491 (1994).

[12] H. Kiyooka and O. Matsumoto, *Reaction scheme of ammonia synthesis in the ECR plasmas*, Plasma Chem. Plasma Process. **16**, 547 (1996).

[13] M. Touvelle, J.L. Muñoz Licea, and M. Venugopalan, *Plasma chemical synthesis II. Effect of wall surface on the synthesis of ammonia*, Plasma Chem. Plasma Process. **7**, 101 (1987).

[14] H. Uyama and O. Matsumoto, *Synthesis of ammonia in high-frequency discharges*, Plasma Chem. Plasma Process. **9**, 13 (1989).

[15] B. Gordiets, C.M. Ferreira, M.J. Pinheiro, and A. Ricard, *Self-consistent kinetic model of low-pressure N_2–H_2 flowing discharges: II. Surface processes and densities of N, H, NH_3*, Plasma Sources Sci. Technol. **7**, 379 (1998).

[16] B. Gordiets, C.M. Ferreira, M.J. Pinheiro, and A. Ricard, *Self-consistent kinetic model of low-pressure N_2–H_2 flowing discharges: I. Volume processes*, Plasma Sources Sci. Technol. **7**, 363 (1998).

[17] A. Ricard, B.F. Gordiets, M.J. Pinheiro, C.M. Ferreira, G. Baravian, J. Amorim, S. Bockel, and H. Michel, *Diagnostic and modeling of N_2–H_2 discharges for iron nitriding*, Eur. Phys. J. Appl. **4**, 87 (1998).

[18] J.L. Jauberteau, I. Jauberteau, and J. Aubreton, *NH_3 and $NH_{x<3}$ radicals synthesis down-*

stream a microwave discharge sustained in an Ar–N_2–H_2 gas mixture. Study of surface reactive processes and determination of rate constants, J. Phys. D: Appl. Phys. **35**, 665 (2002).

[19] J. Amorim, J. Loureiro, and D. Schram, *Formation of H^- ions via vibrational excited molecules produced from recombinative wall desorption of H atoms in a low pressure H_2 positive column,* Chem. Phys. Lett. **346**, 443 (2001).

[20] P. Vankan, D.C. Schram, and R. Engeln, *High rotational excitation of molecular hydrogen in plasmas,* Chem. Phys. Lett. **400**, 196 (2004).

[21] P. Vankan, D.C. Schram, and R. Engeln, *Atomic and molecular hydrogen densities in a plasma expansion,* Plasma Sources Sci. Technol. **14**, 744 (2005).

[22] M.C.M. van de Sanden, R.J. Severens, W.M.M. Kessels, R.F.G. Meulenbroeks, and D. C. Schram, *Plasma chemistry aspects of a–Si:H deposition using an expanding thermal plasma,* J. Appl. Phys. **84**, 2426 (1998), **85**, 1243 (1999).

[23] P. Vankan, S. Mazouffre, R. Engeln, and D. C. Schram, *Inflow and shock formation in supersonic, rarefied plasma expansions,* Phys. Plasmas **12**, 102303 (2005).

[24] S. Mazouffre, I. Bakker, P. Vankan, R. Engeln, and D.C. Schram, *Two-photon laser induced fluorescence spectroscopy performed on free nitrogen plasma jets,* Plasma Sources Sci. Technol. **11**, 439 (2002).

[25] R. Engeln, S. Mazouffre, P. Vankan, D.C. Schram, and N. Sadeghi, *Flow dynamics and invasion by background gas of a supersonically expanding thermal plasma,* Plasma Sources Sci. Technol. **10**, 595 (2001).

[26] P. Vankan, T. Rutten, S. Mazouffre, D.C. Schram, and R. Engeln, *Absolute density measurements of ammonia produced via plasma-activated catalysis,* Appl. Phys. Lett. **81**, 418 (2002).

[27] M.C.M. van de Sanden, J.M. de Regt, G.M. Jansen, J.A.M. van der Mullen, D.C. Schram, and B. van der Sijde, *A combined Thomson-Rayleigh scattering diagnostic using an intensified photodiode array,* Rev. Sci. Instrum. **63**, 3369 (1992).

[28] R.P. Dahiya, M.J. de Graaf, R.J. Severens, H. Swelsen, M.C.M. van de Sanden, and D.C. Schram, *Dissociative recombination in cascaded arc generated Ar-N_2 and N_2 expanding plasma,* Phys. Plasmas **1**, 2086 (1994).

[29] CHEMKIN interface 4, distributed by Reaction Design (available on-line www.ReactionDesign.com).

[30] M. Capitelli, C.M. Ferreira, B.F. Gordiets, and A.I. Osipov, *Plasma kinetics in atmospheric gases,* Springer-Verlag, Berlin (2000).

[31] Private communication with H. van Eck of the FOM–Insitute for Plasma Physics, Rijnhuizen, The Netherlands.

[32] R. Engeln, G. Berden, R. Peeters, and G. Meijer, *Cavity enhanced absorption and cavity enhanced magnetic rotation spectroscopy,* Rev. Sci. Instrum. **69**, 3763 (1998).

[33] G. Berden, R. Peeters, and G. Meijer, *Cavity-enhanced absorption spectroscopy of the 1.5 μm band system of jet-cooled ammonia,* Chem. Phys. Lett. **307**, 131 (1999).

[34] R. Peeters, G. Berden, A. Apituley, and G. Meijer, *Open-path trace gas detection of ammonia based on cavity-enhanced absorption spectroscopy,* Appl. Phys. B **71**, 231 (2000).

[35] L.S. Rothman, A. Barbe, D. Chris Benner, L.R. Brown, C. Camy-Peyret, M.R. Carleer, K. Chance, C. Clerbaux, V. Dana, V.M. Devi, A. Fayt, J.-M. Flaud, R.R. Gamache, A. Goldman, D. Jacquemart, K.W. Jucks, W.J. Lafferty, J.-Y. Mandin, S.T. Massie, V. Nemtchinov, D.A. Newnham, A. Perrin, C.P. Rinsland, J. Schroeder, K.M. Smith, M.A.H. Smith, K. Tang, R.A. Toth, J. Vander Auwera, P. Varanasi, and K. Yoshino, *The HITRAN molecular spectroscopic database: edition of 2000 including updates through 2001,* J. Quant. Spectrosc. Radiat. Transfer **82**, 5 (2003).

[36] L. Lundsberg-Nielsen, F. Hegelund, and F.M. Nicolaisen, *Analysis of the high-resolution spectrum of ammonia ($^{14}NH_3$) in the near-infrared region, 6400-6900 cm^{-1},* 162 , 230 (1993).

[37] A.J.M. Buuron, D.K. Otorbaev, M.C.M. van de Sanden, and D.C. Schram, *Absorption spectroscopy on the argon first excited state in an expanding thermal arc plasma,* Phys. Rev. E **50**, 1383 (1994).

[38] G.J.H. Brussaard, *Remote arc generated plasma in diatomic gases,* PhD thesis, Eindhoven University of Technology, Eindhoven, 1999, available on-line at http://alexandria.tue.nl/extra2/9900312.pdf.

[39] R.F.G. Meulenbroeks, A.J. van Beek, A.J.G. van Helvoort, M.C.M. van de Sanden, and D.C. Schram, *Argon-hydrogen plasma jet investigated by active and passive spectroscopic means,* Phys. Rev. E **49**, 4397 (1994).

[40] M.A. Blauw et al., To be published.

[41] P. Vankan, R. Engeln, and D. C. Schram, *Increased atomic hydrogen flux from a cascaded arc plasma source by changing the nozzle geometry,* Appl. Phys. Lett. **86**, 101501 (2005).

[42] B. Jackson and M. Pearson, *A quantum mechanical study of recombinative desorption of atomic hydrogen on a metal surface,* J. Chem. Phys. **96**, 2378 (1992).

[43] C.T. Rettner, *Dynamics of the direct reaction of hydrogen atoms adsorbed on Cu(111) with hydrogen atoms incident from the gas phase,* Phys. Rev. Lett. **69**, 383 (1992).

[44] G.G. Mannella, *Active nitrogen,* Chem. Rev. **63**, 1 (1963).

[45] J.-P. Sarrette, B. Rouffet, and A. Ricard, *Determination of nitrogen atoms loss probabilities on copper, aluminium, alumina, brass and nylon surfaces,* Plasma Process. Polym. **3**, 120

(2006).

[46] J. Amorim, G. Baravian, and G. Sultan, *Absolute density measurements of ammonia synthetized in N_2-H_2 mixture discharges,* Appl. Phys. Lett. **68**, 1915 (1996).

[47] H. Nagai, M. Hiramatsu, M. Hori, and T. Goto, *Etching organic low dielectric film in ultra-high frequency plasma using N_2/H_2 and N_2/NH_3 gases,* J. Appl. Phys. **94**, 1362 (2003).

[48] J.L. van Hemmen, Modulated beam threshold ionization mass spectrometry: radiical detection in the NH_3/Ar and NH_3/SiH_4/Ar plasma, Master's thesis, Eindhoven University of Technology, 2005.

[49] B. Gordiets, C.M. Ferreira, J. Nahorny, D. Pagnon, M. Touzeau, and M. Vialle, *Surface kinetics of N and O atoms in N_2–O_2 discharges,* J. Phys. D: Appl. Phys. **29**, 1021 (1996).

[50] A. Gelb and S.K. Kim, *Theory of atomic recombination on surfaces,* J. Chem. Phys. **55**, 4935 (1971).

[51] C.J. Hagedorn, M.J. Weiss, and W.H. Weinberg, *Ammonia decomposition on Ru(001) using gas-phase atomic hydrogen,* J. Vac. Sci. Technol. A **16**, 984 (1998).

[52] Z.-P. Liu, P. Hu, and M.-H. Lee, *Insight into association reactions on metal surfaces: Density-functional theory studies of hydrogenation reactions on Rh(111),* J. Chem. Phys. **119**, 6282 (2003).

[53] H. Shi, K. Jacobi, and G. Ertl, *Interaction of hydrogen with nitrogen atoms chemisorbed on a Ru(0001) surface,* J. Chem. Phys. **102**, 1432 (1995).

[54] R.M. van Hardeveld, R.A. van Santen, and J.W. Niemantsverdriet, *Formation of NH_3 and N_2 from atomic nitrogen and hydrogen on rhodium (111),* J. Vac. Sci. Technol. A **15**, 1558 (1997).

Chapter 5

Evidence of surface production of excited molecules*

Abstract

The visual appearance of an expanding nitrogen plasma with and without oxygen is shown. The interaction of the plasma with a substrate leads to the appearance of additional light, which is ascribed to the formation of excited molecules by association of N and/or O atoms at the substrate.

*adapted from: J.H. van Helden, R. Zijlmans, R. Engeln and D.C. Schram, *Molecule formation in N and O containing plasmas,* IEEE Trans. Plasma Sci **33**, 390 (2005)

5.1 Introduction

In the previous two chapters, the generation of ammonia in plasmas containing mixtures of nitrogen and hydrogen was investigated. It was shown that when the surface is exposed to high fluxes of N and H radicals, ammonia can be generated efficiently. It was suggested that in the formation of ammonia an additional layer at a passivated surface could play a role. Ammonia is formed through plasma-surface interactions by the stepwise addition reactions between adsorbed nitrogen and hydrogen containing radicals at the surface and incoming atomic H radicals.

Now, we are interested in the generation of molecules in plasmas containing nitrogen and oxygen. In these plasmas, the so-called mass-defocusing effect observed in N_2–H_2 plasmas, plays a minor role, since nitrogen and oxygen atoms have about equal masses. The formation of NO is generally observed in N_2–O_2 plasmas and also N_2O and NO_2 may be formed. The role of plasma-surface interactions in the generation of NO is not yet clear. Again the question arises whether the formation of molecules may involve weakly bounded particles following the idea of Gordiets et al. [1] to explain the NO production in N_2–O_2 plasmas. If the surface is fully covered, also atoms with less binding energy may be adsorbed and molecules can be formed at the surface with a substantial internal energy. The easiest way to investigate this idea, is by observing the emission in the visible of excited molecules close to a surface.

Previously, additional light emission around a surface and thus the occurrence of excited molecules was observed in nitrogen plasmas, as will be discussed later on. In general, in several experiments aimed at etching and deposition additional light is observed, but the explanation of this effect and the excitation mechanisms are not always discussed.

In the experiments described here, fluxes of radicals are produced with the remote expanding thermal plasma (ETP) technique [2]. A cascaded arc source is used (Fig. 5.1), which operates at flows of typically 3 slm (standard liter per minute). In argon, an ionization degree of typically 10% is reached, equivalent to 10^{20} ions/s (and electrons) emanating from the source [3], and around 1 – 5% in pure nitrogen and mixtures of nitrogen and hydrogen [4, 5]. Molecular gases injected in the arc are almost fully dissociated. The pressure gradient between source (>100 kPa) and process chamber (0.1 – 1 mbar) causes, after a supersonic expansion and a stationary shock, a subsonic expansion towards the copper substrate. Monomers, like oxygen, can be injected in this plasma, which undergo charge transfer and subsequently dissociative recombination reactions leading to atomic radicals which can be used for surface

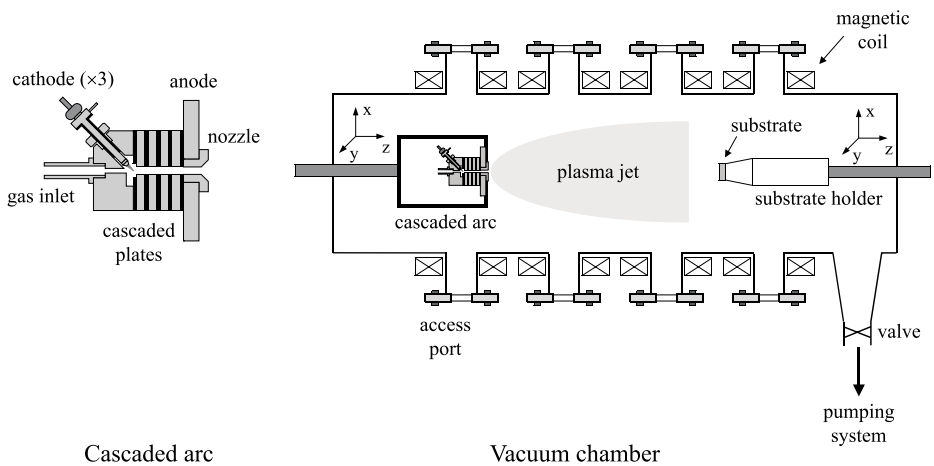

Figure 5.1: Sketch of the setup in which the thermal plasma expansions are created.

modification, e.g. the stripping of photoresist [6, 7]. As there is no power input anymore in the process chamber, the plasma is recombining. In the expansion, the electron temperature decreases to 0.1 – 0.3 eV. At these temperatures, dissociation and excitation by electrons can be neglected [2]. Thus, the remote ETP technique improves the possibility to observe and thus investigate the mechanisms of excitation via association reactions at surfaces which usually are masked by the electronic excitation of the gas particles.

In the experiments, nitrogen plasmas were created with 4 slm nitrogen flowing through the arc, in which the shock occurs at roughly 3 cm, while the distance between the plasma source and substrate was 25 cm. Mazouffre et al. have measured an atomic N density of 4×10^{20} m^{-3} after the shock in a pure nitrogen plasma with a N_2 gas flow of 1.5 slm through the arc at a background pressure of 100 Pa. The flux density of the N atoms is about 2×10^{23} m^{-2} s^{-1}, using a velocity of 500 m/s. Now, 4 slm nitrogen is used, which gives a flux density of the N atoms of 5.3×10^{23} m^{-2} s^{-1}. This means that on the copper substrate, which has the same diameter as the plasma beam, i.e. 0.06 m, a flux density is reached of 5.3×10^{23} m^{-2} s^{-1}, which is equivalent to 10^4 mono-layers/s

The light emission from the plasma in the vessel is detected through one of the access ports and the light is directed through a series of lenses and a mirror to the optical emission spectrometer. The low reflection of the mirror for wavelengths shorter

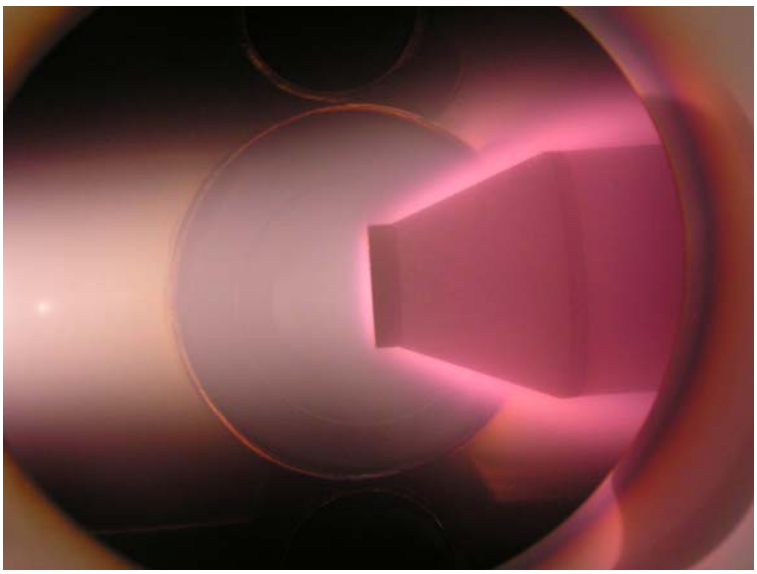

Figure 5.2: Picture of expanding nitrogen plasma produced by a cascaded arc plasma source (4 standard liters per minute (slm) N_2 flow, 75 A) at 100 Pa background pressure.

than 250 nm limited the detection of light at these wavelengths. The optical emission measurements have been performed with a fiber optic spectrometer (Ocean Optics USB2000), which has an optical resolution of ~ 1.5 nm (FWHM).

5.2 Results and discussion

5.2.1 Emission of N_2 plasma

In a pure nitrogen expanding plasma, N^+ and N are produced by the cascaded arc source. The charge exchange reaction of N^+ with N_2 leads to N_2^+ which partially dissociatively recombines to N atoms. The recombination is hampered by the facts that the charge-transfer between N_2 and N^+ is endo-energetic by 1.05 eV and that the temperature of heavy particles (and of electrons) is low, < 0.2 eV. Downstream in the vessel, the main particles in nitrogen plasmas are nitrogen (^{4}S) atoms, nitrogen atomic ions, and as a majority nitrogen molecules, even with a fully dissociated flow of N atoms from the source. The reason is that in a time τ_N (≈ 20 ms), short compared to the residence time of particles in the vessel ($\tau_{res} \approx 2.5$ s), the N atoms

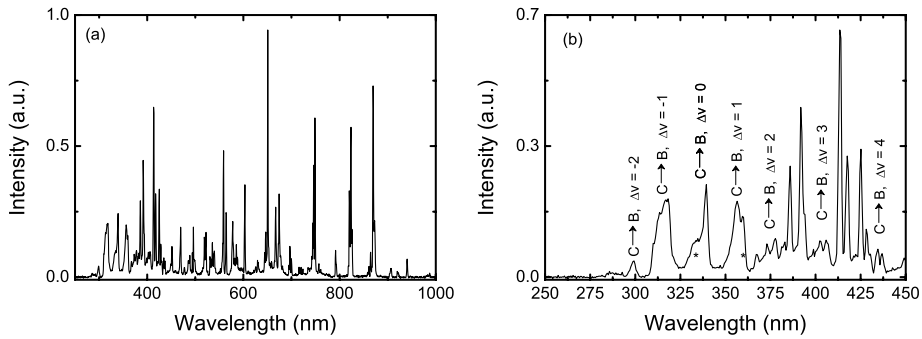

Figure 5.3: a) Spectrum of a nitrogen plasma produced by a cascaded arc plasma source (4 standard liters per minute (slm) N_2 flow, 75 A and 100 Pa background pressure) as measured 25 mm in front of the substrate. b) Most of the spectral features below 450 nm can be assigned to N_2 (C → B) emission. Atomic nitrogen and N_2^+(B → X) (marked by an asterisk) transitions are responsible for the remaining line emission.

will associate at the surface to N_2 molecules. (Volume three particle association of N atoms has insufficient probability at the investigated pressure range). Line emission from atomic nitrogen is observed, which originates from three-particle recombination of atomic ions. A fading of the light with increasing distance from the source is observed. The remaining light is next to line emission also partly from the emission of molecular bands: the first positive system of N_2, this is the (B → A) transition, the second positive system of N_2 this is the (C → B) transition, and the first negative system of N_2^+, this is the (B → X) transition.

However, close to the substrate a strong increase of light is clearly visible (Fig. 5.2 (real colours)). This cannot be attributed to electron excitation as the electron temperature there is below 0.1 eV. The thickness of the additional light layer is about 2.5 mm, which is consistent with a transition probability of 10^5 s^{-1} of the B → A transition and a reflection velocity around 200 m/s. In the spectral analysis, the vibrational transitions in the C → B band of molecular nitrogen and the B → X band of molecular nitrogen ions are clearly visible (Fig. 5.3). The B → A emission is partly outshined by the emission of atomic lines. The N_2(B) and N_2(C) states can be populated by the pooling reactions involving two meta-stable N_2(A) molecules [8, 9]:

$$N_2(A) + N_2(A) \longrightarrow N_2(B) + N_2(X) \qquad k \approx 10^{-16}\ m^3\,s^{-1}, \tag{5.1}$$

$$N_2(A) + N_2(A) \longrightarrow N_2(C) + N_2(X) \qquad k = 1.5 \times 10^{-16}\ m^3\,s^{-1}. \tag{5.2}$$

These processes limit the N_2(A) density to 10^{19} m^{-3}. At low N_2(A) densities, B $\rightarrow$ A emission may be observed and no C $\rightarrow$ B emission. In that case the N_2(A) density is too small for pooling but can still produce N_2(B) in the reaction [10]:

$$N_2(A) + N_2(X, v > 5) \longrightarrow N_2(B) + N_2(X, v - 6) \quad k = 3 \times 10^{-17}\ m^3\, s^{-1}, \quad (5.3)$$

Furthermore, it can explain the N_2^+(B $\rightarrow$ X) radiation: by charge transfer between $N^+$and N_2(A) preferably N_2^+(B, $v = 6, 7$) is produced, as was reported in [11]. The presence of meta-stable $N_2(A^3\Sigma_u^+)$ molecules was observed previously in expanding nitrogen plasmas. It was suggested that N_2(A) molecules are most likely formed at the surface of the plasma reactor [12]. That now less N_2(A) molecules are observed, could be besides to the pooling reactions also be caused by higher ion density in the current plasma conditions than in those experiments. Then the N_2(A) molecules are efficiently lost by charge-transfer reactions with N^+[11]. The extra light emission could also be caused by the generation of N_2(B) directly by association of two atoms at the surface. Apparently, excited molecules are produced if the flux of atoms is high, and the surface is fully covered with atomic nitrogen. Then, in addition, also atoms with less binding energy may be adsorbed, which may produce an excited molecule with substantial internal energy, in a direct pick up reaction with atoms incident at the surface.

5.2.2 Emission of N_2–O_2 plasma

When oxygen is injected in a nitrogen plasma, the O_2 undergoes charge exchange reactions with N^+ and N_2^+, which leads to O atoms. Using an ionization degree of 5% at a flow of 1.7×10^{21} particles/s from the plasma source, gives a flux density of $1.7 \times\ 10^{20}$ O atoms/s. The reaction N + O_2 $\rightarrow$ NO + N could at maximum give a 30% extra O atoms, assuming that 10% of O_2 injected into the background diffuses in the plasma beam. In this case, the plasma brightness decays faster than in a pure nitrogen plasma (Fig. 5.4 (real colours)). Now, the emission spectrum clearly shows features of the first positive system of molecular nitrogen, i.e. N_2(B $\rightarrow$ A). Under these experimental conditions, the quenching of N_2(A) by atomic nitrogen ions is strongly reduced due to the loss of atomic ions in the expansion through the dissociation reaction with molecular oxygen.

A second clear result in Fig. 5.4 is the appearance of an orange glow at and around the substrate. The thickness of the light layer is larger than in the pure nitrogen case, indicating a transition with a lower transition probability. This is consistent with the

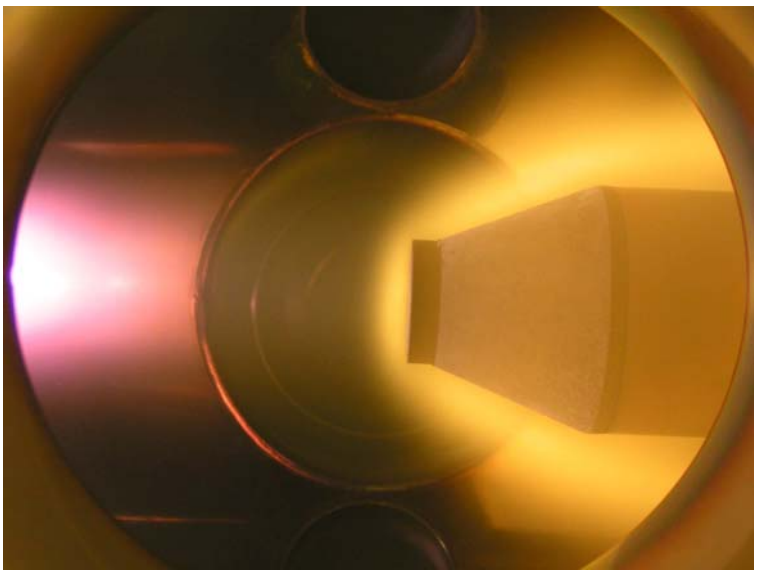

Figure 5.4: Picture of an expanding nitrogen plasma with 1.5 slm O_2 admixed into the background (4 slm N_2 flow, 75 A and 100 Pa background pressure).

broadband feature in the measured emission spectrum (Fig. 5.5). The broadband emission has a resemblance with the emission observed during the re-entry of the space shuttle in the atmosphere (Fig. 5.5). Our spectrum is shifted to the blue of the observed shuttle glow spectrum. This could mean that now more high vibrational states are excited, than in the shuttle-glow. The difference is most likely related to the conditions in the experiments. That the shuttle glow has still almost continuous emission at longer wavelengths and no fall off compared to our spectrum is frequently observed in the comparison between the shuttle-observed emission and the emission measured in laboratory experiments, and the reason for this is not yet clear [13, 14]. However, it is known that the NO_2 emission is continuous and decreases at wavelengths larger than 700 nm [15]. Therefore, the light emission observed during the re-entry is tentatively attributed to the formation of excited NO_2 in an association reaction of O radicals from the atmosphere and NO adsorbed at the surface of space vehicles [13].

To analyze the emission of Fig. 5.5, we performed quantitative mass spectrometry measurements in N_2-O_2 plasmas (see Chapter 6). It is found that around 5% of the N_2 and O_2 was converted into nitric oxide. The observed radiation from 200 to 450 nm is indeed due to the emission of NO(A $\rightarrow$ X) and NO(B $\rightarrow$ X) emission and some

$N_2^+(B \rightarrow X)$ transitions as was deduced from a simulation using LifBase assuming a resolution of 1.5 nm and a temperature of 5000 K. Furthermore, the substrate is exposed to high fluxes of oxygen and nitrogen atomic radicals. As will be shown in Chapter 7, the surface is covered with N and NO. Thus a similar process as in the space vehicle experiments can lead to $NO_2{}^*$ emission:

$$O + NO_{ads} \longrightarrow NO_2(\tilde{A}^2B_2) \longrightarrow NO_2(\tilde{X}^2A_1). \tag{5.4}$$

The reaction leading to NO_2 is exothermic and will result in highly excited molecules in the $NO_2(\tilde{A}^2B_2)$ band state, which radiate light in the wavelength range from 400 to 800 nm. The NO_2 formed at the surface would contain the exothermic energy of the reaction ($\Delta E = 3.1$ eV) minus the adsorption energy of NO on the surface and minus the kinetic energy of the desorbed NO_2 molecule. The kinetic energy of the desorbed NO_2 molecule for a reflection velocity around 200 m/s is about 0.02 eV. If the adsorption energy of NO would be approximately 1 eV, which is reported for crystalline metal surfaces [16], still highly excited NO_2 molecules can be produced in the $NO_2(\tilde{A}^2B_2)$ state, which lies 1.2 eV above the ground state [17]. However, the observed radiation of NO_2 covers the wavelength range from 480 nm to 850 nm, i.e. it involves a maximum energy of the NO_2 molecules of 2.6 eV. Thus apparently part of the absorption energy of the NO is around 0.5 eV and thus indicates the existence of weakly bonded NO at the surface, possibly in an additional layer at a passivated surface, which leads to an excited NO_2 molecule with substantial internal energy. This observation is in agreement with the suggestion of Gordiets et al. [1].

Furthermore, Patten et al. have reported that the radiative fluorescence lifetime in the region between 400 and 750 nm is between 70 and 100 μs [18]. Using a velocity of 200 m/s of the produced $NO_2{}^*$ molecules, this would lead to an additional light layer at the substrate of around 20 mm thickness, which is in agreement with our observation. Note that also in this case the flow pattern is clearly visible: close to the substrate the plasma diverges and flows around the substrate to the section, which is pumped.

5.3 Conclusions

In conclusion, from expanding plasma in interaction with a substrate one can observe additional light close to the substrate. This light shows the flow pattern close to the substrate. The additional light is a very clear visual evidence of the production of excited molecules, presumably by association of atomic radicals at the surface. These

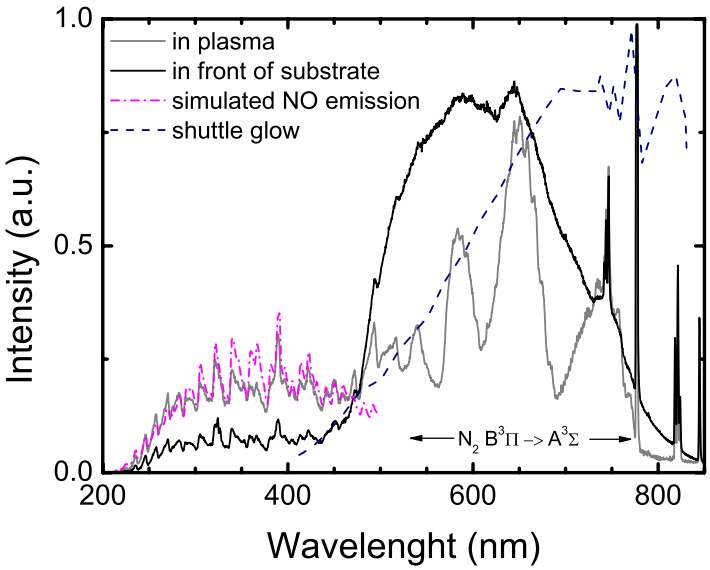

Figure 5.5: Spectra of an expanding nitrogen plasma with 1.5 slm O_2 admixed into the background. (4 slm N_2 flow, 75 A and 100 Pa background pressure) as measured in the plasma, 100 mm from the plasma source, and 17 mm in front of the substrate. In the former, the emission of the first positive system of N_2, i.e. B $\rightarrow$ A emission, is observed. The broadband feature in the latter spectrum is due to NO_2 emission. The emission below 450 nm is due to the emission of NO(A $\rightarrow$ X) and NO(B $\rightarrow$ X) emission and some N_2^+(B $\rightarrow$ X) transitions. The other features are due to N and O atomic line emission. Also the shuttle-glow is plotted, reproduced from Fig. 3 of the paper by Murad [13].

processes take place under conditions of a large flow of atomic radicals and therefore full coverage of the (metallic) surface. The emission around the substrate in an N_2–O_2 plasma indicates that the excited NO_2 molecules responsible for the emission are partly only weakly bonded to the surface, possibly in an additional layer at a passivated surface.

Bibliography

[1] B. Gordiets, C.M. Ferreira, J. Nahorny, D. Pagnon, M. Touzeau, and M. Vialle, *Surface kinetics of N and O atoms in N_2–O_2 discharges*, J. Phys. D: Appl. Phys. **29**, 1021 (1996).

[2] M.C.M. van de Sanden, R.J. Severens, W.M.M. Kessels, R.F.G. Meulenbroeks, and D. C.

Schram, *Plasma chemistry aspects of a–Si:H deposition using an expanding thermal plasma*, J. Appl. Phys. **84**, 2426 (1998), **85**, 1243 (1999).

[3] M.C.M. van de Sanden, J.M. de Regt, G.M. Jansen, J.A.M. van der Mullen, D.C. Schram, and B. van der Sijde, *A combined Thomson-Rayleigh scattering diagnostic using an intensified photodiode array*, Rev. Sci. Instrum. **63**, 3369 (1992).

[4] S. Mazouffre, I. Bakker, P. Vankan, R. Engeln, and D.C. Schram, *Two-photon laser induced fluorescence spectroscopy performed on free nitrogen plasma jets*, Plasma Sources Sci. Technol. **11**, 439 (2002).

[5] R.P. Dahiya, M.J. de Graaf, R.J. Severens, H. Swelsen, M.C.M. van de Sanden, and D.C. Schram, *Dissociative recombination in cascaded arc generated Ar-N_2 and N_2 expanding plasma*, Phys. Plasmas **1**, 2086 (1994).

[6] G.J.H. Brussaard, K.G.Y. Letourneur, M. Schaepkens, M.C.M. van de Sanden, and D.C. Schram, *Stripping of photoresist using a remote thermal Ar/O_2 and $Ar/N_2/O_2$ plasma*, J. Vac. Sci. Technol. B **21**, 61 (2003).

[7] M. Capitelli, C.M. Ferreira, B.F. Gordiets, and A.I. Osipov, *Plasma kinetics in atmospheric gases*, Springer-Verlag, Berlin (2000).

[8] L.G. Piper, *State-to-state $N_2(A^3\Sigma_u^+)$ energy pooling reactions. II. The formation and quenching of $N_2(B^3\Sigma_g, v' = 1–12)$*, J. Chem. Phys. **88**, 6911 (1988).

[9] L.G. Piper, *State-to-state $N_2(A^3\Sigma_u^+)$ energy-pooling reactions. I. The formation of $N_2(C^3\Pi_u)$ and the Herman infrared system*, J. Chem. Phys. **88**, 231 (1988).

[10] L.G. Piper, *The excitation of $N_2(B^3\Sigma_g, v' = 1–12)$ in the reaction between $N_2(A^3\Sigma_u^+)$ and $N_2(X, v \geq 5)$*, J. Chem. Phys. **91**, 864 (1989).

[11] G.J.H. Brussaard, E. Aldea, M.C.M. van de Sanden, G. Dinescu, and D.C. Schram, *Evidence of charge exchange between N^+ and $N_2(A^3\Sigma_u^+)$ in a low-temperature nitrogen plasma*, Chem. Phys. Lett. **290**, 379 (1998).

[12] G.J.H. Brussaard, *Remote arc generated plasma in diatomic gases*, PhD thesis, Eindhoven University of Technology, Eindhoven, 1999.

[13] E. Murad, *The shuttle glow phenomenon*, Annu. Rev. Phys. Chem. **49**, 73 (1998).

[14] O.J. Orient, K.E. Martus, A. Chutjian, and E. Murad, *Recombination of 5-eV $O(^3P)$ atoms with surface-adsorbed NO: Spectra and their dependence on surface material and temperature*, Phys. Rev. A **45**, 2998 (1992).

[15] D.E. Paulsen, W.F. Sheridan, and R.E. Huffman, *Thermal and recombination emission of NO_2*, J. Chem. Phys. **53**, 647 (1970).

[16] R.I. Masel, *Principles of adsorption and reaction on solid surfaces*, Wiley-Interscience, New York (1996).

[17] H.S. Johnston, C.E. Miller, B.Y. Oh, K.o. Patten Jr., and W.N. Sisk, *Internal energy distributions from nitrogen dioxide fluorescence. 1. Cumulative sum method*, J. Phys. Chem. **97**, 9890 (1993).

[18] K.O. Patten Jr., J. D. Burley, and H.S. Johnston, *Radiative lifetimes of nitrogen dioxide for excitation wavelengths from 400 to 750 nm*, J. Phys. Chem. **94**, 7960 (1990).

Chapter 6

Resemblance in gas composition of Ar–N_2–O_2 plasmas and Ar–NO plasmas

Abstract

We measured the steady state gas composition of plasmas produced from Ar–N_2–O_2 mixtures and Ar–NO mixtures with quantitative mass spectrometry. In the former, mainly N_2 and O_2, but also a significant amount of nitric oxide (NO) was formed, i.e. up to 5% of the background gas was NO. In the inverse experiment, in which NO was admixed to an argon plasma, up to 92% of the NO was converted into N_2 and O_2. Thus, the two types of plasmas show a strong resemblance in the steady state gas composition, i.e. $\approx$ 5% NO and $\approx$ 95% N_2 and O_2, although the starting conditions are completely different. It seems that in first order the system prefers to produce the most thermodynamically bonded molecules.

6.1 Introduction

Plasmas containing nitrogen and oxygen are nowadays extensively studied, due to their relevance in various fields of research, e.g. understanding of atmospheric and ionospheric physics [1], in re-entry studies of orbital space vehicles [2] and as sources of active species for applications in plasma chemistry. Examples of the latter include air pollution cleaning by atmospheric pressure discharge treatment [3], sterilization [4, 5], surface treatment of materials, like etching [6]. From various studies, it was concluded that NO molecules are formed in these kind of plasmas [7–9]. Furthermore, the observed NO densities were attributed to the combination of gas phase reactions and plasma-surface processes [10–12].

Also the destruction of NO_x is a subject to which much attention has been given, mainly because of environmental reasons. The toxic nitrogen oxides (NO, NO_2) are present in the emission of combustion gases, and are major sources of acid rain, photochemical smog formation and the green-house effect. The decomposition of NO is currently investigated in various types of plasma, like microwave discharges and microwave discharge-assisted catalytic systems, commonly at atmospheric pressures [13–18]. The measurements are mainly performed in N_2/NO gas mixtures as the reduction process is preferentially done at atmospheric pressures. The results show that NO, if present in small quantities, is converted into N_2 and O_2 with a high decomposition efficiency (up to 100%). In the cases O_2 is admixed the decomposition efficiency decreases, which is attributed to the formation of NO as observed in N_2-O_2 containing plasmas. To the best of our knowledge, there are only a few studies performed on Ar/NO gas mixtures at atmospheric pressure [19, 20]. Also in these cases the NO was almost fully (up to 96%) converted into N_2 and O_2.

For plasma deposition or etching and for surface modification, but also for re-entry studies, a particle flux of ions and/or radicals as high as possible is desirable to obtain sufficiently high process rates. This can be achieved in the remote source approach, in which a plasma is produced in the source and plasma treatment is performed downstream at lower pressure. For the current experiments, the remote expanding thermal plasma (ETP) technique is used, which consists of a high-pressure thermal plasma source and a low-pressure process chamber [21]. In this way, the production of plasma by ionization and the formation of for example N atoms by dissociation of N_2 in the plasma source is geometrically separated from the plasma chemistry in the vessel. The separation of the plasma production, plasma transport and plasma-surface interactions allows independent studies of the different aspects

of the process.

A main advantage of the ETP technique is the fact that there is no power coupled into the plasma in the process chamber. As a result, the plasma is recombining and the downstream electron temperature in the expansion decreases to 0.1 – 0.3 eV [21] and is therefore too low for electronic collisions to play a role in dissociation or excitation processes described in e.g. [22]. The electron density in the downstream is in the order of 10^{18} m^{-3}. Therefore, the plasma chemistry in the vessel is primarily driven by reactions between ions and atomic (N) radicals from the source and injected or produced molecules.

This is in contrast to almost all previous studies on N_2–O_2 or NO containing plasmas, which were mainly performed in non-equilibrium systems, with a high electron temperature. These systems are driven by electron induced excitation and ionization, and therefore knowledge of electron and ion densities and energy distributions, as well as of the density and internal state distributions of reactants and products, is necessary. Moreover, the large number of processes that has to be taken into account to describe the plasma behavior makes the development of complex kinetic models necessary [22–26].

In this chapter, we report on measurements of the steady state gas composition of recombining plasmas produced from $Ar/N_2/O_2$ mixtures and Ar/NO mixtures. The concentrations of stable species present in the background of the plasma were measured using mass spectrometry. We detected molecules like NO, N_2 and O_2, formed in recombining plasmas generated from: (a) Ar plasma to which mixtures of N_2 and O_2 were added; (b) Ar/N_2 plasma to which O_2 was added; (c) N_2 plasma to which O_2 was added and (d) Ar plasma to which NO was added. The added gases were injected in the background of the vessel.

By changing the composition of the mixtures from which the plasmas are created, the amount of N and O radicals in the plasma was varied. This enabled, similar to the experiments in Chapter 4, to study the relation between the molecules produced and the fluxes of N and O atoms in the plasma. The dissociation of N_2 can be optimized by operating the plasma source on N_2 as is done in case (c). Contrary to N_2, O_2 could not be applied through the plasma source, since injection into the arc would damage the plasma source. Since in plasmas produced from mixtures of N_2 and O_2, a few percent of the steady-state gas mixture is measured to be NO, we also investigated the situation in which NO is admixed to a plasma.

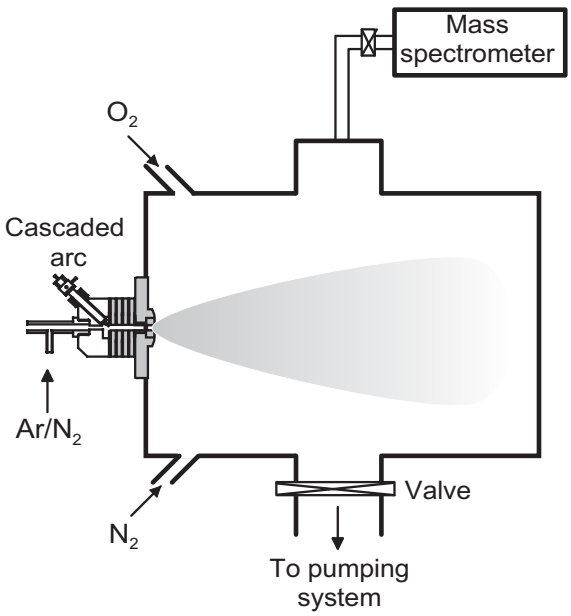

Figure 6.1: Sketch of the setup in which the thermal expansions are created.

6.2 Experimental details

6.2.1 Expanding thermal plasma setup

The recombining plasma generated from mixtures of N_2, O_2 and NO were created with the expanding thermal plasma (ETP) technique, described extensively in the literature (see e.g. [27]). Here, only a short description of the setup is given. The expanding thermal plasma setup consists of a high-pressure thermal plasma source and a low-pressure process chamber as schematically depicted in Fig 6.1.

The plasma source is used to create reactive species for the dissociation of monomers injected into the plasma in the downstream region. A remote plasma is created in a DC cascaded arc source by the generation of a sub-atmospheric (typically 400 kPa) thermal Ar, N_2 or Ar–N_2 plasma with a power of 2 – 5 kW. The cascaded arc source consists of a 30 mm narrow channel of 5 water-cooled insulated copper plates with a centric internal bore of 4 mm diameter. The last plate acts as the common anode for the discharge. Through the channel flows the source gas (Ar, Ar/N_2, or N_2) and a dc current is drawn from the three cathodes to the grounded anode plate producing the plasma. The high heavy particle temperature of approximately 1 eV

leads to almost full dissociation of molecular gases when these are injected in the arc.

The large pressure difference between the source (400 kPa) and the process chamber (typically 20 – 100 Pa), causes a supersonic expansion of the plasma from the nozzle of the cascaded arc into a stainless steel vacuum vessel. After a stationary shock, the plasma expands subsonically towards the other end of the process chamber. The current through the arc channel can be set to 30 – 75 A and the voltage over the arc ranges from 40 to 150 V. In the experiments, the pressure in the vessel was varied between 40 and 300 Pa by adjusting the gate valve to the pump.

6.2.2 Plasma conditions

The formation of molecules in recombining plasmas generated from mixtures of N_2, O_2 and NO were studied for four different experimental situations:
(a) Ar plasma to which mixtures of N_2 and O_2 were added;
(b) Ar/N_2 plasma to which O_2 was added;
(c) N_2 plasma to which O_2 was added;
(d) Ar plasma to which NO was added.

All gases admixed were injected in the background of the vessel, with a maximum flow of 2 slm (standard liter per minute) N_2, 1.8 slm O_2 or 1.8 slm NO.

ad. a)

In the first experimental situation, the cascaded arc source was operated on argon gas with oxygen and nitrogen injected downstream. The characteristics of expanding Ar plasmas have been described extensively in literature [21, 27, 28] and here only the main issues will be discussed briefly. The energy in expanding Ar plasmas is carried by the ions in the expansion and in the form of thermal energy of the particles (mainly atoms). In a typical experiment, the arc was operated at an argon flow rate of 3 slm (standard liter per minute) through the arc and an arc current of 70 A. In that case, the source emanates a partially ionized (15%) argon flow, i.e. an Ar^+ ion flow of 0.45 slm, as determined from ion measurements in the argon expansion using a Langmuir probe [29]. The meta-stable argon density Ar^*_m formed in three particle recombination processes of the argon ions is typically a factor of 10 lower than the argon ion density [30]. Therefore, the contribution of these states to the plasma

chemistry is limited compared to the ion-induced chemistry. Furthermore, the Ar^+ ion flow increases approximately linear with the plasma current for a constant Ar flow through the source over the current range of interest (30 –70 A).

ad. b)

In the second experimental situation, the plasma source was operated on a mixture of argon and nitrogen with oxygen injected downstream. In mixtures of 2 slm argon and 1.1 slm nitrogen used in the experiments, the dissociation degree of N_2 in the arc is expected to be around 50%, while an ionization degree of around 7% is reached as determined from as determined from Langmuir probe measurements in the expansion [29]. The ion flow from the source consisted of Ar^+ and N^+ with approximately a $1:1$ ratio [31, 32]. In an Ar/N_2 plasma, the N atoms will not react in the volume and will arrive at the wall of the plasma reactor, where nitrogen molecules can then be formed by plasma-surface interactions. At first instance the formation efficiency, however, is limited by the low surface recombination probability of N atoms on a stainless steel wall and the N atom will be reflected [33]. The N density will then increase until the density is so high that the net consumed flux producing N_2 molecules is equal to the inflow of N atoms. N_2 molecules formed at the surface reside in the background and diffuse inward into the expanding plasma beam, where they can be dissociated again by charge-transfer reactions with $Ar^+$and N^+followed by dissociative recombination of the formed molecular ion:

$$Ar^+ + N_2 \longrightarrow Ar + N_2^+ \qquad k \approx 2 \times 10^{-16}\ m^3\,s^{-1}, \quad [34] \qquad (6.1)$$

$$N^+ + N_2 \longrightarrow N + N_2^+ \qquad k \approx 10^{-16}\ m^3\,s^{-1}, \quad [35] \qquad (6.2)$$

$$N_2^+ + e \longrightarrow N^* + N \qquad k = 2 \times 10^{-13}\ m^3\,s^{-1}, \quad [36] \qquad (6.3)$$

Note that the N_2^+ ions are short-lived, because of the high loss rate $n_e k_{DR}$ ($n_e \approx 10^{19}$ m^{-3} [29]. Note that the charge-transfer between N_2 and N^+ is endo-energetic by 1.05 eV, which in the subsonic expansion will limit this reaction; in the supersonic expansion the N^+ velocity is high and there the charge-transfer can proceed more easily. From previous experiments, it was concluded that due to above reactions, the main ion in the expansion of an Ar/N_2 plasma is N^+ [31]. Langmuir probe measurements indicated that the ion density increased approximately linear with increasing current through the arc over the investigated range.

The * in reaction (6.11) denotes the fact that the N atoms can be excited into one of the meta-stable ground states N(^{2}P) and N(^{2}D). However, these excited N atoms will

quickly be de-excited by collisions with electrons($k_e \approx 10^{-13}$ m^3 s^{-1} [37]), and with atoms and molecules present in the plasma (rate constant of 4.1×10^{-17} m^3 s^{-1} [33]). Furthermore, in contradiction to previous experiments, it seems that the density of meta-stable $N_2(A^3\Sigma_u^+)$ molecules is an estimated three orders lower. In the current plasma conditions more N^+ ions are produced and then the $N_2(A^3\Sigma_u^+)$ molecules are efficiently lost by charge-transfer reactions with N^+[38]. In conclusion, we can disregard the role of meta-stable atoms and molecules and thus the main chemistry is initiated by N(^{4}S) atoms and N^+ ions.

ad. c)

In the third experimental situation, pure nitrogen was injected into the arc, leading to a pure nitrogen plasma in which the energy is carried out by mainly nitrogen atoms N (around 35%) and by nitrogen atomic ions (1 – 5%) at an arc current of 60 A [31, 33, 34]. The charge-transfer reaction between N^+ and N_2 leads to N_2^+ (reaction (6.2)), which partially dissociatively recombines to N atoms (reaction (6.11)). The densities of the meta-stable N atoms N(^{2}P) and N(^{2}D) emanating from the plasma source are expected to be in the order of 20% of the N(^{4}S) atoms (assuming a thermal population at a temperature of 1 eV). However, in the expansion the N(^{2}D) and N(^{2}D) densities will decrease fast due to de-excitation by collisions with electrons, but also with N(^{4}S) atoms, and N_2 molecules. This also applies to meta-stable N atoms produced in the expansion by dissociative recombination of N_2^+ with electrons, which density is determined by the ionization degree of the plasma. This results in a total density of around 1% for the meta-stable atoms in the plasma beam. Furthermore, also in this experimental situation, the density of $N_2(A^3\Sigma_u^+)$ molecules is too low to be significant for the plasma chemistry. Thus also in this case we disregard reactions involving meta-stable atoms and molecules and thus the main chemistry is initiated by N(^{4}S) atoms and N^+ ions. As in Ar/N_2 plasmas, N_2 molecules are formed by plasma-surface interactions. Also in this type of plasma, the N^+ ion flow increases approximately linear with the plasma current for a constant flow through the source [31].

ad. d)

In the fourth experiment, the same plasma as described under ad. a) was used. However, instead of N_2/O_2 mixtures, NO was injected in the background of the plasma

vessel.

In all four experiments nitrogen and/or oxygen or nitric oxide, are admixed to the plasma by injection in the background of the process chamber, i.e. into the re-circulation flow in the chamber. Oxygen-containing gases need to be injected downstream, since injection into the arc would damage the plasma source. These molecules, together with molecules generated in the plasma, form the basis of influx in the expanding plasma beam. It has been established that diffusion inwards occurs not only in the subsonic region, but also already in the supersonic region if the flow is rarefied at low pressure [39, 40]. As a result, the gas mixture in the re-circulating flow in the periphery of the chamber is mixed into the forward plasma beam emanating from the source. Thus the molecules injected in the background are to a large extend dissociated. If the injected flow is equal or lower then the ion flow from the source, the injected flow can be completely dissociated.

In plasmas containing N_2, O_2 or NO the following charge transfer reactions may occur:

$$\mathrm{Ar^+ + N_2 \longrightarrow Ar + N_2^+} \qquad k \approx 2 \times 10^{-16}\ \mathrm{m^3\,s^{-1}}, \qquad [34] \qquad (6.4)$$

$$\mathrm{Ar^+ + O_2 \longrightarrow Ar + O_2^+} \qquad k \approx 10^{-16}\ \mathrm{m^3\,s^{-1}}, \qquad [34] \qquad (6.5)$$

$$\mathrm{N^+ + N_2 \longrightarrow N + N_2^+} \qquad k \approx 10^{-16}\ \mathrm{m^3\,s^{-1}}, \qquad [35] \qquad (6.6)$$

$$\mathrm{N^+ + O_2 \longrightarrow N + O_2^+} \qquad k = 2.8 \times 10^{-16}\ \mathrm{m^3\,s^{-1}}, \qquad [41] \qquad (6.7)$$

$$\mathrm{N^+ + O_2 \longrightarrow NO^+ + O} \qquad k = 2.5 \times 10^{-16}\ \mathrm{m^3\,s^{-1}}, \qquad [41] \qquad (6.8)$$

$$\mathrm{Ar^+ + NO \longrightarrow Ar + NO^+} \qquad k = 2.7 \times 10^{-16}\ \mathrm{m^3\,s^{-1}}. \qquad [42] \qquad (6.9)$$

Dissociative recombination reactions:

$$\mathrm{O_2^+ + e \longrightarrow O + O}, \qquad (6.10)$$

$$\mathrm{N_2^+ + e \longrightarrow N + N}, \qquad (6.11)$$

$$\mathrm{NO^+ + e \longrightarrow N + O}. \qquad (6.12)$$

Dissociative recombination reactions typically have a rate constant of $1 \times 10^{-13}\sqrt{\hat{T}_e}$ $\mathrm{m^3\ s^{-1}}$ [36], which gives a rate of 2×10^{-13} $\mathrm{m^3\ s^{-1}}$ for an electron temperature around $\hat{T}_e = 0.3$ eV. Note that the reaction rates of dissociative recombination are orders of magnitude higher than those for charge-transfer reactions. Therefore charge-transfer reactions involving the molecular ions O_2^+ and NO^+ are neglected, since both ions have a very short lifetime due to the fast dissociative recombination reactions ($n_e/n_a > 5 \times 10^{-3}$ [33])

The production of molecules out of atomic or molecular radicals in the volume by three particle reactions can be excluded, since these reactions are too slow to lead to any significant production under our low-pressure conditions. Note that the transit time, relevant for "forward" kinetics, is short (< 1 ms), whereas the residence time, relevant to the background kinetics, is relatively long (0.1 – 1 s). Even then at the relevant pressures (mostly ≤ 300 Pa) the particle association of two radicals in a three body reaction is improbable. Instead the formation of molecules at the surface is much more likely; the surface acts as the third body in this case. This means that most of the (atomic) radicals will arrive at the surface at which they will adsorb. At the surface, new molecules can be generated via heterogeneous reactions which subsequently desorb:

$$\mathrm{N} + \mathrm{N} \longrightarrow \mathrm{N_2} \tag{6.13}$$

$$\mathrm{O} + \mathrm{O} \longrightarrow \mathrm{O_2} \tag{6.14}$$

$$\mathrm{N} + \mathrm{O} \longrightarrow \mathrm{NO} \tag{6.15}$$

This process is called plasma-activated catalysis, because a plasma acts as catalyst to produce the radicals for the molecule production [43].

We note that the injected or produced molecules in the plasma may undergo reactions with atomic N in the re-circulating flows background of the plasma vessel leading to more radicals and direct production NO [23]:

$$\mathrm{N} + \mathrm{O_2} \longrightarrow \mathrm{O} + \mathrm{NO} \qquad k = 3.2 \times 10^{-18} \frac{T}{300} \exp(\frac{-3150}{T}) \ \mathrm{m^3\,s^{-1}}, \tag{6.16}$$

or to the loss of NO [23]:

$$\mathrm{N} + \mathrm{NO} \longrightarrow \mathrm{N_2}(\mathrm{X}, \nu \sim 3, 4) + \mathrm{O} \qquad k = 1 \times 10^{-18} T^{0.5} \ \mathrm{m^3\,s^{-1}}. \tag{6.17}$$

The O atom produced in these reactions can be adsorbed at the surface, which can lead to a second NO molecule

6.2.3 Diagnostics

Mass spectrometry

The concentrations of the stable species present in the background of the plasma, NO, N_2 and O_2, were determined with mass spectrometry. The setup was equipped with a quadrupole mass spectrometer (Balzers QMS 421C) on top of the reactor with a secondary electron multiplier (SEM) as detector. The mass spectrometer unit was

pumped to a pressure in the range of 10^{-5} to 10^{-9} mbar with two vacuum pumps in series, a turbo pump (Balzers TPU 180H, 180 litre/s) and a rotary vane pump (Edwards RV3, 3 m^3/h). The mass spectra were measured by sampling the gas through a controlled all-metal regulating valve (UDV 035), while the operating pressure in the mass spectrometer unit was in the 10^{-6} mbar range depending on the chamber pressure.

Absolute concentrations of the stable gas species N_2, O_2 and NO were obtained by calibrating the mass spectrometer signals by injecting the relevant gases into the plasma chamber at various known pressures in the absence of a plasma to avoid conversion of the gases. The sensitivity for N_2O and NO_2 gas was insufficient to detect them. Also from the results of experiments with infrared tunable diode laser absorption spectroscopy (TDLAS) in combination with mass spectrometry, we concluded that N_2O and NO_2 were only minor species in the plasma. The N_2O concentration was below 5% of the NO concentration, except at low ($< 10\%$) O_2 percentages, for which almost no NO was observed and still a significant amount of N_2O was detected. The NO_2 concentration was always below 1% of the NO concentration.

Phase-shift cavity ring-down spectroscopy

In Ar-NO plasmas, the density and temperature of generated O_2 were also determined with the phase-shift cavity ring-down technique. The technique and setup are described in Chapter 2. The measurements were performed on the $^{P}P(15,15)$ transition of the $b^1\Sigma_g^+(\nu' = 0) \leftarrow X^3\Sigma_g^-(\nu'' = 0)$ band of molecular oxygen at 13068.08 cm^{-1}. As mentioned in Chapter 2, a modulation of several times the free spectral range (FSR) was introduced on the grating of the external cavity of the diode laser to enhance the sensitivity of the technique. This modulation introduced a broadening on the absorption spectra. This does not influence the determination of the densities, which is based on the integral absorption (assuming no saturation). However, for the determination of the width of the absorption spectra it is necessary to lower the amplitude of the modulation to about one FSR, at the cost of sensitivity. For the density determination of the produced O_2 in Ar-NO plasmas, the highest sensitivity was required and the large modulation was used.

So, to determine the temperature of the O_2 molecules, the broadening due to the modulation had to be known. Therefore, the vessel was filled with 25 Pa of O_2 at a temperature of 293 K. The lock-in amplifier was set to an integration time of 200 milliseconds. From the baseline of the spectrum, i.e. ϕ_0, a ring-down time of 8

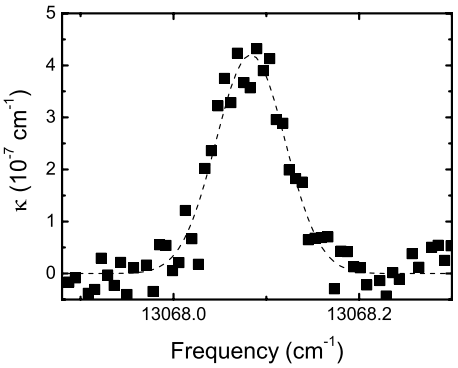

Figure 6.2: A phase-shift cavity ring-down measurement of O_2 in an Ar–NO plasma for the ${}^{P}P(15,15)$ transition of the $b^1\Sigma_g^+(\nu'=0) \leftarrow X^3\Sigma_g^-(\nu''=0)$ band of molecular oxygen. The plasma was created with 6 slm Ar applied through the arc at an arc current of 70 A with 1.8 slm NO injected into the background. The background pressure was 410 Pa.

μs was determined. The recorded absorption lines had a Gaussian spectral profile. This means that the experimentally observed line-width $\Delta\nu$ is a convolution of two Gaussian profiles and is given by:

$$\Delta\nu^2 = \Delta\nu_D^2 + \Delta\nu_B^2, \tag{6.18}$$

where $\Delta\nu_D$ is the Doppler width and $\Delta\nu_B$ the width of the modulation broadening. At $T = 293$ K, $\Delta\nu_D = 0.028$ cm^{-1}, which gives $\Delta\nu_B = 0.081$ cm^{-1}.

In Fig. 6.2, a typical PSCRD measurement in an Ar-NO plasma is shown. An argon plasma was created with 6 slm argon applied through the arc, and 1.8 slm NO was admixed into the background of the vessel. The arc current was set at 70 A and the pressure was 410 Pa. In this case, $\Delta\nu = 0.088$ cm^{-1}; using Eq. 6.18 gives a temperature of 400 K. The O_2 density determined was 7.21×10^{21} m^{-3}. From measurements on various Ar-NO plasma conditions, the O_2 densities measured with mass spectrometry were within 10% of the values obtained with PSCRD spectroscopy, therewith validating the absoluteness of the measured densities determined by mass spectrometry. Furthermore, an average temperature for the O_2 molecules of 420 ± 20 K was determined. The temperature indicates that the detected O_2 was present in the background of the plasma reactor, since molecules in the plasma beam would have a temperature of around 1500 K [44, 45]. This was also to be expected, since O_2 molecules are most likely produced at the wall, so in the background of the plasma.

6.3 Results and discussion

The conversion of the molecules is expressed as a so-called reduced molar fraction, which is the ratio of *measured* values only, i.e. the ratio between *measured* produced molecules under investigation and the *measured* total number of N and O containing molecules present in the plasma. The term "reduced molar fraction" expresses the fact that the molar fractions are calculated with regard to N and O containing gases only, so excluding the argon gas. The advantage of using a reduced molar fraction is that for the calibration of the mass spectrometer signals, we can use ratios of calibration factors, even if differences in the detection system occur, which would lead to a different absolute calibration. It proved that the ratio of the sum of measured densities and the sum of the filling densities of molecules, ($[N_2]$ + $[O_2]$ + [NO])$_m$/($[N_2]$ + $[O_2]$ + [NO])$_f$ was measured to be around one, showing that this procedure gives accurate results. Also in the case of NO conversion to N_2 and O_2 it proved that $[N_2] \approx [O_2]$, indicating again that the mass balance before and after conversion of the precursors was held. The reduced NO molar fraction is defined as:

$$\frac{[NO]}{([NO] + [O_2] + [N_2])}. \tag{6.19}$$

and the reduced O_2 and N_2 molar fraction is defined as:

$$\frac{[O_2] + [N_2]}{([NO] + [O_2] + [N_2])}. \tag{6.20}$$

Thus in fact, this reduced molar fraction is equal to the conversion efficiency. The obtained results using these conversion factors could be reproduced within a 5% error margin while measurements were taken over a one month period.

6.3.1 Ar plasma with N_2 and O_2 injected in the background

In the first experimental situation, an argon plasma was created with 3 slm argon applied through the arc, and oxygen and nitrogen were admixed into the background of the vessel. The arc current was set at 70 A. The N_2 and O_2 molecules are partially dissociated to N and O atoms by charge-transfer reactions between Ar^+ and N_2 and O_2 reactions (6.4) and (6.5), followed by dissociative recombination of the molecular ions, reactions (6.11) and (6.10). The rate coefficients of the reactions differ a factor two, so the amount of N and O atoms formed depends on the injected ratio according to $n_N/n_O = 2n_{N_2}/n_{O_2}$. The reduced NO molar fraction as a function of the injected O_2 flow downstream, for a constant flow of 2 slm N_2 injected into the background

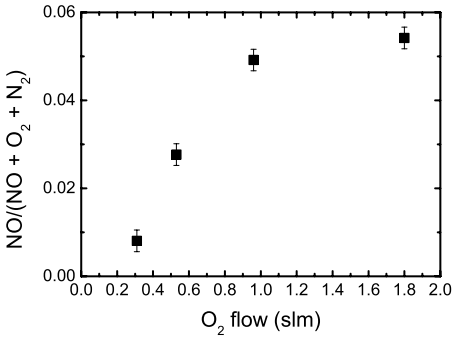

Figure 6.3: Reduced NO molar fraction as a function of the O_2 flow injected in the background. The plasma was created with 3 slm argon applied through the arc and with an arc current of 70 A, and a constant flow of 2 slm nitrogen was injected in the background. The background pressure was kept constant at 100 Pa.

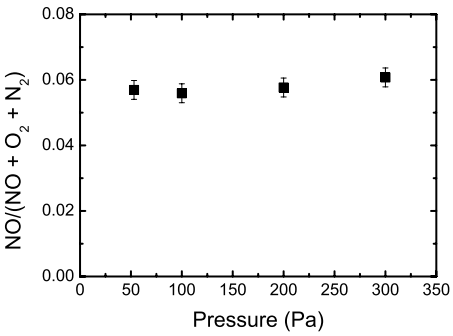

Figure 6.4: Reduced NO molar fraction as a function of the pressure. The plasma was created with 3 slm argon applied through the arc and with an arc current of 70 A. A constant flow of 1.1 slm nitrogen and 1.8 slm oxygen was injected in the background.

is depicted in Fig. 6.3. The pressure in the vessel was kept constant at 100 Pa. The measured reduced NO molar fraction increased with increasing O_2 flow and saturated at around 5% for O_2 flow higher than $\sim$ 1 slm. Furthermore, it seems that a threshold in the NO production is present for small O_2 flows. This is clearly different to the experiments in which ammonia was generated from mixtures nitrogen and hydrogen in which such a threshold was not observed (see Chapter 4).

One could argue that NO is formed via reaction (6.16) in the background of the plasma, where the residence time is approximately 0.3 seconds. The amount of NO produced in the gas phase can be estimated by taking into account the production of NO via reaction (6.16) and its destruction via reaction (6.17):

$$\frac{dn_{NO}}{dt} = n_N \cdot n_{O2} \cdot k_{N-O_2} - n_N \cdot n_{NO} \cdot k_{N-NO}. \tag{6.21}$$

Assuming a temperature of 1000 K, an integration time equal to the lifetime of N atoms, τ_N, of 50 ms [46], and n_N is at maximum 1.1×10^{21} m^{-3} (at the lowest oxygen flow), this results in a NO density which is less than 1% of the measured NO density. This shows that in argon plasmas with N_2 and O_2 injected in the background, NO is not produced in the gas phase, but has to be formed by the association of N and O radicals at the surface.

At relative O_2 flow rates smaller then 0.1, almost no NO was observed. This kind of threshold could be due to the destruction of NO by reactions between NO and N atoms, reaction (6.17). However, under these conditions also other molecules can be formed, i.e. N_2O, from which NO is produced when the O_2 flow increases. Measurements performed using tunable diode laser absorption spectroscopy (see Chapter 7), showed that this threshold in NO production is indeed related to the generation of N_2O. The N_2O molecules cannot be produced in the gas-phase in our low-pressure experiments. N_2O is most probably formed by the association of N radicals and NO adsorbed at the surface of the reactor walls:

$$N + NO_{ads} \longrightarrow N_2O. \tag{6.22}$$

At higher O_2 flows, a transition from N_2O generation to NO generation is observed. As the O_2 flow increases, NO can be produced in the gas phase by the reaction between N_2O and O radicals.

Under maximum NO production conditions, i.e. 1.8 slm O_2 injected in the background, the reduced NO molar fraction was measured as a function of the pressure in the vessel (Fig. 6.4). The reduced NO molar fraction proved to be independent of pressure as is expected due to the remote nature of the plasma. Namely, the Ar^+ ion flow is only dependent on the cascaded arc plasma source parameters and thus remains constant, when the pressure in the vessel is changed. Thus also the amount of N and O atoms, and the amount of produced NO is constant, but the residence time of NO in the vessel increases with increasing pressure, i.e. $n_{NO} \propto \tau$. And since τ is linearly dependent on the pressure in the vessel, the NO density should also increase linearly with increasing pressure. The same reasoning holds for the N_2 and O_2 production from N and O radicals via N respectively O surface association of two radicals at the reactor wall.Furthermore, the N atoms in the plasma background have a lifetime time of typically only 10 – 50 ms (typically a factor 40 shorter than for NO molecules). As a result, the destruction of NO by N radicals is almost pressure independent. This means that the reduced molar fractions as calculated with Eq. 6.19 and Eq. 6.20, would be independent of the pressure. A similar behavior is found for N_2 and O_2 molecules, which leads to the conclusion that NO, N_2 and O_2 are mainly produced at the vessel wall.

In the final experiment, the reduced NO molar fraction was measured on a similar plasma reactor, with only a slightly different geometry. An argon plasma was created with 3 slm argon applied through the arc and the arc current was set at 75 A. Simultaneously N_2 and O_2 were injected in the background with a total flow of

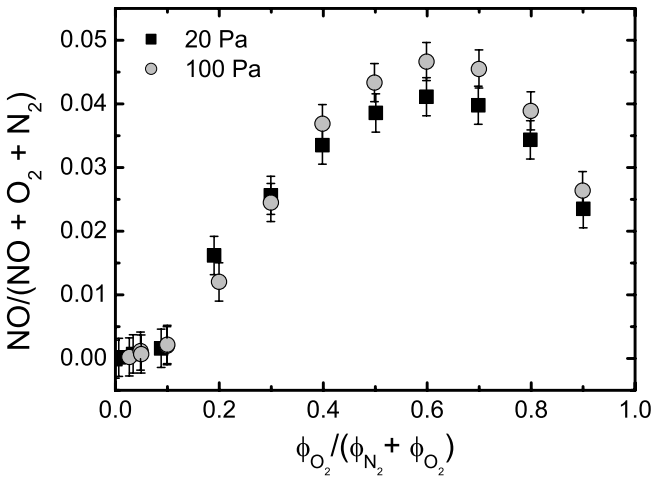

Figure 6.5: Reduced NO molar fraction as a function of the relative oxygen flow to the total N_2 and O_2 flow rate at a pressure of 20 Pa and 100 Pa. The plasma was created with 3 slm argon applied through the arc at an arc current of 75 A. Simultaneously N_2 and O_2 were injected in the background with a total flow of 1.8 slm.

1.8 slm. The reduced NO molar fraction as a function of the relative oxygen flow rate to the total N_2 plus O_2 flow rate is plotted in Fig. 6.5 at a pressure of 20 Pa and 100 Pa. The reduced NO molar fraction for both pressures is the same within the accuracy of the mass spectrometer measurements, which is in agreement with the measurements presented above, from which we concluded that the reduced NO molar fraction is independent of pressure. The maximum in NO production is observed for a relative oxygen flow of 0.6. This slight shift to higher O_2 flows is caused by a lower rate coefficient for the charge-transfer reaction of Ar^+ with O_2 (reaction (6.5)), so that more O_2 than N_2 has to be injected to have equal amounts of O and N radicals. Similar trends in mixtures of oxygen and nitrogen were also observed by others in for example a dc glow discharge [7] and rf plasmas [8].

In conclusion, the maximum of the reduced NO molar fraction is around 5%. The gas composition of the plasma consists of $\approx$ 5% NO and $\approx$ 95% N_2 and O_2. The gas composition at small O_2 flows will be further investigated in Chapter 7.

6.3.2 Ar/N_2 plasma with O_2 injected in the background

In the second experimental situation, the plasma source was operated on a mixture of argon and nitrogen with oxygen injected in the background of the plasma vessel. The

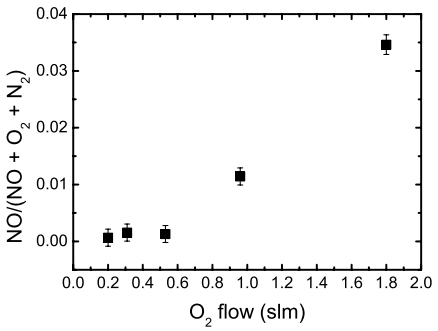

Figure 6.6: Reduced NO molar fraction as a function of the O_2 flow injected in the background. The plasma was created with 2 slm argon and 1.1 slm N_2 applied through the arc at an arc current of 50 A. The background pressure was kept constant at 100 Pa.

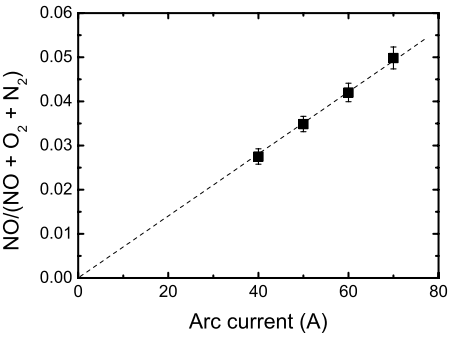

Figure 6.7: Reduced NO molar fraction as a function of the current through the arc. The plasma was created with 2 slm argon and 1.1 slm N_2 applied through the arc and 1.8 slm O_2 injected in the background. The background pressure was kept constant at 100 Pa.

plasma was created with 2 slm argon and 1.1 slm nitrogen applied through the arc at an arc current of 50 A. The pressure was kept constant at 100 Pa. The dissociation of N_2 through the arc is expected to be close to 100%. The injected O_2 and the N_2 molecules formed at the wall are partially dissociated to N and O atoms by reactions (6.4) – (6.12). The difference with the situation in Sec. 6.3.1 is that now more N atoms are present in the plasma. The reduced NO molar fraction as a function of the injected O_2 flow increased with increasing O_2 flow with a sharp increase in NO production for O_2 flows > 0.55 slm (Fig. 6.6). For oxygen flows below this value, we know from other experiments that N_2O is formed, via reaction (6.22). The threshold in reduced NO molar fraction in more pronounced then in a pure argon plasm. Now, more O_2 has to injected to initiate the transition from N_2O to NO generation on the surface. Furthermore, at low O_2 flows, the produced NO can efficiently be destroyed by reactions with N atoms in the gas phase, reaction (6.17). At higher flows, the NO destruction is compensated by more NO production, leading to an increase in measured NO molar fraction.

However, the amount of N^+ ions from the plasma source responsible for the production of O radicals can only explain about 40% of the observed NO. This suggest that NO may be formed by the reaction of N with O_2 molecules (reaction 6.16). In the expansion, the transit time is too short, even if it is assumed that the activation

energy in the supersonic part of the expansion can be overcome by the high energy of the N radicals from the plasma source. NO can be formed via reaction (6.16) in the background of the plasma, where the lifetime of the N atoms is approximately 10 ms [46]. This is a different value than used in the previous section as the lifetime is related to the residence time of stable gases in the reactor ($2\tau_N/\tau_{res} \approx n_N/n_{N_2}$), which is determined by the plasma conditions. The amount of NO produced in the gas phase can be estimated by taking into account the production of NO via reaction (6.16) and its destruction via reaction (6.17) using Eq. 6.21. Using a N atom density in the background of 1×10^{20} and a temperature of 1000 K in the reaction constants, the NO density produced via this channel for an O_2 flow of 1.8 slm is at maximum about 30% of the measured NO density. At lower O_2 flows, the residence of the N atoms increases and thus then more NO can be formed in the gas phase, up to 70%.

This implies that NO is partly also produced through another reaction mechanism. In the production process in the gas phase as described above, two N atom are used to produce two O radicals. The O radicals will not react in the gas phase and will arrive at the surface, where also part of the N atoms will stick. There then NO can be produced by association of N and O radicals and subsequently desorption of NO.

At the condition of maximum NO production, i.e. 1.8 slm O_2 injected in the background, the reduced NO molar fraction was measured as a function of the current through the arc. The NO production had a linear dependence on the arc current as shown in Fig. 6.7. This indicates that the NO production is related to the flow of reactive particles emanating from the plasma source, since the ion flow and most probably also the N flow increases linear with arc current. At higher currents, there are more ions and atoms present which can dissociate O_2 and N_2 molecules. The increased atom and ion flow, will thus lead to a linear increase in the NO production in the gas phase as well as of O radicals. So, the NO production partly via wall association, reaction (6.15), will increase linearly with arc current. We note that since only N_2, O_2 and NO are present in the plasma, the denominator of Eq. 6.19 stays constant while the arc current increases. Since the NO production increases linearly with arc current, this results in the observed trend for the reduced molar fraction in Fig. 6.7.

At the same condition, i.e. 1.8 slm O_2 injected in the background, the reduced NO molar fraction was measured as a function of the pressure in the vessel Fig. 6.8. The NO production was proved again to be independent of pressure; only at pressures above 100 Pa a slight increase could be observed. The NO production was

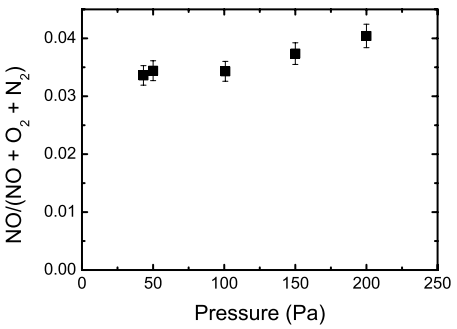

Figure 6.8: Reduced NO molar fraction as a function of the pressure. The plasma was created with 2 slm argon and 1.1 slm N_2 applied through the arc at an arc current of 50 A and 1.8 slm O_2 injected in the background.

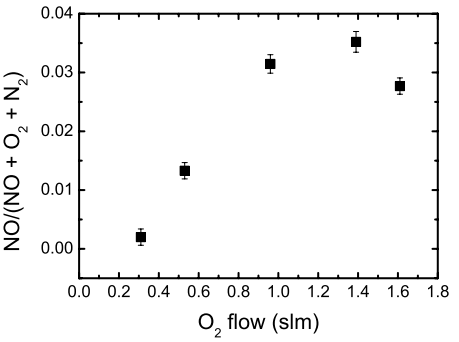

Figure 6.9: Reduced NO molar fraction as a function of the O_2 flow injected in the background. The plasma was created with 2 slm argon and a varying N_2 flow applied through the arc at an arc current of 50 A. A total flow of N_2 and O_2 of 1.5 slm, except for pure oxygen. The background pressure was kept constant at 100 Pa.

also measured for mixtures of N_2 and O_2 with a total flow of 1.5 slm, except for pure oxygen. The reduced NO molar fraction plotted as function of the injected O_2 flow in Fig. 6.9, had now a maximum at approximately 1.25 slm O_2 and 0.25 slm N_2. From Fig. 6.9 it can be concluded that the NO production increases with a higher ratio of O_2 to N_2. The optimum NO production appeared to be at $[O_2]/[N_2] = 5$. This could indicate that at that ratio the NO production is at its maximum whereas the NO destruction via reaction (6.17) is at its minimum. At higher ratios, when the reduced NO molar fraction was measured to decrease, its production is limited by the amount of available N atoms, which is decreasing.

6.3.3 N_2 plasma with O_2 injected in the background

In the third experimental situation, the plasma was created with 1.1 slm nitrogen applied through the arc and oxygen injected in the background. The reduced NO molar fraction as a function of the injected O_2 flow in the background was measured for two arc currents, $I = 50$ A and $I = 70$ A (Fig. 6.10). The pressure was kept constant at 100 Pa. As in the previous plasma, a dissociation degree of N_2 in the arc is expected to be 50 – 100%. The injected O_2 and formed N_2 molecules are partially dissociated to N and O molecules by reactions (6.6) – (6.12). The reduced

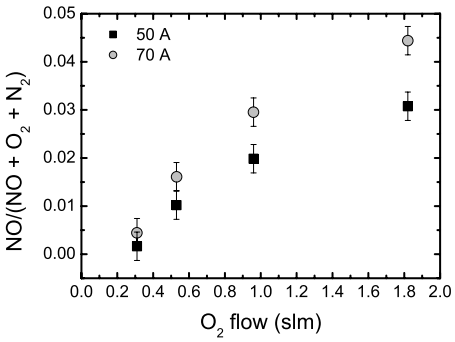

Figure 6.10: Reduced NO molar fraction as a function of the O_2 flow injected in the background for two arc currents, $I = 50$ A and $I = 70$ A. The plasma was created with 1.1 slm N_2 applied through the arc. The background pressure was kept constant at 100 Pa.

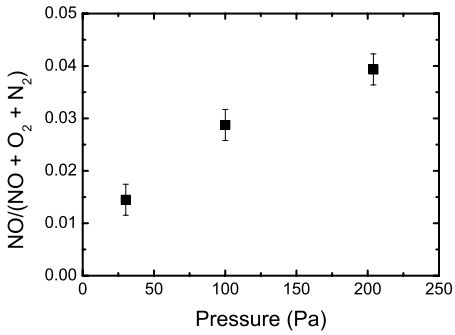

Figure 6.11: Reduced NO molar fraction as a function of the pressure. The plasma was created with 1.1 slm N_2 applied through the arc at an arc current of 50 A and 1.8 slm O_2 injected in the background.

NO molar fraction increases with increasing O_2 flow (Fig. 6.10). Also in this plasma, the amount of N^+ ions is by far not enough to explain the amount of O radicals needed to produce the observed NO by association of N and O at the surface.

This indicates that also in this plasma the reaction between N atoms and O_2 molecules leading to NO production has to be important (reaction 6.16). In the expansion, the transit time is too short, even if it is assumed that the activation energy in the supersonic part of the expansion can be overcome by the high energy of the N radicals from the plasma source. NO can be formed via reaction (6.16) in the background of the plasma, where the lifetime of the N atoms is approximately 20 ms [46]. The amount of NO produced in the gas phase can be estimated by taking into account the production of NO via reaction (6.16) and its destruction via reaction (6.17) using Eq. 6.21. Using a N atom density in the background of 3×10^{20} m^{-3} as previously determined [33], and a temperature of 1000 K in the reaction constants, the NO density produced via this channel for an O_2 flow of 1.8 slm is at maximum about 20% of the measured NO density. At lower O_2 flows, the residence of the N atoms increases and thus then more NO can be formed in the gas phase, up to 100%. Thus also here part of the NO is produced at the wall by the association of N and O atoms. The NO production via this way is of course also counteracted by the destruction of NO, until enough O_2 is injected to create a stable situation in the NO production, as observed

in Fig. 6.10. Except at the lowest O_2 flow, there is a factor 1.5 between the reduced NO molar fractions for the two currents, which is caused by the increase by a factor 1.5 in the ionization degree of the N_2 plasma [31]. At an O_2 flow of 0.3 slm, there is a similar threshold as observed in the two previous cases.

At the condition in which 1.8 slm O_2 is injected in the background, the reduced NO molar fraction was measured as a function of the pressure in the vessel (Fig. 6.11). The NO production increased with increasing pressure. One can calculate using Eq. 6.21, that the contribution of the NO that can be produced in the gas phase via the combination of the reactions (6.16) and (6.17) to the reduced NO molar fraction is constant for all pressures, i.e a reduced NO molar fraction of approximately 0.01. However, since at higher pressures more O_2 is present and thus more NO can be produced and is destroyed again, this means that the amount of O formed increases. And thus also the amount of NO that can be produced at the surface by association of N and O atoms.

6.3.4 Ar plasma with NO injected in the background

In the fourth experimental situation, an argon plasma was created with 3 slm argon applied through the arc, and nitric oxide was admixed into the background of the vessel. The arc current was set at 70 A. The NO molecules are partially dissociated to N and O atoms by charge-transfer reactions between Ar^+ ions and NO molecules, reaction (6.9), followed by dissociative recombination of the molecular ion, reaction (6.12). We note that NO is probably completely dissociated when the injected molecule flow was equal or lower than the ion flow from the source, i.e. NO flow < 0.45 slm. The reduced O_2 + N_2 molar fraction as a function of the injected NO is plotted in Fig. 6.12 as measured at a pressure in the vessel of 100 Pa. Up to 92% conversion of NO to N_2 and O_2 was observed, if the NO flow was below the Ar^+ flow emitted by the plasma source. With further increasing NO flow the measured reduced O_2 + N_2 molar fraction decreased. This is because at a NO flow is higher than the Ar^+ flow, adding more NO does not lead to more dissociation of NO. Then the numerator of Eq. 6.20 does not change anymore, but the denominator of Eq. 6.20 increases as more NO is added, which results in a decreasing reduced O_2 + N_2 molar fraction. We note that thus when more NO was added, still 92% of the dissociated NO was converted into N_2 and O_2.

As we have seen in section 6.3.1, also in plasmas containing N_2 and O_2 with a total flow below the Ar^+ ion flow, only a small amount of NO was observed, up to

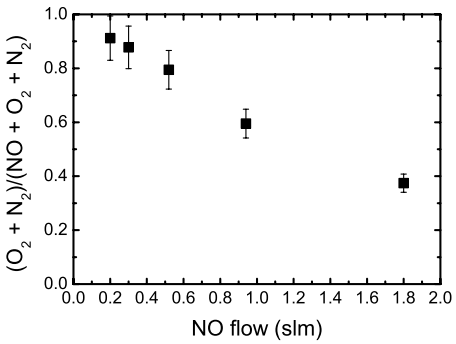

Figure 6.12: Reduced O_2 and N_2 molar fraction as a function of the NO flow. The plasma was created with 3 slm Ar applied through the arc at an arc current of 70 A. The background pressure was kept constant at 100 Pa.

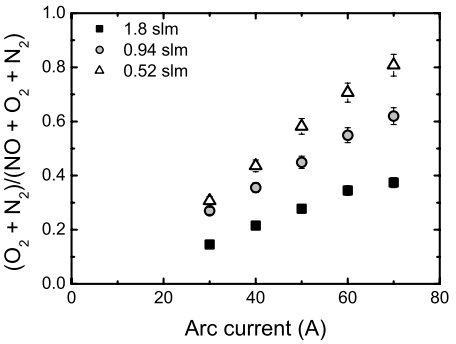

Figure 6.13: Reduced O_2 and N_2 molar fraction as a function of the arc current for three different NO flows. The plasma was created with 3 slm Ar applied through the arc at a constant background pressure of 100 Pa.

8%. Thus, the two types of plasmas show a strong resemblance in the final resulting gas composition, i.e. $\approx$ 8% NO and $\approx$ 92% N_2 and O_2 present in the plasma, although the starting conditions are completely different. We note that since the flows in these experiments are such that all the injected or produced NO or N_2 and O_2 are dissociated, the measured NO in both cases has to be produced in the same way. It points to the observation that for high dissociating conditions not only the injected gases have to be considered in the chemistry, but also the produced molecules.

The reduced O_2 + N_2 molar fraction was measured as a function of the current applied through the arc for three different NO flows. The reduced O_2 + N_2 molar fraction increased approximately linear with increasing arc current as plotted in Fig. 6.13. Up to 85% conversion of NO to N_2 and O_2 was observed. This indicates that the O_2 and N_2 production is related with the ion flow emanating from the plasma source, since the ion flow and thus the O and N production increases linearly with arc current. So the NO destruction as well as the O_2 and N_2 production out of N and O radicals increases linearly with current in the same way, resulting in the observed behavior of the reduced O_2 and N_2 molar fractions as function of the arc current. Note that the denominator of Eq. 6.20 is constant since two NO molecules will give one N_2 and one O_2 molecule.

At the condition of 0.94 slm NO injected, the reduced O_2 + N_2 molar fraction was measured to be independent of pressure in the vessel (Fig. 6.14). This indicates

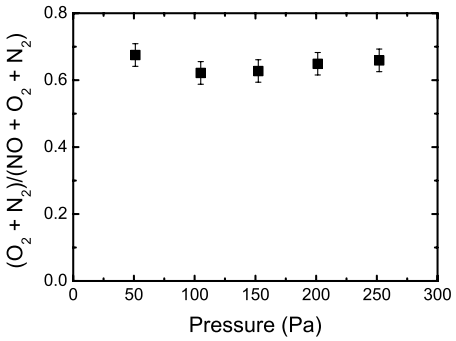

Figure 6.14: Reduced O_2 and N_2 molar fraction as a function of pressure. The plasma was created with 3 slm Ar applied through the arc at an arc current of 70 A with 0.94 slm NO injected in the background.

that the process of NO destruction and O_2 and N_2 formation is ion-chemistry initiated. The NO molecules are dissociated by charge-transfer reactions between Ar^+ and NO followed by dissociative recombination of the molecular ion, leading to O and N atoms. Since the Ar^+ ion flow is only dependent on the cascaded arc source parameters, the Ar^+ flow is independent of pressure, i.e. the amount of N and O atoms produced is independent of pressure. If reactions related to NO, O_2 and N_2 formation are linearly dependent on pressure, the conversion factor calculated with Eq. 6.20 will be independent of pressure as observed in Fig. 6.14.

6.4 Conclusions

We measured the steady state gas composition of plasmas produced from $Ar/N_2/O_2$ mixtures and Ar/NO mixtures with quantitative mass spectrometry. In plasmas containing mixtures of nitrogen and oxygen a significant amount of nitric oxide (NO) was formed, i.e. up to 5% of the background gas was NO. Remarkable is that on average 5% NO was formed in three different types of plasma, i.e. (a) Ar plasma to which mixtures of N_2 and O_2 are added; (b) Ar/N_2 plasma to which O_2 is added; (c) N_2 plasma to which O_2 is added. In the inverse experiment, NO admixed to Ar plasmas, up to 92% of the NO was converted into N_2 and O_2,if the NO flow was equal or lower than the ion flow from the source.

So, in the NO-high depletion case, the situation is dynamically similar to the experiment in which N_2 and O_2 are injected into an argon plasma: in both cases

NO molecules are the minority species and N_2 and O_2 the majority species. Apparently, in both cases there is enough fragmentation and association of radicals to new molecules (for NO injection, mainly N_2 and O_2 molecules), or back to the original molecules (for N_2-O_2 injection). Thus the end situation is the same, if substantial dissociation can be reached in the residence time of the gases in the plasma.

We concluded from the results that in first order the N_2/O_2 system produces and reproduces N_2 and O_2, which are the most thermodynamically bonded molecules. In our low T_e plasmas, the molecules are mostly generated in wall association processes but also by gas phase reactions between N atoms and O_2 molecules leading to NO. It appears from the results, that the two types of plasmas show a strong resemblance in final gas composition, i.e. $\approx$ 5% NO and $\approx$ 95% N_2 and O_2 present in the plasma, although the starting conditions are completely different. This preference for N_2 and O_2 production is in accordance with a picture that molecules are formed by surface processes determined by binding energies.

Bibliography

[1] E.C. Zipf and S.S. Prasad, *Production of nitrous oxide in the auroral D and E regions*, Nature **287**, 523 (1980).

[2] M. Capitelli (Ed), *Molecular Physics and Hypersonic Flows*, (NATO ASI Series C-482), Kluwer, Dordrecht (1996).

[3] B.M. Penetrante and S.E. Schultheis (Ed), *Non-Thermal Plasma Techniques for Pollution Control: Part A—Overview, Fundamentals and Supporting Technologies and Part B—Electron Beam and Electrical Discharge Processing*, Springer-Verlag, Berlin (1993).

[4] S. Moreau, M. Moisan, M. Tabbrizian, J. Barbeau, J. Pelletier, A. Ricard, and L'H. Yahia, *Using the flowing afterglow of a plasma to inactivate Bacilus subtilis spores: Influence of the operating conditions*, J. Appl. Phys. **88**, 1166 (2000).

[5] C.D. Pintassilgo, J. Loureiro, and V. Guerra, *Modelling of a N_2–O_2 flowing afterglow for plasma sterilization*, J. Phys. D: Appl. Phys. **38**, 417 (2005).

[6] G.J.H. Brussaard, K.G.Y. Letourneur, M. Schaepkens, M.C.M. van de Sanden, and D.C. Schram, *Stripping of photoresist using a remote thermal Ar/O_2 and $Ar/N_2/O_2$ plasma*, J. Vac. Sci. Technol. B **21**, 61 (2003).

[7] J. Nahorny, C.M. Ferreira, B. Gordiets, D. Pagnon, M. Touzeau, and M. Vialle, *Experimental and theoretical investigation of a N_2–O_2 DC flowing glow discharge*, J. Phys. D: Appl. Phys. **28**, 738 (1995).

[8] G. Dilecce and S. De Benedictis, *Experimental studies on elementary kinetics in N_2-O_2 pulsed discharges,* Plasma Sources Sci. Technol. **8**, 266 (1999).

[9] R. Ono and T. Oda, *NO formation in a pulsed spark discharge in $N_2/O_2/Ar$ mixture at atmospheric pressure,* J. Phys. D: Appl. Phys. **35**, 543 (2002).

[10] B. Gordiets, C.M. Ferreira, J. Nahorny, D. Pagnon, M. Touzeau, and M. Vialle, *Surface kinetics of N and O atoms in N_2–O_2 discharges,* J. Phys. D: Appl. Phys. **29**, 1021 (1996).

[11] M. Castillo, V.J. Herrero, I. Méndez, and I. Tanarro, *Spectrometric and kinetic study of a modulated glow air discharge,* Plasma Sources Sci. Technol. **13**, 343 (2004).

[12] M. Castillo, I. Méndez, A.M. Islyaikin, V.J. Herrero, and I. Tanarro, *Low-pressure DC air plasmas. Investigation of neutral and ion chemistry,* J. Phys. Chem. **109**, 6255 (2005).

[13] M. Castillo, V.J. Herrero, and I. Tanarro, *Characterization and modelling of the steady state and transients of modulated hollow cathode discharges of nitric oxide,* Plasma Sources Sci. Technol. **11**, 368 (2002).

[14] M. Tsuji, K. Nakano, J. Kumagae, T. Matzuzaki, and T. Tsuji, *Decomposition of NO in a microwave-absorbent assisted discharge of N_2 at atmospheric pressure,* Surf. Coat. Technol. **165**, 296 (2003).

[15] M.A. Wójtowicz, F.P. Miknis, R.W. Grimes, W.W. Smith, and M.A. Serio, *Control of nitric oxide, nitrous oxide and ammonia emissions using microwave plasmas,* J. Hazard. Mater. **74**, 81 (2000).

[16] M. Baeva, H. Gier, A. Pott, J. Uhlenbusch, J. Höschele, and J. Steinwandel, *Studies on gas purification by a pulsed microwave discharge at 2.46 GHz in mixtures of $N_2/NO/O_2$ at atmospheric pressure,* Plasma Chem. Plasma Process. **21**, 225 (2001).

[17] A. Gal, M. Kurahashi, and M. Kuzumoto, *An energy-consumption and byproduct-generation analysis of the discharge nonthermal NO-reduction process,* J. Phys. D: Appl. Phys. **32**, 1163 (1999).

[18] J. Tang, T. Zhang, L. Ma, and N. Li, *Direct decomposition of NO activated by microwave discharge,* Ind. Eng. Chem. Res. **42**, 5993 (2003).

[19] M. Tsuji, K. Nakano, J. Kumagae, and T. Tsuji, *Decomposition of NO by microwave discharge of NO/He or NO/Ar mixtures,* Bull. Chem. Soc. Jpn. **75**, 607 (2002).

[20] K. Kiyokawa, H. Matsuoka, A. Itou, K. Hasegawa, and K. Sugiyama, *Decomposition of inorganic gases in an atmospheric pressure non-equilibrium plasma,* Surf. Coat. Technol. **112**, 25 (1999).

[21] M.C.M. van de Sanden, R.J. Severens, W.M.M. Kessels, R.F.G. Meulenbroeks, and D. C. Schram, *Plasma chemistry aspects of a–Si:H deposition using an expanding thermal plasma,* J. Appl. Phys. **84**, 2426 (1998), **85**, 1243 (1999).

[22] V. Guerra and J. Loureiro, *Self-consistent electron and heavy-particle kinetics in a low-pressure N_2–O_2 glow discharge*, Plasma Sources Sci. Technol. **6**, 373 (1997).

[23] I.A. Kossyi, A. Yu Kostinsky, A.A. Matveyev, and V.P. Silakov, *Kinetic scheme of the non-equilibrium discharge in nitrogen-oxygen mixtures*, Plasma Sources Sci. Technol. **1**, 207 (1992).

[24] B.F. Gordiets, C.M. Ferreira, V.L. Guerra, J.M.A.H. Loureiro, J. Nahorny, D. Pagnon, M. Touzeau, and M. Vialle, *Kinetic model of a low-pressure N_2–O_2 flowing glow discharge*, IEEE trans. Plasma Sci. **23**, 750 (1995).

[25] V. Guerra and J. Loureiro, *Kinetic model of a low-pressure microwave discharge in O_2–N_2 including the effects of O^- ions on the characteristics for plasma maintenance*, Plasma Sources Sci. Technol. **8**, 110 (1999).

[26] G. Cartry, L. Magne, and G. Cernogora, *Experimental study and modelling of a low-pressure N_2–O_2 time afterglow*, J. Phys. D: Appl. Phys. **32**, 1894 (1999).

[27] M.C.M. van de Sanden, J.M. de Regt, G.M. Jansen, J.A.M. van der Mullen, D.C. Schram, and B. van der Sijde, *A combined Thomson-Rayleigh scattering diagnostic using an intensified photodiode array*, Rev. Sci. Instrum. **63**, 3369 (1992).

[28] M.C.M. van de Sanden, J.M. de Regt, and D.C. Schram, *Recombination of argon in an expanding plasma jet*, Phys. Rev. E **47**, 2792 (1993).

[29] M.A. Blauw et al., To be published.

[30] A.J.M. Buuron, D.K. Otorbaev, M.C.M. van de Sanden, and D.C. Schram, *Absorption spectroscopy on the argon first excited state in an expanding thermal arc plasma*, Phys. Rev. E **50**, 1383 (1994).

[31] R.P. Dahiya, M.J. de Graaf, R.J. Severens, H. Swelsen, M.C.M. van de Sanden, and D.C. Schram, *Dissociative recombination in cascaded arc generated Ar-N_2 and N_2 expanding plasma*, Phys. Plasmas **1**, 2086 (1994).

[32] G.J.H. Brussaard, M.C.M. van de Sanden, and D.C. Schram, *Ion denisties in a high intensity, low flow nitrogen–argon plasma*, Phys. Plasmas **4**, 3077 (1997).

[33] S. Mazouffre, I. Bakker, P. Vankan, R. Engeln, and D.C. Schram, *Two-photon laser induced-fluorescence spectroscopy performed on free nitrogen plasma jets*, Plasma Sources Sci. Technol. **11**, 439 (2002).

[34] G.J.H. Brussaard, *Remote arc generated plasma in diatomic gases*, PhD thesis, Eindhoven University of Technology, Eindhoven, 1999, available on-line at http://alexandria.tue.nl/extra2/9900312.pdf.

[35] S.C. Brown, *Basic Data of Plasma Physics*, MIT Press, Cambridge MA (1966).

[36] J. Perrin, O. Leroy, and M.C. Bordage, *Cross-sections, rate constants and transport coefficients*

in silane plasma chemistry, Contrib. Plasma Phys. **36**, 3 (1996).

[37] J.A.M. van der Mullen, *Excitation equilibria in plasmas; a classification,* Phys. Rep. **191**, 110 (1990).

[38] G.J.H. Brussaard, E. Aldea, M.C.M. van de Sanden, G. Dinescu, and D.C. Schram, *Evidence of charge exchange between N^+ and $N_2(A^3\Sigma_u^+)$ in a low-temperature nitrogen plasma,* Chem. Phys. Lett. **290**, 379 (1998).

[39] R. Engeln, S. Mazouffre, P. Vankan, D.C. Schram, and N. Sadeghi, *Flow dynamics and invasion by background gas of a supersonically expanding thermal plasma,* Plasma Sources Sci. Technol. **10**, 595 (2001).

[40] P. Vankan, S. Mazouffre, R. Engeln, and D. C. Schram, *Inflow and shock formation in supersonic, rarefied plasma expansions,* Phys. Plasmas **12**, 102303 (2005).

[41] M. Capitelli, C.M. Ferreira, B.F. Gordiets, and A.I. Osipov, *Plasma kinetics in atmospheric gases,* Springer-Verlag, Berlin (2000).

[42] R.J. Shul, B.L. Upschulte, R. Passarella, R.G. Keesee, and A.W. Castleman Jr., *Thermal energy charge-transfer reactions of Ar^+ and Ar_2^+,* J. Phys. Chem. **91**, 2556 (1987).

[43] P. Vankan, T. Rutten, S. Mazouffre, D.C. Schram, and R. Engeln, *Absolute density measurements of ammonia produced via plasma-activated catalysis,* Appl. Phys. lett. **81**, 418 (2002).

[44] J.P.M. Hoefnagels, Y. Barrell, W.M.M. Kessels, and M.C.M. van de Sanden, *Time-resolved cavity ringdown study of the Si and SiH_3 surface reaction probability during plasma deposition of a–Si:H at different substrate temperatures,* J. Appl. Phys. **96**, 4094 (2004).

[45] P.J. van den Oever, J.H. van Helden, C.C.H. Lamers, R. Engeln, D.C. Schram, M.C.M. van de Sanden, and W.M.M. Kessels, *Density and production of NH and NH_2 in an Ar–NH_3 expanding plasma jet,* J. Appl. Phys. **98**, 093301 (2005).

[46] I.S.J. Bakker, Properties of an expanding thermal nitrogen plasma, Master's thesis, Eindhoven University of Technology, 2001.

Chapter 7

Mechanisms of molecule formation in $Ar/N_2/O_2$ plasmas

Abstract

The mechanisms of molecule formation in expanding plasmas containing mixtures of nitrogen and oxygen were investigated using time-resolved tunable diode laser absorption spectroscopy. In these plasmas fluxes of atomic N and O radicals are created, leading to the formation of NO and N_2O, but also NO_2 molecules, produced to a large extend in surface processes. At low relative O_2 flows (between 5 and 15%), a transition from N_2O generation to NO generation is observed. We show that when the nitrogen or oxygen flow is stopped, the generation of NO and N_2O molecules is still observed on time-scales much longer than the residence time of the gases in the plasma reactor. From this observation, we conclude that mainly NO and N are present at the surface and stored in the metal wall.

7.1 Introduction

The generation of NO and N_2O is observed in expanding plasmas containing mixtures of nitrogen and oxygen (Chapter 6). We showed that by using an atomic nitrogen and oxygen source by dissociation of N_2, O_2 or NO precursors that N_2, O_2 and NO molecules are (re-)formed. From various experimental studies on dc, microwave and rf discharges in N_2–O_2 at low pressures [1–4] and theoretical studies [5–9], the main reactions concerning the production of NO, N_2O, and NO_2 molecules have been determined. It was found that in these active plasmas reactions involving atoms and molecules in excited or meta-stable states, e.g. $N_2(X, \nu > 12)$, $N_2(A)$, $N(^2D)$, $N(^2P)$ and $O(^1D)$, are the key processes leading to these molecules. Furthermore, also plasma-surface processes, especially the wall processes of N and O atoms, could play a role in the observed NO densities [10–12].

Most of the experiments on N_2–O_2 plasmas have been performed in non-equilibrium active plasmas, in which a large number of processes has to be taken into account: electron kinetics, vibrational kinetics, chemical kinetics for a large number of species and surface processes. We studied passive recombining plasmas in which the electron temperature is only around 0.3 eV and therefore dissociation and excitation by electrons can be neglected at these temperatures [13]. It will be discussed in the next section that the densities of meta-stable atoms and molecules are too low to be responsible for the observed NO density in the current experiments.

In our low-pressure plasmas, the NO, N_2O and NO_2 molecules will primarily be formed in wall association processes of N and O radicals, possibly in combination with subsequent gas phase reactions, i.e. NO maybe formed by gas phase reactions out of N_2O and NO_2, both formed at the surface. Also other studies performed on N_2–O_2 plasmas showed that the densities of the molecules and radicals present in the plasma are directly related to processes at the surface [10–12]. The evolution of the time decay as function of the "history" of the surface has been studied mainly in O_2 plasmas, e.g. [14, 15] and a few studies have been done in N_2–O_2 afterglows [16].

Here, we present results on a more detailed study of the NO and N_2O generation in expanding thermal plasmas containing mixtures of nitrogen and oxygen, in which the oxygen percentage was varied from 0 – 100%. Furthermore, to characterize the surface coverage of the reactor wall in our experiments, we monitored the time-behavior of the densities of the NO and N_2O molecules after switching off the N_2 or O_2 flow into the plasma reactor. The densities were determined using high time-resolution tunable diode laser absorption spectroscopy (TDLAS).

Here, the TDLAS measurements were performed with the compact and transportable infrared multi-component acquisition (IRMA) system based on infrared absorption spectroscopy developed at the INP-Institute in Greifswald in Germany [17]. Absorption spectroscopy with the IRMA system has been performed previously to measure for example, the effect of combining plasma and photocatalyst for VOC removal in a low-pressure pulsed discharge in dry synthetic air [18], the line strength and transition dipole moment of the ν_2 fundamental band of the methyl radical [19], to study the composition of plasmas containing hydrocarbons [20–22], to investigate the gas composition of H_2–Ar–N_2 microwave plasmas containing methane [23] and to detect neutral species in a low-pressure plasma containing boron and hydrogen [24].

The TDLAS technique has several advantages. Firstly, the lead salt diode lasers in the spectral region between 3 and 20 μm have a very high spectral resolution of about 10^{-4} cm^{-1}. Secondly, the transitions in molecules and radicals in the IR region, especially in the fundamental bands, have large transition probabilities. Thirdly, the measured absorptions can easily be calibrated. And finally, the TDLAS technique is very suitable for time-resolved measurements [17, 25].

In this chapter, we will first describe the basics of the expanding recombining plasmas and the primary chemistry (Sec. 7.2.1). Next, in Sec. 7.2.2, the experimental details of the tunable diode laser absorption technique used to measure the NO and N_2O molecules will be outlined. In the results section (Sec. 7.3), the measured NO and N_2O densities will be discussed and time resolved measurements on these molecules, when the nitrogen or oxygen flow into the system is stopped, will be presented. Also a simple model to explain the observed densities will be proposed. In the last section the conclusions are presented.

7.2 Experiment details

7.2.1 Expanding thermal plasma setup

We present measurements of the densities of NO and N_2O produced in a plasma reactor in which a recombining plasma expanded generated from mixtures of argon, nitrogen and oxygen. Atomic N and O radicals were created with the expanding thermal plasma (ETP) technique [26]. In this remote technique, a high-density argon or nitrogen plasma is created in a high-pressure cascaded arc plasma source and the plasma processes take place downstream at lower pressure. In the DC cascaded arc

plasma source a high-pressure (typically 400 kPa) plasma is created in a channel with a diameter of 4 mm and a total length of 30 mm formed by 5 water-cooled insulated copper plates. The cascaded plates are at floating potential and the last plate acts as the common anode for the plasma. A dc current of 60 A is drawn in flowing argon or nitrogen gas from the three cathodes concentrically placed around one end of the channel to the grounded anode plate, producing the plasma. In the case of an expanding argon plasma, the plasma source emanates a partially ionized (12%) argon flow. The plasma expands supersonically through a conically shaped nozzle into a low-pressure vessel (typically 20 Pa), and after a stationary shock, expands subsonically towards the other end of the process chamber. The wall of the process chamber are made of stainless steel. In the expansion, the plasma is recombining as there is no power coupled into the plasma anymore. The downstream electron temperature decreases to 0.1 – 0.3 eV.

The plasma source was operated in two different ways. In the first one the arc source was operated on argon gas. In that case, the Ar^+ ions in the flow form the primary enthalpy reservoir. The meta-stable argon density is directly linked to the ion density, but a factor of 10 lower than the argon ion density [27] and we neglect the contribution of these states to the plasma chemistry. By charge transfer of argon ions with N_2 and O_2 molecules injected downstream, followed by dissociative recombination, atomic radicals are produced [28, 29]:

$$Ar^+ + N_2 \longrightarrow Ar + N_2^+ \qquad k \approx 2 \times 10^{-16}\ \mathrm{m^3\,s^{-1}}, \tag{7.1}$$

$$Ar^+ + O_2 \longrightarrow Ar + O_2^+ \qquad k \approx 10^{-16}\ \mathrm{m^3\,s^{-1}}, \tag{7.2}$$

$$N_2^+ + e \longrightarrow N(^4S) + N^* \tag{7.3}$$

$$O_2^+ + e \longrightarrow O(^3P) + O^* \tag{7.4}$$

The dissociative recombination reactions typically have a rate constant of $10^{-13}/\sqrt{\hat{T}_e}$ $m^3\ s^{-1}$ [30], which gives a rate of 2×10^{-13} $m^3\ s^{-1}$ for an electron temperature of about $\hat{T}_e = 0.3$ eV. Meta-stable atoms, $N^*(^2P, ^2D)$ and $O^*(^1D, ^1S)$ are produced by dissociative recombination of the molecular ions [31, 32]. However, these excited atoms will quickly be de-excited by collisions with electrons ($k_e \approx 10^{-13}$ $m^3\ s^{-1}$) [33], and with atoms and molecules present in the plasma (rate constant of 4.1×10^{-17} $m^3\ s^{-1}$ [34]).

In Chapter 4, it was shown that by increasing the amount of radicals in the plasma and thus flux to the surface, the production efficiency of ammonia increased. Therefore, we also optimized the nitrogen dissociation by operating the plasma source on nitrogen gas. O_2 could not be applied through the plasma source, since injection

into the arc would damage the plasma source. In the second experimental series, nitrogen gas was injected in the arc; in that case the primary enthalpy was carried in mainly nitrogen atoms and by nitrogen atomic ions. In a pure nitrogen plasma, the dissociation degree of N_2 in the arc is expected to be around 35% at high currents, while an ionization degree of around 1 – 5% is attained [34, 35]. The densities of the meta-stable N atoms N(^{2}P) and N(^{2}D) emanating from the plasma source are expected to be in the order of 20% of the N(^{4}S) atoms (assuming a thermal population at a temperature of 1 eV). In the expansion, the N(^{2}P) and N(^{2}D) densities will decrease fast due to de-excitation by collisions with electrons, but also with N(^{4}S) atoms, and N_2 molecules. This also applies to meta-stable N atoms produced in the expansion by dissociative recombination of N_2^+ with electrons; the produced density is limited by the ionization degree of the plasma. It results in a total density of around 1% for the meta-stable atoms in the plasma beam.

Previously, also a significant density of meta-stable $N_2(A^3\Sigma_u^+)$ molecules has been observed in expanding nitrogen plasmas [28]. These N_2(A) molecules were assumed to be produced by surface association of N atoms. This observation was made in a low-flow, low-current nitrogen plasma with a relatively low N^+ ion density. These N^+ ions are responsible for a major loss channel for N_2(A) molecules, i.e. a resonant charge transfer reaction. In the present plasma conditions more N^+ ions are produced, and as a result, the N_2(A) molecules are efficiently lost by this reaction [36]. Therefore we assume the role of N_2(A) molecules to be small. A finite contribution of excited molecules (as N_2(X,v)) can however not totally excluded.

By charge-transfer with N^+ from the plasma source the O_2 injected in the background is dissociated [37]:

$$N^+ + O_2 \longrightarrow N + O_2^+ \qquad k = 2.8 \times 10^{-16}\ \mathrm{m^3\,s^{-1}}, \tag{7.5}$$

$$N^+ + O_2 \longrightarrow NO^+ + O \qquad k = 2.5 \times 10^{-16}\ \mathrm{m^3\,s^{-1}}, \tag{7.6}$$

followed by dissociative recombination of the molecular ion (reaction(7.4)) and [37]:

$$NO^+ + e \longrightarrow N + O \qquad k = 2 \times 10^{-13}\ \mathrm{m^3\,s^{-1}}, \tag{7.7}$$

N and O radicals are produced.

In conclusion, ions are created in the plasma source and gases injected downstream interact with these ions, which results in atomic N and O radicals as is schematically depicted for both experimental configurations in Fig. 7.1. Since three-particle reactions are too slow to lead to any significant production under our low-pressure conditions (mostly < 100 Pa), most of the radicals will arrive and finally

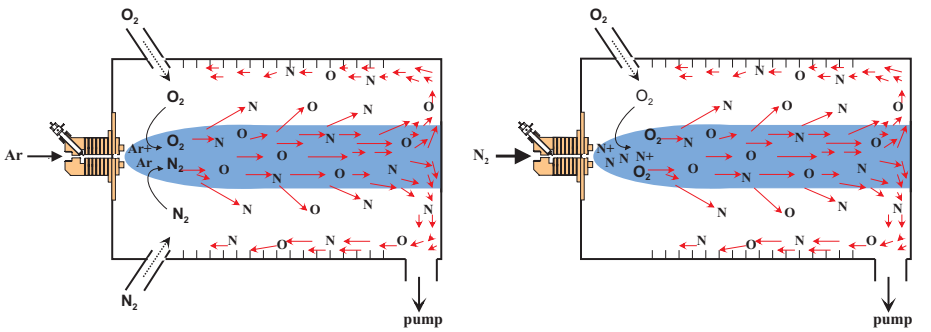

Figure 7.1: Schematic representation of the expanding plasma jet for both types of plasmas: Expanding Ar plasma to which O_2 was injected in the background (left figure); Expanding N_2 plasma with O_2 added in the background (right figure).

interact at the surface. In an argon plasma with an ionization degree of 16% at a current of 75 A and 3000 sccm of gas flow, 4×10^{20} radicals/s are produced. With a total surface area of about 1 m^2, this gives a flux density for the radicals of 4×10^{20} m^{-2} s^{-1}. Thus within the residence time (0.4 – 1 s) many mono-layers (> 10) can cover the surface. The same holds for nitrogen plasmas.

7.2.2 Tunable infrared diode laser absorption spectroscopy

The densities of the generated NO and N_2O molecules were measured with tunable diode laser absorption spectroscopy (TDLAS) using the infrared multi-component acquisition (IRMA) system [17]. Detailed descriptions of the diode laser spectrometer, data acquisition and data processing can be found elsewhere [17, 25, 38] and here only a brief description of the main constituents are given.

The IRMA system consists of four independent tunable lead salt diode lasers. The narrow band laser light (line-width 10^{-4} cm^{-1}) of the four lasers can be multiplexed in time. We used two different diode lasers to monitor NO and N_2O. The diode lasers were mounted in two different cold stations thermally coupled to the cold finger of a Helium closed-cycle cryostat. The temperature of each laser could be controlled at milli-Kelvin precision in the range between 30 and 100 K. The laser light was directed twice through the plasma vessel by the use of a retro-reflector outside the second quartz window to increase the path length ($L = 1.65$ m) and thus the sensitivity. The light was then passed through a monochromator, to ensure single-mode laser light to be analyzed, and then focused onto a liquid nitrogen cooled MCT detector. Both

Table 7.1: The molecular absorption lines used for concentration measurements of NO and N_2O.

Molecule	Frequency (cm^{-1})	Line strength S_1 @ 296 K $cm^{-1}/(cm^{-2}$ molecule)	Line strength S_2 @ 450 K $cm^{-1}/(cm^{-2}$ molecule)
NO	1852.885	1.04×10^{-20}	8.84×10^{-21}
NO	1884.293	1.26×10^{-20}	7.72×10^{-21}
N_2O	2193.54	3.75×10^{-19}	4.09×10^{-19}
N_2O	2203.733	7.90×10^{-19}	5.87×10^{-19}

are placed on the same table of the IRMA system as the diode lasers. The spectra were recorded and analyzed by means of the TDLWintel rapid scan software. The software provided a sophisticated sweep integration method which fits the recorded spectra on-line. If the pressure and spectral positions of the absorption lines are known the mole fractions of the molecules in their ground state can be obtained with a time resolution of a few millisecond. The absorption spectrum of NO or N_2O gas, measured in a reference cell, was used to identify the recorded absorption lines in the plasma [39, 40]. The frequency scan of the laser was linearized with an etalon of known free spectral range. The integrated absorption was determined by integration over frequency of the nonlinear least-squares fit to the known spectral line profile [17, 39]. Then the total density of absorbing species was determined using the line strength of the measured transition (see Sec. 7.2.2). Finally, the measured molar fraction is plotted as a function of time. As the line strength is temperature dependent, the temperature of the species is required to determine the density of the species. The molecular densities were determined for $T_{ref} = 296$ K, which is the so-called reference temperature utilized in the HITRAN database [39] from which the molecular input parameters for the TDLWintel software were taken. The line positions and line strengths S_1 (at $T_{ref} = 296$ K) for the molecular absorption lines, used for the concentration measurements of NO and N_2O are given in Table 7.1. The software package allows the simultaneous analysis of multiple absorptions as low as 10^{-5} with signal averaging of a few seconds or as low as 10^{-4} with time resolution of a few milliseconds. The detection limit in our experiments of both NO and N_2O was about 2×10^{17} m^{-3}.

Determining densities from absorption measurements

The determination of the frequency-dependent absorption coefficient $\kappa(\nu)$ in the tunable diode laser absorption spectroscopy measurements is based on the measurement of a small change of the transmitted intensity at a certain frequency $I(\nu)$ through the absorbing medium. The absorption coefficient $\kappa(\nu)$ for a homogeneous medium is according to Beer-Lambert law:

$$I(\nu) = I_0(\nu) \exp[-\kappa(\nu)L], \tag{7.8}$$

where $I_0(\nu)$ is the incident intensity and L the total absorption path length. The integrated absorption coefficient over frequency is linked to the total density of the absorbing species N under consideration:

$$\kappa_\nu = \int \kappa(\nu)\mathrm{d}\nu = N \int S(T)\mathrm{d}\nu, \tag{7.9}$$

where $S(T)$ is the line strength of the ro-vibrational transition at temperature T. It should be noted that the line strength used here includes the temperature dependence of the partition function and the Boltzmann relation between the total density N and the density $n_{v,J}$ of the level for which the absorption is measured.

The temperature was determined by measuring several NO-transitions around 1870 cm^{-1}. The relative integrated absorptions of these transitions show a strong temperature dependence, which allowed for an accurate determination of the gas temperature; this turned out to be 450 K. This temperature is merely determined by the gas in the observation arms and does not resemble the temperature of the plasma in the reactor chamber. However, it is in agreement with the previously measured temperature of O_2 molecules in expanding Ar-NO plasmas with phase-shift cavity ring-down spectroscopy (Chapter 6). The line strength S(T) at $T = 450$ K was calculated from the HITRAN quantity $S(T_{ref})$ via [39]:

$$S(T) = S(T_{ref}) \frac{Q(T_{ref})}{Q(T)} \frac{\exp\left(-\frac{hcE_\eta}{kT}\right)}{\exp\left(-\frac{hcE_\eta}{kT_{ref}}\right)} \frac{\left[1 - \exp\left(-\frac{hc\nu_{\eta\eta'}}{kT}\right)\right]}{\left[1 - \exp\left(-\frac{hc\nu_{\eta\eta'}}{kT_{ref}}\right)\right]}. \tag{7.10}$$

The second term on the right in Eq. 7.10 is the ratio of the total internal partition functions. The third term on the right takes into account the ratio of Boltzmann populations and the fourth term the effect of stimulated emission. $Q(T)$ and $Q(T_{ref})$ as well as E_η, the energy of the lower level, were obtained from the HITRAN database The resulting line strengths S_2 (at $T = 450$ K) for the transitions at which NO and

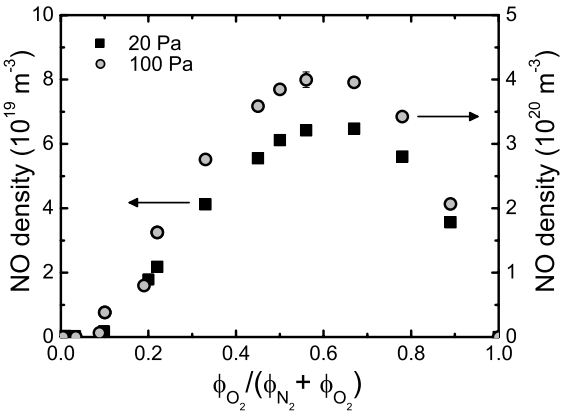

Figure 7.2: NO density as a function of the oxygen flow rate relative to the total N_2 and O_2 flow rate in Ar plasma with N_2 and O_2 injected in the background. The argon plasma was created with a flow of 3000 sccm Ar flowing through the arc. Simultaneously N_2 and O_2 were injected in the background with a total flow of 1800 sccm. The arc current was set at 75 A; the background pressure was 20 and 100 Pa.

N_2O were detected are given in Table 7.1. The relatively low temperature indicates that the detected species were present in the background of the plasma reactor, since molecules in the plasma beam would have a much higher temperature of around 1500 K [41, 42].

7.3 Results

7.3.1 Ar plasma with N_2 and O_2 injected in the background

Steady state molecule densities

The results of the TDLAS measurements on NO, formed when mixtures of N_2 and O_2 (total flow of 1800 standard cubic centimeters per minute (sccm)) are injected in the background of an expanding Ar plasma are depicted in Fig. 7.2. The plasma source is operated at 75 A and a flow of 3000 sccm Ar is applied, which results in an ion flow of 450 sccm [43]. The NO density was determined for two background pressures, i.e. 20 and 100 Pa. The maximum in NO production is observed for a oxygen flow relative to the total flow of nitrogen and oxygen of 0.6. That the maximum in NO production is not observed at a relative oxygen flow of 0.5, is probably due to the lower rate coefficient for the charge-transfer reaction of Ar^+ with O_2 (reaction (7.2)),

so that more O_2 than N_2 has to be injected to have equal amount of O and N radicals. At relative O_2 flow rates smaller than 0.1, almost no NO is observed. Similar trends in mixtures of oxygen and nitrogen were also observed by others in for example a dc glow discharge [1] and rf plasmas [2].

To explain the trend of the NO density as function of the O_2 flow rate relative to the total O_2 and N_2 flow rate at low O_2 flows, we assume that mainly N radicals are present at the surface and that NO is formed by the association of N and O radicals at the surface:

$$\mathrm{N} + \mathrm{surface} \longrightarrow \mathrm{N(s)}, \tag{7.11}$$

$$\mathrm{O} + \mathrm{N(s)} \longrightarrow \mathrm{NO}(s) \longrightarrow \mathrm{NO}(g). \tag{7.12}$$

The NO produced at low O_2 flow and thus high N_2 flow could efficiently be lost in the gas phase by the reaction [5]:

$$\mathrm{N} + \mathrm{NO} \longrightarrow \mathrm{N_2(X}, \nu \sim 3, 4) + \mathrm{O} \qquad k = 1 \times 10^{-18} T^{0.5}\ \mathrm{m^3\,s^{-1}}, \tag{7.13}$$

with a rate constant of 3×10^{-17} $\mathrm{m^3\ s^{-1}}$ in the background at 1000 K. But, oxygen atoms could also be lost in the formation of other molecules like N_2O or, although much less probable at low O_2 flows, NO_2.

To investigate the importance of the generation of N_2O the N_2O density as function of the O_2 percentage has been measured. The results are plotted for two pressures in Fig. 7.3. The N_2O density has its maximum at flows where almost no NO is observed and when the N_2O density starts to decrease, NO starts to increase (7.2). At low O_2 flows, the N_2O density is higher at 100 Pa then at 20 Pa, as expected, since its residence time in the background is longer at higher pressure. But, at 100 Pa the N_2O density starts to decrease at lower relative O_2 flows as compared to the 20 Pa case. This can be explained by a destruction reaction with O atoms, since this reaction becomes more important at higher pressure.

The N_2O molecules can not be produced in the gas phase in our low-pressure experiments. Therefore, N_2O must be formed primarily by the association of N radicals and NO molecules adsorbed at the surface of the reactor wall:

$$\mathrm{N} + \mathrm{NO_{ads}} \longrightarrow \mathrm{N_2O}. \tag{7.14}$$

As the O_2 flow and thus the O flux increases, NO can be produced in the gas phase by the reaction [37]:

$$\mathrm{O} + \mathrm{N_2O} \longrightarrow \mathrm{NO} + \mathrm{NO} \qquad k = 1.5 \times 10^{-16} \times \exp(-1.4 \times 10^4 / T)\ \mathrm{m^3\,s^{-1}}, \tag{7.15}$$

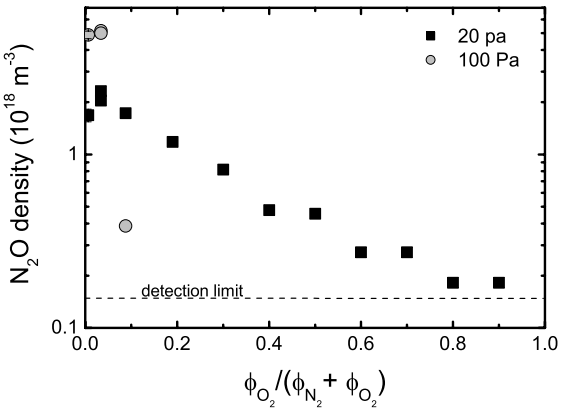

Figure 7.3: N_2O density as a function of the oxygen flow rate relative to the total N_2 and O_2 flow rate in Ar plasma with N_2 and O_2 injected in the background for the same conditions as in Fig. 7.2.

where T is the temperature in Kelvin. The branching to N_2 and O_2 is less probable. Different values for the rate of this reaction are reported, which indicate that the rate could be 5 to 40 times lower than for reaction (7.15):

$$O + N_2O \longrightarrow N_2 + O_2 \qquad k = (0.4-3)\times 10^{-17}\times\exp(-1.4\times 10^4/T)\ \mathrm{m^3\,s^{-1}}. \quad (7.16)$$

Both reactions have an energy threshold of 1.2 eV ($\approx 1.4 \times 10^4$ K). However, we note that the reaction (7.14) is exothermic. The N_2O formed at the surface would at maximum contain the exothermic energy of the reaction ($\Delta E = 4.93$ eV) minus the adsorption energy of NO on the surface and minus the kinetic energy of the desorbed N_2O molecule. One could speculate that the thus formed N_2O molecule has a significant internal energy and that this could lead to NO formation in collisions with O atoms, before the N_2O molecule is de-activated.

In conclusion, the threshold in NO production at low O_2 flows is related to the generation at the surface of N_2O. If the O_2 flow, and thus the O density, increases, NO can be formed in the gas phase by two particle reactions out of N_2O, formed at the surface. The transition of N_2O generation to NO generation at higher O_2 flows could next to formation of N_2O also be caused by a change in surface processes; whereas at low O density only N_2O is formed, at higher O fluxes also NO_2 (vide infra) and NO desorption becomes probable.

Now we discuss the NO production at relative O_2 flows larger than 0.2. At these relative O_2 flows one can expect NO_2 to be formed. The NO_2 density as measured

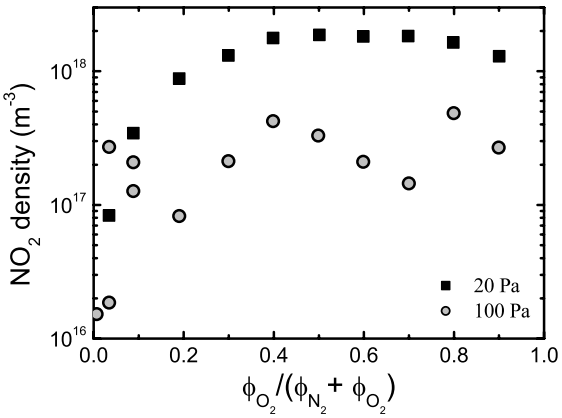

Figure 7.4: The NO_2 densities in the plasma as measured with mass spectrometry as a function of the oxygen flow rate relative to the total N_2 and O_2 flow rate under the same plasma conditions as in Fig. 7.2

with mass spectrometry under the same plasma conditions as before is plotted in Fig. 7.4. As for N_2O, also NO_2 is most probably formed at the wall in an association reaction of O radicals (in stead of N radicals) and NO adsorbed at the surface [44]:

$$O + NO_{ads} \longrightarrow NO_2. \tag{7.17}$$

In contrast to N_2O, the NO_2 densities for O_2 flows larger than 0.1, are lower at 100 Pa than at 20 Pa. This indicates that the produced NO_2 molecules are partially lost in the gas phase by reactions with N and O atoms (no temperature dependence) [5, 45]:

$$N + NO_2 \longrightarrow O + N_2O \qquad k = 8 \times 10^{-18}\ m^3\,s^{-1}, \tag{7.18}$$

$$N + NO_2 \longrightarrow NO + NO \qquad k = 6 \times 10^{-18}\ m^3\,s^{-1}, \tag{7.19}$$

$$N + NO_2 \longrightarrow 2O + N_2 \qquad k = 2.4 \times 10^{-18}\ m^3\,s^{-1}, \tag{7.20}$$

$$N + NO_2 \longrightarrow N_2 + O_2 \qquad k = 1.9 \times 10^{-18}\ m^3\,s^{-1}, \tag{7.21}$$

$$O + NO_2 \longrightarrow NO + O_2 \qquad k = 9.8 \times 10^{-18}\ m^3\,s^{-1}. \tag{7.22}$$

These reactions also show that part of the observed NO could be produced out of NO_2.

We are also interested in the use of the injected gases for the production of NO, N_2O and NO_2 molecules, since this can give an indication of the processes leading to the observed densities of the molecules. The use of a gas is defined by the amount of O(N) atoms in te measured NO, N_2O and NO_2 molecules divided by the amount

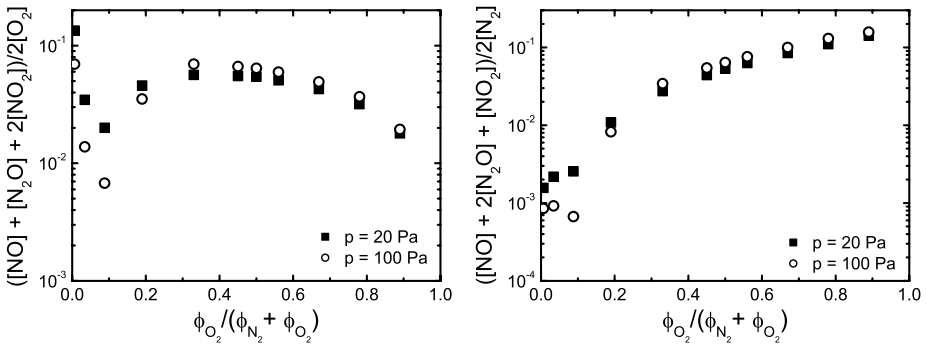

Figure 7.5: The use of O_2 (left figure) and N_2 (right figure) as a function of the oxygen flow rate relative to the total N_2 and O_2 flow rate in Ar plasma with N_2 and O_2 injected in the background for the same conditions as in Fig. 7.2.

of O(N) atoms admitted to the system in the form of $O_2(N_2)$. For example, NO_2 and O_2 molecules contain two O radicals, while NO and N_2O contain only one O radical and therefore the amount of O atoms in the molecules is calculated as:

$$\frac{[NO] + [N_2O] + 2[NO_2]}{2[O_2]}. \tag{7.23}$$

The use of N_2 and O_2 gases is plotted in Fig. 7.5 as a function of the O_2 flow rate relative to the total N_2 and O_2 flow rate. The use of O_2 at O_2 flow rates larger than 0.2 is almost constant at a level of 2–5% and is almost independent of pressure. That the O_2 use is high at low oxygen flows, where no NO is observed, shows that the apparent threshold in NO production at low O_2 flows is due to the generation of N_2O and NO_2. Hence, the explanation that for low O_2 flows N_2O is produced rather than NO seems valid and that the apparent threshold is connected with the reaction (7.15). The dip in the O_2 use al low O_2 flows could be caused by the loss of O atoms to O_2 molecules via reaction (7.16). As in the case of the use of O_2, also the use of N_2 is almost independent of pressure. However, the use of N_2 increases to 15% with increasing O_2 flow. To fully understand the meaning of this 15% use of N_2 one should remember that the maximum amount of injected $N_2(O_2)$ molecules that can be dissociated is 50% (example for relative nitrogen flow of 0.1, assuming full dissociation, and with flows in sccm):

$$\frac{[N_2]_{\text{diss}}}{[N_2]_{\text{injected}}} = \frac{[Ar^+]}{[N_2]} * \frac{[N_2]}{[N_2] + [O_2]} = \frac{2 \times 450}{180} * \frac{180}{1800} = 0.5. \tag{7.24}$$

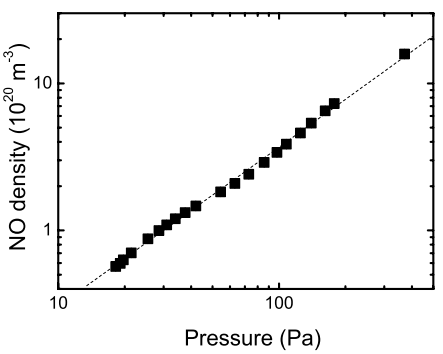

Figure 7.6: NO density as a function of the background pressure in Ar plasma with N_2 and O_2 injected in the background. The argon plasma was created with a flow of 3 slm Ar flowing through the arc. Simultaneously 0.8 slm N_2 and 1.0 slm O_2 were injected in the background at an arc current of 75 A (dotted line: linear behavior)

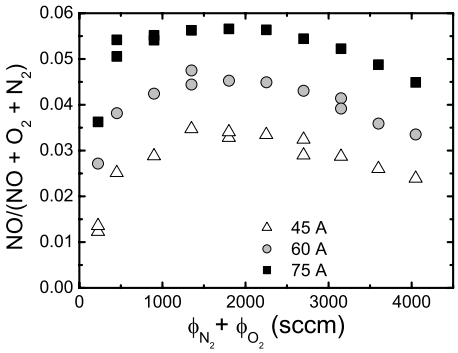

Figure 7.7: NO density as a function of total N_2 and O_2 flow for three currents through the plasma source. The argon plasma was created with a flow of 3 slm Ar flowing through the arc. Simultaneously N_2 and O_2 were injected at the ratio $\phi_{O_2}/(\phi_{O_2} + \phi_{N_2}) = 0.6$ at a pressure of 80 Pa.

Taking this into account and remembering that N radicals can also be lost in the gas phase via reactions (7.13) and (7.18) – (7.21), this means that a significant amount of the N atoms is used in the production of NO and NO_2 molecules.

The NO density was also measured as a function of pressure in the vessel at the ratio where the maximum NO production is observed, i.e. $\phi_{O_2}/(\phi_{O_2} + \phi_{N_2}) = 0.6$ (Fig. 7.6). The NO density is proportional to the pressure with slope 1, which is in line with NO formation by surface processes. The production process of NO via the association of N and O radicals is independent of pressure, since the amounts of N and O radicals produced depend only on the plasma source parameters. But the residence time in the vessel increases with increasing pressure, i.e. $n_{NO} \propto \tau$. And since τ is linearly dependent on the pressure in the vessel, the NO density should also increase linearly with increasing pressure. Furthermore, the N and O atoms in the plasma have a residence time of typically 10 – 30 ms in the background of our plasma (typically a factor 40 lower than for stable molecules, like e.g. NO).

A remarkable result is shown in Fig. 7.7, in which the NO reduced molar fraction is plotted as a function of the total flow of N_2 and O_2 injected in the background for three currents through the plasma source. The measurements were again performed

at the ratio where the maximum NO production is observed. The densities of N_2O and NO_2 under the measured conditions are less than 1% and can be neglected. The reduced molar fraction is only slightly dependent on the total flow of N_2 and O_2 and scales linearly with the arc current. The explanation of the latter is the linear scaling of the Ar^+ flow emanating form the plasma source with arc current. This leads to a higher dissociation of the injected N_2 and O_2 and thus more radicals are available for NO production. The trend of the reduced molar fraction can be explained as follows. With increasing total flow, more and more NO is produced, because more N_2 and O_2 is dissociated. At a certain total flow of N_2 and O_2, all Ar^+ ions are used for the production of N and O radicals, which leads to a maximum in the NO density. Adding more N_2 and O_2 molecules does not lead to the production of more NO, while the total density increases, resulting in a decreasing NO reduced molar fraction.

Time-resolved measurements

In order to validate that surface processes play a role in the NO production and to investigate the surface coverage of the reactor wall in the experiments, we monitored the time-behavior of the densities of the NO and N_2O molecules after switching off the N_2 or O_2 flow. The analysis was made in view of the question whether time constants could be indicative of the processes of molecule formation. The time dependencies were measured first in plasmas created with 5000 sccm Ar flowing through the arc at a current of 60 A. Simultaneously, 300 sccm N_2 and 300 sccm O_2 were injected in the background of the vessel. At 60 A, the Ar flow is partially ionized (12%), i.e. an Ar^+ ion flow of 600 sccm, as determined from Langmuir probe measurements in the argon expansion [43]. Thus the Ar^+ ion flow is chosen to be approximately equal to the total flow of N_2 and O_2 molecules to ensure an effective dissociation of the molecules and thus high fluxes of N and O radicals towards the surface, i.e. 2.5×10^{20} m^{-2} s^{-1}.

The time behavior of NO when either the N_2 or O_2 flow was stopped is shown in Fig. 7.8. The time traces shown in Fig. 7.8 were recorded after N and O exposure to the wall for respectively 1, 3 (only N_2 exposure is shown) and 10 minutes. At $t = 0$ the N_2 or O_2 flow was stopped[†]. When the O_2 injection was stopped, the NO density dropped below the detection limit in ≈ 6 seconds, independent of the exposure time of O_2. This decay can be explained to a large extend by the residence time of 1.2 s. The

[†]The NO density of the 3 minutes exposure of N_2 starts at a somewhat lower value. It was measured in a separate measurement campaign with TDLAS and apparently the condition of the vessel wall was somewhat different in that experiment.

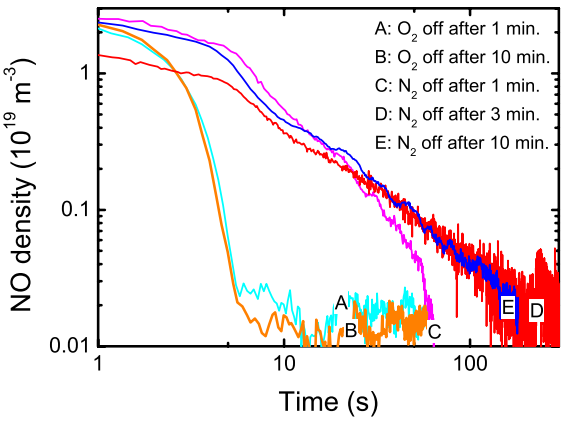

Figure 7.8: Time behavior of the NO density after switching off the N_2 or O_2 flow in Ar plasma with N_2 and O_2 injected in the background. The argon plasma was created with a flow of 5000 sccm Ar flowing through the arc. 300 Sccm N_2 and 300 sccm O_2 were injected in the background. The arc current was set at 60 A; the background pressure was 66 Pa. At $t = 0$ the O_2 flow (A,B) or the N_2 flow (C,D,E) is stopped.

decay is even faster than exponential, again related to a predominant N_2O production at low O_2 densities. That NO is not observed over long time-scales indicates that almost no O atoms are present on the surface.

In the opposite experiment, so stopping the N_2 injection, again a decrease in the first ~ 6 seconds is observed. However, this decay is slower than in the case of stopping the O_2 flow. Apparently NO is produced from a reservoir. The second part of the decrease of the NO density to below the detection limit takes has a 1/e time of 15 s for 1 minute of exposure and 30 s for 3 or 10 minutes of exposure. The sharp decrease after 60 seconds in the NO density for 1 minute of exposure is because the O_2 flow was stopped.

The residence time of particles in the reactor is given by:

$$\tau_{residence} = \frac{V \times (p/kT)}{\phi_{gases}}. \tag{7.25}$$

In these experiments, the pressure is 66 Pa at a background gas temperature of 450 K, the volume of the plasma reactor is 268 liters and the total flux of gases is $\phi = 5600$ sccm $\triangleq 2.3 \times 10^{21}$ particles/s. Thus the residence time is 1.2 seconds. This means that the observed behavior of the NO density is not related to processes in the volume, but must be due to surface processes.

After exposure times longer than 3 minutes, no change in the trend in the NO density was observed. That NO is still detected over such long times scales after the N_2 flow was stopped, raises the question where the reservoir of N is, needed to produce NO over such a long period. It implies that N is not only present *on* the wall, but also *in* the wall of the reactor. This can be elucidated as follows. When both the O_2 and N_2 gas flow are applied, 1% of the background is detected to be NO, which is equal to 24 sccm. Assuming that in stationary state all 600 sccm of N_2 and O_2 molecules are dissociated, only $24/600 = 4\%$ of the dissociated N_2 and O_2 are used to form NO. A fully covered surface with 1 mono-layer of particles corresponds to 10^{19} particles m^2 present at the surface. If all these particles would desorb from the surface within the residence time of 1 second, while only 4% would be NO, that would result in 4×10^{17} NO molecules m^{-3} or a flow of only 0.96 sccm. In total 2.4×10^{20} m^{-3} NO molecules are formed over 200 seconds; with a reactor volume of 0.27 m^3 this is equal to a flow of 0.84 sccm on average for 200 seconds. This requires thus 200 mono-layers for the NO and the N_2 and O_2 production. Such an amount can never be present on the surface and thus N has to be present in the wall of the reactor. The slow decrease in NO density is then caused by the reaction of N diffusing out of the wall with O atoms from the plasma impinging on the wall, leading to NO. That there is a difference for 1 minute of exposure compared to 3 or 10 minutes of exposure indicates that it takes more than 1 minute to fully saturate the stainless steel wall with N atoms.

In Fig. 7.9, the time behavior of the N_2O density as the O_2 flow is stopped after 1 minute is plotted for three different arc currents. As the amount of O_2 in the vessel is decreasing after $t = 0$, the same transition from NO to N_2O generation occurs as was also observed when in static conditions the amount of O_2 in mixtures of nitrogen and oxygen was smaller than 10% (Fig. 7.2 and Fig. 7.3). The N_2O first reaches a maximum, and at even lower O_2 presence the N_2O density decreases again. The maximum of the N_2O density increased when more current was applied to the plasma source. The amount of ions and thus of produced O and N radicals in the plasma (reactions (7.1) – (7.4)) increases with higher arc current, so more radicals are available to generate N_2O. When all the O_2 is pumped out of the vessel, the N_2O density decreases according to a second order exponential decay, i.e. $\exp(t/\tau_1) + \exp(t/\tau_2)$. This is shown in Fig. 7.9, in which the background level is subtracted. The relevant time constant τ_1 decreases with increasing current, from 20 seconds at 45 A to 10 seconds at 75 A. This short time constant is most likely caused by the reaction of NO on the wall and N atoms impinging on the wall, leading to N_2O.

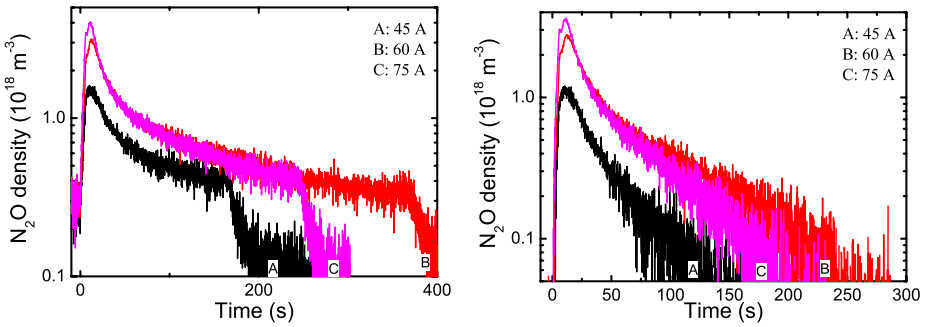

Figure 7.9: Time behavior of the N_2O density after switching off the O_2 flow after 1 minute for three arc currents in Ar plasma with N_2 and O_2 injected in the background under the same plasma conditions as in Fig. 7.8. The final fast decrease in the N_2O density is caused by stopping the N_2 flow into the vessel, after which the N_2O decreases to below the detection limit. In the right figure the background level is subtracted.

At higher currents, more N atoms are produced, so the NO at the surface is faster converted into N_2O, resulting in a shorter τ_1. That there is a decrease in NO density with a different time constant suggests that not only N atoms, but also NO radicals are stored in the wall.

Summary

When the O_2 injection is stopped, the NO density dropped below the detection limit in $\sim$ 6 seconds, independent of the exposure time of O_2. Furthermore, a transition from NO to N_2O generation is observed, after which the N_2O density slowly decreases below the detection limit. Both effects suggest that O is mainly present in the form of NO at and below the surface and that NO is stored in the metal wall; the NO molecules diffuse out of the wall when the O_2 flow is stopped. In the opposite experiment, so stopping the N_2 injection, a slow decrease of the NO density is observed, which suggests the presence of N atoms at and in the wall of the reactor. We note that also the time-behavior of the NO density after the O_2 flow was switched off indicates that almost no O atoms are present on the surface. Moreover, if also O atoms would have been present on the wall in large amounts, the time-resolved measurements of N_2O after the O_2 flow was stopped should have shown not two exponential decay related to NO on the wall and diffusing out of the wall, but also an

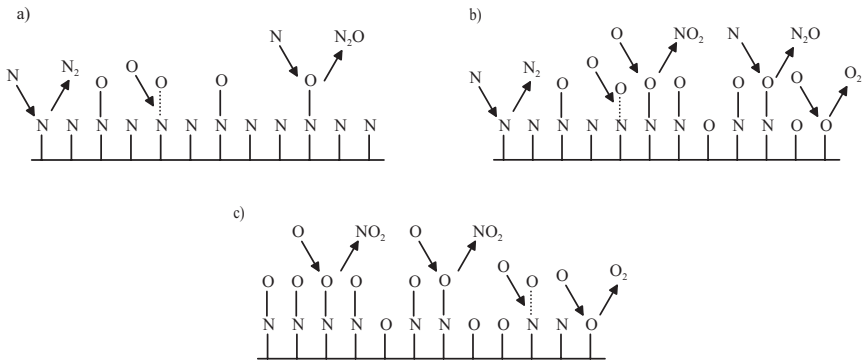

Figure 7.10: Schematic representation of the surface and the surface processes in three regimes: a): $\phi_{O_2}/\phi_{O_2+N_2} < 0.2$, b): $0.2 < \phi_{O_2}/\phi_{O_2+N_2} < 0.8$ and c): $\phi_{O_2}/\phi_{O_2+N_2} > 0.8$.

exponential decay, due to the formation of N_2O from O atoms present on or in the wall. From the results of the time-resolved measurements, we conclude that mainly N and NO radicals are present at the surface and stored in the stainless steel wall.

The generation of molecules in expanding Ar plasmas containing mixtures of nitrogen and oxygen, in which the oxygen percentage was varied from 0 – 100%, can be divided in three regimes. In the first regime, $\phi_{O_2}/\phi_{O_2+N_2} < 0.2$, the surface is mainly covered with N atoms and some NO molecules. The surface coverage and the basic surface processes are illustrated in Fig. 7.10a. The few O atoms impinging at the surface will form adsorbed NO by association with N atoms present on the surface. Incoming N radicals form N_2 molecules by association with N atoms on the surface or will form N_2O by association of N radicals with NO molecules adsorbed at the surface of the reactor wall; the thus formed N_2O molecules will subsequently desorb. When the O_2 flow is increased the O radical density increases and NO can be produced by the reaction between N_2O and O radicals. The apparent threshold in NO production at low O_2 flows is connected to these processes. Next to NO formation out of N_2O, also the direct desorption of NO formed by the association of N and O radicals at the surface may become possible at higher O_2 flows.

With increasing O_2 flow, also the surface processes and surface coverage are changing. This is the second regime illustrated in Fig. 7.10b, which is valid for $0.2 < \phi_{O_2}/\phi_{O_2+N_2} < 0.8$. With increasing O_2 flow, the wall is mainly covered by NO and some N and O atoms. Now, next to N_2O and N_2 molecules also NO_2

molecules can be formed by association of O atoms impinging on the surface and the NO adsorbed at the surface. By reactions with N and O atoms, the NO_2 can be converted to NO. Due to the changing surface coverage, i.e. mainly NO at the surface, also the formed NO can desorb directly, which is most likely the dominant process. Furthermore, the incoming O radicals can form O_2 molecules by association with O atoms at the surface.

Also, in the third regime, $\phi_{O_2}/\phi_{O_2+N_2} > 0.8$, (Fig. 7.10c), we assume that the surface is mainly covered with N atoms and NO molecules and some O atoms. The N atoms impinging on the surface adsorb and react with O atoms impinging on the surface leading to NO on the surface and almost no N_2 molecules are formed. Also here, the incoming O radicals can form O_2 molecules by association with O atoms on the surface. Next, NO_2 molecules are formed by the association of O atoms imping on the surface and the NO adsorbed at the surface. The desorbed NO_2 molecules then react with O atoms, leading to NO and O_2 molecules. As a result the use of N_2 in producing NO_x, which is a significant amount of the 50% of the N_2 that is dissociated.

7.3.2 N_2 plasma with O_2 injected in the background

Steady state molecule densities

To study the effect of the amount of radicals on the NO production, we performed also experiments with an optimized nitrogen dissociation by operating the plasma source on nitrogen gas. Oxygen could not be applied through the plasma source, since injection into the arc would damage the plasma source. Therefore, the plasma was created with 1800 sccm nitrogen applied through the arc and oxygen injected in the background. The arc current was set at 60 A and the pressure was kept constant at 94 Pa. The expanding N_2 plasma is substantially dissociated ($\approx 30\%$) and partially ionized ($\approx 5\%$). The injected O_2 molecules are partially dissociated to O atoms by charge-transfer reactions of the N^+ ions emanating from the plasma source, reactions (7.26) and (7.6), followed by dissociative recombination of the molecular ions, reactions (7.4) and (7.7). The NO density increased with increasing O_2 flow and saturated at $\sim 3.5 \times 10^{20}$ m^{-3} for O_2 flows higher than 2000 sccm (Fig. 7.11). We note that approximately 90 sccm of the nitrogen flow are N^+ ions, so a saturation was expected at approximately 10 times lower oxygen flows. This implies that the NO formation is not only related to the dissociation of O_2 by N^+, but that NO is formed

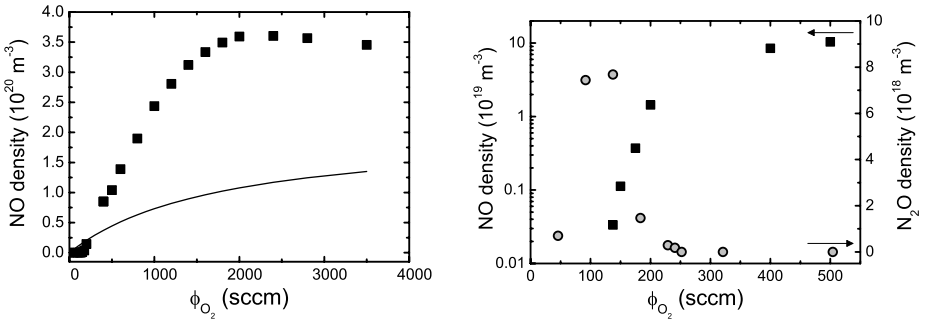

Figure 7.11: The NO density as a function of the O_2 flow injected in the background in expanding N_2 plasmas (left figure). A blow up of the NO density for relative oxygen flows up to 500 sccm and the N_2O density in the same range (right figure). The nitrogen plasma was created with a flow of 1800 sccm N_2 flowing through the arc. The arc current was 60 A and the background pressure was 94 Pa. The curve represents the NO production in the gas phase (see text).

in the expanding plasma beam ($T = 1500$ K) via the reaction:

$$\mathrm{N} + \mathrm{O_2} \longrightarrow \mathrm{O} + \mathrm{NO} \qquad k = 3.2 \times 10^{-18} \frac{T}{300} \exp(\frac{-3150}{T}) \ \mathrm{m^3\,s^{-1}}. \tag{7.26}$$

We assume that the activation energy of 3150 K for this reaction is overcome in the supersonic expansion by the high energy of the N radicals in the supersonic expansion. However, the transit time relevant in the supersonic expansion is only 10^{-5} s. Furthermore, the relevant transient time for "forward" kinetics is too short (< 1 ms) to form significant amount of NO via this reaction in the subsonic expansion, where the rate constant with activation energy is 2×10^{-18} m^3 s^{-1}. The reaction could be relevant for the background kinetics, since the residence time, relevant to the background kinetics, is long (≈ 3 s). The lifetime of N atoms, τ_N, in the background can be estimated to be approximately 75 ms [46]. To estimate the maximum contribution of this reaction to the NO production, we take a temperature of 1000 K, which is most probably slightly low for the average temperature of the nitrogen atom during its lifetime. The rate constant of reaction (7.26) is then 4.5×10^{-19} m^3 s^{-1}. To calculate the NO density, we also have to take into account that NO is easily destroyed in the background chemistry in the plasma reactor (assuming also T = 1000 K) via the reaction:

$$\mathrm{N} + \mathrm{NO} \longrightarrow \mathrm{N_2(X}, \nu \sim 3, 4) + \mathrm{O} \qquad k = 3.3 \times 10^{-17} \ \mathrm{m^3\,s^{-1}}. \tag{7.27}$$

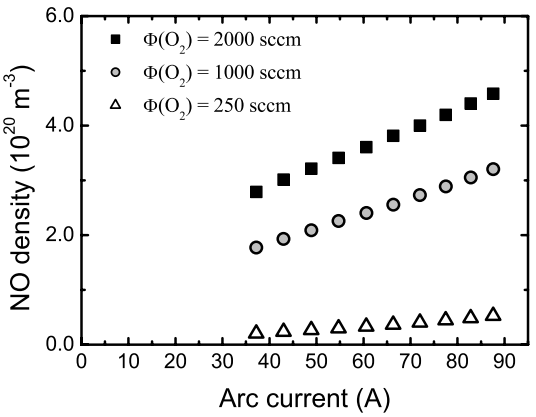

Figure 7.12: NO density as a function of the arc current in expanding N_2 plasmas with O_2 injected in the background. The nitrogen plasma was created with a flow of 1800 sccm N_2 flowing through the arc. The background pressure was 67 Pa.

The density of NO can be written as:

$$n_{NO} = \frac{n_N \cdot n_{O2} \cdot k_{N-O_2} \cdot \tau_N}{n_N \cdot k_{N-NO} \cdot \tau_N}. \tag{7.28}$$

The NO density using this formula and $n_N = 3{\times}10^{20}$ m^{-3} is plotted in Fig. 7.11; with this choice about 30% of the NO can be attributed to this reaction. Furthermore, the time-resolved measurements on the NO density, when O_2 is injected after exposure of the wall to N atoms for some time, show that the NO formation process occurred at time-scales which are typical for wall processes rather than gas phase (example presented in Sec. 7.3.2). This implies that NO is mainly produced through another reaction mechanism. The production of NO can also be explained as follows. In both reactions (7.26) and (7.27) an O atom is produced. The combination of both reactions plus the dissociation of O atoms by N^+ ions would results in an O atom density of $\approx 3.5 \times 10^{20}$ m-3 in the background. Then NO can be produced by association of N and O radicals and subsequently desorption of NO from the surface.

Also in this plasma a threshold in the NO production is observed and also here it is related to the generation of N_2O. The N_2O density and the NO density at low O_2 flows are plotted as an insert in Fig. 7.11. As in Sec. 7.3.1, the N_2O density has its maximum at flows were no NO is observed. When NO starts to appear, the N_2O density decreases quickly to below the detection limit of the IRMA system of 1.5×10^{17} m^{-3}. Apparently, for higher O_2 flows N_2O is converted by a reaction

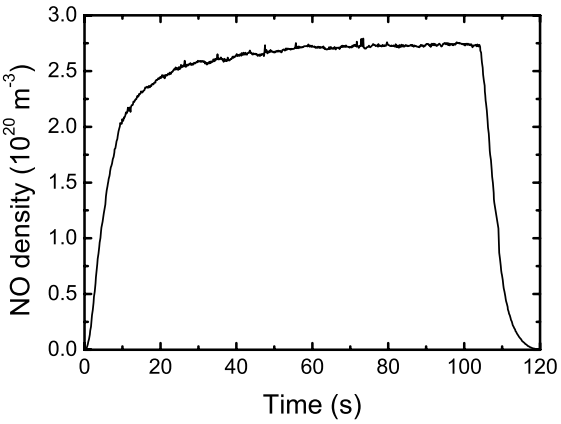

Figure 7.13: Time behavior of the NO density after switching on the O_2 flow ($t = 0$ s) and switching off the O_2 flow ($t = 104$ s) in expanding N_2 plasmas with O_2 injected in the background. The nitrogen plasma was created with a flow of 1800 sccm N_2 flowing through the arc, while 1000 sccm O_2 was injected in the background. The arc current was set at 60 A; the background pressure was 100 Pa.

with O atoms into NO. But in addition, also the surface coverage and thus processes could change, leading to direct desorption of NO produced by association of N and O radicals at the wall.

To study the influence of the N^+ ions and N atoms on the NO formation, the NO density was measured as a function of the current through the arc for three O_2 flows (Fig. 7.12). As expected, the NO density scales linearly with arc current. The NO production is determined by the amount of O radicals formed in the plasma and thus the NO density should have a linear dependence on arc current. Both the N atom and N^+ ion fluxes from the plasma source scale approximately linear with the arc current, i.e oxygen atom production roughly increases linearly with arc current [35].

Time-resolved measurements

Also during these measurements, the surface coverage and the role of surface processes was characterized by monitoring the time-behavior of the densities of the NO and N_2O molecules after switching off the O_2 flow into the plasma reactor. The time behavior of NO density in a nitrogen plasma with oxygen injected in the background is plotted in Fig. 7.13 for an O_2 flow of 1000 sccm. The plasma source was operated

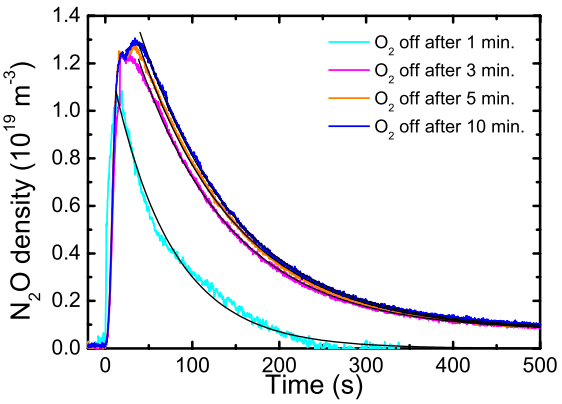

Figure 7.14: Time behavior of the N_2O density after switching off the O_2 flow in expanding N_2 plasmas with O_2 injected in the background. The nitrogen plasma was created with a flow of 1800 sccm N_2 flowing through the arc, while 500 sccm O_2 was injected in the background. The arc current was set at 60 A; the background pressure was 57 Pa. The curves represent fits with a single exponential decay function.

at a current of 60 A and with 1800 sccm N_2 flowing through the arc. When O_2 was added the NO density reached a steady state value after 45 seconds. The average residence time of the gases in the plasma reactor is 3.5 seconds at a pressure of 90 Pa. Thus, the long time until the NO density saturates has again to be related to surface processes leading to the formation of NO. When the O_2 flow was stopped, the NO density decreased to below the detection limit in 12 seconds. In this time, also a transition from NO to N_2O generation is observed under these circumstances as will be discussed in more detail below. This time is independent of the amount of O_2 flow injected. As concluded in Sec. 7.3.1, this time behavior is due to the fact that it takes roughly 12 seconds to pump down the long O_2 gas line behind the mass flow controllers.

Next the N_2O density was monitored, after the O_2 flow was stopped. The N_2O density as a function of time is plotted in Fig. 7.14 for a nitrogen plasma to which 500 sccm O_2 was added for respectively 1, 3, 5 and 10 minutes. After exposure times longer than 3 minutes, almost no change in the trend of the N_2O density is observed. As the amount of O_2 in the vessel is decreasing, the same transition from NO to N_2O generation occurs as was also observed in static conditions at low O_2 flows, see Fig. 7.11. The N_2O first reaches a maximum, and at even lower O_2 presence the N_2O

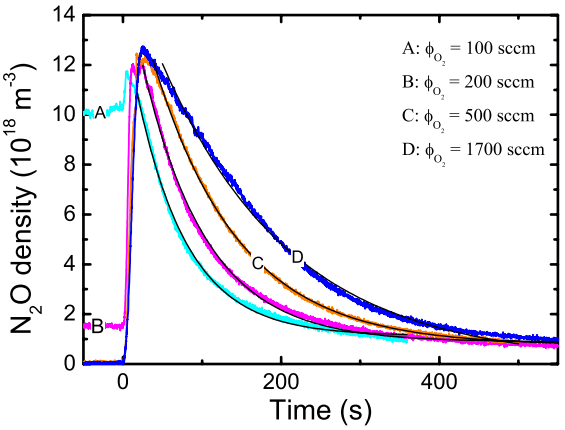

Figure 7.15: Time behavior of the N_2O density after switching off the O_2 flow after 3 minutes for four O_2 flows. The nitrogen plasma was created with a flow of 1800 sccm N_2 flowing through the arc. The arc current was set at 60 A; the background pressure was 57 Pa. The curves represent fits with a single exponential decay function.

density decreases again[‡]. Once all O_2 is pumped out of the vessel, it takes minutes before the density of N_2O is below the detection limit. The time trace of this slow decrease can be described with a single order exponential decay (see Fig. 7.14). In all four experiments, the time constant of the decay was $\tau \approx 110$ s. For such long time-scale, one can calculate in the same way as done for N_2O in Sec. 7.3.1, that at least 21 mono-layers are needed for the measurement in which the O_2 flow was stopped after 1 minute. For exposures longer than 1 minute, even 30 mono-layers are necessary. This indicates that N_2O is most probably produced by the reaction of NO diffusing out of the wall with N atoms from the plasma impinging on the wall.

The time behavior of the N_2O density after switching off the O_2 flow was also recorded for 4 different O_2 flows injected for 3 minutes into the vessel (Fig. 7.15). At $t = 0$ the O_2 flow was stopped. For O_2 flows of 100 and 200 sccm, N_2O is already formed, while the oxygen flow is on, but at higher O_2 flows, no N_2O is detected. This is in agreement with measurements on N_2O as a function of the injected O_2 flow in stationary conditions (see Fig. 7.11). When the O_2 flow was stopped, the N_2O density increased for the two lowest flows. Again, the NO to N_2O transition is observed as the amount of O_2 in the vessel is decreasing. The maximum in the N_2O density

[‡]The maximum of N_2O is somewhat lower for 1 minute exposure of O_2. It was measured in a separate measurement campaign with TDLAS and apparently the condition of the vessel wall was somewhat different in that experiment.

is independent of the O_2 flow, which indicates that there is a limit in the amount of N_2O that can be produced, related to the maximum surface coverage and bulk storage. The N_2O first reaches a maximum, and at even lower O_2 presence the N_2O density decreases again. When all the O_2 is pumped out of the vessel, the N_2O slowly decreases. The time trace of this slow decrease can be described with a single order exponential decay (see Fig. 7.15). The time constant increased from $\tau = 62$ seconds for $\phi_{O_2} = 100$ sccm to $\tau = 158$ seconds for $\phi_{O_2} = 1700$ sccm. The slow decrease is most likely caused by supply of NO at the surface by NO diffusing out of the metal to the surface. Now, at least 21 mono-layers are needed to explain the N_2O production for $\phi_{O_2} = 100$ sccm. At the surface, the NO reacts with N atoms from the plasma impinging on the wall, leading to N_2O. At higher O_2 flows more NO could be built into the wall and thus it takes longer before all NO has diffused out of the wall.

Summary

Also in nitrogen plasmas with oxygen injected in the background mainly NO and N are present at the surface and are built in the surface and their diffusion out of the wall is observed when the nitrogen flow is stopped. The generation of molecules in expanding nitrogen plasmas to which oxygen is added in the background of the vessel can be divided in two regimes. The first regime, low oxygen flows, the same reasoning is applicable as in Sec. 7.3.1. With increasing O_2 flow, the NO density is determined by the combination of two processes. Firstly, NO is produced by besides reactions between N and O_2 by the association of N and O radicals at the wall, with subsequent desorption of the NO molecules. But also, the NO is lost by the reaction of NO with N atoms. When as much oxygen is injected in the background as N_2 is fed through the plasma source, the NO density saturates.

7.4 Conclusion

We investigated the mechanisms of molecule formation in expanding plasmas containing mixtures of nitrogen and oxygen using time-resolved tunable diode laser absorption spectroscopy. In the expanding recombining plasma, the generation of molecules by reactions involving atoms and molecules in excited states can be excluded. The main primary chemistry is made up by the high fluxes of atomic N and O radicals created, leading to the formation of mainly NO, but also N_2O and NO_2 molecules produced in surface processes.

We have shown that when the nitrogen or oxygen flow is stopped, the generation of NO and N_2O molecules is observed on time-scales long compared to the residence time. From the results, it is concluded that mainly NO and N are present at the surface and diffuse in the metal wall as their diffusion out of the wall is observed after the nitrogen or oxygen flow is stopped. In our low-pressure plasmas, the NO, N_2O, and NO_2 molecules are primarily formed in wall association processes of N and O radicals, in combination with subsequent gas phase reactions, i.e. part of the observed NO is formed out of N_2O and NO_2 by gas phase reactions.

The generation of molecules in expanding argon plasmas containing mixtures of nitrogen and oxygen, in which the oxygen percentage was varied from 0 – 100%, can be divided in three regimes. At low O_2 flows (around 10%), the surface is mainly covered with N atoms and some NO molecules. Furthermore, at low O_2 flows a transition from N_2O generation to NO generation is observed. This transition is caused by a change in the surface coverage and thus processes at the reactor wall. Furthermore, at low O_2 flows N_2O is produced and the O density is too small to destruct N_2O. At higher O_2 flows NO can be produced by the destruction of N_2O by a reaction with O radicals. The apparent threshold in NO production at low O_2 flows is connected to these processes.

The second regime, oxygen flows between 20% and 80%, the wall is mainly covered by NO and by N and O atoms. Now, next to N_2O and NO, also NO_2 molecules can be formed by the association of O and N atoms impinging at the surface. Due to the changing surface coverage, also the formed NO can desorb directly, which is most likely the dominant process.

Also in the third regime, oxygen flow > 80%, the surface is mainly covered by O atoms and NO molecules and some N atoms. The N atoms impinging on the surface are used to form NO on the surface and almost no N_2 molecules are formed. Then only NO_2 and almost no N_2O molecules are formed. The NO_2 molecules will react with O atoms, leading to NO and O_2 molecules. We note that the results indicate that at high O_2 flows, and thus low N_2 flows, almost all N atoms produced in the plasma are used in the production of NO and NO_2 molecules.

The generation of molecules in expanding nitrogen plasmas to which oxygen is added in the background of the vessel can be divided in two regimes. The first regime, low oxygen flows, again a transition from N_2O to NO is observed. With increasing O_2 flow, the NO production is determined by the competition between the generation of NO at the surface by the association of N and O radicals at the wall and the NO destruction by the reaction of NO with N atoms.

Bibliography

[1] J. Nahorny, C.M. Ferreira, B. Gordiets, D. Pagnon, M. Touzeau, and M. Vialle, *Experimental and theoretical investigation of a N_2–O_2 DC flowing glow discharge,* J. Phys. D: Appl. Phys. **28**, 738 (1995).

[2] G. Dilecce and S. De Benedictis, *Experimental studies on elementary kinetics in N_2-O_2 pulsed discharges,* Plasma Sources Sci. Technol. **8**, 266 (1999).

[3] R. Ono and T. Oda, *NO formation in a pulsed spark discharge in $N_2/O_2/Ar$ mixture at atmospheric pressure,* J. Phys. D: Appl. Phys. **35**, 543 (2002).

[4] Y. Ionikh, A.V. Meshchanov, J. Röpcke, and A. Rousseau, *A diode laser study and modeling of NO and NO_2 formation in a pulsed DC air discharge,* Chem. Phys. **322**, 411 (2006).

[5] I.A. Kossyi, A. Yu Kostinsky, A.A. Matveyev, and V.P. Silakov, *Kinetic scheme of the non-equilibrium discharge in nitrogen-oxygen mixtures,* Plasma Sources Sci. Technol. **1**, 207 (1992).

[6] B.F. Gordiets, C.M. Ferreira, V.L. Guerra, J.M.A.H. Loureiro, J. nahorny, D. Pagnon, M. Touzeau, and M. Vialle, *Kinetic model of a low-pressure N_2–O_2 flowing glow discharge,* IEEE trans. Plasma Sci. **23**, 750 (1995).

[7] V. Guerra and J. Loureiro, *Self-consistent electron and heavy-particle kinetics in a low-pressure N_2–O_2 glow discharge,* Plasma Sources Sci. Technol. **6**, 373 (1997).

[8] V. Guerra and J. Loureiro, *Kinetic model of a low-pressure microwave discharge in O_2–N_2 including the effects of O^- ions on the characteristics for plasma maintenance,* Plasma Sources Sci. Technol. **8**, 110 (1999).

[9] B.F. Gordiets and C.M. Ferreira, *Self-consistent modeling of volume and surface processes in air plasma,* AIAA Journal **36**, 1643 (1998).

[10] B. Gordiets, C.M. Ferreira, J. Nahorny, D. Pagnon, M. Touzeau, and M. Vialle, *Surface kinetics of N and O atoms in N_2–O_2 discharges,* J. Phys. D: Appl. Phys. **29**, 1021 (1996).

[11] M. Castillo, V.J. Herrero, I. Méndez, and I. Tanarro, *Spectrometric and kinetic study of a modulated glow air discharge,* Plasma Sources Sci. Technol. **13**, 343 (2004).

[12] M. Castillo, I. Méndez, A.M. Islyaikin, V.J. Herrero, and I. Tanarro, *Low-pressure DC air plasmas. Investigation of neutral and ion chemistry,* J. Phys. Chem. **109**, 6255 (2005).

[13] M.C.M. van de Sanden, R.J. Severens, W.M.M. Kessels, R.F.G. Meulenbroeks, and D. C. Schram, *Plasma chemistry aspects of a–Si:H deposition using an expanding thermal plasma,* J. Appl. Phys. **84**, 2426 (1998), **85**, 1243 (1999).

[14] G. Cartry, L. Magne, and G. Cernogora, *Atomic oxygen recombination on fused silica: modelling and comparison to low-temperature experiments (300 K),* J. Phys. D: Appl. Phys. **33**, 1303 (2000).

[15] Y.C. Kim and M. Boudart, *Recombination of O, N, and H atoms on silica: kinetics and mechanism,* Langmuir **7**, 2999 (1991).

[16] G. Cartry, L. Magne, and G. Cernogora, *Experimental study and modelling of a low-pressure N_2–O_2 time afterglow,* J. Phys. D: Appl. Phys. **32**, 1894 (1999).

[17] J. Röpcke, L. Mechold, M. Käning, J. Anders, F.G. Wienhold, D. Nelson, and M. Zahniser, *IRMA: A tunable infrared multicomponent acquisition system for plasma diagnostics,* Rev. Sci. Instrum. **71**, 3706 (2000).

[18] A. Rousseau, O. Guaitella, L. Gatilova, F. Thevenet, C. Guillard, J. Röpcke, and G.D. Stancu, *Photocatalyst activation in a pulsed low pressure discharge,* Appl. Phys. Lett. **87**, 221501 (2005).

[19] G.D. Stancu, J. Röpcke, and P.B. Davies, *Line strengths and transition dipole moment of the ν_2 fundamental band of the methyl radical,* J. Chem. Phys. **122**, 014306 (2005).

[20] J. Röpcke, L. Mechold, X. Duten, and A. Rousseau, *A time resolved laser study of hydrocarbon chemistry in H_2–CH_4 surface wave plasmas,* J. Phys. D: Appl. Phys. **34**, 2336 (2001).

[21] V. Schulz von der Gathen, J. Röpcke, T. Gans, M. Käning, C. Lukas, and H.F. Döbele, *Diagnostic studies of species concentrations in a capacitively coupled RF plasma containing CH_4–H_2–Ar,* Plasma Sources Sci. Technol. **10**, 530 (2001).

[22] G. Lombardi, K. Hassouni, F. Bénédic, F. Mohasseb, J. Röpcke, and A. Gicquel, *Spectroscopic diagnostics and modeling of $Ar/H_2/CH_4$ microwave discharges used for nanocrystalline diamond deposition,* J. Appl. Phys. **96**, 6739 (2004).

[23] F. Hempel, P.B. Davies, D. Loffhagen, L. Mechold, and J. Röpcke, *Diagnostic studies of H_2–Ar–N_2 microwave plasmas containing methane or methanol using tunable infrared diode laser absorption spectroscopy,* Plasma Sources Sci. Technol. **12**, S98 (2003).

[24] M. Osiac B.P. Lavrov, A.V. Pipa, and J. Röpcke, *On the spectroscopic detection of neutral species in a low-pressure plasma containing boron and hydrogen,* Plasma Sources Sci. Technol. **12**, 576 (2003).

[25] J.B. McManus, D. Nelson, M. Zahniser, L. Mechold, M. Osiac, J. Röpcke, and A. Rousseau, *TOBI: A two-laser beam infrared system for time-resolved plasma diagnostics of infrared active compounds,* Rev. Sci. Instrum. **74**, 2709 (2003).

[26] M.C.M. van de Sanden, J.M. de Regt, G.M. Jansen, J.A.M. van der Mullen, D.C. Schram, and B. van der Sijde, *A combined Thomson-Rayleigh scattering diagnostic using an intensified photodiode array,* Rev. Sci. Instrum. **63**, 3369 (1992).

[27] A.J.M. Buuron, D.K. Otorbaev, M.C.M. van de Sanden, and D.C. Schram, *Absorption spectroscopy on the argon first excited state in an expanding thermal arc plasma,* Phys. Rev. E **50**, 1383 (1994).

[28] G.J.H. Brussaard, *Remote arc generated plasma in diatomic gases,* PhD thesis, Eindhoven University of Technology, Eindhoven, 1999, available on-line at http://alexandria.tue.nl/extra2/9900312.pdf.

[29] M. Hawley and M.A. Smith, *Charge-transfer chemistry of $Ar^+(^2P_{3/2})$ and $Kr^+(^2P_{3/2})$ at very low collision energies,* J. Phys. Chem. **96**, 6693 (1992).

[30] J. Perrin, O. Leroy, and M.C. Bordage, *Cross-sections, rate constants and transport coefficients in silane plasma chemistry,* Contrib. Plasma Phys. **36**, 3 (1996).

[31] J.R. Peterson, A. Le Padellec, H. Danared, G.H. Dunn, M. Larsson, A. Larson, R. Peverall, C. Strömholm, S. Rosén, M. af Ugglas, and W.J. van der Zande, *Dessociative recombination and excitation od N_2^+: Cross sections and product branching ratios,* J. Chem. Phys. **108**, 1978 (1998).

[32] R. Peverall, S. Rosén, J.R. Peterson, M. Larsson, A. Al-Khalili, L. Vikor, J. Semaniak, R. Bobbenkamp, A. Le Padellec, A.N. Maurellis, and W.J. van der Zande, *Dissociative recombination and excitation of O_2^+: Cross sections, product yields and implications for studies of ionospheric airglows,* J. chem. Phys. **114**, 6679 (2001).

[33] J.A.M. van der Mullen, *Excitation equilibria in plasmas; a classification,* Phys. Rep. **191**, 110 (1990).

[34] S. Mazouffre, I. Bakker, P. Vankan, R. Engeln, and D.C. Schram, *Two-photon laser induced-fluorescence spectroscopy performed on free nitrogen plasma jets,* Plasma Sources Sci. Technol. **11**, 439 (2002).

[35] R.P. Dahiya, M.J. de Graaf, R.J. Severens, H. Swelsen, M.C.M. van de Sanden, and D.C. Schram, *Dissociative recombination in cascaded arc generated Ar-N_2 and N_2 expanding plasma,* Phys. Plasmas **1**, 2086 (1994).

[36] G.J.H. Brussaard, E. Aldea, M.C.M. van de Sanden, G. Dinescu, and D.C. Schram, *Evidence of charge exchange between N^+ and $N_2(A^3\Sigma_u^+)$ in a low-temperature nitrogen plasma,* Chem. Phys. Lett. **290**, 379 (1998).

[37] M. Capitelli, C.M. Ferreira, B.F. Gordiets, and A.I. Osipov, *Plasma kinetics in atmospheric gases,* Springer-Verlag, Berlin (2000).

[38] D.D. Nelson, J.H. shorter, J.B. McManus, and M.S. Zahniser, *Sub-part-per-billion detection of nitric oxide in air using a thermoelectrically cooled mid-infrared quantum cascade laser spectrometer,* Appl. Phys. B **75**, 343 (2002).

[39] L.S. Rothman, C.P. Rinsland, A. Goldman, S.T. Massie, D.P. Edwards, J.-M. Flaud, A. Perrin, C. Camy-Peyret, V. Dana, J.-Y. Mandin, J. Schroeder, A. McCann, R.R. Gamache, R.B. Wattson, K. Yoshino, K.V. Chance, K.W. Jucks, L.R. Brown, V. Nemtchinov, and P. Varanasi, *The HITRAN molecular spectroscopic database and HAWKS (HITRAN Atmospheric WorKStation): 1996 edition,* J. Quant. Spectrosc. Radiat. Transfer **60**, 665 (1998).

[40] G. Guelachvili and K.N. Rao, *Handbook of infrared standards: with spectral maps and transition assignments between 3 and 2600 μm*, Academic press London (1986).

[41] J.P.M. Hoefnagels, Y. Barrell, W.M.M. Kessels, and M.C.M. van de Sanden, *Time-resolved cavity ringdown study of the Si and SiH_3 surface reaction probability during plasma deposition of a–Si:H at different substrate temperatures*, J. Appl. Phys. **96**, 4094 (2004).

[42] P.J. van den Oever, J.H. van Helden, C.C.H. Lamers, R. Engeln, D.C. Schram, M.C.M. van de Sanden, and W.M.M. Kessels, *Density and production of NH and NH_2 in an Ar–NH_3 expanding plasma jet*, J. Appl. Phys. **98**, 093301 (2005).

[43] M.A. Blauw et al., To be published.

[44] B.F. Gordiets and C.M. Ferreira, *Self-consistent modeling of volume and surface processes in air plasma*, AIAA J. **36**, 1643 (1998).

[45] L.F. Phillips and H.I. Schiff, *Mass-spectrometric studies of atomic reactions. V. The reaction of nitrogen atoms with NO_2*, J. Chem. Phys. **42**, 3171 (1965).

[46] I.S.J. Bakker, Properties of an expanding thermal nitrogen plasma, Master's thesis, Eindhoven University of Technology, 2001.

Chapter 8

General conclusions

Abstract

The subject of the study presented in this thesis has been the generation of molecules in plasmas characterized by high fluxes of reactive particles. The various investigations have been presented as separate chapters. The chapters are written in the form of stand-alone articles with their own conclusion based on the results in that chapter. Here, the conclusions of each chapter are combined to give a general conclusion for the two model systems studied.

Diagnostics

For the determination of the density of the molecular radicals and molecules various diagnostics have been applied. A new diagnostic technique, phase-shift cavity ring-down technique has been introduced. With this technique, the line intensities of transitions in the spin-forbidden $b^1\Sigma_g^+(\nu' = 0) \leftarrow X^3\Sigma_g^-(\nu'' = 0)$ band of molecular oxygen can be obtained within 4% of values obtained from the HITRAN molecular spectroscopic database. Absorptions down to $2 \times 10^{-8}\mathrm{cm}^{-1}$ can be recorded in an integration time of 500 milliseconds. The high sensitivity together with its simplicity and high duty cycle makes phase-shift cavity ring-down a very promising technique to accurately measure densities in any type of plasma or gas. Furthermore, a simple model has been introduced to correct the measured signals for phase shifts introduced by the off-resonance amplified spontaneous emission of the laser used in the experiments.

To measure the NH_x radicals in plasmas of mixtures of nitrogen and hydrogen a relative new technique, i.e. cavity ring-down spectroscopy has been used. This technique allows for the detection of absolute NH and NH_2 radical densities in N_2–H_2 plasmas. The advantage of this technique is that when the frequency-dependent absorption cross section is known, absolute densities are obtained with a high sensitivity.

The molar fractions of the molecules have been determined with quantitative mass spectrometry. The molar fraction is defined as the ratio of *measured* values only, i.e. the ratio between *measured* produced molecules under investigation and the *measured* total number of molecules present in the plasma. The advantage of using a molar fraction is that the calibration of the mass spectrometer signals is always valid, even if differences in the detection system occur, which would lead to a different absolute calibration.

In collaboration with colleagues from the INP-Institute in Greifswald in Germany, it was shown that time-resolved tunable diode laser absorption spectroscopy can also be applied in our plasmas. By directing the laser twice through the plasma, absorptions as low as 10^{-5} with signal averaging of a few seconds or as low as 10^{-4} with time resolution of a few milliseconds can be obtained. A detection limit of 2×10^{17} m^{-3} has been achieved, which is sensitive enough to study the presence of newly formed molecules in our low pressure, high-flux plasma expansion.

Plasmas containing mixtures of nitrogen and hydrogen

From the measured densities and spectra of the NH and NH_2 radicals it was deduced that the molecular radicals are produced in the plasma expansion. The difference in the measured spectra for the two types of plasmas investigated as function of the position from the plasma source showed that the generation of the NH_x radicals is governed by two different mechanisms. A remarkable result is that in expanding N_2 plasma with H_2 injected in the background the high rotational levels were overpopulated at a distance of 10 cm from the plasma source. Furthermore, the vibrational distribution in both types of plasmas is non-Boltzmann.

The densities of the NH_x radicals are in the order of 10^{17}– 10^{19} m^{-3}, which is a few percent of the ammonia density in these plasmas. The NH_x radicals are formed by reactions of NH_3 molecules, produced at the walls of the plasma reactor, with H atoms emitted by the plasma source. The NH radicals are also formed via reactions between nitrogen atoms and H_2 molecules in the plasma expansion. It is concluded that NH_x radicals play an important, though indirect, role in the ammonia production at the surface.

Studies on four different types of expanding plasmas containing mixtures of nitrogen and hydrogen showed that the ammonia production is strongly dependent on the fluxes of N and H radicals to the surface. Furthermore, the ammonia density was the highest in the plasma reactor with the highest "active" surface to volume ratio. By using an atomic nitrogen and hydrogen source, ammonia can be formed efficiently, i.e. more than 10% of the total background pressure is measured to be ammonia. The maximum ammonia molar fraction that could have been produced in our experiments determined by the fluxes of N and H radicals would have been 30% for a mixture containing 70% hydrogen. This means that an efficiency in the ammonia generation of 33% is achieved in our experiments.

Because of the high fluxes of N and H radicals in our experiments, the ammonia production proved to be independent of wall material, which is in contrast with previous studies. Thus at high fluxes, it seems that the actual chemistry may take place in an additional layer at a passivated surface, covered with N, H and NH and NH_2 radicals. Then, ammonia is formed via plasma-surface interactions by the stepwise addition reactions between adsorbed nitrogen and hydrogen containing radicals at the surface and incoming atomic H radicals, i.e. by the successive hydrogenation of adsorbed nitrogen atoms and the intermediates NH and NH_2 at the surface of the plasma reactor.

Plasmas containing mixtures of nitrogen and oxygen

The visual appearance of an expanding nitrogen plasma with or without oxygen in interaction with a substrate leads to the appearance of additional light, which is ascribed to the formation of excited molecules by association of N and/or O atoms at the substrate.

Ar–N_2–O_2 plasmas and Ar–NO plasmas showed a remarkable resemblance in gas composition. In three different types of plasmas containing mixtures of nitrogen and oxygen on average 5% NO was formed. In the inverse experiment, NO admixed to Ar plasmas, up to 92% of the NO was converted into N_2 and O_2. So, in the NO-high depletion case, the situation is dynamically similar to the experiment in which N_2 and O_2 are injected into an argon plasma: in both cases NO molecules are the minority species and N_2 and O_2 the majority species. Apparently, in both cases there is enough fragmentation and association of radicals to new molecules (for NO injection, mainly N_2 and O_2 molecules), or back to the original molecules (for N_2-O_2 injection). Thus the end situation is the same, if substantial dissociation can be reached within the residence time of the gases in the plasma. Thus, the two types of plasmas show a strong resemblance in the gas composition, i.e. $\approx$ 5% NO and $\approx$ 95% N_2 and O_2 present in the plasma, although the starting conditions are completely different. This preference for N_2 and O_2 production is in accordance with the picture that molecules are formed by surface processes determined by binding energies.

The main primary chemistry in expanding plasmas containing mixtures of nitrogen and oxygen is made up by the high fluxes of atomic N and O radicals created, leading to the formation of mainly NO, but also N_2O and NO_2 molecules, produced to a large extend in surface processes. Mainly NO and N are present at the surface and are stored in the metal wall as the generation of NO and N_2O molecules is still observed after the nitrogen or oxygen flow is stopped, on time-scales much longer than the residence time of the gases in the plasma reactor. In our low-pressure plasmas, the NO, N_2O, and NO_2 molecules are primarily formed in wall association processes of N and O radicals, in combination with subsequent gas phase reactions. The observed NO is mainly generated in the association of N and O radicals at the wall of the reactor and partly formed out of N_2O and NO_2 by gas phase reactions with N and O radicals and by a reaction between N atoms and O_2 molecules in the gas phase.

Summary

Molecules are often synthesized in catalytic processes. A well-known example is ammonia synthesis from nitrogen and hydrogen gas by the Haber-Bosch process. In catalysis, a specific surface material is used as a catalyst in order to dissociate the precursor molecules as well as to enhance the production of a specific molecule. The subject of this thesis is the generation of molecules in plasma, in which plasma acts as catalyst to dissociate the precursor molecules already before they come in contact with a surface. Then the surface is mainly exposed to fluxes of atomic and molecular *radicals* rather than molecules. The question investigated is: which molecules are formed and how? Especially, the role of plasma-surface interactions in the generation of molecules is investigated. In plasma chemistry, but also in interstellar space research, a debate on the importance of surface processes besides volume processes is a central theme.

The generation of molecules in plasmas by association of radicals at a surface was studied at the hand of two systems. In the first one, surfaces are exposed to fluxes of atomic nitrogen and hydrogen leading among others to ammonia formation. In the second one, surfaces are exposed to fluxes of atomic nitrogen and oxygen resulting in a significant amount of NO molecules besides regenerated N_2 and O_2 molecules. The importance of plasma-surface interactions is quantified by studying the generated molecules present in the gas phase. The molecules have been monitored using mass spectrometry and three laser-based diagnostic techniques, i.e. time resolved tunable diode laser absorption spectroscopy, cavity enhanced absorption spectroscopy and cavity ring-down spectroscopy.

A new diagnostic has also been introduced, phase-shift cavity ring-down spectroscopy (PSCRD). In the PSCRD technique, a narrow band cw diode laser is used in combination with a high-finesse optical cavity to perform very sensitive high-resolution, direct absorption spectroscopy in a simple experimental setup using ideas

from the field of cavity ring-down spectroscopy (CRDS). Furthermore, by quantifying the role of amplified spontaneous emission (ASE) in CRDS measurements, absolute line intensities and densities are obtained.

An evaluation of the role of NH and NH_2 radicals in ammonia producing plasmas has been performed using cavity ring-down spectroscopy. With this technique, absolute densities of NH and NH_2 radicals were obtained. The NH_x radicals are formed by reactions between ammonia and H atoms and subsequently the reaction between NH_2 and H atoms. The NH radicals are also formed via reactions between nitrogen atoms and H_2 molecules in the plasma expansion. Furthermore, the density distribution of NH over the vibrational levels is non-Boltzmann and the high rotational levels in the beginning of the expansion are overpopulated.

The experiments on plasmas containing mixtures of nitrogen and hydrogen performed, indicate that the ammonia production occurs at the wall of the plasma reactor. It was shown that an efficiency of 33% in the ammonia generation can be achieved, if the admitted nitrogen and hydrogen gas flows are appreciable dissociated, resulting in high atomic N and H radical fluxes. It appeared that the efficiency of the ammonia production is related to the fluxes of the N and H radicals from the plasma to the surface. There are indications that the amount of molecules formed is similar for different wall materials. The presence of an additional layer at a passivated surface could play a role in the formation of these molecules at the surface. Radicals arriving at the surface adsorb and interact to generate new molecules. For instance, ammonia is most likely formed by the successive hydrogenation of adsorbed nitrogen atoms at the surface of the plasma reactor via the intermediates NH and NH_2.

Perhaps the most clear indication of the surface production of molecules in an additional layer, in which the precursor radicals or molecules are only weakly bonded to the surface, is the appearance of additional light around a substrate placed in expanding nitrogen plasmas with and without oxygen added. Apparently, excited molecules are formed by association of N and/or O atoms at the substrate.

The gas composition of plasmas produced from $Ar/N_2/O_2$ mixtures and Ar/NO mixtures has been studied. The plasmas show a striking resemblance in the steady state gas composition, i.e. $\approx$ 5% NO is formed and $\approx$ 95% N_2 and O_2 are formed in the plasma, despite the fact that the starting conditions are completely different.

In plasmas containing mixtures of nitrogen and oxygen, besides NO also N_2O and NO_2 are formed. It appeared that below a certain threshold in the O_2 flows, primarily N_2O is formed and almost no NO. This can be explained by a surface that is primarily covered with N and NO. At higher O_2 flows, the production of NO

becomes dominant, but also a finite amount of NO_2 is measured.

In the course of the investigations presented in this thesis a more detailed view on the role of atomic radicals and surface processes in the generation of molecules through plasma-surface processes is established. The obtained knowledge can serve as a starting point to study more complex systems. The high efficiency in molecule generation suggests that when a plasma is used to dissociate the precursor molecules, the surface material, which is no longer selected to dissociate molecules, can be optimized to facilitate the formation of specific molecules.

Samenvatting

Moleculen worden vaak geproduceerd via katalytische processen. Een algemeen bekend voorbeeld is de productie van ammoniak uit stikstof en waterstof gas via het Haber-Bosch proces. In katalyse wordt een specifiek materiaal als katalysator gebruikt om de precursor moleculen te dissociëren alsmede om de productie van een bepaald soort molecuul te bevorderen. Het onderwerp van dit proefschrift is de generatie van moleculen in plasma's, waarbij het plasma fungeert als katalysator om de precursor moleculen te dissociëren, voordat ze in contact komen met een oppervlak. In dat geval wordt het oppervlak voornamelijk blootgesteld aan fluxen van atomaire en moleculaire *radicalen*, in plaats van moleculen. De vraag die onderzocht wordt is: welke moleculen worden gevormd en hoe? In het bijzonder, de rol van plasma-wand interacties in de generatie van moleculen wordt bestudeerd. In plasma chemie, maar ook in het onderzoek van de interstellaire ruimte, is het belang van processen aan oppervlakken naast volume processen een belangrijk thema.

De generatie van moleculen in plasma's door de associatie van radicalen aan een oppervlak is bestudeerd aan de hand van twee systemen. In het eerste systeem wordt een oppervlak blootgesteld aan fluxen van atomair stikstof en waterstof, hetgeen onder anderen leidt tot de productie van ammoniak. In het tweede systeem wordt een oppervlak blootgesteld worden aan fluxen van atomair stikstof en zuurstof, hetgeen resulteert in een significante hoeveelheid NO en vooral opnieuw gevormde stikstof en zuurstof moleculen. Het belang van plasma-wand interacties is gekwantificeerd door het bestuderen van de gevormde moleculen aanwezig in de gas fase. De moleculen zijn gemeten met behulp van massaspectrometrie en drie op lasers gebaseerde technieken, namelijk tijdsopgeloste verstembare diode laser absorptie spectroscopie, "cavity enhanced" absorptie spectroscopie en "cavity ring-down" spectroscopie.

Ook is er een nieuwe meetmethode geïntroduceerd, namelijk "phase-shift cavity

ring-down" spectroscopie (PSCRD). In de PSCRD techniek wordt een smalbandige continue diode laser gebruikt in combinatie met een optische trilholte met een hoge finesse. Daarmee wordt zeer gevoelige, hoge resolutie, directe absorptie spectroscopie mogelijk met een simpele experimentele opstelling, gebaseerd op de principes van de "cavity ring-down" techniek. Door de rol van spontane gestimuleerde emissie in "cavity ring-down" metingen te kwantificeren zijn absolute lijnintensiteiten en dichtheden bepaald.

De rol van NH en NH_2 radicalen in ammoniak producerende plasma's is bepaald met behulp van "cavity ring-down" spectroscopie. Hiermee zijn absolute dichtheden van NH en NH_2 radicalen gemeten. De NH_x radicalen worden gevormd via reacties tussen ammoniak en H atomen gevolgd door reacties tussen NH_2 en H atomen. De NH radicalen worden ook gevormd via reacties tussen stikstof atomen en H_2 moleculen in de plasma expansie. Verder blijkt dat de dichtheidsverdeling van NH over de vibrationele toestanden geen Boltzmann verdeling is en dat de hoge rotationele aangeslagen toestanden aan het begin van de expansie overbezet zijn.

Experimenten uitgevoerd aan stikstof en waterstof bevattende plasma's, laten zien dat de productie van ammoniak plaatsvindt aan de wand van de plasma reactor. Er wordt aangetoond dat een 33% efficiëntie in de ammoniak productie wordt bereikt indien een aanzienlijke hoeveelheid van de toegevoerde stikstof en waterstof gassen gedissocieerd worden, hetgeen resulteert in een hoge atomaire N en H flux. Het blijkt dat de efficiëntie in ammonia productie is gerelateerd aan de N en H radicalen flux van het plasma naar de wand. Er zijn aanwijzingen dat de hoeveelheid gevormde moleculen hetzelfde is voor verschillende materialen. De aanwezigheid van een additionele laag op een gepassiveerd oppervlak zou hierbij een rol kunnen spelen. Radicalen die in contact komen met het oppervlak worden geadsorbeerd en vormen nieuwe moleculen. Een illustratie hiervan is dat ammoniak waarschijnlijk wordt gevormd door de opeenvolgende hydrogenatie van geadsorbeerde stikstof atomen en de tussenproducten NH en NH_2 aan het oppervlak van de plasma reactor.

De meest duidelijke ondersteuning van de productie van moleculen aan een oppervlak in een additionele laag waarin de precursor radicalen of moleculen slecht zwak gebonden zijn aan het oppervlak, is de observatie van extra licht rond een substraat geplaatst in een expanderend plasma van puur stikstof of van een stikstof/zuurstof mengsel. Klaarblijkelijk worden geëcxiteerde moleculen gevormd door de associatie van N en/of O atomen aan een oppervlak.

De gas composities van plasma's geproduceerd van mengsels van $Ar/N_2/O_2$ en Ar/NO zijn bestudeerd. De plasma's vertonen een saillante gelijkenis in de station-

aire gas compositie, d.w.z. $\approx$ 5% NO moleculen en $\approx$ 95% N_2 and O_2 moleculen worden gevormd, ondanks dat de begincondities compleet verschillend zijn.

In stikstof en zuurstof bevattende plasma's wordt naast NO, ook N_2O en NO_2 gevormd. Het blijkt dat beneden een bepaalde drempel in de zuurstof toevoer, voornamelijk N_2O wordt gevormd en bijna geen NO. Dit kan verklaart worden met een oppervlak dat voornamelijk bezet is met N en NO. Met toenemende zuurstof toevoer wordt de productie van NO dominant, maar wordt ook een beperkte hoeveelheid NO_2 gemeten.

Gedurende het onderzoek gepresenteerd in dit proefschrift is een meer gedetailleerd beeld van de rol van de atomaire radicalen en de processen aan oppervlakken in de generatie van moleculen door plasma-wand processen vastgelegd. De verkregen kennis kan als startpunt dienen voor de bestudering van meer complexe systemen. De hoge efficiëncie in molecuul generatie suggereert dat wanneer een plasma wordt gebruikt om de precursor moleculen te dissociëren, het oppervlak niet meer geselecteerd hoeft te worden om moleculen te dissociëren, maar geoptimaliseerd kan worden om de vorming van specifieke moleculen te bevorderen.

Dankwoord

Het werk beschreven in dit proefschrift had nooit tot stand kunnen komen zonder de bijdrage van de vele mensen die ik bij deze wil danken.

Ten eerste wil ik Daan bedanken, je enthousiasme was elke keer weer aanstekelijk en je zorgde voor een inspirerende werkomgeving. Daan, een aparte eigenschap van jou is dat jij op ieder moment datgene kan verklaren wat ik als promovendus aan bevindingen krijg gedurende het onderzoek. Het kostte soms wat moeite om te doorgronden wat je bedoelde als we weer eens een discussie hadden over de fysica, maar dacht achteraf toch steeds: niet zo gek bedacht! Daarnaast wil ik ook Richard bedanken. In de dagelijkse gang van zaken was jij de persoon waar ik altijd terecht kon. Mijn huidige experimentele vaardigheden en spectroscopische kennis zijn grotendeels aan jou te danken. Tenslotte wil ik Richard van de Sanden graag bedanken voor het kritisch en nauwkeurig doorlezen van mijn manuscript, hetgeen uiteindelijk nog behoorlijk heeft bijgedragen aan de wetenschappelijke inhoud.

Een gedeelte van de gegevens waarop dit proefschrift is gebaseerd is te danken aan de inzet van een aantal studenten. Ik wil daarom als eerste de afstudeerders Rens Zijlmans en Göksel Yagci bedanken voor hun bijdrage. Daarnaast ben ik erkentelijk voor de bijdrage van de stagairs: Wiebe Wagemans, Petr Hlavenka, Abdel El Fattahi, Carolien Lamers en Philip Somers. Verder wil ik ook collega-promovendi Peter Vankan, Peter van den Oever en Rens Zijlmans bedanken (Rens zorg goed voor de HNO-opstelling) voor de gezamenlijke uren in het lab.

Onmisbaar in het experimentele werk was de technische begeleiding van Ries van de Sande, Jo Jansen, Herman de Jong en Bertus Hüsken. Vooral voor de reparaties, wanneer de HNO-opstellingt het weer eens begaf. Maar uiteindelijk heb ik nog het heugelijke feit mogen meemaken dat ook de kleinste, maar fijnste opstelling, waar ik veel van mijn metingen op heb verricht in een nieuw jasje gestoken uiteindelijk ook in de labtuin staat. Ook Jeanne Loonen, Lianne Doms en Marion Nolet wil ik hier

noemen, voor de vele zaken die jullie voor mij hebben geregeld en georganiseerd; dank hiervoor.

Dan wil ik ook mijn kamergenoten noemen die vaker mijn gedachten voorgeschoteld kregen of ze wilden of niet: Marco van de Sande, Maikel van Hest, Peter van den Oever (dat jaar meten met zijn tweeën heeft uiteindelijk veel opgeleverd), Ioana Volintiru (die wel eens gek werd van al die discussies over fysica tussen Peter en mij).

Verder wil ik alle ETP collega's van de laatste vier en half jaar bedanken, die nog niet zijn genoemd: Erwin, Igor, Joost, Stephan, Bram, Erik, Alquin, Christian, Adriana, Michiel, Eugen, Paul, Menno, Kerim, Onno, Terje, Hans, Johan, Greg, Chiel, Bas, Roland, Peter, Arno en de enkele mensen die ik hoogstwaarschijnlijk vergeten ben. De sfeer binnen ETP is naar mijn mening uniek en zorgt ervoor dat grootse prestaties geleverd kunnen worden, houden zo! Speciaal wil ik het PEST-team (Plasma Enhanced Soccer Team) noemen, waarin ik de laatste 4 jaar met veel plezier heb gevoetbald.

I would also like to acknowledge the people of the Centre for Plasma physics at the International Research Centre for Experimental Physics (IRCEP) of the Queen's University in Belfast for the hospitality during my three months working visit. Especially Bill Graham, Damian Della Croce, Gagik Narsisyan, Fernando Garcia, Brendan Dromey, thank you for the pleasant time (and all the hours in the pub).

Als laatste wil ik mijn ouders, mijn zus en schoonbroer en kinderen bedanken. Jullie onvoorwaardelijke steun en vertrouwen is onmisbaar geweest in het tot stand komen van dit proefschrift, maar ook in de vorming van mij als persoon.

Curriculum Vitae

1977, August 22	Born in Susteren, The Netherlands
1989 – 1995	VWO College Sittard, Sittard
1995 – 2001	Student Applied Physics, Eindhoven University of Technology
	Five months traineeship (fall/winter 1999/2000) at the New York State Center for Advanced Thin Film Technology, State University of New York at Albany, New York, U.S.A.
	Master thesis project in the group Equilibrium and Transport in Plasmas
2001 – 2006	PhD student, group Equilibrium and Transport in Plasmas, Center for Plasma Physics and Radiation Technology, Department of Applied Physics, Eindhoven University of Technology
	Three months working visit (fall 2004) to the group of Prof. W.G. Graham at the Plasma and Laser Interactions Physics Research Division, Queen's university Belfast